THESE

Pour l'obtention du Grade de

DOCTEUR DE L'ECOLE NATIONALE SUPERIEURE DE MECANIQUE ET D'AEROTECHNIQUE

(Diplôme National - Arrêté du 25 mai 2016)

Ecole Doctorale:
Sciences et Ingénierie en Matériaux, Mécanique, Energétique et Aéronautique

Secteur de Recherche: Mécanique des solides, des Matériaux, des Structures et des Surfaces

Présentée par:

Ahmad Al Takash

Development of numerical methods to accelerate the prediction of the behavior of multiphysics under cyclic loading

-

Développement de méthodes numériques en vue d'une prédiction plus rapide du comportement multiphysique sous chargement cyclique

Directeur de thèse: Jean-Claude GRANDIDIER

Co-encadrants: Marianne BERINGHIER et Mohammad HAMMOUD

Soutenue le 23 Novembre 2018

devant la Commission d'Examen

JURY

Président :	
Sylvain DRAPIER	Professeur, Ecole des Mines de Saint-Etienne, Saint-Etienne
Rapporteurs :	
Francisco CHINESTA	Professeur, Arts et Métiers ParisTech, Paris
Elias CUETO	Full professor, Université de Saragosse, Espagne
Membres du jury :	
Virgine EHRLACHER	Chercheur, ENPC, Paris
Christine ESPINOSA	Maître de conférence HDR, ISAE-SUPAERO, Toulouse
Jean-Claude GRANDIDIER	Professeur, ENSMA Poitiers
Marianne BERINGHIER	Maître de conférence, ENSMA Poitiers
Mohammad HAMMOUD	Associate professor, LIU Beirut, Liban

ACKNOWLEDGMENT

To soul of my father.

I would like to express my sincere gratitude to my advisor; Dr Marianne Beringhier, I want to thank you for the continuous support of my PH.D study, guidance and immense knowledge. To Dr Hammoud for your motivation and knowledge. To Dr Grandidier, for your knowledge.

I would like to thank my committee members, Professor Francisco Chinesta, Professor Elias Cueto, Professor Sylvain Drapier, Dr. Chirstine Espinosa and Dr. Virginie Ehrlacher for serving as my committe members.

A special thank to my family, my mother your prayers for me was what sustained me thus far, for my beloved fiance Aya for supporting me for everything. For my two brother Khalil and Abbas for being beside me through all stages of my life. Finally I thank my god for letting me through all the difficulties.

Abstract

In the framework of structural calculation, the reduction of computation time plays an important role in the proposition of failure criteria in the aeronautic and automobile domains. Particularly, the prediction of the stabilized cycle of polymer under cyclic loading requires solving of a thermo-viscoelastic problem with a high number of cycles. The presence of different time scales, such as relaxation time (viscosity), thermal characteristic time (thermal), and the cycle time (loading) lead to a huge computation time when an incremental scheme is used such as with the Finite Element Method (FEM). In addition, an allocation of memory will be used for data storage. The objective of this thesis is to propose new techniques and to extend existent ones. A transient thermal problem with different time scales is considered in the aim of computation time reduction. The proposed methods are called model reduction methods. First, the Proper Generalized Decomposition method (PGD) was extended to a nonlinear transient cyclic 3D problems. The non-linearity was considered by combining the PGD method with the Discrete Empirical Interpolation Method (DEIM), a numerical strategy used in the literature. Results showed the efficiency of the PGD in generating accurate results compared to the FEM solution with a relative error less than 1%. Then, a second approach was developed in order to reduce the computation time. It was based on the collection of the significant modes calculated from the PGD method for different time scales. A dictionary assembling these modes is then used to calculate the solution for different characteristic times and different boundary conditions. This approach was adapted in the case of a weak coupled diffusion thermal problem. The novelty of this method is to consider a dictionary composed of spatio-temporal bases and not spatial only as used in the POD. The results showed again an exact reproduction of the solution in addition to a huge time reduction. However, when different cycle times are considered, the number of modes increases which limits the usage of the approach. To overcome this limitation, a third numerical strategy is proposed in this thesis. It consists in considering a priori known time bases and is called the mixed strategy. The originality in this approach lies in the construction of a priori time basis based on the Fourier analysis of different simulations for different time scales and different values of parameters. Once this study is done, an analytical expression of time bases based on parameters such as the characteristic time and the cycle time is proposed. The related spatial bases are calculated using the PGD algorithm. This method is then tested for the resolution of 3D thermal problems under cyclic loading linear and nonlinear and a weak coupled diffusion thermal problem.

Keywords: Model Reduction, Proper Generalized Decomposition, A priori time bases, Transient problem, Fourier analysis, Multi-time.

Résumé

La réduction du temps de calcul lors de la résolution de problèmes d'évolution dans le cadre du calcul de structure constitue un enjeu majeur pour, par exemple, la mise en place de critères de rupture des pièces dans le secteur de l'aéronautique et de l'automobile. En particulier, la prédiction du cycle stabilisé des polymères sollicités sous chargement cyclique nécessite de résoudre un problème thermo-viscoélastique à grand nombre de cycles. La présence de différentes échelles de temps telles que le temps de relaxation (viscosité), le temps caractéristique associé au problème thermique et le temps du cycle de chargement conduit à un temps de calcul significatif lorsqu'un schéma incrémental est utilisé comme c'est le cas avec la méthode des éléments finis (MEF). De plus, un nombre important de données doit être stocké (au moins à chaque cycle). L'objectif de cette thèse est de proposer de nouvelles méthodes ainsi que d'étendre des méthodes existantes. Il est choisi de résoudre un problème thermique transitoire cyclique impliquant différentes échelles de temps avec l'objectif de réduire le temps de calcul réduit. Les méthodes proposées font partie des méthodes de réduction de modèles. Tout d'abord, la méthode de décomposition propre généralisée (PGD) a été étendue à un problème transitoire cyclique 3D non linéaire, la non-linéarité a été traitée en combinant la méthode PGD à la Méthode d'interpolation empirique discrète (DEIM), stratégie numérique déjà proposée dans la littérature. Les résultats ont montré l'efficacité de la PGD pour générer des résultats précis par rapport à la solution FEM avec une erreur relative inférieure à (1%). Ensuite, afin de réduire le temps de calcul, une autre approche alternative a été développée. Cette approche est basée sur l'utilisation d'une collection de modes, les modes les plus significatifs, issus de solutions PGD pour différentes échelles de temps et différentes valeurs de paramètres. Un dictionnaire regroupant ces modes est alors utilisé pour construire des solutions pour différents temps caractéristiques et différentes conditions aux limites, uniquement par projection de la solution sur les modes du dictionnaire. Cette approche a été adaptée pour traiter un problème faiblement couplé diffuso-thermique. La nouveauté de cette approche est de considérer un dictionnaire composé de bases spatio-temporelles et non pas uniquement de bases spatiales comme dans la fameuse méthode POD. Les résultats obtenus avec cette approche sont précis et permettent une réduction notable du temps de calcul online. Néanmoins, lorsque différents temps de cycles sont considérés, le nombre de modes dans le dictionnaire augmente, ce qui en limite son utilisation. Afin de pallier cette limitation, une troisième stratégie numérique est proposée dans cette thèse. Elle consiste à considérer comme a priori connues des bases temporelles, elle est appelée stratégie mixte. L'originalité dans cette approche réside dans la construction de la base temporelle a prior basée sur l'analyse de Fourier de différentes simulations pour différents temps et différentes valeurs des paramètres. Une fois cette étude réalisée, une expression analytique des bases temporelles fonction des paramètres tels que le temps caractéristique et le temps du cycle est proposée. Les bases spatiales associées sont calculées à l'aide d'un algorithme type PGD. Cette méthode est ensuite testée pour la résolution de problèmes thermiques 3D sous chargement cyclique linéaires et non linéaires et un problème faiblement couplé thermo-diffusion.

Mots-clés: Réduction de modèle, Décomposition propre généralisée, Bases a priori, problème transitoire, Analyse de Fourier, multi-temps.

Education is the most powerful weapon, you can use to change the world

---

Nelson Mandela

Contents

Acknowledgements ii

Abstract iii

List of Figures ix

List of Tables ix

Introduction 1

1 Literature review 5
- 1.1 Introduction . . . 8
- 1.2 FEM and the incremental scheme . . . 8
- 1.3 Model Order Reduction (MOR) . . . 10
  - 1.3.1 A posteriori . . . 10
    - 1.3.1.1 Proper Orthogonal Decomposition (POD) . . . 10
  - 1.3.2 A priori . . . 11
    - 1.3.2.1 A Priori Hyper Reduction (APHR) . . . 11
    - 1.3.2.2 LArge Time INcrement (LATIN) . . . 11
    - 1.3.2.3 Proper Generalized Decomposition (PGD), non-incremental scheme 12
  - 1.3.3 MOR strategies in the context of fatigue . . . 15
- 1.4 Numerical issues to deal with nonlinearities . . . 17
  - 1.4.1 Newton-Raphson method . . . 17
  - 1.4.2 Picard's method . . . 19
  - 1.4.3 Asymptotic Numerical Method (ANM) . . . 20
  - 1.4.4 Discrete Empirical Interpolation Method (DEIM) . . . 21
- 1.5 Frequency domain analysis . . . 21
  - 1.5.1 Fourier analysis . . . 22
  - 1.5.2 Application of the Fast Fourier Transform method (FFT) in mechanics and more particularly materials under fatigue . . . 23
- 1.6 Discussion . . . 24

2 3D thermal problem: linear, nonlinear and multitime 27
- 2.1 Introduction . . . 30
- 2.2 3D thermal problem within the Finite Element framework . . . 30
  - 2.2.1 3D linear thermal problem . . . 30
    - 2.2.1.1 Modeling . . . 30
    - 2.2.1.2 Finite Element approximation . . . 33
  - 2.2.2 3D non-linear thermal problem . . . 36
    - 2.2.2.1 Modeling . . . 36
    - 2.2.2.2 Finite Element approximation . . . 36
- 2.3 Discussion and conclusion . . . 37

3 PGD method to deal with 3D heat problem **39**
3.1 Introduction . . . 42
3.2 PGD solution of 3D transient thermal problem . . . 42
3.2.1 Problem description . . . 42
3.2.2 Progressive construction of the separated representation . . . 42
3.3 Solution with an incremental scheme with FE framework . . . 45
3.4 Numerical results . . . 47
3.4.1 PGD for linear 3D thermal problem under cyclic loading . . . 47
3.4.1.1 Influence of the physical time on the solution . . . 47
3.4.1.2 Influence of the time discretization on the PGD solution . . . 52
3.4.1.3 Influence of the spatial position . . . 52
3.4.2 PGD for nonlinear 3D thermal problem under cyclic loading . . . 53
3.4.2.1 DEIM-PGD combination for nonlinear problems . . . 53
3.5 Conclusion . . . 58

4 Numerical approach based on the collection of the most significant modes to solve cyclic transient thermal problems involving different time scales **59**
4.1 Introduction . . . 62
4.2 Presentation of the method . . . 62
4.3 Algorithm . . . 63
4.3.1 Problem description . . . 63
4.3.2 Creation of the dictionary and algorithm of the proposed approach . . . 63
4.4 Numerical results . . . 66
4.4.1 Dictionary 1 for a fixed cycle time and different physical times . . . 66
4.4.1.1 Dictionary creation . . . 66
4.4.1.2 Dictionary evaluation . . . 69
4.4.2 Dictionary 2 for fixed physical time and different cycle times . . . 73
4.4.2.1 Dictionary creation . . . 73
4.4.2.2 Dictionary evaluation . . . 75
4.5 Extension to many harmonics . . . 77
4.5.1 Dictionary evaluation . . . 79
4.6 Extension to coupled problems . . . 81
4.6.1 Problem description . . . 82
4.6.2 Algorithm of the coupled thermo-diffusion problem . . . 83
4.6.3 Dictionary evaluation of the thermo-diffusion problem . . . 84
4.7 Conclusion . . . 85

5 Towards a priori timebasis - proposal of a mixed strategy **89**
5.1 Introduction . . . 92
5.2 Presentation of the method . . . 92
5.3 Mixed strategy for 3D linear problem . . . 94
5.3.1 Algorithm . . . 94
5.3.1.1 Problem description . . . 94
5.3.1.2 Strategy to generate the time bases . . . 95
5.3.1.3 Algorithm to compute the spatial bases . . . 100
5.3.2 Numerical results . . . 101
5.3.2.1 Homogeneous Dirichlet boundary conditions . . . 101
5.3.2.2 Non-homogeneous Dirichlet boundary conditions . . . 104
5.3.2.3 Opposite non-homogeneous Dirichlet boundary conditions . . . 107
5.3.2.4 Robin boundary conditions . . . 109
5.3.2.5 Non-constant source and non-homogeneous Dirichlet with different cycle times . . . 109
5.3.3 Effect of the time basis order . . . 111
5.3.4 Usage of the time basis to generate solution with larger number of cycles . . . 113

5.3.5 Usage of the time basis to generate solution with larger time domain 114
5.3.6 Influence of the load 116
5.3.6.1 Sinusoidal 117
5.3.6.2 Heaviside 122
5.3.6.3 Influence of the ratio ($\frac{T_{min}}{T_{max}} = -1$) 126
5.3.6.4 Influence of the load amplitude 127
5.3.7 Extension to coupled problem 131
5.3.8 Discussion on the use of the mixed strategy for linear problem 135
5.4 Mixed strategy for 3D non linear problem 135
5.4.1 Algorithm 135
5.4.1.1 Choice of the time bases 135
5.4.1.2 Algorithm to compute spatial basis and to solve the non-linearity . 136
5.4.2 Numerical results 136
5.4.2.1 Nonlinear heat equation with one cycle time 136
5.4.2.2 Nonlinear heat equation with two cycle times 143
5.4.3 Discussion on the use of the mixed strategy for nonlinear problem 145
5.5 Conclusion 145

Conclusion and Perspective **149**

Résumé substantiel **153**

Bibliography **184**

A Appendix A **185**
A.1 Progressive construction of the PGD 185
A.2 Sampling in the frequency domain 186
A.3 Finite Element Method using ABAQUS software 186
A.3.1 Linear 3D transient thermal problem 186
A.3.2 Nonlinear problem 188

B Appendix B **189**
B.1 Construction of the separated representation 189

C Appendix C **193**
C.1 Chapter 5: simulations summary 193

List of Figures

1.1 Domain and sub domain for Finite Element Method [Reddy, 1993] . . . 9
1.2 Finite Element approximation [Reddy, 1993] . . . 9
1.3 The iterative procedure in the LATIN algorithm [Ladeveze *et al.*, 2010] . . . 12
1.4 Comparison of computational costs (PGD VS FEM) [Giner *et al.*, 2013] . . . 13
1.5 The classical algorithm of PGD method . . . 14
1.6 Newton-Raphson algorithm [Larson et Bengzon, 2013] . . . 18
1.7 Picard algorithm [Larson et Bengzon, 2013] . . . 19
1.8 DEIM-based PGD algorithm from [Aguado *et al.*, 2013] . . . 22
1.9 The Fast Fourier Transform of $f(t)$ . . . 23

2.1 Thermal equilibrium on a solid domain Ω [Bergheau et Fortunier, 2010] . . . 30
2.2 The linear shape function [Bergheau et Fortunier, 2010] . . . 34
2.3 Non-linear solver with the two steps [Bergheau et Fortunier, 2010] . . . 37

3.1 The first five cycles of the cyclic loading T_∞ . . . 43
3.2 The boundary conditions applied to the model . . . 43
3.3 The evolution of temperature for constant load and cyclic load at $(x, y, z) = (25, 50, 25)$ 46
3.4 The computation time for case of cyclic loading and constant loading with the FEM using Abaqus software. . . . 47
3.5 The evolution of the temperature under cyclic load $\tau_c = 20s$ (50 cycles) with $\tau_\phi = 0.1s$ at $(x, y, z) = (25, 25, 50)$ . . . 49
3.6 The evolution of the temperature under cyclic load $\tau_c = 20s$ (50 cycles) with $\tau_\phi = 10s$ at $(x, y, z) = (25, 25, 50)$ . . . 50
3.7 The evolution of the temperature under cyclic load $\tau_c = 20s$ (50 cycles) with $\tau_\phi = 1000s$ at $(x, y, z) = (25, 25, 50)$ . . . 50
3.8 The evolution of the temperature under cyclic load $\tau_c = 20s$ (2000 cycles) and $L_t = 40000s$ with $\tau_\phi = 1000s$ at $(x, y, z) = (25, 25, 50)$ . . . 51
3.9 The partition of the first 10 modes in x, y, z and t dimensions for $\tau_\phi = 1000s$ . . . 51
3.10 The evolution of the temperature for $\tau_\phi = 10s$ using different time discretization $(x, y, z) = (25, 25, 50)$ . . . 52
3.11 The evolution of the temperature for $\tau_\phi = 1000s$ using different time discretization $(x, y, z) = (25, 25, 50)$ . . . 53
3.12 The evolution of temperature for different spatial positions with respect to the physical time . . . 54
3.13 Temperature evolution for case 1 $Cp = 9.2 \times T + 1366.66$ . . . 56
3.14 Temperature evolution for case 2 $Cp = T + 25$ . . . 56
3.15 Temperature evolution for case 3 $Cp = 27 \times T + 25$ . . . 57

4.1 Creation of the dictionary issued from 3 different cases . . . 63
4.2 The evolution of $\frac{|\alpha_i^j|}{\max\limits_i |\alpha_i^j|}$ with respect to the number of modes for each case j . . . 66
4.3 The evolution of the temperature under cyclic load $\tau_c = 20s$ (50 cycles) with $\tau_\phi = 0.1s$ at $(x, y, z) = (25, 25, 50)$ . . . 68
4.4 The evolution of the temperature under cyclic load $\tau_c = 20s$ (50 cycles) with $\tau_\phi = 10s$ at $(x, y, z) = (25, 25, 50)$ . . . 68

4.5 The evolution of temperature under cyclic load $\tau_c = 20s$ (50 cycles) with $\tau_\phi = 1000s$ at $(x, y, z) = (25, 25, 50)$ . . . 69
4.6 The partition of the first 12 most significant modes in x, y, z directions of the dictionary 70
4.7 The time evolution of the modes $F_i(x)G_i(y)H_i(z)U_i(t)$ of the dictionary 1 at $(x, y, z) = (25, 25, 25)$ . . . 70
4.8 The evolution of the α_i coefficient for $\tau_\phi = 3s$ with respect to the modes of the dictionary 1 . . . 71
4.9 The evolution of temperature under cyclic load $\tau_c = 20s$ (50 cycles) with $\tau_\phi = 3s$ at $(x, y, z) = (25, 25, 50)$ . . . 71
4.10 The evolution of temperature under $\tau_c = 20s$ with $\tau_\phi \approx 10s$ and different boundary conditions at $(x, y, z) = (25, 25, 50)$ - case 1-BC . . . 72
4.11 The evolution of temperature under $\tau_c = 20s$ with $\tau_\phi = 100s$ and different boundary conditions at $(x, y, z) = (25, 25, 50)$ - case 2-BC . . . 73
4.12 The evolution of temperature for different cycle times at $(x, y, z) = (25, 25, 50)$ . . . 74
4.13 The time part of the first 12 most significant modes of the dictionary 2 . . . 74
4.14 The time evolution of the modes $F_k(x)G_k(y)H_k(z)U_k(t)$ of the dictionary 2 at $(x, y, z) = (25, 25, 50)$ . . . 75
4.15 The evolution of the coefficient α for $\tau_c = 20s$ with respect to the modes of the dictionary 2 . . . 76
4.16 The evolution of temperature under $\tau_c = 20s$ with $\tau_\phi = 10s$ at $(x, y, z) = (25, 25, 25)$ 76
4.17 The evolution of the coefficient α for $\tau_c = 20s$ with respect to the modes of the dictionary 3 . . . 77
4.18 The evolution of temperature using different dictionaries . . . 78
4.19 The evolution of T_∞ under $(T_\infty(\tau_c = 10) + T_\infty(\tau_c = 50) + T_\infty(\tau_c = 100))$ . . . 79
4.20 The evolution of the coefficient α for $\tau_\phi = 3s$ with respect to the modes of the dictionary 4 . . . 80
4.21 The evolution of temperature under $(\tau_\phi = 3s)$ and cycle time ($\tau_c = 10$,$\tau_c = 50$,$\tau_c = 100s$) at $(x, y, z) = (25, 25, 50)$ . . . 80
4.22 The evolution of temperature under $(\tau_\phi = 3s)$ and cycle time ($\tau_c = 10$,$\tau_c = 50$, $\tau_c = 100s$) at $(x, y, z) = (25, 25, 50)$ using the summation of different solutions obtained from each dictionary independently. . . . 81
4.23 The first five cycles of the cyclic loading with a cycle time $\tau_c = 100s$ . . . 83
4.24 The evolution of the α_i coefficient for $\tau_\phi = 3s$ (same physical time) with respect to the modes of the coupled dictionary denoted by dictionary 5 in case of the coupled problem for the temperature . . . 85
4.25 The evolution of temperature under same physical time $(\tau_\phi = 3s)$ and $\tau_c^T = 100s$ and $\tau_c^D = 10s$ at $(x, y, z) = (25, 25, 25)$ . . . 86
4.26 The evolution of the α_i coefficient for $\tau_\phi = 20s$ (different physical times) with respect to the modes of the dictionary 5 in case of the coupled problem for the temperature 86
4.27 The evolution of temperature under $\tau_\phi^T = 3s$ and $\tau_c^T = 100s$ with $\tau_\phi^D = 20s$ and $\tau_c^D = 10s$ at (x, y, z) = (25, 25, 25) . . . 87
4.28 Uncoupled case : the evolution of concentration under $\tau_\phi^D = 3s$ and $\tau_\phi^D = 20s$ with $\tau_c^D = 10s$ at $(x, y, z) = (25, 25, 25)$ . . . 87
4.29 The evolution of temperature under $\tau_\phi = 3s$ and cycle time $\tau_c^T = 100$ without coupling effect . . . 88

5.1 Combination between transient part and a fluctuation part . . . 93
5.2 Presentation of the algorithm and the ingredient of the approach . . . 93
5.3 The first four cycles of the cyclic loading with a cycle time $\tau_c = 10s$ . . . 94
5.4 The evolution of the temperature for different values of $R_\tau = \frac{\tau_\phi}{\tau_c}$ with a constant cycle time $\tau_c = 10s$. . . . 95
5.5 The FFT of a fixed spatial point at the center of the cube for different values of $R_\tau = \frac{\tau_\phi}{\tau_c}$ and a constant cycle time $\tau_c = 10s$ . . . 96

5.6 The variation of the amplitude of the peaks in the frequency domain for 4 different points . . . 97
5.7 The evolution of the temperature in the time domain and frequency domain at the center point $(x, y, z) = (25, 25, 25)$ . . . 98
5.8 Generation of the time basis for the first peak . . . 98
5.9 The time basis generated from the first peak with $S_1 = 1 - A \times exp(\frac{-5t}{\tau_\phi})$ . . . 99
5.10 The FFT of the load applied . . . 99
5.11 The evolution of the phase angle with respect to R_τ . . . 100
5.12 Normalized time modes for $\tau_\phi = 1000s$ issued from the analytical expressions . . . 102
5.13 Convergence with respect to the number of modes for $\tau_\phi = 1000s$ . . . 102
5.14 Comparison between the temperature for $\tau_\phi = 1000s$ resulting from the mixed strategy and FEM at $(x, y, z) = (25, 25, 25)$ . . . 103
5.15 Different points in the model . . . 103
5.16 Normalized time modes for $\tau_\phi = 100s$ issued from the analytical expressions . . . 104
5.17 Convergence with respect to the number of modes for $\tau_\phi = 100s$ . . . 105
5.18 Comparison of the case where physical time $\tau_\phi = 100s$ resulting from the mixed strategy and FEM at $(x, y, z) = (25, 25, 25)$ . . . 105
5.19 Convergence of the solution with respect to the number of modes . . . 106
5.20 Comparison of the solution, for the case of non-homogeneous boundary condition, resulting from the mixed strategy and the FEM at $(x, y, z) = (25, 25, 25)$ . . . 107
5.21 Convergence with respect to the number of modes for opposite loads . . . 107
5.22 Comparison between the solution obtained within the mixed strategy and FEM for opposite loads at $(x, y, z) = (37.5, 25, 25)$ . . . 108
5.23 Comparison between the solution obtained using the mixed strategy and the FEM at the center point for opposite loads . . . 108
5.24 Convergence with respect to the number of modes for Robin boundary conditions . . . 110
5.25 Solution from the mixed strategy compared to the Finite Element solution for Robin boundary conditions at $(x, y, z) = (25, 25, 25)$ . . . 110
5.26 Bases issued from different cycle times imposed by a volumetric heat source (right) and a Dirichlet boundary condition (left) . . . 112
5.27 The evolution of temperature using the approach (using the order of bases from case 1) compared to FEM solution at $(x, y, z) = (25, 25, 25)$ . . . 112
5.28 The evolution of $\frac{T_n}{T_{n-1}}$ . . . 113
5.29 Evolution of temperature at $(x, y, z) = (25, 25, 25)$ for larger number of cycles: 5 cycles (case 1) . . . 114
5.30 Evolution of temperature at $(x, y, z) = (25, 25, 25)$ for larger number of cycles: 10 cycles (case 2) . . . 115
5.31 Evolution of temperature at $(x, y, z) = (25, 25, 25)$ for larger number of cycles: 20 cycles (case 3) . . . 115
5.32 The evolution of the temperature with larger time domain $L_t = 2000s$ at $(x, y, z) = (25, 25, 25)$ . . . 116
5.33 The evolution of two types of sinusoidal load . . . 118
5.34 The evolution of the temperature for fixed spatial point (25,25,25) under sinusoidal load 1 . . . 119
5.35 Comparison of the bases: old and new bases . . . 120
5.36 Case 1: Evolution of the temperature using the approach and the reference solution at $(x, y, z) = (25, 25, 25)$ . . . 121
5.37 Case 2: Evolution of the temperature using the approach and the reference solution at $(x, y, z) = (25, 25, 25)$ . . . 121
5.38 Case 3: Evolution of the temperature using the approach and the reference solution at $(x, y, z) = (25, 25, 25)$ . . . 122
5.39 Different types of Heaviside load . . . 123
5.40 Load type 1: Solution using the approach at $(x, y, z) = (25, 25, 25)$ with $\tau_c = 20s$ . . . 125

5.41 Load type 2: Solution using the approach at $(x, y, z) = (25, 25, 25)$ with $\tau_c = 10s$ . . 125
5.42 Solution using the approach at $(x, y, z) = (25, 25, 25)$ with $\tau_\phi = 100s$ 126
5.43 Load type 4: Solution using the approach at $(x, y, z) = (25, 25, 25)$ with $\tau_\phi = 100s$. 127
5.44 Heat source $\boldsymbol{R} = -1$, $\tau_c = 20s$, $n_{cycles} = 10$ 128
5.45 The evolution of temperature using the old bases at $(x, y, z) = (25, 25, 25)$ 128
5.46 The variation of the amplitude and the phase angle in frequency domain for fixed spatial point $(x, y, z) = (25, 25, 25)$, $(\boldsymbol{R} = -1)$ and $(\boldsymbol{R} = 0)$ 129
5.47 Solution using the approach compared to reference solution at $(x, y, z) = (25, 25, 25)$ 129
5.48 Evolution of temperature for new amplitude with old bases at $(x, y, z) = (25, 25, 25)$ 130
5.49 The first 4 cycles of the cyclic loading with a cycle time $\tau_c^D = 2.5s$ for $F_D(t)$ and $\tau_c^T = 50s$ for $F_T(t)$ 133
5.50 The evolution of temperature under the same physical time $(\tau_\phi = 3s)$ and $\tau_c^T = 50s$ and $\tau_c^D = 2.5s$ at $(x, y, z) = (25, 25, 25)$ 133
5.51 The evolution of temperature under $(\tau_\phi = 3s)$ and $\tau_c^T = 50s$ without coupling effect 134
5.52 The evolution of temperature under different physical times $(\tau_\phi^T = 3s$ and $\tau_\phi^D = 10s)$ and $\tau_c^T = 50s$ and $\tau_c^D = 2.5s$ at $(x, y, z) = (25, 25, 25)$ 134
5.53 The evolution of the temperature with $\tau_c = 10s$ and $Cp = 9.2 \times T + 1366.6$ at $(x, y, z) = (25, 25, 25)$ - case 1 138
5.54 The evolution of the relative error with respect to the Picard iterations and the number of modes - case 1 138
5.55 The evolution of the relative error with respect to the number of Picard iterations - case 2 139
5.56 The evolution of temperature with $\tau_c = 10s$, $C_p = T + 25$ and $3.2 < R_\tau < 10$ at $(x, y, z) = (25, 25, 25)$ - case 2 139
5.57 The evolution of temperature with $\tau_c = 10s$, $C_p = 27 \times T + 25$ with $3.2 < R_\tau < 181.4$ at $(x, y, z) = (25, 25, 25)$ - case 3 140
5.58 The evolution of temperature using the approach compared to the FEM at $(x, y, z) = (25, 25, 25)$ - quadratic dependence of $C_p(T)$ 141
5.59 The evolution of the specific heat with respect to the temperature - rectangular dependence of $C_p(T)$ 142
5.60 The evolution of temperature using the approach compared to the FEM at $(x, y, z) = (25, 25, 25)$- rectangular dependence of $C_p(T)$ 142
5.61 The evolution of specific heat C_p with respect to the temperature - case 1 sinusoidal dependence 143
5.62 The evolution of specific heat C_p with respect to the temperature - case 2 sinusoidal dependence 144
5.63 The evolution of temperature case 1 and case 2 using FEM at $(x, y, z) = (25, 25, 25)$ 144
5.64 The evolution of temperature using the approach and compared to the FEM - case 1 $(\tau_c^{C_p} = 10s)$ at $(x, y, z) = (25, 25, 25)$ 145
5.65 The evolution of temperature using the approach and compared to the FEM - case 2 $(\tau_c^{C_p} = 20s)$ at $(x, y, z) = (25, 25, 25)$ 146
5.66 Représentation de la Transformée de Fourier Rapide (TFR) de $f(t)$ 157
5.67 Evolution de la température pour le cas 3 $Cp = 27 \times T + 25$ 165
5.68 Evolution de la température pour $(\tau_\phi = 3s)$ et le dictionnaire 4 ($\tau_c = 10$,$\tau_c = 50$,$\tau_c = 100$) en (x, y, z) = (25, 25, 50) 168
5.69 Evolution de la température pour $\tau_\phi^T = 3s$ et $\tau_c^T = 100s$ avec $\tau_\phi^D = 20s$ et $\tau_c^D = 10s$ à (x, y, z) = (25, 25, 25) 169
5.70 Evolution de la température pour un même temps physique $(\tau_\phi = 3s)$ pour les deux phénomènes et deux temps de cycle différents $\tau_c^T = 50s$ et $\tau_c^D = 2.5s$ à $(x, y, z) = (25, 25, 25)$ 172

A.1 The Fast Fourier Transform of $f(t)$ with different sampling numbers 187

List of Tables

3.1 Material properties and boundary conditions . . . 48
3.2 The physical time τ_ϕ with respect to the specific heat coefficient C_p . . . 48
3.3 Number of modes with respect to the physical time . . . 49
3.4 Time saving PGD VS FEM ratio with respect to the physical time . . . 50
3.5 The relative error calculated for different points for the three linear cases . . . 51
3.6 Appropriate time discretization . . . 52
3.7 Number of the Iterations and time-saving for the different non-linear cases . . . 57
3.8 The relative error calculated for different points for the three non-linear cases . . . 57

4.1 Material properties and boundary conditions . . . 66
4.2 The physical time τ_ϕ with respect to the specific heat coefficient C_p . . . 67
4.3 Number of modes for the full PGD and number of most significant modes with respect to the physical time τ_ϕ (dictionary 1 - $\tau_c = 20s$) . . . 67
4.4 The relative error calculated for different points for $\tau_\phi = 3s$ and dictionary 1 . . . 70
4.5 The relative error for different spatial points in the domain for cases 1-BC and 2-BC 72
4.6 Number of modes for the full PGD and number of most significant modes for $\tau_\phi = 10s$ with respect to cycle time (dictionary 2). . . . 74
4.7 Number of modes for the full PGD and number of the most significant modes for $\tau_\phi = 10s$ with respect to cycle time (dictionary 3). . . . 75
4.8 Number of most significant modes with respect to the physical time τ_ϕ and constant cycle time for dictionary 4 . . . 79
4.9 The relative error for different spatial points in the domain . . . 80
4.10 Different combination of the dictionaries (✓ refers to valid and x refers to invalid) . 81
4.11 The physical times τ_ϕ^D and τ_ϕ^T with respect to the specific heat coefficient C_p and the diffusion coefficient D respectively . . . 82
4.12 Material properties and the coupling coefficient . . . 82
4.13 Number of most significant modes with respect to the physical time and cycle time τ_c of each dictionary for diffusion and thermal problem only (uncoupled problems) . . 84

5.1 The physical time τ_ϕ with respect to the specific heat C_p . . . 96
5.2 The relative error calculated for different points for $\tau_\phi = 1000s$, $\tau_\phi = 100s$ and $\tau_\phi = 0.1s$ . . . 102
5.3 The relative error calculated for different points for non-homogeneous Dirichlet boundary conditions . . . 106
5.4 The relative error calculated for different points for opposite non-homogeneous Dirichlet boundary conditions . . . 108
5.5 Separated form of the LHS and RHS for Robin boundary conditions . . . 109
5.6 The relative error calculated for different points for Robin boundary conditions . . . 109
5.7 The relative error calculated for different points for different cycle time . . . 111
5.8 The relative error and the number of modes for different number of cycles . . . 114
5.9 The relative error calculated for different points with larger time domain $L_t = 2000s$ 116
5.10 The relative error calculated for different points for the sinusoidal case . . . 120
5.11 The location of the peaks for the case of load type 1 with $\tau_c = 20s$ . . . 124
5.12 The location of the peaks for the load of type 2 ($\tau_c = 10s$) . . . 124

5.13 Material properties and the coupling coefficient . . . 132
5.14 The relative error calculated for different points for linear dependence of specific heat 140
5.15 The relative error calculated for different points for the quadratic case . . . 141
5.16 The relative error calculated for different spatial points - rectangular dependence of $C_p(T)$ . . . 142
5.17 The relative error calculated for different points for the sinusoidal case . . . 145
5.18 Gain en temps PGD VS FEM en fonction des différents temps physiques . . . 164
5.19 Nombre de modes PGD et nombre de modes les plus significatifs pour différents temps physiques (dictionnaire 1 - $\tau_c = 20s$) . . . 167

A.1 The notation for different integrals . . . 185
A.2 Diffusive heat transfer or mass diffusion elements . . . 187

B.1 Separated forms of the LHS of the first term . . . 190
B.2 Separated forms of the LHS and RHS of the second term . . . 191
B.3 Separated forms of the LHS and RHS of the third term . . . 191
B.4 Separated forms of the LHS and RHS of the fourth term . . . 191

C.1 The relative error calculated for different spatial points for $\tau_c = 10s$ with heat source and null boundary conditions . . . 194
C.2 The relative error calculated for different spatial points for $\tau_c = 20s$ with heat source and null boundary conditions . . . 194
C.3 The relative error calculated for different spatial points for $\tau_c = 40s$ with heat source and null boundary conditions . . . 195
C.4 Summary of the simulations . . . 196

Introduction

***

General introduction

This thesis is in the context of mechanics of materials, importantly in the field of multiphysics and fatigue to achieve tools of performing successful life prediction in fatigue for industrial applications.

To point out, polymer and metals under fatigue concern a large domain of applications like automotive, aerodynamics, aircraft engines, turbines, biomechanics, pressure vessels ... etc. Indeed, these applications are subjected to thermo-mechanical loading cycles which can be more damaging compared to the isothermal fatigue (constant temperature). For example, pipes are used in the industries, power plant, these pipelines are under internal pressure and cyclic temperature. Also, in gas turbines during the transient regimes (start-up and shut-down operations) it is subjected to temperature variation leading to the variation of the strain consequently affects the fatigue. The effect of these loading may lead to the failure of the structure and lead to a catastrophic condition [Nayebi et Hamidpour, 2016]. Thus, the challenge is to predict the service life of these components.

A lot of criteria exist to predict the service life of components for the automotive and aviation industry. Yet, the criterion in fatigue is based on the parameters calculated in a stabilized state such as the maximal stress [Nguyen *et al.*, 2013]. Initially, the literature of the fatigue in some metal shows that the parameters are often calculated in the first cycle, by assuming the material behaves elastically or exhibits plasticity. However, in other metals, the stabilized cycle is not obtained directly where the thermal loading has a major effect on the response of the material. On the contrary, it is very difficult to predict the stabilized cycle in the case of polymers which exhibit a viscoelastic behavior. Recent developments showed that 1000 cycles are required [Berrehili, 2010]. Thus, a major challenge is to define and predict the stabilized state with a reduced computation time.

From a numerical point of view, the literature in fatigue of polymers shows difficulties in solving the thermoviscoelastic upon using an incremental method. It is due to the presence of different time scales such as:

- the relaxation time due to the effect of viscoelasticity. It can be described by a large number of times if a large number of internal variables is used to described the viscosity.
- the characteristic time associated with the thermal effect.
- the time scale related to the cycle time.

To obtain an accurate prediction for simulations using an incremental scheme, the time step is very fine as it is required by the phenomenon with the smallest characteristic time and usually the mesh has to be fine due to either the gradient phenomena or the time step.
Thermoviscoelasticity has been solved through Finite Element Method (FEM) in a large number of works. We can cite for example [Othman et Abbas, 2012]. In [Nguyen, 2013], Nguyen et al. indicate that using classical Finite Element Method (FEM) to solve polymers thermoviscoelasticity under cyclic loading leads to large computation time due to the fine mesh, a large number of cycles needed to reach the stabilized cycle, nonlinearities from the parameters (for example dependence of specific heat and convection coefficient on temperature). Furthermore, storage memory can be another problem due to the number of cycles and the number of variables to be stored, the phenomenon being history dependent.

Model Order Reduction, and in particular the Proper Generalized Decomposition (PGD) method [Ammar *et al.*, 2006, Ammar *et al.*, 2007, Chinesta *et al.*, 2010b], can be a solution and promising method to overcome the mentioned problems. This method is used by a large community of scientists [Chinesta *et al.*, 2011b]. In the French community, they are grouped in the GDR AMORE. In one of my thesis laboratory, the PPRIME Institute, this method has been studied in the particular context of multiphysics couplings [Nguyen, 2012], viscoelasticity [Hammoud *et al.*, 2014], themoviscoelasticity [Beringhier *et al.*, 2010]. In the case of viscoelasticity and thermoviscoelasticity, the

PGD method was restricted for one-dimensional case.

The prediction of a large number of cycles and coupled problems are considered to be one of the most important issue in scientific and industrial research. Efficient numerical tools through efficient methods have to be developed. To clearly understand the numerical issues, it is required to:

- analyze the existing methods,
- check their time saving with a good accuracy,
- analyze their range of applications (for coupling, nonlinearity, ...)

and this is one of the objective of this thesis, the main objective is being to propose efficient numerical strategies.

The thesis manuscript is organized as follows:

- Chapter 1 is dedicated to a review concerning the numerical methods widely used in mechanics of materials and more particularly for polymers materials under fatigue. These materials are in the domain of linear transient problems, nonlinear problems, and coupled problems. These problems raise different issues for which different approaches are used in the literature. These approaches are briefly described.
  In this chapter, we try to answer the concerns that have arisen: What are the alternative approaches used to predict problems with different time scales? What are the numerical techniques that can lead to a large time-saving? What are the linearization schemes that can deal with the non-linearity?

  Another concern will be an overview of the Fourier analysis and its application as the Fourier Transform will be used as a tool to develop a new numerical method in Chapter 5.

- In Chapter 2 at first glance, a modeling of a 3D transient problem is constructed by highlighting the main parameters (material properties, boundary conditions, timescales and the initial conditions, etc.)

  In summary, the major issues treated in this chapter are:

  1. Generation of the mathematical modeling of 3D linear transient problem.
  2. Generation of the mathematical modeling of 3D non-linear transient problem.
  3. Introduction of the multi-time scales present in the 3D transient problem.
  4. Introduction of the algorithm of the FEM to solve the linear and non-linear thermal problems.

- In Chapter 3 the PGD method, referred as approach 1 in this manuscript, is developed for a 3D thermal problem. This method is validated and compared with the FEM to enhance the interest of using this alternative method. The studied problem is a thermal problem under cyclic thermal loading. Equally important, this chapter shed lights on the coupling between the Proper Generalized Decomposition method (PGD) and the A priori Discrete Empirical Interpolation Method (DEIM) to solve the non-linearity associated with the temperature parameters dependence such as specific heat $C_p(T)$ and convection coefficient $h(T)$ on temperature. In these simulations, the effect of the characteristic time associated with the physical phenomena and the effect of the cycle time are discussed. In particular, the effect of the characteristic time on the time discretization and the effect of the spatial position are studied. The question arises here: how to obtain more time-saving? The next chapters aim to construct two different techniques to achieve more time saving by using always MOR.

- Chapter 4 presents a numerical method, referred as approach 2 in this manuscript, based on the use of a collection of the most significant modes to solve cyclic transient thermal problems involving different time scales. These space-time modes are issued from the PGD method. This technique is interesting in our context where different time scales control the evolution of the polymer behavior, the aim is to construct an efficient dictionary that can be used for different problems. In the first place, the efficiency of the most significant modes is evaluated, then the dictionary that contains the most significant modes is used to solve different problems. This approach is validated with different applications, harmonic problems (different cycle times) and coupled problems. The efficiency with respect to time saving is analyzed. Furthermore, the limitation of the proposed method with respect to cycle time is discussed.

- Chapter 5 presents a new approach, referred as approach 3 in this manuscript, based on the observation that in the context of cyclic problems, the solution consists of a combination of a transient part and a fluctuation part. This strategy is based on the knowledge of an a priori known basis like the well-known Proper Orthogonal Decomposition (POD): the time basis, and the construction of the basis within an iterative procedure like the Proper Generalized Decomposition method (PGD): the spatial basis. This method can be seen similar to the Large Time INcrement (LATIN) method as the solution is sought under a space-time representation. The novelty of the approach is the construction of the a priori time basis. To propose an efficient time basis, the study of the solution within the frequency domain via the Fast Fourier Transform (FFT) is considered and an analytical expression of the time basis is provided. Accordingly, it is possible to construct an a priori basis that will be related to the transient part and the fluctuation part. First, this method is studied and validated especially regarding the convergence of such algorithm. This method is extended for different problems (different physical times, different cycle times, different load...etc.) and is called the mixed strategy. The mixed strategy is then extended to more complex cases : a coupled problem and a nonlinear case. The non-linearity is introduced with the material properties such as the specific heat $C_p(T)$. This non-linearity affects the evolution of the temperature, then the generation of the bases is related to the evolution of $C_p(T)$. A linearization procedure is then added to the PGD algorithm to compute the spatial modes. The efficiency of the mixed is then discussed.

- Conclusion summaries the work and presents several future perspectives to develop an efficient technique to solve thermoviscoelasticity to predict the response of polymers under fatigue.

- Appendices A, B, C present the summary of the additional simulations and results related to chapter 3, chapter 4, and chapter 5.

Thesis collaboration. This thesis was carried out through a collaboration agreement between the "Lebanese International University" (LIU) and the "Ecole Nationale Supérieure de Mécanique et d'Aérotechnique(ISAE-ENSMA). Under this collaboration, the duration spending in France is 5 months and in Lebanon 7 months including teaching (around 120h) per year. The purpose of this agreement is to examine and propose new numerical approaches for thermo-viscoelastic behavior under cyclic loading. As such, I would like to thank all of these partners for their financial support as well as for their pronounced scientific interest.

Chapter 1

Literature review

—

If we knew what it was we were doing,
it would not be called research, would it?
Albert Einstein

Contents

1.1 Introduction . . . 8
1.2 FEM and the incremental scheme . . . 8
1.3 Model Order Reduction (MOR) . . . 10
1.3.1 A posteriori . . . 10
1.3.1.1 Proper Orthogonal Decomposition (POD) . . . 10
1.3.2 A priori . . . 11
1.3.2.1 A Priori Hyper Reduction (APHR) . . . 11
1.3.2.2 LArge Time INcrement (LATIN) . . . 11
1.3.2.3 Proper Generalized Decomposition (PGD), non-incremental scheme 12
1.3.3 MOR strategies in the context of fatigue . . . 15
1.4 Numerical issues to deal with nonlinearities . . . 17
1.4.1 Newton-Raphson method . . . 17
1.4.2 Picard's method . . . 19
1.4.3 Asymptotic Numerical Method (ANM) . . . 20
1.4.4 Discrete Empirical Interpolation Method (DEIM) . . . 21
1.5 Frequency domain analysis . . . 21
1.5.1 Fourier analysis . . . 22
1.5.2 Application of the Fast Fourier Transform method (FFT) in mechanics and more particularly materials under fatigue . . . 23
1.6 Discussion . . . 24

1.1 Introduction

Scientists have been studied and proposed over the years different strategies in the context of fatigue of mechanical materials such as polymer or metals. As a matter of fact, these materials are widely used in industrial applications such as aerodynamics, internal-combustion engine, turbines, biomechanics etc. We can cite for example [Anderson, 1991, Anderson, 2017, Sauer et Richardson, 1980, ...]. To point out, these products are subjected to thermomechanical loading cycles (for example, the variation of the pressure and the variation of the temperature). Accordingly, different numerical methods and strategies were used and developed to predict the behavior of the material under cyclic loading. In fact, models involving transient fields and different time scales must be solved in large time intervals using very fine time steps. Using an incremental time scheme, researchers encounter the following difficulties: large computation time, stability requirements, storage memory, non-convergence [Le Bris, 2006, Chinesta *et al.*, 2013a]. In this case, the standard increment method becomes inefficient. Definitely, other numerical techniques must be investigated and developed. Consequently, the large computation time is widely considered to be the most important issue in scientific research especially in solving structural evolution problems. Yet, the researchers work on developing numerical techniques such as the Model Order Reduction (MOR) to predict the lifetime by generating accurate results and a reasonable computation time in industrial applications. In this chapter, we will present in particular different numerical strategies in the context of fatigue. Hence, the goal of this chapter is to shed light on the numerical techniques especially model reduction classically used for evolution problems.
In summary, the major issues treated in this chapter are:

1. Give an overview of the Finite Element Method (FEM) and in particular the use of an incremental scheme in the context of fatigue.
2. Present the alternative methods: Model Order Reduction methods (MOR). In this class of methods, the Proper Generalized Decomposition method will be more detailed and discussed since this method is used in this thesis.
3. Address the linearization schemes and the issue of treating non-linear models.
4. Specify the different use of Model Order Reduction in the particular context of fatigue.
5. Discuss the use of the Fast Fourier Transform (FFT) techniques in mechanics.

1.2 FEM and the incremental scheme

In this section, an overview of the Finite Element Method (FEM) is given. FEM represents one of the most important techniques used in computational mechanics and in particular to deal with coupled problems and fatigue. Let us note advanced commercial finite element software such as ABAQUS and ANSYS [Rao, 2010] have the capability to solve different kinds of problems [Khennane, 2013, Bhatti, 2005].
To illustrate, FEM is based on the collection of sub-domains of a given domain Fig. 1.1 where the governing equation is approximated by the variational method Fig. 1.2. According to [Reddy, 1993] this method can be illustrated by three features:

1. The geometrical complex domain is represented by the collection of simple sub-domains.
2. The governing equation is solved in each element.
3. The elements are assembled to the global system.

To explain, the approximation solution is written under the form:

$$u(x) \approx U_N(x) = \sum_{j=1}^{N} c_j \phi_j(x)$$

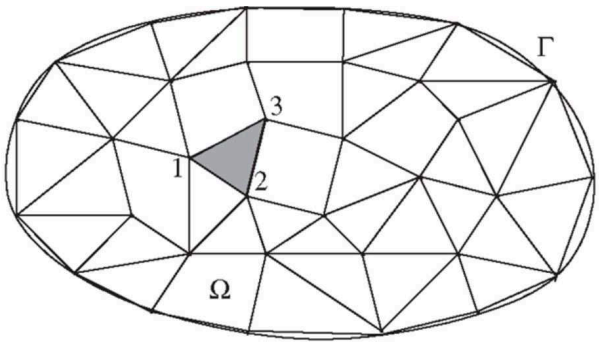


Figure 1.1: Domain and sub domain for Finite Element Method [Reddy, 1993]

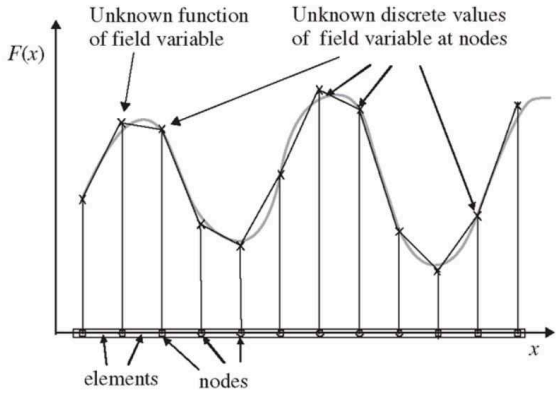


Figure 1.2: Finite Element approximation [Reddy, 1993]

where $u(x)$ represents the solution of a differential equation, U_N refers to the approximated solution, N is number of nodes in the physical domain, c_j are real constants and ϕ_j represent the shape functions.
Accordingly, to choose the shape functions the following methods can be used:

- the Ritz method
- the Galerkin method
- the Petrov-galerkin method
- the least squares method
- the collocation method.

To sum up, the steps that are used in the FEM are the followings [Reddy, 1993]:

1. Discretization by constructing the finite element mesh and the number of nodes and elements.
2. Derivation of element equations for all typical elements in the mesh.
    - construct the variational formulation and obtain element equations in the form: $[K^e]u^e = F^e$
3. Assembly of the element equations.
4. Identify the boundary conditions.
5. Solution and post-processing.

Incremental scheme for transient problems. In the case of transient problems, an increment scheme has to be used. At each time step, the spatial FEM is solved, which increases the computation time in the case of many time steps. Moreover, the choice of the time step has to satisfy the stability requirement (related to the spatial scale) and a very fine time step is required to converge and accurately describe the solution.
In case of 3D finite element simulation, it can be very costly depending on the spatial discretization and the time step required for the incremental mesh.
For the time integration, several schemes exist in the literature for example the explicit scheme and the implicit scheme. The stability analysis of the implicit and explicit schemes [Ascher *et al.*, 1997] showed that an unconditionally stability is achieved with the implicit scheme and for explicit a critical time step is needed [Hughes et Liu, 1978].

The incremental scheme combined with FEM has been widely used in solid mechanics [Zienkiewicz et Taylor, 2000, Zienkiewicz et Taylor, 2005, ...] to cite a few. Let us note that the literature on the usage of the Finite Element Method in the mechanics showed that it requires high computation efforts. For example, Nguyen et al [Nguyen, 2013] have shown that 1000 cycles are required to describe accurately the stabilized cycle of an high density polyethylene and leads to a large computation time mainly due to the use of the incremental scheme. Namely, a small time step is used linked to the presence of different time scales: time associated with cyclic loading and one related to the physical properties.
Therefore, much techniques and research are dedicated for finding a robust and accurate approach for reducing the computational time by reducing the size of the equation using reduced basis. To this end, the accuracy of the reduced model depends on the choice of the bases. In what follows we will shed light on the usage of the Model Reduction in the context of the mechanics and in particular fatigue.

1.3 Model Order Reduction (MOR)

Despite the numerical progressive improvements in term of solving mechanical problems. Some challenging problems still infeasible or they cost a huge computational time. Thus, many techniques were developed with the aim of reducing the computational costs. To begin with, the Model Order Reduction (MOR) is used as an alternative method. The objective of the Model Order Reduction is to represent the distributed state of a system with few shape functions. MOR has been developed to solve multiphysics, complex problems [Chinesta *et al.*, 2011b, Benner *et al.*, 2015, Stein *et al.*, 2004, Guérin *et al.*, 2018] and showed efficient results. Classically it is divided into two main categories:

- a posteriori methods.
- a priori methods.

1.3.1 A posteriori

A posteriori methods use direct simulations to create basis. The most famous a posteriori method is the Proper Orthogonal Decomposition (POD) [Chatterjee, 2000]. For these methods, a knowledge of the solution of the problem is required.

1.3.1.1 Proper Orthogonal Decomposition (POD)

In this section, the discussion will point to the Proper Orthogonal Decomposition (POD), which refers to extract an important information from full order problems and use them in similar problems. We will refer to the illustration presented in [Chinesta et Ladevèze, 2014]. To introduce this method, assume that you have a full solution $u(x,t)$, the POD generates an efficient tool to obtain the most relevant and important information by maximizing the functional:

$$\alpha = \frac{\sum_{m=1}^{p}[\sum_{i=1}^{M}\phi(x_i)u^m(x_i)]^2}{\sum_{i=1}^{M}(\phi(x_i))^2} \tag{1.1}$$

where $\phi(x)$ is the characteristic structure among these $u^m(x)$. Eq. (1.1) is equivalent to solve the eigenvalue problem:

$$c\phi = \alpha\phi \tag{1.2}$$

where c is the two-point correlation matrix. For more details reader can refer to [Chinesta et Ladevèze, 2014]. Definitely, POD has been used in wide applications such as image processing [Benaarbia et Chrysochoos, 2017], chemical engineering, turbulent fluid flows [Noack, 2013, Holmes, 2012], structural vibration [Feeny et Kappagantu, 1998] including, but not limited to the linear transient thermal problem [Białecki *et al.*, 2005]. This method is very efficient and accurate results are obtained with a reduced computation time online.

1.3.2 A priori

Methods in this category do not require any prior information on the studied problem. The basis functions are not known but calculated using an iterative procedure. The PGD method is one of the examples of this category that will be more detailed as it will be used in this thesis.

1.3.2.1 A Priori Hyper Reduction (APHR)

A Priori Hyper Reduction [Ryckelynck et Benziane, 2010] is considered as a model reduction method since it is used to decompose implicitly a state of evolution. APHR is an incremental scheme based on a classical step by step time integration as introduced in [Ryckelynck, 2005]. To illustrate, the Hyper Reduction is based on choosing the integration point of the finite element model to estimate the evolution of the reduced state. Indeed, APHR is a development of Karhunen-Loève expansion [Newman, 1996] to create an a posteriori approach. The main idea behind this method is to avoid the preliminary construction of the basis from an incremental solution of state evolution where the basis functions are updated. So that the most significant basis functions are selected for state evolution representation. To sum up the adaptive strategy with the APHR, Ryckelynck et al. [Ryckelynck, 2005] points out the followings:

- In the whole time domain, a set of basis function is defined.
- Selection of the basis based on Karhunen-Loève expansion.
- Selection of the most significant basis.
- A reduced integration domain smaller than the whole domain is used for the formulation.

Several studies through the APHR method have been carried out. They concern nonlinear problems [Ryckelynck, 2005], nonlinear thermal problems [Ryckelynck, 2002]. This method has been extended to mechanical models involving internal variables by Ryckelynck et al. [Ryckelynck et Benziane, 2010]. Recently Miled et al. [Miled *et al.*, 2013] developed APHR to solve coupled viscoelastic-viscoplastic composites leading to accurate results and computation time saving (60% compared to FEM). Moreover, Ryckelynck [Ryckelynck *et al.*, 2015] applied an error estimator to validate the domain of hyper-reduced predictions and in the case of time-dependent problem the equations are solved backward in time and he used an elasto-visco-plastic behavior to check the validity of domain of hyper reduction. By the same token, in [Nasri, 2017] they used an a-priori adaptive approach by using APR to have a reduced model, it was used to solve cyclic elasto-visco-plastic problem leading to an accurate solution.

1.3.2.2 LArge Time INcrement (LATIN)

Another a priori method is the LATIN method. This method has been introduced by Ladeveze [Ladevèze, 1985] in 1985. The space-time separation was one of the ingredients of this method and contributes largely to its performance in term of time saving. Let us illustrate this approach. The steps of the LATIN method are as follows:

- Separate the solution into two subspaces

1. The space A_d refers to global linear equations.
2. The space Γ refers to local non-linear equations.

- The second principle is to use a two-stage iterative scheme to have the solution of the problem. One iteration of this method consists of two stages as shown in Fig. 1.3

  1. Local stage.
  2. Linear stage.

  However the local stage is represented by non linear curve since it accounts the non-linear set and a straight line is used to represent the linear stage.

- Use adapted approximation of the unknowns.

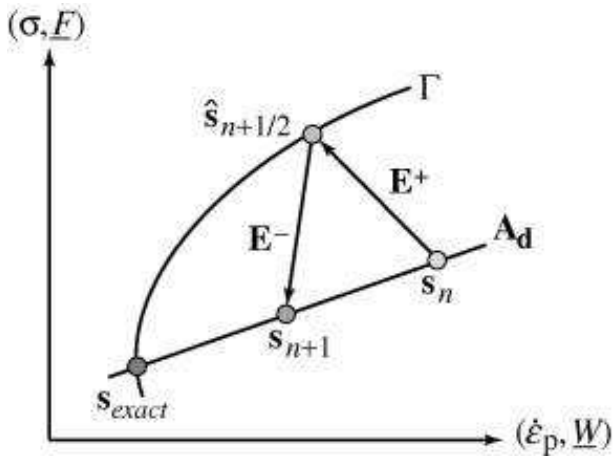


Figure 1.3: The iterative procedure in the LATIN algorithm [Ladeveze *et al.*, 2010]

This method has been widely used in multiphysics problems [Néron *et al.*, 2004]. In the domain of the fatigue, LATIN method has been used widely [Bhattacharyya *et al.*, 2016, Stehly et Remond, 2002].

1.3.2.3 Proper Generalized Decomposition (PGD), non-incremental scheme

Ladeveze in his work initiates the use of a separated representation in computational mechanics [Ladeveze *et al.*, 2010] in the context of the LATIN method to build a non-incremental scheme [Ladeveze et Nouy, 2003]. In 2006 and 2007 Ammar et al. [Ammar *et al.*, 2006, Ammar *et al.*, 2007] generalized the use of a separated representation for multi-dimensional problems (separation of each dimension) and called this method the PGD. The PGD is an a priori method [Chinesta *et al.*, 2013a, Chinesta *et al.*, 2011a], it has been used by many researchers to deal with: multi-physics, viscoelastic, dynamic... etc. To point out, Chinesta et al. [Chinesta *et al.*, 2010a, Chinesta *et al.*, 2007] extended the separated representation for chemical and stochastic equations in the Brownian configuration. In the fluid mechanics, PGD has been developed in [Aghighi *et al.*, 2013]. In the field of thermal problems in composite materials, PGD was used by Pruliere [Prulière *et al.*, 2010b]. Interestingly, the new paradigm for scientific computing has been developed within the PGD method to solve different models [Chinesta *et al.*, 2010b, Prulière *et al.*, 2010a]. Furthermore, PGD has been used in computational mechanics in models that involve many time scales (time-multiscale) [Chinesta *et al.*, 2016]. PGD has shown its potential, it generates efficient computation in plate or shell domains [Bognet *et al.*, 2012]. Nguyen et al. [Nguyen, 2012] used PGD method to solve coupled transient multi-physics problems in 2D with different characteristic times. In the same way, Nouy [Nouy, 2010] extended the PGD for solving time-dependent partial differential equations. Also, it is not restricted to the cubic domain and can be addressed in complex domains as presented

in [Ghnatios *et al.*, 2016]. PGD has the capability to consider any material properties as an extra coordinate [Chinesta *et al.*, 2013a], increasing the dimensionality of the problem. But, PGD scales are linear with space dimensions so this will be efficient and not a problem. The review on the PGD showed efficient and accurate results with a small number of modes. Importantly, Giner et. al [Giner *et al.*, 2013] proved the effectiveness of using PGD to solve 3D cracked plates in linear elastic fracture mechanics. The comparison of the computational costs for PGD and standard FEM is shown in Fig. 1.4 it indicates that accurate results with a reduced computational time compared to FEM. Indeed, PGD is efficient to solve many engineering problems that could not be solved using the standard technique such as quantum mechanics, complex fluid, and genetic process. Moreover, in the case of geometrical domains where one of the dimensions is too small compared to others where the standard grid based on discretization becomes impractical, PGD can be efficient.
As a matter of fact, for problem defined in space by dimension D, and M is the number of nodes discretized at each coordinate, thus the total number of degrees of freedom is $M \times D$ whereas in the standard mesh based it is M^D. Thus, the upshot of the PGD method is the ability to reduce the number of degrees of freedom.
To solve a problem using the PGD, the classical algorithm of PGD is illustrated in Fig. 1.5 (1 dimensional heat equation), to clarify, the field is sought in a separated form. This separated form is introduced into the weak form of the problem with a particular test field as illustrated in Fig. 1.5 leading to a nonlinear system to determine the new mode $R(x)S(t)$. This nonlinear system is usually solved with an alternating strategy.
To be more precise, let us detail the different steps of the PGD algorithm within an illustrative example of which considers the conductivity k as an extra coordinate [Chinesta *et al.*, 2010a].

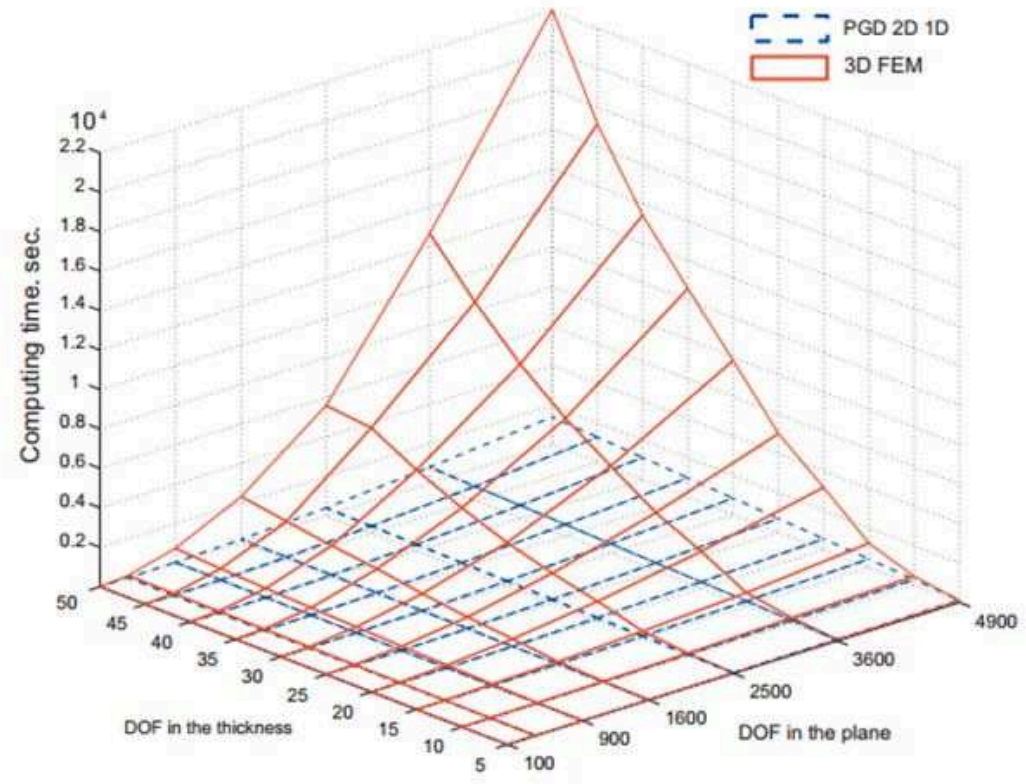


Figure 1.4: Comparison of computational costs (PGD VS FEM) [Giner *et al.*, 2013]

PGD steps and solution for heat equation with k as an extra-coordinate. Let us consider the following heat equation :

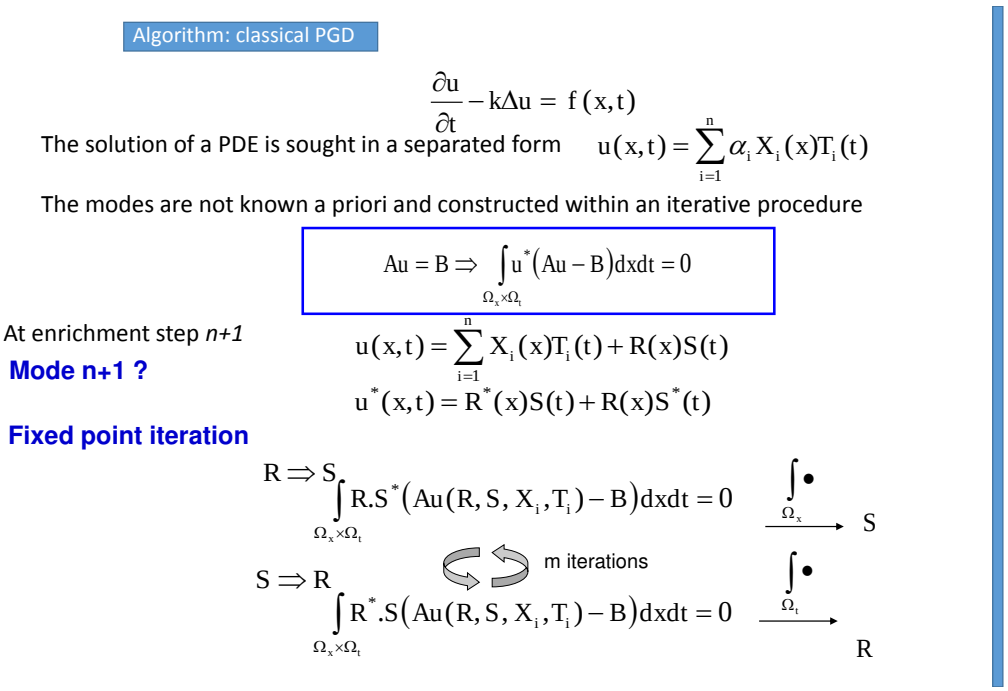


Figure 1.5: The classical algorithm of PGD method

$$\frac{\partial u}{\partial t} - k\triangle u - f = 0$$

where u refers to the temperature and k refers to the conductivity and f is the heat source term and is assumed constant here, and $(x, t, k) \in \omega \times I \times K$. k is here considered as an extra coordinate, the problem is solved for all values of $k \in K$. In this example, null initial and boundary conditions are considered.

- The weak formulation is :

$$\int_{\omega \times I \times K} u^*.(\frac{\partial u}{\partial t} - k\triangle u - f)dxdtdk = 0$$

  where u^* is a test function choosen in an appropriate functional space.

- The PGD solution is sought under a separated representation:

$$u(x,t,k) \approx \sum_{i=1}^{N} X_i(x).T_i(t).K_i(k)$$

  .

- At enrichment step n of PGD algorithm, the following approximation is known:

$$u(x,t,k) \approx \sum_{i=1}^{n} X_i(x).T_i(t).K_i(k)$$

  .

- The next function $X_{n+1}(x).T_{n+1}(t).K_{n+1}(k)$ is searched and is denoted by $R(x).S(t).W(k)$.

- The test function is choosen under the form:

$$u^* = R^*(x).S(t).W(k) + R(x).S^*(t).W(k) + R(x).S(t).W^*(k)$$

- To find R, S and W, a nonlinear system is solved. This system is usually solved by using an iterative procedure, an alternating directions fixed point algorithm [Ammar *et al.*, 2006]. At each iteration of the linearization procedure, it consists of three steps:

  1. Computing $R(x)$ from $S(t)$ and $W(k)$. As S and W are assumed known, it leads to a linear system with respect to R.
  2. Computing $S(t)$ from $R(x)$ and $W(k)$. As R and W are assumed known, it leads to a linear system with respect to S.
  3. Computing $W(k)$ from $R(x)$ and $S(t)$. As R and S are assumed known, it leads to a linear system with respect to W.

- These iterations proceed until reaching a fixed point within a user defined tolerance (ϵ).

$$\frac{\left\|X_n^i(x)T_n^i(t)K_n^i(k) - X_n^{i-1}(x)T_n^{i-1}(t)K_n^{i-1}(k)\right\|}{\left\|X_n^{i-1}(x)T_n^{i-1}(t)K_n^{i-1}(k)\right\|} < \epsilon$$

- The enrichment step ends with an appropriate measure of error ($E < \epsilon^1$).

$$E = \frac{\|X_n(x).T_n(t).K_n(k)\|}{\|u^n\|}$$

  $\|\|$ stand for the L^2 norm

The interested reader can refer to Appendix A.1 for a more detailed presentation of the PGD algorithm in this particular example.
Of course, the review of the PGD showed impressive results in all the life domains, in what follows we will shed light on the usage of the PGD on the resolution of fatigue.

1.3.3 MOR strategies in the context of fatigue

In 2016, Bergheau et al. [Bergheau *et al.*, 2016] published a paper in which they used Proper Generalized Decomposition as a space-time integrator for elastoplastic problems. Bergheau reminds us in his introduction that the usage of an incremental scheme leads to a large computation time and that the FEM becomes inefficient for a large number of cycles. Bergheau used an alternative method, the PGD method, where he points out that PGD has not been generalized in the treatment of solid mechanics. To illustrate Bergheau used the FEM to compute stress and the PGD for the displacement field. He discussed different strategies that can be used to solve coupled space-time problem:

- The first strategy of resolution is based on the computation of the full solution in space until convergence. Note that the time function is not computed. Then, a full solution in time is carried out with the previous space functions. This technique may lead to non-accurate results as the spatial resolution and the time resolution are completely uncoupled.

- The second strategy of resolution is based on considering the space-time as a whole problem and it is solved until convergence. This approach is applied to solve elastoplasticity under cyclic loading but only 3 cycles have been tested.

- The third strategy of resolution is based on considering only the elastic behavior: for each spatial mode, a displacement is determined. Then a time resolution is carried out until convergence. This method may lead to a larger number of modes than the previous strategies. Despite this, the approach is efficient in the prediction of the solution.

Other studies in the field of viscoelasticity using PGD has been done by Hammoud et al. [Hammoud *et al.*, 2014]. They discussed a non-equilibrium state under creep and cyclic loading. Moreover, they showed that a combination of PGD and adaptive time step could be efficiently used to predict the

viscoelastic behavior. They found that when the relaxation time is smaller than the cycle time the stabilized cycle is reached directly. However, when the relaxation time and the cycle time have the same order, the stabilized cycle is reached at the end of the simulation. It was not the case when the relaxation time is larger than the cycle time, the stabilized cycle is not reached. In like manner, Ammar et al. [Ammar *et al.*, 2015] studied a transient simulation of viscoelastic behavior where the characteristic time of the mechanical response is less than the time of interest. A very small time step will be required within the FEM. Also, they used space-time separated representation to simulate an integro-differential model within the PGD framework. They mentioned that for the case of viscoelastic behavior (time dependent), the standard incremental simulations are inefficient. Nasri el al. [Nasri *et al.*, 2018] solved polycrystalline problem under cyclic loading within PGD framework. In their work, they developed three methods: incremental-right method by keeping constant stiffness matrix, and two versions of the PGD method (each version differs from its convergence criterion (see [Nasri *et al.*, 2018]). Importantly, they showed that the usage of incremental-right method leads to a large time saving compared to the two versions of PGD method the FEM with an incremental schema. It is noted that the second PGD version was slow compared to the incremental scheme since the nonlinear term is updated with a displacement field at each enrichment of PGD.

Not to mention, Beringhier et al. [Beringhier *et al.*, 2010] solved a thermoviscoelastic coupled problem for one-dimensional case, where two different characteristics times were used. They applied different shape functions for space and time to adjust discretization to different characteristic times, where a coupled strategy is used. Forthwith, the displacement and temperature are simultaneously determined.

From the author's knowledge, an alternative method, the LArge Time INcrement (LATIN), is the first method applied to solve evolution problems under cyclic loading. Preliminary work on this domain was undertaken by Boisse et al. [Boisse *et al.*, 1990]. They use the LArge Time Increment(LATIN) in elastoplastic for cyclic viscoplastic problems.

Straightaway, Cognard et al. [Cognard et Ladevèze, 1993] used LATIN for cyclic viscoplasticity and he draws our attention to the advantages of the LATIN method in solving cyclic viscoplastic behavior:

- The convergence for one hundred cycles computed in a single increment is obtained with a small number of iterations.
- The saving in the computation time is important compared to FEM, with error less than 5%.
- With only a few time functions and space fields, the stresses and the displacement can be predicted.

Another more recent solution using LATIN is described in [Stehly et Remond, 2002]. Authors show the advances in using the LATIN method. In their paper, Stehly and Remond check the performance of this approach in solving cyclic viscoplastic and viscoelastic. The results obtained were satisfactory and they are fully justified by the reduction of computation time by a factor of 7 up to 15. The limitation of their study is that the approach was performed in the one-dimensional case. More recently a combination of LATIN and wavelet transform has been proposed by Comte et al. [Comte *et al.*, 2006], this combination refers to a direct method. Thereupon, it is applied to solve the structural evolution problem. To clarify, the problem is solved on the whole time interval and the wavelet transform is applied in the global stage of the LATIN method. Comte et al. conclude that LATIN method accelerates the convergence of the solution and the decomposition of the load plays the main role in reducing the computation time. Particularly, this method has been applied to the elasto-plastic behavior under thermomechanical loading leading to a good accuracy with the FEM. Moreover, an approach for thermomechanical fatigue is developed by Constantinescu et al. [Constantinescu *et al.*, 2004] to determine the global behavior of the structure. Three computations are required:

- 1. Fluid flow computation by taking into account the heat exchange coefficient and the thermal flux,

- 2. Transient thermal diffusion computation,
- 3. Mechanical computation with the temperature field.

Recently Bhattacharyya et al. [Bhattacharyya, 2018], use LATIN-PGD techniques to solve continuum damage problems to predict the service life of the components that involves cyclic fatigue. However they applied their techniques only on academic problems.

So far, Montebello et al. [Montebello, 2015] used Proper Orthogonal Decomposition to describe the phenomenon of fretting-fatigue. As an illustration, POD generates a basis from a set of time-dependent fields [Chatterjee, 2000]. POD has been used in materials science, thermal science [Liang *et al.*, 2002, Efe et Ozbay, 2003] and other fields like fluid mechanics.

A combination of the Fourier analysis and Model Reduction in specific Proper Orthogonal Decomposition has been used by Ichihashi et al. [Ichihashi *et al.*, 2010] to analyze the energy released from experimental data, where Fast Fourier Transform (FFT) generates the temporal characteristic and POD provides the significant information. Equally important, a Priori Hyper-Reduction [Ryckelynck *et al.*, 2006] has been used to accurately solve a nonlinear behavior involving internal variable to predict the fatigue life [Ryckelynck et Benziane, 2010]. Not to mention, Ryckelynck et al [Ryckelynck *et al.*, 2015] developed a posteriori error estimator of hyper reduced prediction for elastoviscoplastic problems. To say nothing of, an optimal approach by the minimization of the problem is used of an inelastic structure under cyclic loading [Peigney et Stolz, 2003]; with this intention, a thermomechanical problem is studied for the validation. Comparatively, Spilipoulos [Spiliopoulos, 2002] developed a simplified method to predict the steady cyclic stress state by decomposing the residual stress in Fourier series.

1.4 Numerical issues to deal with nonlinearities

Nonlinear models are presented in different applications, traditionally non-linearities in a thermal conduction problem are associated with parameters dependencies such as physical properties depending on the temperature, volumetric heat source depending on the temperature, etc. The solution of such models requires a linearization scheme to deal with the nonlinearity. In this section, different linearization schemes will be presented.
In fact, the LATIN method has been used to solve thermo-mechanical models involved with non-linearity [Néron et Ladevèze, 2010], more standard linearization strategies were analyzed in [Ammar *et al.*, 2010] and it is applied in thermo-mechanical models [Prulière *et al.*, 2010b], more recently Chinesta et al. [Chinesta *et al.*, 2013b] solved a nonlinear parametric thermal model defined in degenerated geometries. An appealing alternative strategy is based on the interpolation of the non-linear term as proposed in [Barrault *et al.*, 2004]. This strategy was extended to the PGD method in [Chinesta *et al.*, 2013c]. The linearization schemes that will be discussed in this section are:

1. Newton-Raphason method
2. Picard's method
3. Asymptotic Numerical Method
4. Discrete Empirical Interpolation Method

1.4.1 Newton-Raphson method

The nonlinear solver, the Newton-Raphson method, is the most famous especially within FEM. To illustrate this non-linear solver, the following non-linear problem [Larson et Bengzon, 2013] is considered:

$$-\nabla.(a(u)\nabla u)) = f \in \Omega \tag{1.3}$$

A null boundary condition is considered, where a is a parameter depending on u, f is a source function, and u is the unknown field (temperature in our problem). To proceed with the Newton's method the field u is written as follows:

$$u = u^0 + \delta \tag{1.4}$$

where u^0 is the current approximation of u and δ is the correction, the finite element approximation is written as:

$$(a(u^0)\nabla\delta_h + a_u^{'}(u_h^0)\delta_h\nabla u_h^0, \nabla v) = (f, v) - (a(u^0)\nabla u^0, \nabla v) \tag{1.5}$$

where v is the virtual field and by considering $\delta = \sum_{j=1}^{N} d_j\varphi_j$ with d_j the unknown coefficient to be determined.
Eq. 1.3 can be written as:

$$\sum_{j=1}^{N} d_j(a(u_h^0)\nabla\varphi_j + a_u^{'}(u_h^0)\varphi_j\nabla u_h^0, \nabla\varphi_i) = (f, \varphi_i) - (a(u^0)\nabla u^0, \nabla\varphi_i) \tag{1.6}$$

Then the Jacobian matrix can be defined as:

$$J_{ij} = (a(u_h^0)\nabla\varphi_j, \nabla\varphi_i) + (a_u^{'}(u_h^0)\varphi_j\nabla u_h^0, \nabla\varphi_i) \tag{1.7}$$

and the residual writes:

$$R_i = (f, \varphi_i) - (a(u^0)\nabla u^0, \nabla\varphi_i) \tag{1.8}$$

The linear system with the unknown d_j reads:

$$Jd = R \tag{1.9}$$

The algorithm of Newton's method is depicted in Fig. 1.6.

In case of the Proper Generalized decomposition, at each iteration of the Newton method the Jacobian (J) and the residual (R) have to be updated and evaluated, then it is projected to Reduced Order Basis then the system is solved. Thus, the complexity and the computation depends on the order of the size of the discretization of the Reduced Order Basis [Capaldo *et al.*, 2014]. The combined Newton- PGD method is usually done as follows:

- the Newton's method is first applied to the continuous problem leading to a linearized equation,
- the PGD algorithm is then applied at each iteration of the Newton's procedure to solve the linearized equations.

1.4.2 Picard's method

The Picard's method is an other linearization scheme. With the Picard scheme, it starts with an initial guess of the nonlinear term for example if the specific heat (C_p) is dependent on temperature ($C_p = a \times T + b$), assume $T = 0$ and proceeds. To illustrate the Picard's method, let us consider the problem in Eq. 1.3. The variational formulation reads:

$$(a(u)\nabla u, \nabla v) = (f, v) \tag{1.10}$$

where v is the virtual field. The finite element approximation leads to:

$$(a(u_h)\nabla u_h, \nabla v) = (f, v) \tag{1.11}$$

where $u_h = \sum_{j=1}^{N} \xi_j\varphi_j$, with $\{\varphi_j\}$ the shape function. By introducing the stiffnes matrix $M_{ij} = (a(u_h)\nabla\varphi_j, \nabla\varphi_i)$, and the load vector $b_i = (f, \varphi_i)$, Eq. 1.3 can be written as:

$$M(\xi)\xi = b \tag{1.12}$$

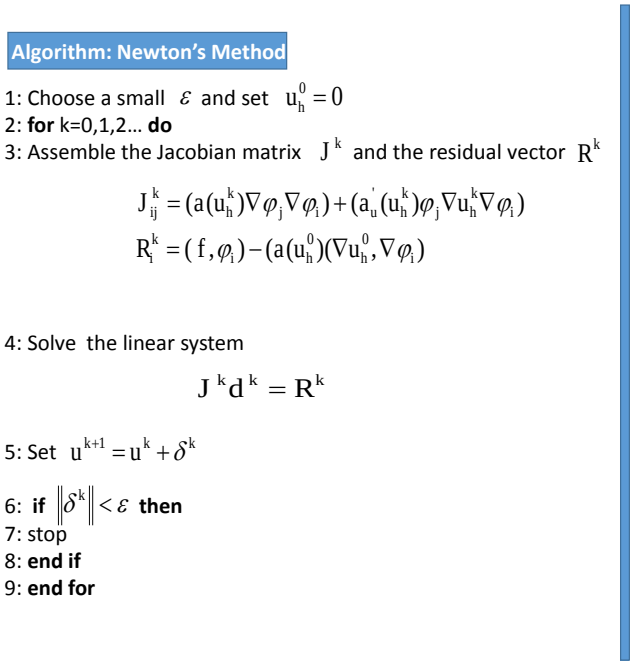


Figure 1.6: Newton-Raphson algorithm [Larson et Bengzon, 2013]

This equation is always nonlinear. To proceed, the Picard's method consists in evaluating the stifness matrix from the previous iteration as illustrated in the Picard's algorithm in Fig. 1.7 [Larson et Bengzon, 2013].

The PGD based Picard solution is sought in the separated form. At each enrichment step, the previous term sum is known (from the linearization using Picard scheme). Thus, the non-linear term is evaluated from the previous enrichment step. However, in the case of Newton's method the equation is linearized and then the PGD is applied at each Newton iteration where a linear problem is to be solved. Let us note that the Picard method will be extended and used to compute the non-linearity, generated from the dependence of the specific heat on temperatures in our proposed approach the mixed strategy presented in Chapter 5.

Illustrative example of Newton's and Picard's method based-PGD In this illustrative example, the nonlinear term appears as an heat source in the heat equation as follows:

$$\frac{\partial u}{\partial t} - k.\Delta u = -u^2 + f(x,t) \tag{1.13}$$

Let us consider a homogenous boundary condition and initial conditions.
The Newton's method and the Picard's Method are used as linearization schemes.
With the Picard scheme, the field is written as:

$$u(x,t) = \sum_{i=1}^{N} X_i(x)T_i(t) \tag{1.14}$$

At enrichment step n, the $n-1$ terms are known, consequently the term u^2 is evaluated by means of the solution at the previous iteration that is:

$$u^2 = (\sum_{i=1}^{n-1} X_i(x)T_i(t))^2 \tag{1.15}$$

then the iterative procedure proceeds until convergence.
However, in case of Newton's method, the governing equation is linearized such that at each iteration

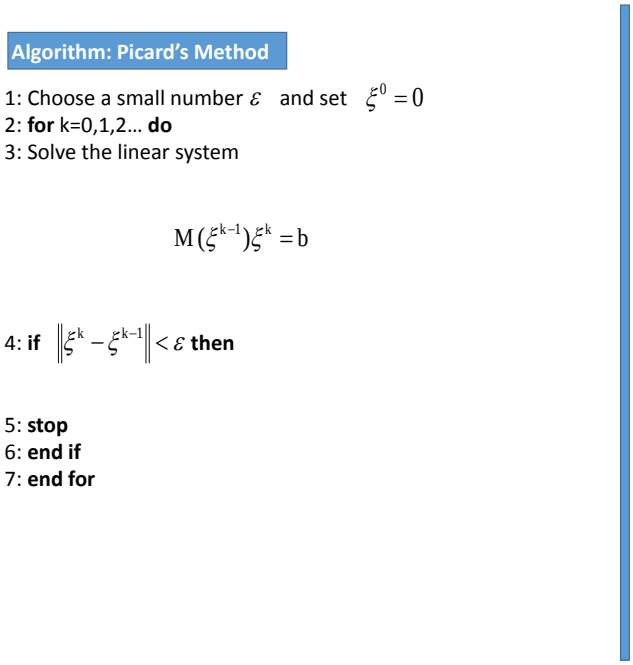


Figure 1.7: Picard algorithm [Larson et Bengzon, 2013]

j, the solution is given by:

$$u^{j+1} = u^j + \tilde{u} \tag{1.16}$$

where $\tilde{u}$ is the linearized solution:

$$\frac{\partial \tilde{u}}{\partial t} - k.\Delta\tilde{u} + 2u^j\tilde{u} = -R(u^j) \tag{1.17}$$

and the residual is written as:

$$R(u^j) = \frac{\partial u^j}{\partial t} - k.\Delta u^j + (u^j)^2 - f(x,t) \tag{1.18}$$

Then, the linear equation obtained is solved with PGD. Thus, $\tilde{u}$ is obtained in the separated form and proceed with PGD algorithm.

In the context of the PGD, it is noted that the Picard and Newton procedure converge, with a simular number of iterations. However, the Newton strategy converges slightly faster [Chinesta *et al.*, 2013a].

In the context of reduced basis, it is noted that by using Newton iteration to solve the nonlinear PDE, the global Jacobian matrix has to be updated and solved at each Newton step leading to more challenging regarding the time saving. For the Picard's method, the nonlinear term can lead to a very large number of modes which increases the memory storage. Thus other methods have been studied with the Model Order Reduction framework such as the Asymptotic Numerical Method and the Discrete Empirical Interpolation Method.

1.4.3 Asymptotic Numerical Method (ANM)

In general, the Newton's and Picard's method are successfully used to determine the solution of non-linear problems, however, such methods encounter the following difficulties: the computation time (usually larger cost compared to the linear case), the storage memory etc. In this section, an alternative approach called Asymptotic Numerical Method (ANM) is discussed. Such method has been proposed by [Noor et Peters, 1980, Damil et Potier-Ferry, 1990], where the nonlinear branches are evaluated in the asymptotic expansion form, then, they are determined by solving linear problems with Finite Element Method. This method has been used to solve the non-linear elastic problems [Cochelin

et al., 1994b, Cochelin *et al.*, 1994a]. In the context of the Model Order Reduction, this strategy has been extended with Chinesta et al. [Chinesta *et al.*, 2013b], where the PGD method was combined with an advanced non-linear solver (the Asymptotic Numerical Method) on the context of non-linear transient parametric thermal models. The upshot of their study showed that this approach can be used for challenging thermal problems and parametric models.In the real simulation developments, Cueto et.al [Cueto et Chinesta, 2014] gave a review about the usage of the ANM with the MOR and in particular with the POD. Moreover, Niroomandi et al. have been used POD-ANM to solve hyperelastic problems [Niroomandi *et al.*, 2009].

To illustrate we use the example:

$$\frac{\partial u}{\partial t} - k.\Delta u = \lambda.u^2 + f(x,t) \tag{1.19}$$

where λ is the loading parameter. The asymptotic expansion of the unknown field u and the coefficient λ are written as follows:

$$u = u_0 + a.u_1 + a^2.u_2 + ... \tag{1.20}$$

$$u^2 = (u^2)_0 + a.u_1 + a^2.u_2 + ... \tag{1.21}$$

The detailed procedure is illustrated in [Chinesta *et al.*, 2013b], it is noticed that the differential operator is always the same. To illustrate the PGD-based ANM, the original problem Eq. (1.13) is modified by adding the loading parameter, then ANM treats the non-linear model by unique expansion Eq. (1.20) and Eq. (1.21). At each order, the resulting equation is solved by PGD method. they found that an expansion of order 4 is sufficient to capture the nonlinearity.

1.4.4 Discrete Empirical Interpolation Method (DEIM)

The DEIM is used to reduce the computational cost resulted from the nonlinearities by using interpolation with the projection. This method is applied to arbitrary ODEs. It is based on interpolating a pre-computed base (offline solution) for the non-linear terms, then it approximated the non-linear term and the Jacobian matrix. The nonlinear terms are interpolated using set of points, some authors called these points the magic points [Maday *et al.*, 2009]. Consequently, the nonlinear term is calculated at the magic points with the pre-computed bases. This method has widely used in the domain of the model reduction. The first development of an empirical interpolation in the reduced-basis can be found in [Barrault *et al.*, 2004, Grepl, Martin A. *et al.*, 2007]. The authors used empirical interpolation for partial differential equations with non-affine parameter dependence.

The discrete variant of the empirical interpolation has been developed in [Chaturantabut et Sorensen, 2010] and so-called the Discrete Empirical Interpolation Method (DEIM). It has been carried out and extended to POD [Chaturantabut et Sorensen, 2010], interestingly, they showed that this combination leads to an accurate reduced system, generating accurate results. DEIM-POD has been widely used in the domain of mechanics, for example, Ghavamian et.al [Ghavamian *et al.*, 2017] used this method to solve strain-softening viscoplasticity. Similarly, in [Benjamin *et al.*,] authors applied to deal with the dependence of the parameter in the heat conduction. In fact, there is a considerable amount of literature on the use of DEIM-POD. We here only cite some of the recent works [Lihong *et al.*, 2017, Fu *et al.*, 2018]. To sum, the DEIM has provided very satisfactory results in the term of solving nonlinear with the POD. Likewise, Fritzen et. al [Fritzen *et al.*, 2016] used Hyper-Reduction (HR) and the DEIM to solve a nonlinear thermal problem, the results obtained by the authors showed both HR and DEIM generates accurate results and acceleration of the computation time. Recently the DEIM has been extended to PGD [Aguado *et al.*, 2013], Aguado et al. have been coupled the EIM with the PGD by searching for the new points at each iteration related to a new ROB, compared to the POD the bases are a priori unknown, thus the nonlinear term need to be computed and interpolated during the resolution using the PGD algorithm. To this end, DEIM has already provided satisfactory results in the aim of saving time compared to the other nonlinear methods. To emphasize, the nonlinear term is interpolated using the reduced basis instead of being

fully evaluated [Aguado *et al.*, 2013]. The algorithm of coupling DEIM with PGD issued from [Aguado *et al.*, 2013] is illustrated in Fig. 1.8.

In our work, the DEIM-PGD is used to solve the 3D non-linear problem, the non-linearity will be generated from the dependence of the material properties such as the specific heat, convection coefficient on cyclic temperature as it will be presented in Chapter 3.

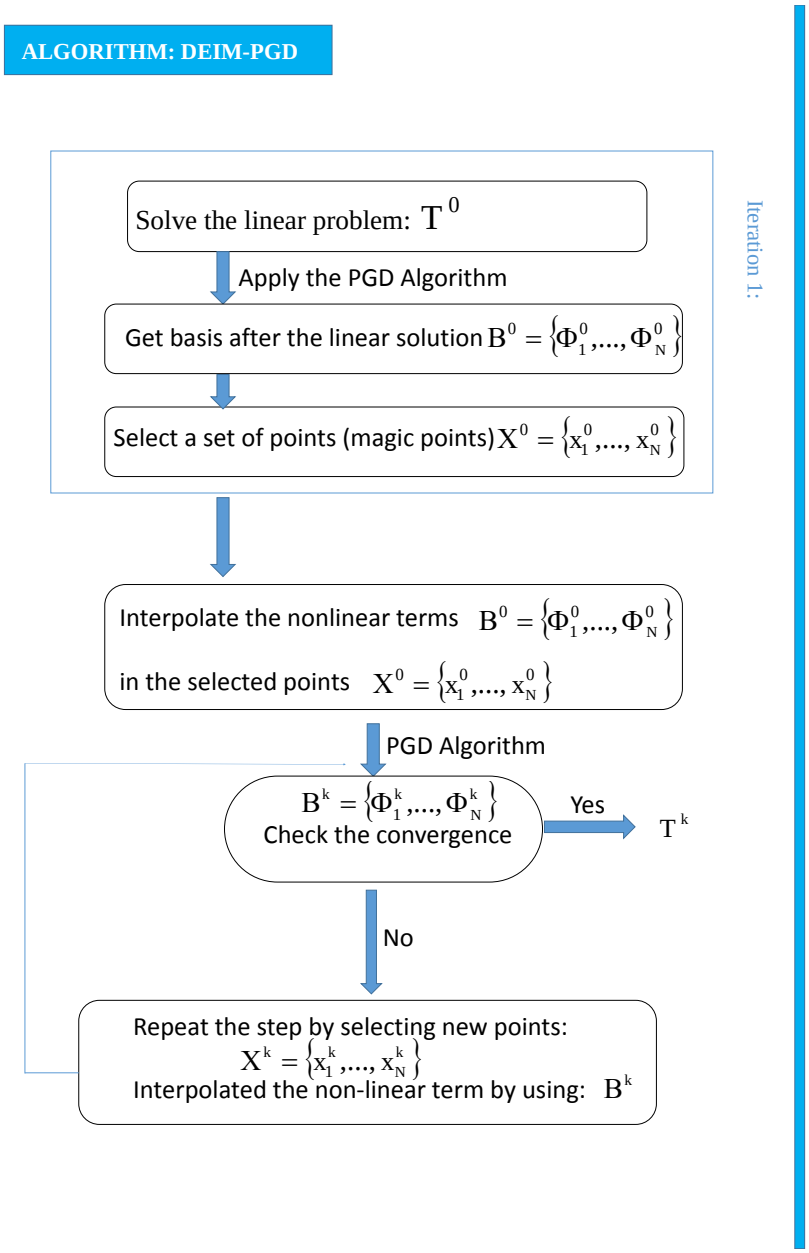


Figure 1.8: DEIM-based PGD algorithm from [Aguado *et al.*, 2013]

1.5 Frequency domain analysis

The Fast Fourier Transform (FFT) is a signal processing technique used in different domains and applications such as structural dynamics, vibration analysis, diffusion equation, numerical integration, etc. FFT computes in an efficient way the Discrete Fourier Transform (DFT) of a signal in the time domain into the frequency domain. There exists an inverse transformation to reconstruct a solution from the frequency domain to the time domain (Inverse Fast Fourier Transform: IFFT). The development of the algorithm of the FFT has been passed through modification and improvement

since it is originating in 1965 by Cooley and Tukey [Cooley, 1987, Van Loan, 1992].
In this section, only an illustration of the FFT is given. For more information on the FFT and its algorithm, the interested reader can refer to [Brandolini, 2004, Walnut, 2013] and the reference therein. In this thesis, this technique will only be used as a black box to analyze and study the effect of characteristic times such as cycle time and physical time in the frequency domain.

1.5.1 Fourier analysis

Fourier transform technique uses the spectrum of a function in the time domain and generates a representation of this function in the frequency domain. Mathematically, this relationship is stated as:

$$S(f) = \int_{-\infty}^{\infty} s(t) \exp(-j2\pi f) dt$$

where $S(f)$ is the Fourier transform of $s(t)$. t, f are the time and frequency respectively, and $j = \sqrt{-1}$.
To illustrate the procedure of the Fourier transform, let us consider the following function (combination of periodic and exponential functions):

$$f(t) = cos(2\ \pi\ f_1\ t) + 2cos(2\ \pi\ f_2\ t) + 10(1 - exp(\frac{5}{100}t) \tag{1.22}$$

where $f_1 = 0.5Hz$, $f_2 = 1Hz$ and t(s) is the time domain. A MATLAB tool that uses the Fast Fourier Transform returns the discrete Fourier Transform (DFT) from the time signal $(f(t))$. Fig. 1.9 represents the evolution of the $f(t)$ in time domain, and the corresponding amplitude and phase angle in the frequency domain (output of the MATLAB tool). It is noted that:

1. The function $f(t)$ consists of a combination of a transient part (due to the presence of an exponential function) and a fluctuation part (cyclic due to the presence of periodic function (cosine)).

2. In the frequency domain, three fundamental peaks are appeared:

   (a) The first peak at $f = 0$Hz, this peak is related to the transient part, particularly the exponential function $(10(1 - exp(\frac{5}{100}t))$.

   (b) The second peak at $f = 0.5$Hz is related to the frequency of the periodic function $(cos(2\ \pi\ f_1\ t))$ where $f_1 = 0.5Hz$.

   (c) The third peak at $f = 1Hz$ is related to the frequency of the periodic function $(2 \times cos(2\ \pi\ f_2\ t))$ where $f_2 = 1$Hz.

Remark. The effect of the sampling number on the signal in the frequency domain is discussed in Appendix A.2.

1.5.2 Application of the Fast Fourier Transform method (FFT) in mechanics and more particularly materials under fatigue

Fourier series and Fast Fourier Transform has to do a lot with data analysis in the mechanical domain. For instance, it is very useful for determining the properties of vibrating systems. To point out, in industrial applications, machines such as dishwashers, turbine etc. can produce harmonic signal, thus this signal needs to be analyzed in order to know the natural frequency of the machine and understand the behavior. For example, Harcarik et al. [Harčarik *et al.*, 2012] used the Fast Fourier Transform to analyze the frequency obtained with different domestic appliances, indeed the upshot of their study showed that the FFT is a good choice for transforming time signal recorded from the appliances to a frequency signal thus the mechanical properties can be understood.

Various authors have been using FFT method for the prediction of the micromechanical fields in polycrystalline [Lebensohn *et al.*, 2012]. By the same token, Felder et al. [Felder *et al.*, 2017] have driven the further development of the usage of FFT, they have used finite element and the FFT for

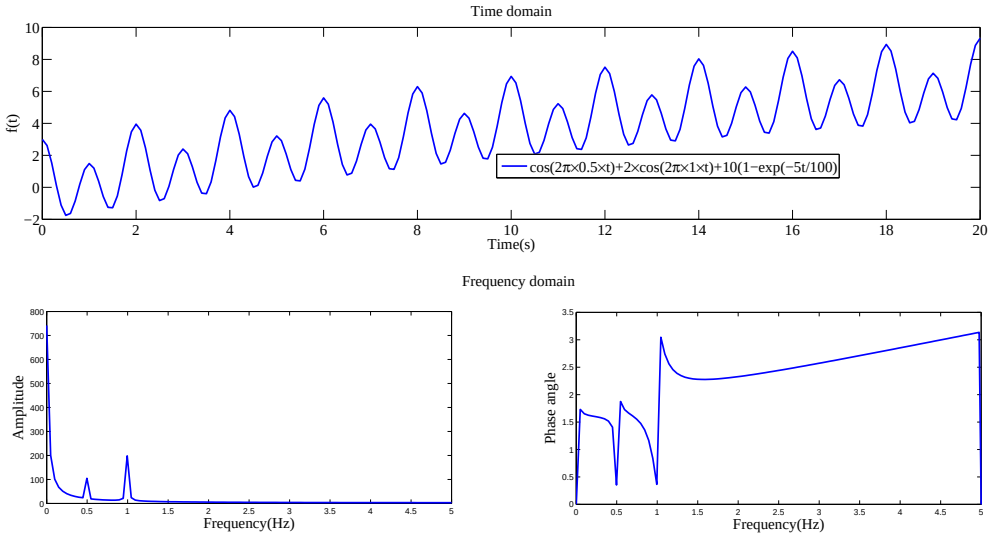


Figure 1.9: The Fast Fourier Transform of $f(t)$

the prediction of the material behavior and the local fields viscoplastic material. To illustrate for the macro scale, FEM has been applied, whereas, for the micro scale the Fast Fourier Transform has been used. Eyre et al. [Eyre et Milton, 1999] carried out the use of Fourier transform to compute the response in a composite material by computing the tensor through the use of an experimental value. They have extended the use of the FFT to compute the response in the case of the nonlinear and thermoelastic materials.

Equally important, the FFT originally developed as the fast algorithm to compute the mechanical response from an image in the mechanics of materials [Lebensohn *et al.*, 2011]. In the context of the fatigue, Sutherlan [Sutherland, 1996] use the Inverse Fast Fourier Transform to determine the fatigue load on the turbine blade by transforming the frequency spectrum to an equivalent time series suitable for the cycle time. To our knowledge from the literature on FFT in mechanics, the FFT has not been applied as a direct tool to establish bases for model reduction.

1.6 Discussion

To sum up, in this chapter, an overview of the different numerical approaches for solving multiphysics problems according to their classification as an incremental scheme and a non-incremental scheme is presented. Within the FE framework, a considerable amount of literature points out the numerical limitations: large computation time, non-convergence, and need of large memory. To overcome these limitations, Model Reduction methods seem to be an efficient way. Some of these methods have already been used in the context of different time scales and fatigue but only the LATIN method dealt with 3D cases for a long time. Nevertheless, the LATIN method needs the knowledge of directions and a particular writing of the problem to be used. Some articles have already discussed the use of the PGD method in the context of fatigue, but they are usually limited to one-dimensional case. More recently the 3D case has been investigated with the model reduction. Despite this interest, it was limited to 10 cycles and the time saving obtained with authors compared to the standard incremental method was of order 10 [Nasri *et al.*, 2018]. Also in [Bergheau *et al.*, 2016] their work was limited to 3 cycles and a small time has been considered. Important to realize, that PGD has been used widely for different kind of domains for instance fluid mechanics, biomechanics, chemistry, etc. In detail, the PGD is here introduced to avoid the non-incremental scheme. But the PGD can be combined to a non-incremental scheme to deal with transient problems. The findings of the review on the non-linear problems showed that a combination of the PGD with a non-linear solver such as Newton's or Picard's method can be used to solve a non-linear problem- but the main difficulty mentioned

related to the evaluation of the non-linear terms that can lead to the increase of the computational time. Besides, a technique based on the Asymptotic Numerical Method has been used with PGD to solve a non-linear problem. Discrete Empirical Interpolation Method (DEIM) is used to reduce the computational cost resulted from the non-linearities by using interpolation projection and seems a promising method. Particularly, this chapter provides an overview of the usage of the Fast Fourier Transform as a mean to solve thermomechanical problems. To our knowledge from the literature on FFT in mechanics, the FFT has not been applied as a direct tool to establish bases for the model reduction. Where, in the domain of the multiphysics, there is a lack of approach that relies on a priori time-basis which can be a promising solution for saving a large amount of time. However, as mentioned in the literature, enhancing the computation time of solving multiphysics problem is an important need. It was previously stated that the Model Order Reduction and the Reduced Basis are usually used to decrease the computational time for problems involving different time scales. Correspondingly, in this thesis, three approaches in the framework of model order reduction are developed and used to solve cyclic transient thermal problems involving different time scales and are the followings:

- Approach 1. This approach is based on the well known method, the Proper Generalized Decomposition (PGD), this method is related to the construction of the unknown field (temperature in this thesis) in a separated representation.
- Approach 2. The second numerical approach is based on the use of a collection of the most significant modes to solve cyclic transient thermal problems involving different time scales. The dictionary of the significant modes is given by Proper Generalized Decomposition (PGD) solutions for different time scales. The originality behind this approach lies in the fact that space-time modes are considered instead of only spatial modes as in the Proper Orthogonal Decomposition (POD).
- Approach 3. This approach is based on the knowledge of an a priori time bases to reduce the computation time by avoiding the use of an incremental scheme. The originality behind this approach is the construction of the a priori time basis that are based on an analytical expression using the Fast Fourier Transform (time bases are known), then the PGD method is used to compute the spatial modes (the spatial modes are unknown). This method is called the mixed strategy.

The benefits of each approach are discussed in the term of time saving and accuracy compared to FEM or the usual PGD.

Chapter 2

3D thermal problem: linear, nonlinear and multitime

—

Research is creating new knowledge
Neil Armstrong

Contents

2.1 Introduction 30
2.2 3D thermal problem within the Finite Element framework 30
2.2.1 3D linear thermal problem 30
2.2.1.1 Modeling 30
2.2.1.2 Finite Element approximation 33
2.2.2 3D non-linear thermal problem 36
2.2.2.1 Modeling 36
2.2.2.2 Finite Element approximation 36
2.3 Discussion and conclusion 37

2.1 Introduction

Transient diffusion problems play an important role in engineering and science domains such as heat transfer problems [Annaratone, 2011], heat conduction in solids [Carslaw et Jaeger, 1986], thermal conductivity behavior of polymers [dos Santos *et al.*, 2013], temperature effects of the machinery [Rizk et Awad, 2018]. The study of transient heat problems requires the consideration of the thermal capacitance of materials. Accordingly, under a thermal load, the steady state is unreached directly, and it takes time depending on the diffusivity of the material. In order to obtain the variation with respect to time, the Finite Element Method coupled with a time integration is needed. Of course, the transient problem can be linear or nonlinear. As a matter of fact non-linearity can be generated from the dependence of the conductivity on the temperature. Certainly, the phenomenon generated from the transient problems is controlled by the characteristic times: physical time (related to the material properties) and the cycle time (related to an harmonic load). Practically speaking, the modeling of transient problems depends on the problem formulation of linear and nonlinear equations. In this chapter, a modeling of a 3D transient problem is constructed by highlighting the primary parameters (material properties), boundary conditions, timescales, initial conditions, etc.

In summary, the major issues treated in this chapter are:

1. Generation of the mathematical modeling of a 3D linear transient problem.
2. Generation of the mathematical modeling of a 3D non-linear transient problem.
3. Introduction of the multi-time scales presented in the 3D transient problem.
4. Introduction of the algorithm of the FEM to solve the linear and non-linear thermal problems.

The presentation of the 3D thermal within the Finite Element Method is based on the work of Bergheau et al. [Bergheau et Fortunier, 2010].

2.2 3D thermal problem within the Finite Element framework

2.2.1 3D linear thermal problem

2.2.1.1 Modeling

According to the thermal equilibrium, the heat produced on a solid portion is equal to the heat flux coming out. In this way, the thermal equilibrium of the portion Ω_A is written as follows at any point of the solid Ω as shown in Fig. 2.1:

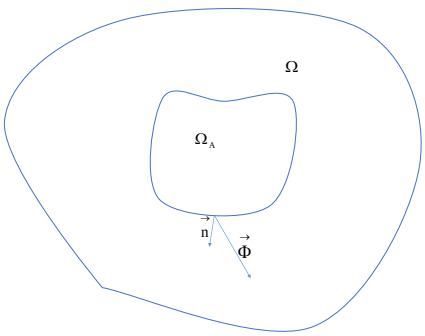


Figure 2.1: Thermal equilibrium on a solid domain Ω [Bergheau et Fortunier, 2010]

$$\forall\ \Omega_A,\quad \int_{\Omega_A} Q dv = \int_{\partial\Omega_A} \overrightarrow{\Phi}.\overrightarrow{n} ds \tag{2.1}$$

where $\overrightarrow{\phi}$ is a vector that identifies the heat flux ($W.m^{-2}$), $\overrightarrow{n}$ is the outward unit normal to this surface and Q is the volumetric heat source ($W.m^{-3}$).

The Fourier law states that the variation of temperature in spatial direction ($\overrightarrow{grad}(T)$) will generate a heat flux such that:

$$\overrightarrow{\Phi} = -\underline{k}.\overrightarrow{grad}(T) \tag{2.2}$$

where $\underline{k}$ is the second order tensor in which each component generates the thermal gradient. Let us consider an isotropic material (the conductivity is the same in all directions) therefore, $\underline{k}$ is written as $\underline{k} = k\underline{I}$ with $\underline{I}$ is the identity matrix. Substitute Eq. (2.2) in Eq. (2.1), it writes:

$$div(\underline{k}.\overrightarrow{grad}(T)) + Q = 0 \tag{2.3}$$

In case 3D $div(\underline{k}.\overrightarrow{grad}(T))$ writes:

$$div(\underline{k}.\overrightarrow{grad}(T)) = k(\frac{\partial^2 T}{\partial x^2} + \frac{\partial^2 T}{\partial y^2} + \frac{\partial^2 T}{\partial z^2}) \tag{2.4}$$

Transient. In fact, according to the first law of thermodynamics, the equilibrium state in Eq. (2.3) produces an internal energy change that can be expressed as $\rho\dot{H}$ where $\dot{H}$ represents the variation with respect to time of its specific enthalpy H and ρ the density. However, in case of steady state $\dot{H}$ is null. In case of transient Eq. (2.3) is written as follows:

$$div(\underline{k}.\overrightarrow{grad}(T)) + Q = \rho\dot{H} \tag{2.5}$$

Boundary conditions. The thermal boundary conditions that can be applied to the solid are:

1. Heat flux on the boundary $\partial\Omega$ of Ω, is generally written as in Eq. (2.6)

$$\overrightarrow{\Phi}.\overrightarrow{n} = -q(T) \tag{2.6}$$

   and it can be as follows:

   - Convection of the form: $q = h(T - T_\infty)$, where h is the convection coefficient ($W.m^{-2}.K^{-1}$) and T_∞ is the ambient temperature (K).
   - Radiation of the form: $q = \sigma\epsilon(T_\infty^4 - T^4)$, where σ is the Stefan Boltzman coefficient ($WK^4.m^{-2}$) and ϵ is the emissivity of the surface. In our model, a null radiation is assumed.
   - $q = 0$ in case of adiabatic or symmetry boundary conditions.
   - q is constant (independent of the temperature) it is referred to the Neuman condition.

2. A known temperature on the boundary T_d (which represents the Dirichlet boundary condition).

The portion where the temperature is defined is represented by ∂_{Ω_T}, and ∂_{Ω_q} is the portion where the heat flux is applied. In the transient case, the boundary conditions and the heat source vary with respect to time. Thus, the objective is to find $T(x, y, z, t)$ at any point $\mathbf{x} = (x, y, z) \in \Omega$ and any

time $t \in 0 < t < t_f$ verifying the boundary (BC) and initial conditions (IC):

$$\begin{cases} \bullet \ IC \\ T(\overrightarrow{\mathbf{x}}, 0) = T_0(\mathbf{x}) \\ \mathbf{x} = (x, y, z) \\ \bullet \ \forall t, \ t \in \ 0 < t < t_f : \\ R(T,t) = div(\underline{k}.\overrightarrow{grad}(T)) + Q - \rho\dot{H} = 0 \\ \bullet \ BC \\ (\underline{k}.\overrightarrow{grad}(T)).\overrightarrow{n} = q \text{ on } \partial\Omega_q \\ T = T_d \text{ on } \partial\Omega_T \end{cases} \tag{2.7}$$

Where $\partial\Omega_T \cup \partial\Omega_q = \partial\Omega$ and $R(T,t)$ represents the residual of the problem. It is equal to zero at any point on Ω between $t = 0$ and $t = t_f$.

The different time scales involved in a transient heat transfer phenomena [Marin, 2010] are discussed in this section. It is well known that heat propagates from the region of the higher temperature to the lower one. This transfer depends on the following:

1. The physical time scale which is mainly related to the material properties (conductivity, density, and specific heat) and the length of the sample.

2. The time scale related to the load applied (cycle time).

The physical time scale depends strongly on the geometry (characteristic length) and its thermal diffusivity. The thermal diffusivity $(\alpha(m^2.s^{-1}))$ is related to the rate at which the temperature propagates through the material and is defined as:

$$\alpha = \frac{k}{\rho C_p} \tag{2.8}$$

where k $(\mathrm{W.m^{-1}})$ is the thermal conductivity, ρ $(\mathrm{kg.m^{-3}})$ represents the density of the material, C_p $(J.kg^{-1}.^{\circ}\mathrm{C}^{-1})$ its specific heat. Let us recall that the specific heat C_p is related to the amount of heat needed to raise the temperature of a unit mass by one degree. Hence, the diffusivity is the ratio of the heat conducted through the material to the heat stored per unit volume. Accordingly, the physical time τ_ϕ(s) can be seen as:

$$\tau_\phi = \frac{\rho C_p L_c^2}{k} \tag{2.9}$$

Where L_c is a characteristic length. To illustrate, the physical time is inversely proportional with respect to the diffusivity. So, low diffusivity will generates high physical time.

Another characteristic time scale is related to the harmonic loads (volumetric heat source, heat flux, and defined temperature). This time scale is referred to the cycle time $(\tau_c(s))$ that is the frequency of the load $(\frac{1}{\tau_c})$. In this case, the new time scale will affect the behavior of the polymer. So, the understanding of the link between the different time scales presented in the multi-physics problem is very essential.

To determine the temperature, the weak formulation of Eq. (2.7) after applying the divergence theorem (integration by parts) is written as:

$$\begin{cases} \bullet \text{ at } t = 0 : \\ T(\overrightarrow{\mathbf{x}}, 0) = T_0(\overrightarrow{\mathbf{x}}) \\ \bullet \ \forall t, \ t \in \ 0 < t < t_f : \\ \int_\Omega \Psi(Q - \rho\dot{H})dv + \int_{\partial\Omega_q} \Psi q ds - \int_\Omega \overrightarrow{grad}^T(\Psi).\underline{k}.\overrightarrow{grad}(T)dv = 0 \end{cases} \tag{2.10}$$

where Ψ refers to the virtual field.

Remark.

The Galerkin method constructs at any instant a temperature approximation by n-dimensional spaces. The finite element approximation is only used for space variations, while, another technique is required for time integration such as the Finite Difference method.

2.2.1.2 Finite Element approximation

The temperature $T(\overrightarrow{\mathbf{x}}, t)$ is estimated inside each element e of a mesh, where it is determined at the nodes of the corresponding element (e).

The functions $\Psi(\overrightarrow{\mathbf{x}})$ and $T(\overrightarrow{\mathbf{x}}, t)$ are estimated as follows:

$$\begin{aligned} \forall \mathbf{x} \in \Omega^e, \ \forall t, \ t \in \ \ 0 \leq t < t_f, \ \ T(\overrightarrow{\mathbf{x}}, t) \ &= \textstyle\sum_{i=1}^{n^e} N_i^e(\overrightarrow{\mathbf{x}}) T_i^e(t) \\ &= \left\langle N_1^e(\overrightarrow{\mathbf{x}}), ..., N_{n^e}^e(\overrightarrow{\mathbf{x}}) \right\rangle . \begin{Bmatrix} T_1^e(t) \\ . \\ . \\ . \\ T_{n^e}^e(t) \end{Bmatrix} \\ &= \left\langle N^e(\overrightarrow{\mathbf{x}}) \right\rangle . \{T^e(t)\} \end{aligned} \tag{2.11}$$

$$\begin{aligned} \forall \mathbf{x} \in \Omega^e, \ \forall t, \ t \in \ \ 0 \leq t < t_f, \ \ \Psi(\overrightarrow{\mathbf{x}}) \ &= \textstyle\sum_{i=1}^{n^e} \Psi^e N_i^e(\overrightarrow{\mathbf{x}}) \\ &= \left\langle \Psi_1^e, ..., \Psi_{n^e}^e \right\rangle . \begin{Bmatrix} N_1^e(\overrightarrow{\mathbf{x}}) \\ . \\ . \\ . \\ N_{n^e}^e(\overrightarrow{\mathbf{x}}) \end{Bmatrix} \\ &= \left\langle \Psi^e \right\rangle . \{N^e(\overrightarrow{\mathbf{x}})\} \end{aligned} \tag{2.12}$$

where

- $\{T\}$ represents the temperature vector.
- $\langle \Psi \rangle$ represents the weighting function values.
- N represents shape function related to the temperature.
- The upper script e will refer to the number of an element, and i is the local number of an element e.

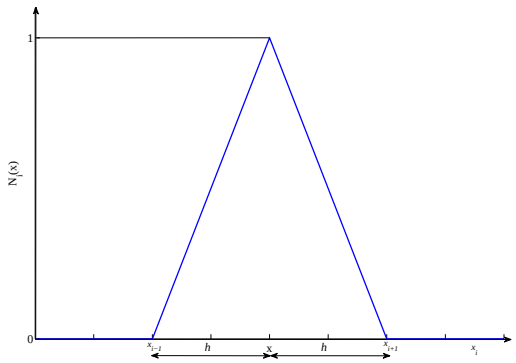


Figure 2.2: The linear shape function [Bergheau et Fortunier, 2010]

$T_i^e(t)$ represents the temperature at instant t of element e and node i, Ψ_i^e represents the weighting function value at the node number i of element e, and $N_i^e(\overrightarrow{\mathbf{x}})$ refers to the shape function as seen in Fig. 2.2 where $N_i(x)$ is expressed as follows:

$$N_i(x) = \begin{cases} \frac{x-x_{i-1}}{h} & \text{if } \; x_{i-1} < x < x_i \\ \\ \frac{x_{i+1}-x}{h} & \text{if } \; x_i < x < x_{i+1} \\ \\ 0 \;\; \text{if not} \end{cases} \tag{2.13}$$

The terms of the discrete problem Eq. (2.10) are expressed as follows:

$$\int_\Omega \Psi(Q - \rho\dot{H})dv = \sum_{e=1}^{m} \langle \Psi^e \rangle . \int_{\Omega^e} \{N^e\} (Q - \rho\dot{H})dv \tag{2.14}$$

$$\int_{\partial\Omega} \Psi q ds = \sum_{e=1}^{m} \langle \Psi^e \rangle . \int_{\partial\Omega^e \cap \partial\Omega_q} \{N^e\} q ds \tag{2.15}$$

$$\int_\Omega \overrightarrow{grad}(\Psi).k.\overrightarrow{grad}(T)dv = \sum_{e=1}^{m} \langle \Psi^e \rangle . \int_{\Omega^e} \overrightarrow{grad}^T(N^e).k.\overrightarrow{grad}(T)dv \tag{2.16}$$

The variation rate of the enthalpy $\dot{H}$ is $C_p = \frac{dH}{dT}$. Thus, $\rho\dot{H} = \rho C_p \dot{T}$, where $\dot{T}$ can be approximated by a nodal expression as:

$$\begin{aligned} \forall \; \overrightarrow{\mathbf{x}} \in \Omega^e, \;\; 0 \leq t < t_f \;\; \dot{T}(\overrightarrow{\mathbf{x}}, t) \;\; &= \textstyle\sum_{i=1}^{n^e} N_i^e(\overrightarrow{\mathbf{x}}) \dot{T}_i^e(t) \\ &= \langle N^e(\overrightarrow{\mathbf{x}}) \rangle . \left\{ \dot{T}^e(t) \right\} \end{aligned} \tag{2.17}$$

where $\left\{ \dot{T}_i^e(t) \right\}$ consists of the rate of the temperature change at the nodes of element e.

Insert Eq. (2.14), Eq. 2.15, and Eq. 2.16 into Eq. 2.10, then the residual expression writes:

$$\begin{aligned} \{R^e(T,t)\} = &\int_{\Omega^e} \{N^e\} Q dv + \int_{\partial\Omega^e \cap \partial\Omega_q} \{N^e\} q ds \\ &-(\int_{\Omega^e} \rho C_p \{N^e\} \langle N^e \rangle dv). \left\{ \dot{T}^e \right\} \\ &- \int_{\Omega^e} \left\{ \overrightarrow{grad}^T(N^e) \right\} .k.\overrightarrow{grad}(T)dv \end{aligned} \tag{2.18}$$

The internal energy change $\rho\dot{H}$ generates a new symmetrical matrix called the capacitance matrix (similar to the mass matrix in dynamic problems) defined as:

$$[M^e] = \int_{\Omega^e} \rho C_p \{N^e\} \langle N^e \rangle \, dv \tag{2.19}$$

The modeling in this section is restricted to a linear case where:

- The material properties (conductivity k, density ρ, and specific heat C_p) are independent of temperature.
- The boundary condition such as the heat flux: $q = h(T - T_\infty) + q_0$, where the convection coefficient h and q_0 (constant flux) are independent of temperature.
- The volumetric heat source Q is independent of temperature.

The load term is written as follows:

$$\{F^e\} = \int_{\Omega}^{e} \{N^e\} Q dv + \int_{\partial\Omega^e \cap \partial\Omega_q} \{N^e\} (q_0 + hT_\infty) ds \tag{2.20}$$

and the conductance matrix is expressed as:

$$[K^e] = [k^e] + [H^e] \tag{2.21}$$

where

$$\begin{cases} [k^e] = & \int_{\Omega^e} \left\{ \overrightarrow{grad}^T (N^e) . \underline{k} . \right\} \left\langle \overrightarrow{grad} (N^e) \right\rangle \\ [H^e] = & \int_{\partial\Omega^e \cap \partial\Omega_q} \{N^e\} \, h \, \langle N^e \rangle \end{cases} \tag{2.22}$$

Finally, the element residual can be written as:

$$\{R^e(T)\} = \{F^e\} - [M^e] . \left\{ \dot{T}^e \right\} - [K^e] . \{T^e\} \tag{2.23}$$

Where $\{F^e\}$ represents the load vector, $[M^e]$ referred to the capacitance matrix or the mass matrix, and $[K^e]$ is the conductance matrix.

After defining the elementary matrices, an assembly is required to generate the global matrix:

$$\{R(T)\} = \{F\} - [M] . \left\{ \dot{T} \right\} - [K] . \{T\} \tag{2.24}$$

Thus, Eq. (2.24) is a first order differential equation where a time integration is needed to solve it:

$$[M] . \left\{ \dot{T} \right\} + [K] . \{T\} = \{F\} \tag{2.25}$$

Remark. To recall, in the case of transient problems, an incremental scheme will be used. At each time step, the spatial FEM will be solved, which increases the computation time. Moreover, the choice of the time step should satisfy the requirement related to the spatial scale. This issue will be discussed in the coming sections.

Time integration. The time evolution of the temperature at the mesh nodes of the element requires the integration of the differential system, that is the temperature and its gradient at any point of the model. The implicit finite difference scheme can be used where:

$$\left\{ \dot{T}(t + \Delta t) \right\} = \frac{\{T(t + \Delta t)\} - \{T(t)\}}{\Delta t} \tag{2.26}$$

In case of the linear problem, the column vector $\{F\}$, the capacitance matrix and the conductance matrix are being known at instant $t + \Delta t$. Using the finite difference scheme, starts with an initial

condition at $t = 0$, that is T_0, followed by the estimation of the temperature at each instant by consecutive time steps Δt. The nodal temperatures at this instant are obtained by solving the differential equation where the space is approximated by the finite element method and the time is approximated by the finite difference method, leading to the following equation:

$$([M] + \Delta t\,[K]).\{T(t + \Delta t)\} = \Delta t\,\{F\} + [M]\,.\,\{T(t)\} \tag{2.27}$$

Other time integration methods might be used as: direct time integration and the modal analysis. The modal method is widely used in mechanics [Subbaraj et Dokainish, 1989, Dokainish et Subbaraj, 1989], but rarely used in heat transfer.

2.2.2 3D non-linear thermal problem

2.2.2.1 Modeling

Previously, it was considered that the material properties are independent of the temperature. However, the non-linearity in a thermal conduction problem can appear in the form of:

1. The dependence of the physical properties on the temperature, such as the specific heat $C_p(T)$.
2. The dependence of the volumetric heat source $Q(T)$.
3. The dependence of the boundary heat flux $q(T)$.

In this thesis, the dependance of the material properties and the boundary condition (convection coefficient) on the temperature will be studied.

2.2.2.2 Finite Element approximation

When the material properties such as, the conductivity k, the specific heat C_p and the density ρ depend on the temperature, then the matrices $[K]$ and $[M]$ depend on temperature. Thus, the residual vector is a nonlinear function, which depends on the temperature and it is expressed as follows:

$$\{R(T)\} = \{F\} - [M(T)]\,.\,\left\{\dot{T}\right\} - [K(T)]\,.\,\{T\} \tag{2.28}$$

In order to solve Eq. 2.28 (non-linear equation), two steps usually are considered:

1. Initialisation step. This step consists in choosing an initial guess for the solution. A solution of the associated linear problem is usually used. In our example it can be the solution of the temperature for $C_p = C_p(T = 0)$.
2. This step consists in an iterative procedure. At each iteration i, the non-linear equation is linearized with a linearization scheme such as Newton as illustrated in Fig. 2.3 where $\{\Delta T\}^i$ is the solution of the associated linear system. A convergence test is carried out at each iteration by comparing the norm of residual denoted by $\{R^i\}$ (the Euclidean norm) with a certain tolerance.

Remark. To recall, common methods used to solve non-linear equations are:

- Newton-Raphson method [Chama *et al.*, 2018]
- Modified Newton-Raphson method
- Substitution method known as Picard iterative method (fixed point method).

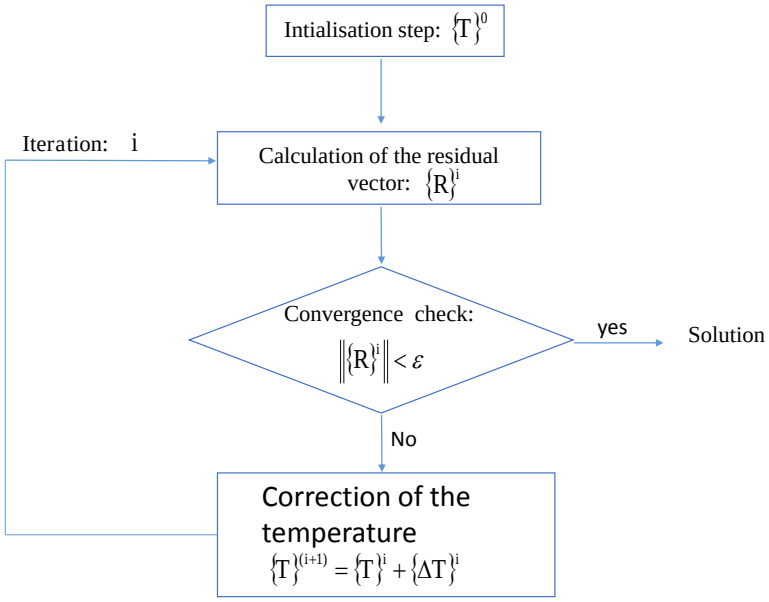


Figure 2.3: Non-linear solver with the two steps [Bergheau et Fortunier, 2010]

In case of the dependence of the physical properties on the temperature for example, the conductivity $k(T)$, then term involved in the residual for the transient case is :

$$\begin{aligned} R_i^k &= -\int_{\Omega^e} \left\{\overrightarrow{grad}^T(N_i^e)\right\}.k(T).\overrightarrow{grad}(T)dv \\ &= -\sum_j (\int_{\Omega^e} \left\{\overrightarrow{grad}^T(N_i^e)\right\}.k(T).\overrightarrow{grad}(N_j^e)dv)T_j^e \end{aligned} \tag{2.29}$$

Using the Newton-Raphson, the tangent matrix generated is:

$$M_{ij}^{(k)} = -\frac{\partial R_i^k}{\partial T_j^e} = \begin{cases} \int_{\Omega^e} \overrightarrow{grad}^T(N_i^e).k.\overrightarrow{grad}(N_j^e)dv \\ + \int_{\Omega^e} \overrightarrow{grad}^T(N_i^e).\frac{dk}{dT}.\overrightarrow{grad}(N_j^e)dv \end{cases} \tag{2.30}$$

It is noted from the Eq. 2.30, appearance of a new term (second term) due to the effect of the dependence of the conductivity on temperature.

Note that the dependence of the material properties on the temperature can generate another characteristic time. Such as the nonlinear heat equation will have two cycle times: the first is related to the cycle time of the harmonic load applied and the second through the dependence of specific heat on temperature. This second cycle time can exist if the dependence has a sinusoidal form with a different cycle. To this end, it is important to understand the relationship of the different time scales that exist in the transient heat problem. These time scales might necessitate a very dense mesh for small characteristic time.

2.3 Discussion and conclusion

In this chapter, the governing equations for a 3D transient thermal problem are presented. The mathematical modeling of a 3D linear and non-linear transient thermal problem was highlighted and derived. To summarize, the presence of the non-linearity that can be generated from the physical

properties such as the specific heat was illustrated. This presence leads to the dependence of the capacitance and mass matrices on the temperature. Additionally, the characteristic times involved in the thermal problem are illustrated and discussed. To point out, two different time scales controlling this phenomenon are presented: the physical time τ_ϕ related to the material properties and the cycle time τ_c associated with the loading. To this end, the algorithm used in FEM to solve 3D transient linear and non linear problem is discussed.

The major outcomes of this chapter are:

- The model has two characteristic times (cycle time and physical time).
- The internal energy generated is related to the variation of the specific enthalpy with respect to time (transient case).
- The time integration scheme is an implicit incremental scheme.
- The non-linearity is solved with an iterative scheme. This scheme is referred to Newton method (in Abaqus) as detailed in Appendix A.3.

The next chapters aim to investigate the following points:

1. The behavior of the material under cyclic loading.
2. The effect of the characteristic times involved in transient problems in the behavior.
3. The effect of cyclic loading on the computation time.
4. The importance of using model reduction MOR, especially the Proper Generalized Decomposition (PGD) instead of the FEM in the context of the fatigue.

Chapter 3

PGD method to deal with 3D heat problem

—

Without data, you're just
another person with an opinion
Edwards Deming

Contents

3.1 Introduction 42
3.2 PGD solution of 3D transient thermal problem 42
3.2.1 Problem description 42
3.2.2 Progressive construction of the separated representation 42
3.3 Solution with an incremental scheme with FE framework 45
3.4 Numerical results 47
3.4.1 PGD for linear 3D thermal problem under cyclic loading 47
3.4.1.1 Influence of the physical time on the solution 47
3.4.1.2 Influence of the time discretization on the PGD solution 52
3.4.1.3 Influence of the spatial position 52
3.4.2 PGD for nonlinear 3D thermal problem under cyclic loading 53
3.4.2.1 DEIM-PGD combination for nonlinear problems 53
3.5 Conclusion 58

3.1 Introduction

In this chapter, the Proper Generalized Decomposition method (PGD) is presented. Such a non-incremental method is related to the construction of a separated representation of the unknown field [Chinesta *et al.*, 2013a], revealing valuable results in computational time-saving. To this end, the computational time-saving generated from the non-incremental solution is discussed first. Then, this chapter extends to study a cyclic transient 3D thermal problem involving different time scales under cyclic loading with emphasis on the effect of the different time scales and the spatial position [AL Takash *et al.*, 2019]. Finally, a linearization procedure has been extended to PGD framework to solve the non-linearity.

Thus, the main objectives of this chapter are listed as follows:

1. Overcome the huge time computation we may face with FEM.
2. Link the behavior of the material under cyclic load.
3. Understand the link between cycle time and physical time.
4. Shed lights on the effect of the spatial position.
5. Solve non-linear models using a combination of Proper Generalized Decomposition (PGD) and Discrete Empirical Interpolation Method (DEIM).

3.2 PGD solution of 3D transient thermal problem

3.2.1 Problem description

Consider a cube of side L subjected to a Robin boundary condition $\Phi = h(T - T_\infty)$ where Φ is the heat flux, h is the convection coefficient, T_∞ (surrounding temperature: environmental temperature) is cyclic (triangular form as shown in Fig. 3.1) with $\boldsymbol{R} = \frac{T_{min}}{T_{max}} = 0$ and a particular cycle time denoted by τ_c. In order to predict the temperature field $T(x, y, z, t)$ on the domain $\Omega = \Omega_x \times \Omega_y \times \Omega_z \times \Omega_t$, the thermal problem is written as follows:

$$\rho C_p \frac{\partial T}{\partial t} - k\Delta T - Q = 0 \tag{3.1}$$

where k is the thermal conductivity of the material used, ρ represents its density, and C_p its specific heat. Let us note that the heat source Q is assumed null in the studied simulations in this chapter.

Two different values of convection coefficient will be considered in the simulations: a convection coefficient $h_{vertical}$ in the direction of x and y, and a convection coefficient $h_{horizontal}$ in the z direction as shown in Fig. 3.2. Symmetry boundary conditions are considered (only a eighth of the cube is simulated).

3.2.2 Progressive construction of the separated representation

The three-dimensional thermal problem is written as follows:

$$\rho C_p \frac{dT}{dt} - k\left(\frac{\partial^2 T}{\partial^2 x} + \frac{\partial^2 T}{\partial^2 y} + \frac{\partial^2 T}{\partial^2 z}\right) - Q = 0 \tag{3.2}$$

A null initial condition is considered i.e $T(x, y, z, t = 0) = 0$. The boundary conditions are considered as follows:

1. Neumann condition at $x = \frac{L}{2}$ $(h_{vertical})$
2. Neumann condition at $y = \frac{L}{2}$ $(h_{vertical})$

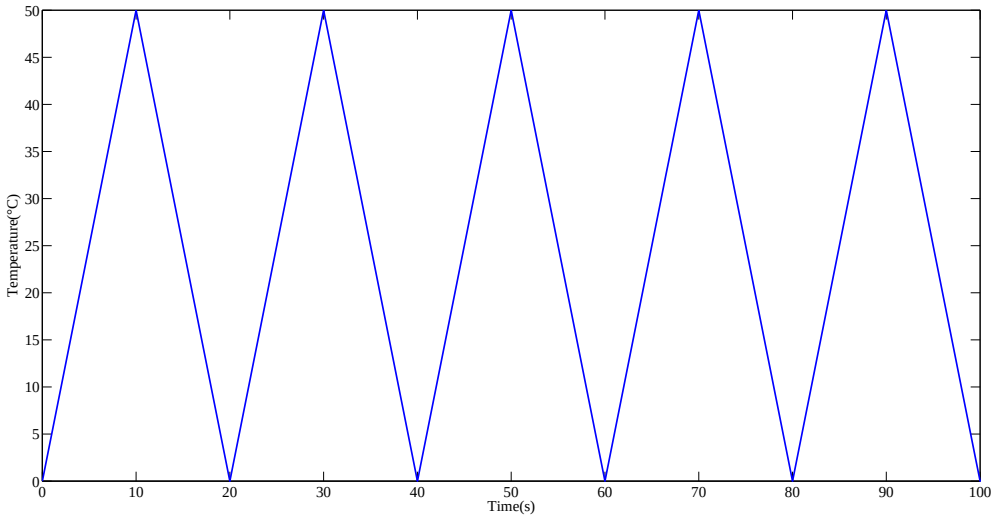


Figure 3.1: The first five cycles of the cyclic loading T_∞

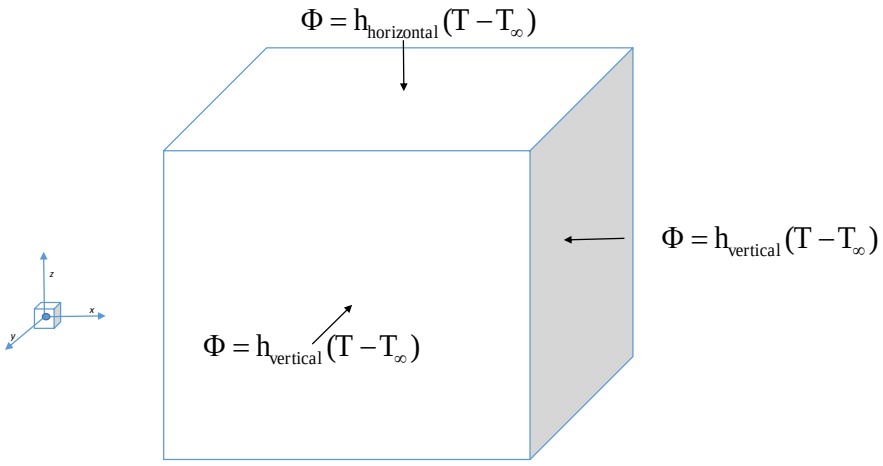


Figure 3.2: The boundary conditions applied to the model

3. Neumann condition at $z = \frac{L}{2}$ ($h_{horizontal}$)

4. Due to symmetry no heat flux in the symmetrical sides ($x = 0$, $y = 0$, $z = 0$).

The Neuman conditions are written as:
$\Phi_x = -k\frac{\partial T}{\partial x} = h_{vertical}(T(x = L/2, y, z) - T_\infty)$
$\Phi_y = -k\frac{\partial T}{\partial y} = h_{vertical}(T(x, y = L/2, z) - T_\infty)$
$\Phi_z = -k\frac{\partial T}{\partial z} = h_{horizontal}(T(x, y, z = L/2) - T_\infty)$

For all suitable test function T^*, the weighted residual form of Eq. 3.2 reads

$$\int_\Omega T^* \rho C_p \frac{dT}{dt} \mathrm{d}\Omega - k \int_\Omega T^* (\frac{\partial^2 T}{\partial^2 x} + \frac{\partial^2 T}{\partial^2 y} + \frac{\partial^2 T}{\partial^2 z}) \mathrm{d}\Omega = 0 \tag{3.3}$$

By taking into account the Robin condition, the Galerkin variational formulation can be written as follows:

$$\begin{aligned} &\int_\Omega T^* \rho C_p \frac{\partial T}{\partial t} \mathrm{d}\Omega + k \int_\Omega [(\frac{\partial T^*}{\partial x}\frac{\partial T}{\partial x} + \frac{\partial T^*}{\partial y}\frac{\partial T}{\partial y} + \frac{\partial T^*}{\partial z}\frac{\partial T}{\partial z})] \mathrm{d}\Omega \\ &+ \int_{S_{yz}\times\Omega_t} T^*(\frac{L}{2}, y, z, t)\ h_{vertical}(T(\frac{L}{2}, y, z, t) - T_\infty) \mathrm{d}y\mathrm{d}z\mathrm{d}t \\ &+ \int_{S_{xz}\times\Omega_t} T^*(x, \frac{L}{2}, z, t)\ h_{vertical}(T(x, \frac{L}{2}, z, t) - T_\infty) \mathrm{d}x\mathrm{d}z\mathrm{d}t \\ &+ \int_{S_{xy}\times\Omega_t} T^*(x, y, \frac{L}{2}, t)\ h_{horizontal}(T(x, y, \frac{L}{2}, t) - T_\infty) \mathrm{d}x\mathrm{d}y\mathrm{d}t = 0 \end{aligned} \tag{3.4}$$

The objective is to obtain a solution of Eq. 3.2 using PGD approximation in a separated form as written in Eq. 3.5:

$$T(x, y, z, t) = \sum_{i=1}^{N} F_i(x) G_i(y) H_i(z) U_i(t) \tag{3.5}$$

where N refers to the number of modes of the PGD solution. Each term of the expansion form is computed at each step of an iterative process. Thus, enriching the PGD approximation until a suitable convergence criterion is satisfied.

At each enrichment step n ($n \geq 1$) of the iterative process, the $n-1$ first terms of the PGD approximation are known:

$$T(x, y, z, t)^{n-1} = \sum_{i=1}^{n-1} F_i(x) G_i(y) H_i(z) U_i(t) \tag{3.6}$$

The objective is to compute the n^{th} mode $F_n(x)G_n(y)H_n(z)U_n(t)$ to obtain the enriched PGD solution. The solution is written as:

$$T(x, y, z, t) = \sum_{i=1}^{n-1} F_i(x) G_i(y) H_i(z) U_i(t) + F_n(x) G_n(y) H_n(z) U_n(t) \tag{3.7}$$

$F_n(x)$,$G_n(y)$, $H_n(z)$, and $U_n(t)$ are unknown at the current enrichment step n. To search the n^{th} mode, the resulting problem is non-linear due to the separated form of the solution and a suitable iterative scheme is required. The most used iterative scheme is an alternating direction strategy by starting an arbitrary guess T_n^0. The convergence is reached when Eq. 3.8 is satisfied where the non-linear iterations proceed until reaching a fixed point.

$$\frac{\left\| F_n^i(x) G_n^i(y) H_n^i(z) U_n^i(t) - F_n^{i-1}(x) G_n^{i-1}(y) H_n^{i-1}(z) U_n^{i-1}(t) \right\|}{\left\| F_n^{i-1}(x) G_n^{i-1}(y) H_n^{i-1}(z) U_n^{i-1}(t) \right\|} < \epsilon \tag{3.8}$$

where the index i refers to the iteration of the alternating direction strategy at enrichment step n. The enrichment process itself stops according to the following stopping criterion:

$$E = \frac{\|F_n(x).G_n(y).H_n(z).U_n(t)\|}{\|T^n\|} \tag{3.9}$$

The enrichment ends when $E < \epsilon^1$, $\|\|$ stands for the L^2 norm.

In the PGD, we choose to separate with respect to each coordinate x, y, z and t. Each iteration of the alternating direction scheme consists of the following 4 steps (equal to the number of coordinates):

1. Step 1: Calculating $F_n(x)$ from $G_{n-1}(y)$, $H_{n-1}(z)$,$U_{n-1}(t)$
2. Step 2: Calculating $G_n(x)$ from $F_n(x)$, $H_{n-1}(z)$,$U_{n-1}(t)$
3. Step 3: Calculating $H_n(z)$ from $F_n(x)$, $G_n(y)$,$U_{n-1}(t)$
4. Step 4: Calculating $U_n(t)$ from $F_n(x)$, $G_n(y)$,$H_n(z)$

For example for Step 1, the approximation reads:

$$T(x,y,z,t) = \sum_{i=1}^{n-1} F_i(x)G_i(y)H_i(z)U_i(t) + F_n(x)G_{n-1}(y)H_{n-1}(z)U_{n-1}(t) \tag{3.10}$$

where all functions are known except $F_n(x)$ The simplest choice for the weight function T^* in the weighted residual formulation Eq. 3.3 is

$$T(x,y,z,t)^* = F_n(x)^*G_{n-1}(y)H_{n-1}(z)U_{n-1}(t) \tag{3.11}$$

Once Eq. 3.11 is inserted in Eq. 3.4, the weighted residual form of a one dimensional problem over Ω_x can be solved. The discretization of the unknown functions followed by the integration (on the domain x, y ,z , and t) allows to obtain a linear system of the form represented in Eq. 3.12

$$[K]\{R\} = \{b\} \tag{3.12}$$

At each step of the alternating direction scheme, a linear system is solved to compute each function separately as shown in Appendix B. Note that the size of the linear system is equal to the number of discretization for a particular coordinate (e.g. x for Step 1).

The used version of the PGD method is the progressive one. At each enrichment step, the functions are normalized using L^2 norm and the solution is sought under the form:

$$T(x,y,z,t) = \sum_{i=1}^{N} \alpha_i F_i(x)G_i(y)H_i(z)U_i(t) \tag{3.13}$$

where F_i, G_i, H_i, U_i are the normalized functions and the coefficients α_i are computed through a projection step as detailed in [Chinesta *et al.*, 2016, Cueto *et al.*, 2016].

3.3 Solution with an incremental scheme with FE framework

In this section, the increase in the computation time to deal with cyclic loading is illustrated within the Finite Element framework. Let us note that the use of the FEM implies the use of an incremental scheme compared to the PGD method.
Two cases are investigated:

1. Case 1: Applying robin boundary condition as shown in Fig. 3.2 with $T_\infty = 25°C$ (constant load).

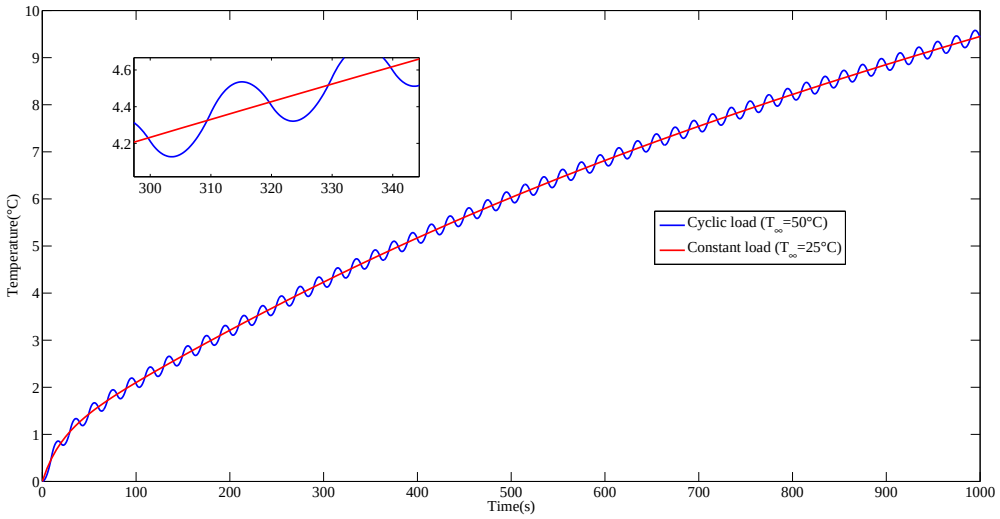


Figure 3.3: The evolution of temperature for constant load and cyclic load at $(x, y, z) = (25, 50, 25)$

2. Case 2: Applying robin boundary condition as shown in Fig. 3.2 where T_∞ is cyclic load with $T_{max} = 50°C$, $\boldsymbol{R} = 0$, $\tau_c = 20s$ and a triangular form as shown in Fig. 3.1.

The two cases are solved using ABAQUS (Finite Element commercial software).

It is important to realize the presence of one time scale (physical time: τ_ϕ) in case of a constant load is applied (case 1). However, another characteristic time is generated once a cyclic load is applied (case 2). Thus, in case 2 two time scales are present, one related to the cycle time (τ_c) and the other related to the physical time (τ_ϕ).

Remark. The physical time is defined as $\tau_\phi = \frac{\rho C_p}{k} L_c^2$, where L_c is the characteristic length. For our simulations, we choose L_c equals to $\frac{L}{4}$ where L is the length of the cube.

Two questions arise here:

1. What is the effect of the cyclic loading?
2. What is the effect of the new timescale on the computational time?

The simulation test is a cube of length $L = 100$mm with null initial condition. The time domain denoted by L_t is 1000s and the material properties are reported in Table 3.1. Particularly, the specific heat is chosen $C_p = 757\text{J.kg}^{-1}\text{.C}^{-1}$. Same spatial mesh has been used for both cases ($h = 5mm$). The time discretization for case 1 (constant load) is chosen based on the following criteria with the implicit scheme in case of the transient problem [Szabó, 2009]:

$$\frac{h^2 \rho C_p}{6 \times 0.5 \times k} \leq \Delta t \tag{3.14}$$

Then, $13.7 \leq \Delta t$, in this case $\Delta t = 14s$ has been chosen. However, for case 2 (cyclic load) due to the presence of cycle time and according to the convergence of the solution it is chosen $\Delta t = 0.5s$. Fig. 3.3 depicts the evolution of the temperature for the two cases (constant load and cyclic load). It shows that for constant load $T_\infty = 25°C$, the evolution matches the average of the evolution obtained from the cycle load with $T_{max} = 50°C$.
Markedly, the computation time has been increased in case of the cyclic load compared to the constant load case (of order 27) for a given spatial mesh as shown in Fig. 3.4. In fact, this is explained by the presence of different time scales - related to the thermal characteristic time and the cycle

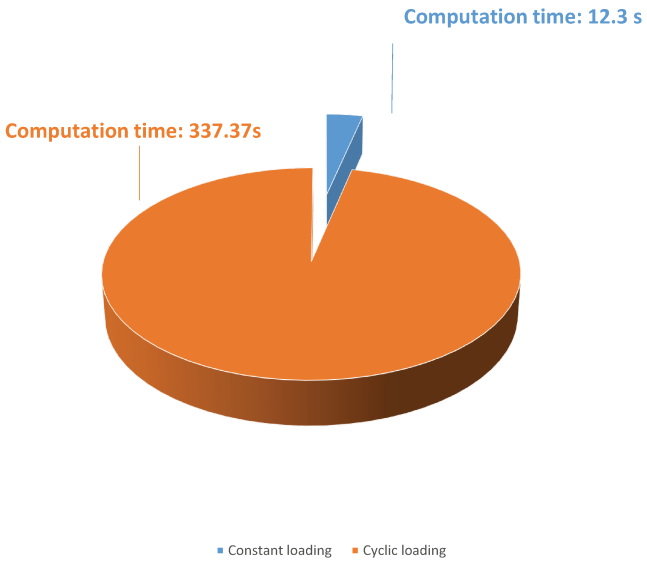


Figure 3.4: The computation time for case of cyclic loading and constant loading with the FEM using Abaqus software.

time - thus, the mesh will be dense as required by the phenomenon for the smallest characteristic time (in this case, the cycle time). This will lead to a large computation time within the classical Finite Element Method (FEM). Moreover, a large number of cycles is needed to reach the stabilized cycle under fatigue which may also generate a prohibitive and huge computation time. Thereupon, in case of fatigue, the computation time will increase.

Thus, PGD method will be used. The PGD has already been studied in the case of creep load by different authors for example Hammoud el al. [Hammoud *et al.*, 2014] leading to a large time saving compared to FEM for a good accuracy (around 31 for creep load). Moreover, the usage of PGD in the case of fatigue is well discussed in the previous chapter (chapter 1).

Can we obtain a large time saving with PGD when a cyclic load is applied? Could the PGD method capture the cyclic effect? In what follows, PGD method is used to solve a thermal problem to predict linear and nonlinear problem under fatigue. In the first place, the time saving obtained with PGD is discussed.

3.4 Numerical results

3.4.1 PGD for linear 3D thermal problem under cyclic loading

3.4.1.1 Influence of the physical time on the solution

The simulation test is a 100 mm long three-dimensional cube subjected to cyclic heat flux at all sides, with null initial condition. Symmetry boundary conditions are applied and the other surfaces are under Neumann condition. The model encounters a cyclic load with amplitude $(50°C)$. The time domain is denoted by L_t equals 1000 s which leads to consider 50 cycles (20s/cycle). The material properties are reported in Table 3.1. The values for the stopping criteria for the PGD are: $\epsilon = 10^{-3}$ (fixed point) and $\epsilon_1 = 10^{-3}$(enrichment).

Remark. To deal with different physical times, the specific heat is considered variable. Table 3.2

ρ	k	$h_{vertical}$	$h_{horizontal}$	T_∞
950 $(\mathrm{kg.m^{-3}})$	0.45($\mathrm{W.m^{-1}{}^\circ C^{-1}}$)	4.6($\mathrm{W.m^{-2}.K^{-1}}$	6.36$\mathrm{W.m^{-2}.K^{-1}}$)	$T_{min} = 0^\circ\mathrm{C}, \mathrm{T_{max}} = 50^\circ\mathrm{C}$

Table 3.1: Material properties and boundary conditions

$C_p(\mathrm{J.kg^{-1}.C^{-1}})$	0.075	7.5	757
$\tau_\phi(\mathrm{s})$	0.1	10	1000

Table 3.2: The physical time τ_ϕ with respect to the specific heat coefficient C_p

lists the physical time with respect to the specific heat.

Three different physical times are investigated:

1. Case 1: $\tau_\phi = 0.1s$ less than the cycle time $\tau_c = 20s$
2. Case 2: $\tau_\phi = 10s$ same order of the cycle time $\tau_c = 20s$
3. Case 3: $\tau_\phi = 1000s$ larger than the cycle time $\tau_c = 20s$

Remark. The relative error is computed using the following equation for all cases:

$$E(\%) = \frac{\|T_{PGD} - T_{ref}\|}{\|T_{ref}\|} \times 100 \tag{3.15}$$

where T_{ref} is the FEM solution, T_{PGD} is the full PGD solution, and $\| \ \|$ is the L^2 norm.

Case 1: Let us consider a problem where $\tau_\phi = 0.1s$ is smaller than the cycle time $\tau_c = 20s$. Fig. 3.5 depicts the evolution of temperature for $\tau_\phi = 0.1s$ with respect to time using the PGD and compared to FEM solution. Interestingly, PGD method leads to an accurate solution with a relative error less than 0.4% as shown in Table 3.5 compared to the FEM solution with same spatial step ($h = 5mm$) and same time step ($\Delta t = 0.1s$) are used. Importantly, 10 modes (space and time modes) as summarized in Table 3.3 were needed to generate this accurate solution.
With attention to the stabilized cycle, it is noticed that the stabilized cycle is quickly reached. This can be explained by the high thermal diffusivity (low physical time).

Case 2: Comparatively, when $\tau_\phi = 10s$ is in the same order of the cycle time $\tau_c = 20s$ the solution is depicted in Fig. 3.6, where same spatial step ($h = 5mm$) and same time step ($\Delta t = 0.2s$) are used for both solutions. It is worth noting that there is an agreement between both solutions (PGD and FEM solution) with a relative error less than 0.4%. In this case, a greater number of modes is required (40 modes) as seen in Table 3.3 since the solution is composed by two parts: a transient and a stationary parts.
The stabilized cycle is attained after 4 cycles as shown in Fig. 3.6.

Case 3: When $\tau_\phi = 1000s$ is larger than the cycle time, the stabilized cycle is not reached at the end of the simulation due to the low thermal diffusivity (high physical time). The temperature evolves very slowly in this time scale ($\tau_\phi = 1000s$), more than 50 cycles are required to reach the stabilized cycle. The solution is obtained with 50 modes using the PGD as illustrated in Table 3.3. The solution obtained with PGD is compared to the FEM one in Fig. 3.7, where same spatial step ($h = 5mm$) and same time step($\Delta t = 0.5s$) are used. It reveals an accurate solution with a relative error less than 0.6%.
Importantly, the number of cycles needed in this case are more than 1800 cycles to reach the stabilized cycle as shown in Fig. 3.8 once a large time domain is used $L_t = 40000s$, it is worth noted

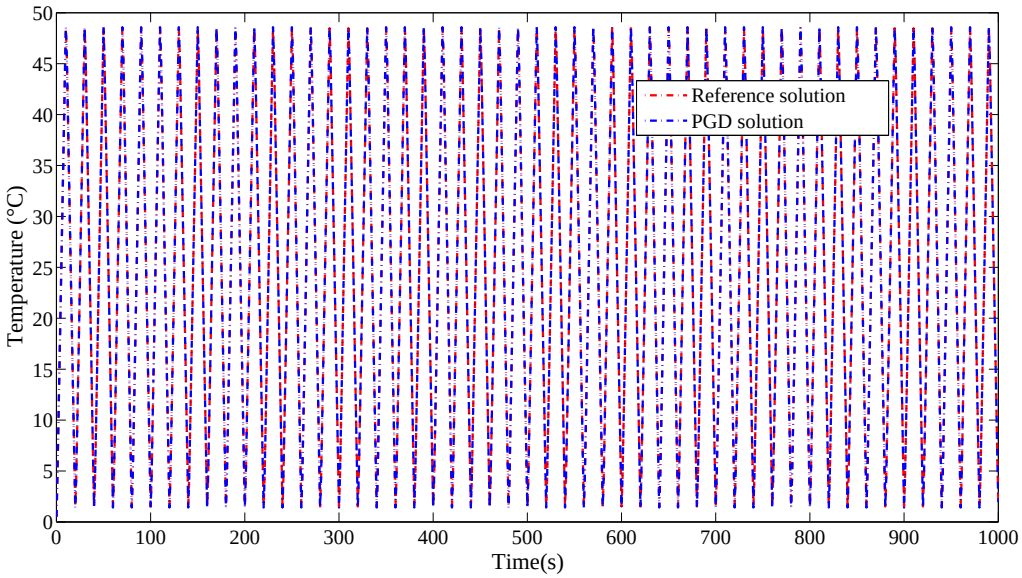


Figure 3.5: The evolution of the temperature under cyclic load $\tau_c = 20s$ (50 cycles) with $\tau_\phi = 0.1s$ at $(x, y, z) = (25, 25, 50)$

τ_ϕ	Number of modes
0.1	10
10	40
1000	50

Table 3.3: Number of modes with respect to the physical time

that the average solution at the end of this simulation is equal to $25°C$.

Three different behaviors due to the characteristic time have been noticed and illustrated. Thus, PGD method allows predicting the behavior of the heat problem under cyclic loading. The number of PGD modes depends on the physical time. In case of transient state ($\tau_\phi = 1000s$), a higher number of modes is required than the other states. Fig. 3.9 presents the 10 spatial and time modes that are used to construct the solution of case 3. It is noticed that:

1. The spatial modes are different

2. The modes components $F_i(x)$ and $G_i(y)$ are the same. This can be explained by the same convection coefficient in x and y directions. However it is noticed that the $H_i(z)$ is different by magnitude since the convection coefficient is different (for example at position $x = 10mm$, $F_i(x = 10) = -1.02$, $G_i(y = 10) = 1.02$ and $H_i(z = 10) = 0.06124$).

3. The time modes are composed of a deviation and a periodic function. Large value of $\tau_\phi = 1000$ implies important deviation of the time modes.

Under those circumstances, PGD leaded to accurate results compared to FEM. A time-saving is obtained using PGD compared to the FEM as illustrated in Table 3.4 with a relative error for all the cases less than 0.6% as summarized in Table 3.5 for different spatial points.

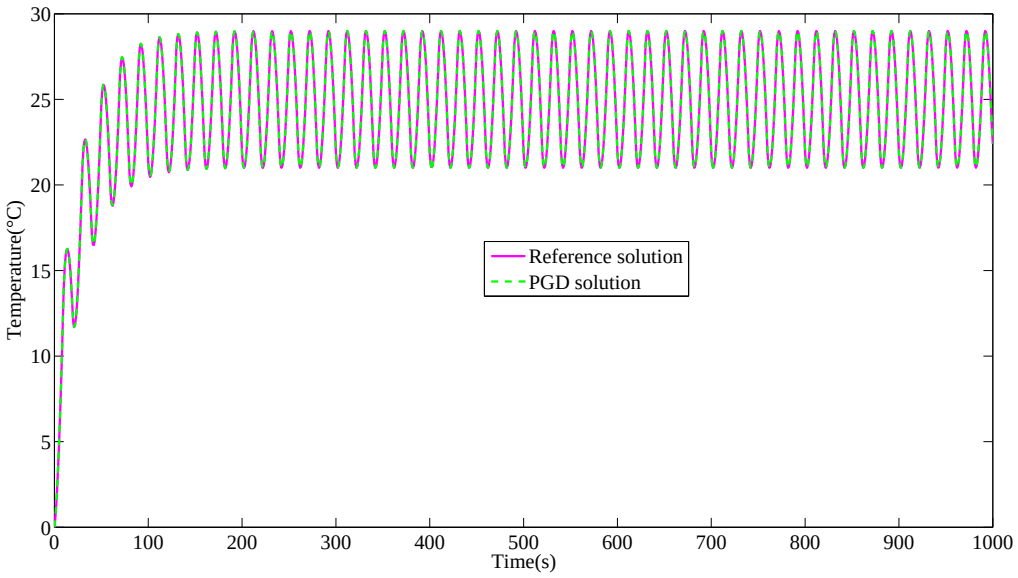


Figure 3.6: The evolution of the temperature under cyclic load $\tau_c = 20s$ (50 cycles) with $\tau_\phi = 10s$ at $(x, y, z) = (25, 25, 50)$

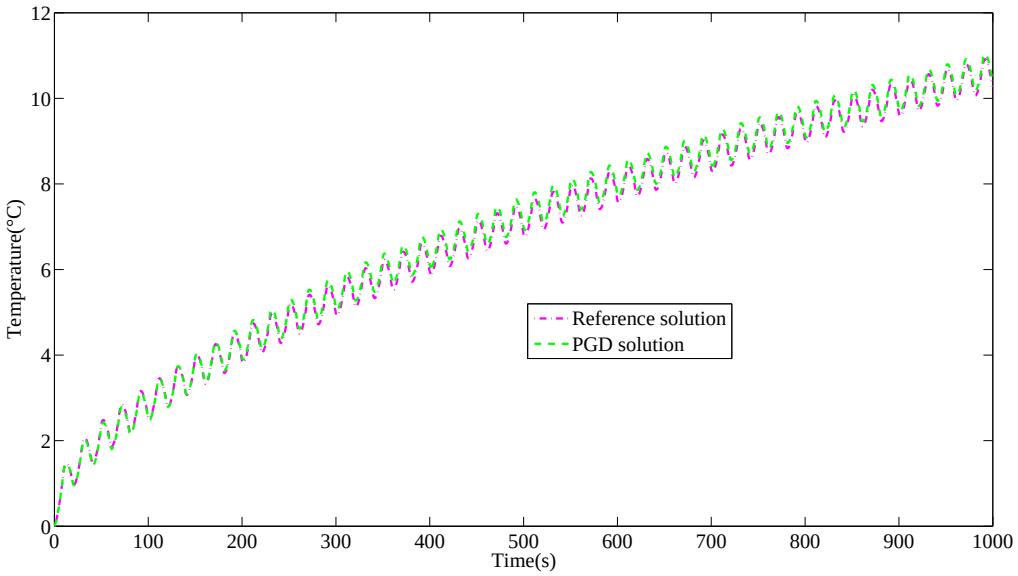


Figure 3.7: The evolution of the temperature under cyclic load $\tau_c = 20s$ (50 cycles) with $\tau_\phi = 1000s$ at $(x, y, z) = (25, 25, 50)$

τ_ϕ	CPU(FEM)	CPU(PGD)	Time-saving ratio
0.1	1342.2	8.48	158.51
10	780	9.89	78.86
1000	373.31	16.75	22.28

Table 3.4: Time saving PGD VS FEM ratio with respect to the physical time

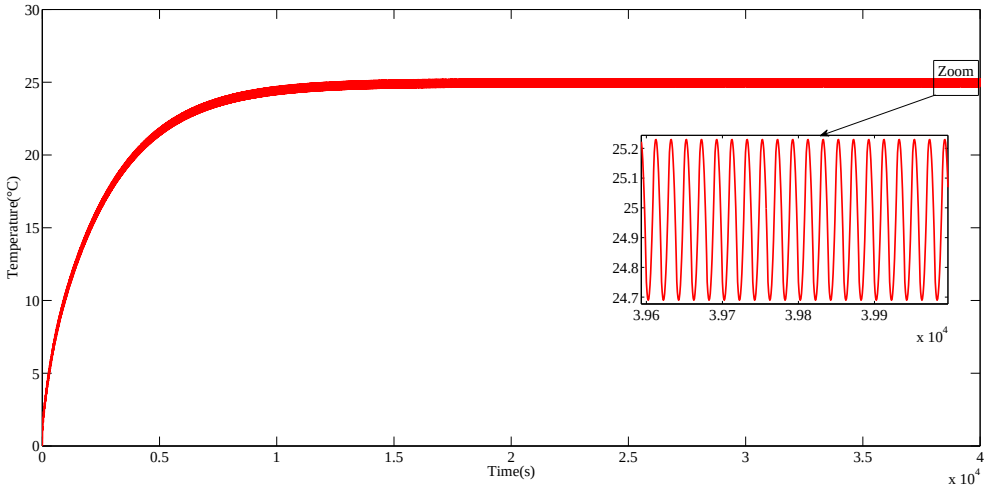


Figure 3.8: The evolution of the temperature under cyclic load $\tau_c = 20s$ (2000 cycles) and $L_t = 40000s$ with $\tau_\phi = 1000s$ at $(x, y, z) = (25, 25, 50)$

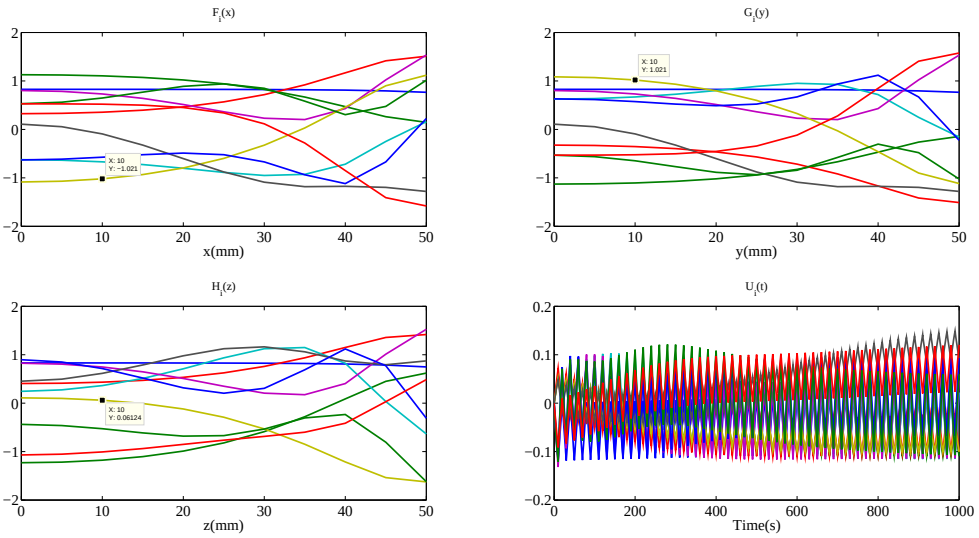


Figure 3.9: The partition of the first 10 modes in x, y, z and t dimensions for $\tau_\phi = 1000s$

Spatial point (x,y,z)	$(25, 25, 25)$	$(25, 25, 50)$	$(37.5, 37.5, 37.5)$	$(37.5, 12.5, 37.5)$
Relative error for case 1 (%)	0.15	0.23	0.35	0.25
Relative error for case 2 (%)	0.34	0.32	0.36	0.3
Relative error for case 3 (%)	0.45	0.51	0.56	0.47

Table 3.5: The relative error calculated for different points for the three linear cases

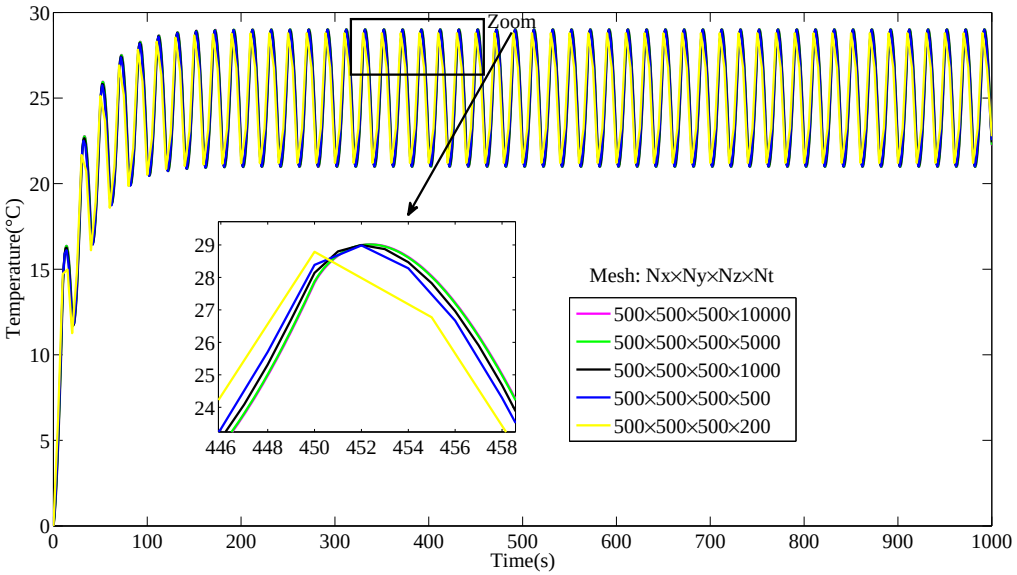


Figure 3.10: The evolution of the temperature for $\tau_\phi = 10s$ using different time discretization $(x, y, z) = (25, 25, 50)$

$\tau_\phi(s)$	0.1	10	1000
Nt	8000	5000	2000

Table 3.6: Appropriate time discretization

3.4.1.2 Influence of the time discretization on the PGD solution

As the considered time domain will be larger than the one used here ($L_t = 1000s$), can we limit the computation time by considering an adapted time discretization depending on the physical time? For this purpose, the three different cases $\tau_\phi = 0.1$, $\tau_\phi = 10$, $\tau_\phi = 1000s$ are considered for different time discretizations denoted by $\Delta t = \frac{L_t}{N_t}$ where N_t is the number of time intervals. These time discretizations related to the cycle time $\tau_c = 20s$ are as follows: $N_t = [10000, 5000, 1000, 500, 200]$ they represent $[200, 100, 20, 10, 4]$ points per cycle, respectively. Consider the example of $\tau_\phi = 10s$. Fig. 3.10 depicts the evolution of temperature for a fixed point using different time discretization. Notably, the general shape of the evolution of temperature is similar for all time discretizations, specifically when the number is larger than 25 points per cycle. With this intention, the zoom in Fig. 3.10 of the evolution showed that for coarse discretization a phase shift between the fine and coarse scale has been noticed. However, this showed that $N_t = 5000$ an intermediate discretization for the case of $\tau_\phi = 10s$ is required. However, for $\tau_\phi = 1000s$, Fig. 3.11 depicts the evolution of the temperature for a fixed point using different time discretization. It is noticed that $N_t = 2000$ can be used to generate an accurate solution. In case $\tau_\phi = 0.1s$, $N_t = 8000$ is required.
Thus, time discretization depends on the physical time (τ_ϕ) and the cycle time (τ_c). Once the physical time is small, a fine discretization is required, leading us to conclude that fine discretization is required when the physical time decreases as summarized in Table 3.6.

3.4.1.3 Influence of the spatial position

As the spatial position affects the evolution of the temperature, we will analyze whether the spatial position is linked to the timescales or not. Three cases are investigated:

1. Case 1: $\tau_\phi = 0.1s << \tau_c = 20s$

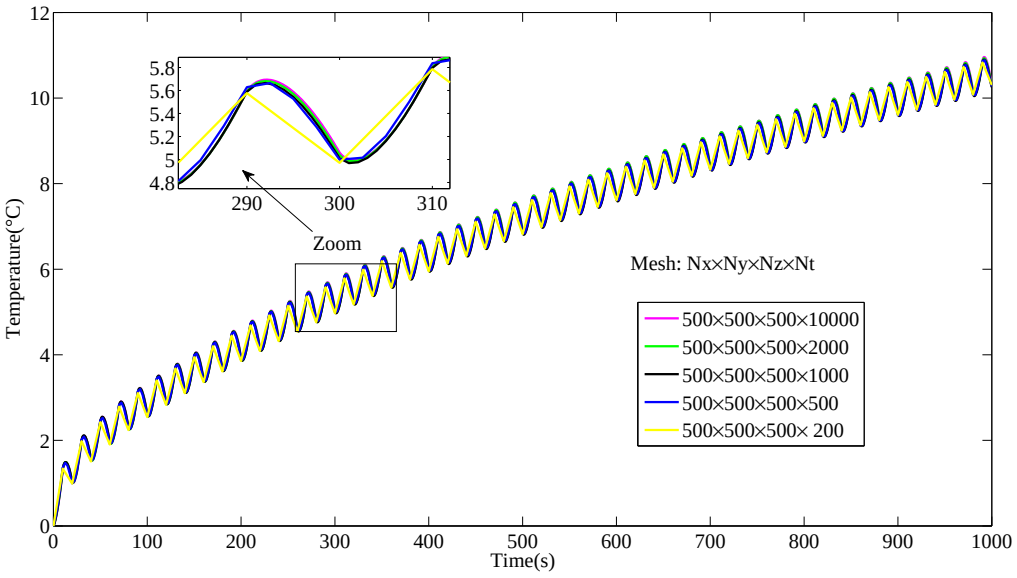


Figure 3.11: The evolution of the temperature for $\tau_\phi = 1000s$ using different time discretization $(x, y, z) = (25, 25, 50)$

2. Case 2: $\tau_\phi = 10s \approx \tau_c = 20s$
3. Case 3: $\tau_\phi = 1000s >> \tau_c = 20s$

Case 1: When $\tau_\phi << \tau_c$, it is noticed from Fig. 3.12(a) that regardless of the spatial position, the evolution of the temperature is very fast. Where the results match together in the three different positions. Thus, the effect of spatial position is less important in case the physical time is less than the cycle time. This confirms that small physical time leads to high thermal diffusivity, consequently, the stabilized cycle is attained quickly.

Case 2: τ_ϕ is the same order as the cycle time. As it can be seen in Fig. 3.12(b), the stabilized cycle is attained after a certain time for all the spatial positions. Accordingly, the effect of the spatial position is noticed with the amplitude of the temperature at each point. With this in mind, the amplitude decreases far from the boundary.

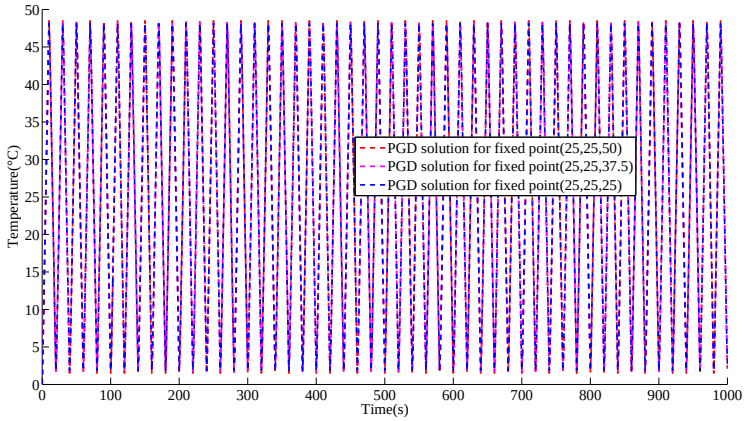
Case 3: In case $\tau_\phi >> \tau_c$, the first thing to remember is that the stabilized cycle is not reached at the end of the simulation. To emphasize, it is noticed from Fig. 3.12(c), that for the first spatial position (25,25,50) located at the boundary the stabilized cycle is not reached. Additionally, for the other points far from the boundary, it is noticed that the cyclic effect is negligible. This indicates that the amplitude and the behavior are affected far from the boundary.

Thus, the relaxation time affects the evolution of temperature. It can be concluded the relaxation time is small, the evolution is fast in all the domain. However, in the case of high relaxation time the effect of cyclic load starts to be negligible as we go far from the boundary.

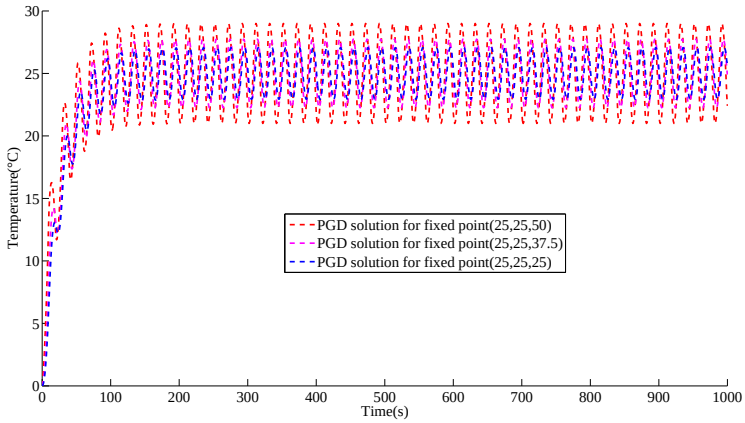
3.4.2 PGD for nonlinear 3D thermal problem under cyclic loading

3.4.2.1 DEIM-PGD combination for nonlinear problems

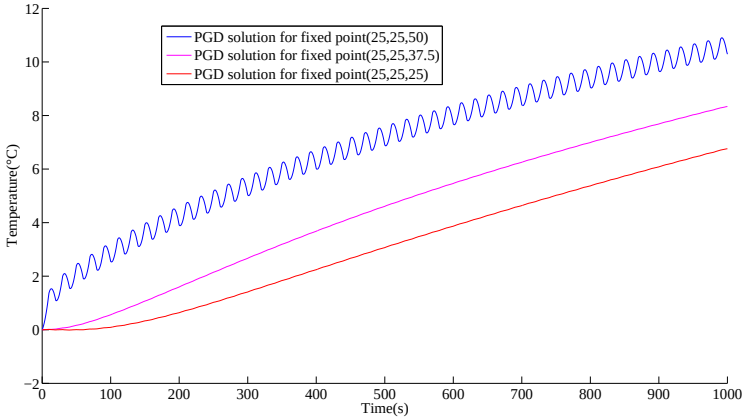
Among the Model Order Reduction methods, the Proper Generalized Decomposition (PGD) showed its efficiency to solve linear problems in the time domain. In this section, the non-linearity due to the material properties is introduced. Thus, a linearization technique is required. This technique



(a) Different spatial position with $\tau_\phi = 0.1s$ and $\tau_c = 20s$



(b) Different spatial position with $\tau_\phi = 10s$ and $\tau_c = 20s$



(c) Different spatial position with $\tau_\phi = 1000s$ and $\tau_c = 20s$

Figure 3.12: The evolution of temperature for different spatial positions with respect to the physical time

is based on the Discrete Empirical Interpolation Method (DEIM) [Aguado *et al.*, 2013]. The PGD method is combined with DEIM to solve a 3D nonlinear transient problem, where the nonlinear term is interpolated using the reduced basis. The combination of DEIM-PGD is not detailed in this thesis as it is only used. This method has been developed in the thesis of Aguado Jose [Aguado, 2015].

Let us consider the dependence of the specific heat on the temperature. Thus Eq. (3.1) can be written as follows:

$$\rho C_p(T)\frac{\partial T}{\partial t} - k\Delta T = 0 \tag{3.16}$$

Steps to proceed to solve the non-linearity:

1. Solve the linear problem.
2. Select a set of points (magic points).
3. Interpolate the nonlinear terms using these selected points.
4. The solution T^{k+1} is constructed where the index k refers to the nonlinear iteration.
5. The first three steps (1-2-3) are repeated until a convergence criteria ($\frac{\|T^{k+1}-T^k\|}{\|T^k\|} < \epsilon$) is reached ($\epsilon = 10^{-3}$).

Remark. The detailed algorithm of the DEIM based PGD is discussed in Chapter 1 and the interested reader can refer to [Aguado, 2015] for further details.

Consider a cube of side L subjected to a Robin boundary condition $\phi = h(T - T_\infty)$, where T_∞ is cyclic as shown in Fig. 3.1 with $\tau_c = 20s$. Same material properties as the linear case are considered. However, the specific heat is a temperature dependent. The form of specific heat is considered linear as follows:

$$Cp = a \times T + b \tag{3.17}$$

where a and b are constants to be chosen.
Three cases are considered:

1. Case 1: $C_p = 9.2 \times T + 1366.6$.
2. Case 2: $C_p = T + 25$.
3. Case 3: $C_p = 27 \times T + 25$.

Case 1 Note that the form of this non-linearity has been used in [Nguyen, 2013].
Fig. 3.13 depicts the evolution of the temperature for case 1. It is worth noting that the transient state is generated due to the high physical time. Indeed, regardless the value of T, Cp has a minimum value of 1366.6 J.kg^{-1}.C^{-1}, which leads to high physical time.
2 iterations are needed to generate a solution with a relative error less than 0.5% compared to the reference solution.

Case 2 Depending on the maximum value of temperature applied ($T_{max} = 50°C$), the specific heat has a maximum value $C_p = 75$ J.kg^{-1}.C^{-1} leading to physical time ($\tau_\phi = 100s$) which generates a solution composed of transient and stationary. Henceforth, Fig. 3.14 depicts the evolution of the temperature for case 2. The solution consists of two parts (transient and stationary). Accordingly, 3 iterations are needed to generate a solution with a relative error less than 0.5%.

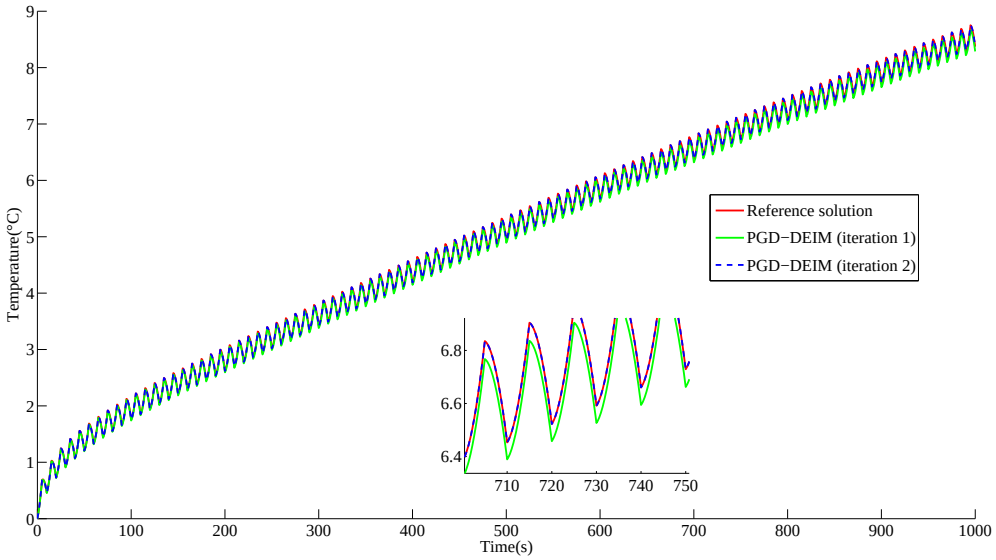


Figure 3.13: Temperature evolution for case 1 $Cp = 9.2 \times T + 1366.66$

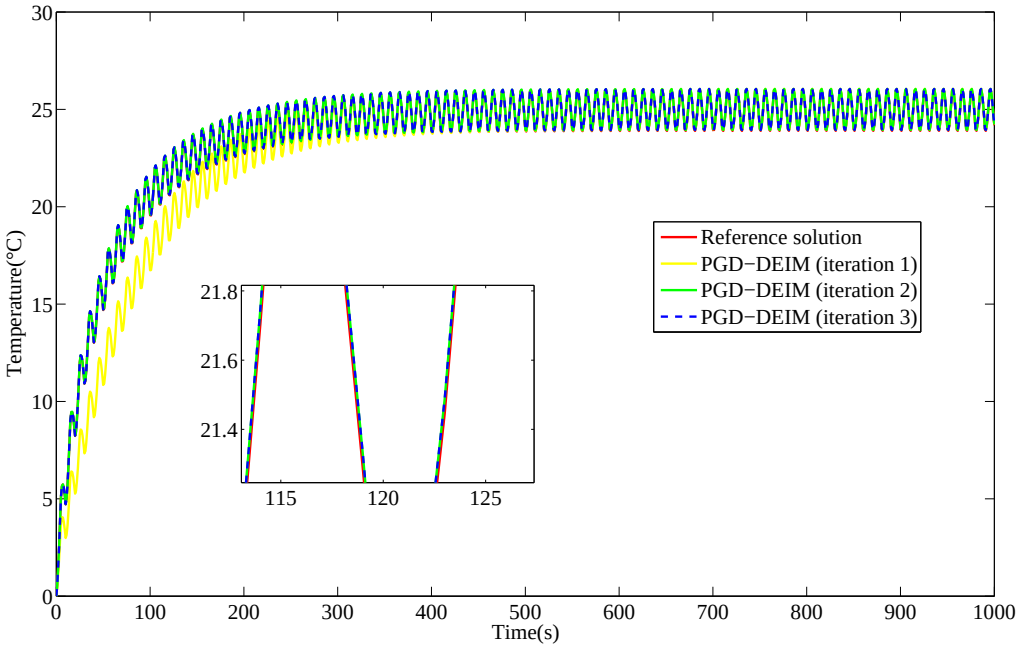


Figure 3.14: Temperature evolution for case 2 $Cp = T + 25$

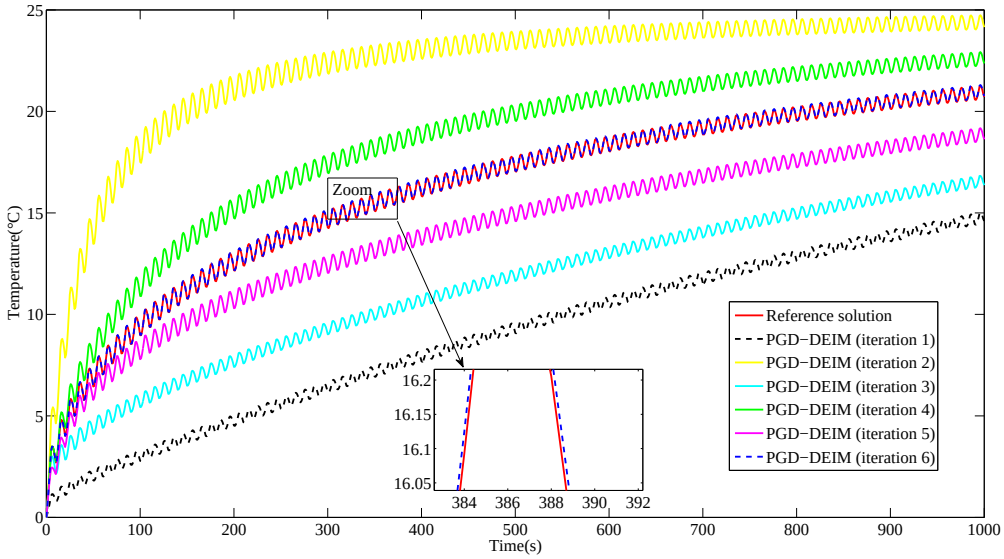


Figure 3.15: Temperature evolution for case 3 $Cp = 27 \times T + 25$

Cases	Case 1	Case 2	Case 3
Number of Iterations	2	3	6
Time saving PGD VS. FEM	50.94	50.57	12.55

Table 3.7: Number of the Iterations and time-saving for the different non-linear cases

Case 3 The form of $C_p = 27 \times T + 25$ generates two different behaviors. When $T = 0$, the specific heat is $C_p = 25\ \mathrm{J.kg^{-1}.C^{-1}}$ which generates a small physical time and a stationary behavior. However, when the temperature is maximum, $C_p = 1375\ \mathrm{J.kg^{-1}.C^{-1}}$ leads to high physical time with a transient behavior. Thus, the solution is a combination of two different time scales (high physical time and low physical time). To illustrate, Fig. 3.15 pinpoints the evolution of the temperature for case 3. Notably, the solution tends to reach the stabilized cycle which is not the same as case in 1 where a high transient solution is generated. Importantly, 6 iterations are needed to generate a solution with a relative error less than 0.6%.

As a summary, the number of iteration increases as the specific heat varies between two different values (high and small). Table 3.7 depicts the number of iteration for each case. It is clear that for case 3, 6 iterations are needed since the behavior is different (behavior with high physical time and behavior with low physical time). A time saving is obtained compared to FEM of order 12 for case 3.The relative error for different points for the three different cases is summarized in Table 3.8.

Remark. Another kind of nonlinearity has been evaluated: the dependence of the convection coefficient on temperature. Good results have been obtained. Showing the ability of the PGD coupled with DEIM to solve nonlinear thermal problems.

Spatial point (x,y,z)	$(25, 25, 25)$	$(25, 25, 50)$	$(37.5, 37.5, 37.5)$	$(37.5, 12.5, 37.5)$
Relative error for case 1 $(\%)$	0.44	0.4	0.41	0.4
Relative error for case 2 $(\%)$	0.45	0.42	0.4	0.46
Relative error for case 3 $(\%)$	0.55	0.53	0.57	0.55

Table 3.8: The relative error calculated for different points for the three non-linear cases

3.5 Conclusion

This chapter has revealed that the PGD approach can be extended to a 3D cyclic transient problem leading to a time-saving of order 30 compared to FEM. Equally important, this chapter illustrates the results obtained with the DEIM-based PGD technique [Aguado *et al.*, 2013] to solve the non-linearity generated from the dependence of the material properties on the temperature. The findings of this chapter indicate that PGD can capture the different behaviors generated from the different time scales.

The efficiency of the PGD method was investigated using two different characteristic times: the cycle time of the loading applied and the physical time related to the material properties. The investigations showed three different behaviors. Remarkably, the stabilized cycle obtained after a number of cycles when the characteristic times are of the same order. However, it was obtained directly in a unique case when the physical time is less than the cycle time. However, the stabilized cycle is not reached in case the physical time is higher than the cycle time.

Moreover, a way to decrease the computation time was presented, by decreasing the number of time discretizations depending on the physical time. For example, for the high physical time a coarse time discretization can be used which is not the case when we have small physical time. Also, the effect of the spatial position with respect to the physical time showed that for high physical time, the cyclic effect vanishes as we are far from the boundaries (where the load is applied) due to the low evolution of temperature when we have a low diffusivity. Let us note that same responses as in the 1D viscoelastic case [Hammoud *et al.*, 2014] have been obtained.

Finally, this chapter showed the capacity of the PGD to solve the nonlinear 3D thermal problem with a time-saving of order 20. Yet, the question arises here how to obtain more time-saving using the MOR? Two different approaches in the following chapters will be addressed with the aim of obtaining significant time-saving for cyclic transient thermal problems.

Chapter 4

Numerical approach based on the collection of the most significant modes to solve cyclic transient thermal problems involving different time scales

—

All of science is nothing more than,
the refinement of everyday thinking.
Albert Einstein

Contents

4.1 Introduction . . . 62
4.2 Presentation of the method . . . 62
4.3 Algorithm . . . 63
4.3.1 Problem description . . . 63
4.3.2 Creation of the dictionary and algorithm of the proposed approach . . . 63
4.4 Numerical results . . . 66
4.4.1 Dictionary 1 for a fixed cycle time and different physical times . . . 66
4.4.1.1 Dictionary creation . . . 66
4.4.1.2 Dictionary evaluation . . . 69
4.4.2 Dictionary 2 for fixed physical time and different cycle times . . . 73
4.4.2.1 Dictionary creation . . . 73
4.4.2.2 Dictionary evaluation . . . 75
4.5 Extension to many harmonics . . . 77
4.5.1 Dictionary evaluation . . . 79
4.6 Extension to coupled problems . . . 81
4.6.1 Problem description . . . 82
4.6.2 Algorithm of the coupled thermo-diffusion problem . . . 83
4.6.3 Dictionary evaluation of the thermo-diffusion problem . . . 84
4.7 Conclusion . . . 85

4.1 Introduction

The present work focuses on dealing with models that involved different characteristic times. In chapter 3, it was shown that 3D thermal problems under cyclic thermal loads present a similar behavior as the viscoelastic phenomena. Moreover, it has been proved the ability of the PGD method to solve 3D thermal problems under cyclic loading with time saving of order 50 compared to the FEM (PGD with a decomposition $x \times y \times z \times t$). Let us note that for viscoelastic study, more time scales are needed, and thus more time consuming. The following question arises: Is it possible to achieve more time saving by using MOR? To answer this question, a dictionary of the most significant spatial and temporal modes, with respect to energy, generated using the PGD method will be developed [AL Takash *et al.*, 2018]. In this particular context, another question is noticed: Can this dictionary be used widely for problems with various characteristic times, cycle times, boundary conditions? In order to answer these questions, the major issues of this chapter are:

1. Prove accuracy when using significant modes only.

2. Validate the usage of the collection of the significant modes for problems with different parameters.

3. Discuss the ability of this approach in case of cycle time.

4. Check the computation time saving by using the significant modes for cyclic load.

4.2 Presentation of the method

In the case of cyclic thermal problem, the different responses are related to the presence of different characteristic times: physical time and cycle time. Yet, is it possible to establish a dictionary of significant modes that can be used for a family of problems?
The idea of our approach is to construct a dictionary of significant modes generated from PGD modes taken together as a priori modes for different problems. The originality lies on the fact that space-time modes are used whereas only spatial modes are considered in the POD.

Let us start by investigating the steps to obtain an efficient collection of modes:

- As preliminary step, solutions for different given time scales (physical time and cycle time) are searched. The physical time is defined as $\tau_\phi = \frac{\rho C_p}{k} L_c^2$ where ρ is the density, k is the conductivity and C_p is the specific heat, and L_c is a characteristic length. Each physical time (or cycle time) leads to a different response. With this in mind, the idea is to find the solution for a physical time range (or cycle time range) with defined significant modes.

- The significant modes are then collected. First, these significant modes are tested by rebuilding the direct solution using these modes (space-time modes). Straightaway, a collection of significant modes is built.

- Then, a solution in the same family with new time scale is searched within the different time scales and boundary conditions. In this step, the modes are a priori known and a projection of the solution on a discrete basis (generated by the significant modes) is done to calculate the coefficients of projection denoted by $(\alpha) = (\alpha_i)$ in this chapter for each mode i.

- Finally, the solution is built by using the calculated coefficients (α_i) and a priori modes.

Fig. 4.1 depicts the procedure to collect the significant modes. The dictionary is here composed of the significant modes deduced from 3 different cases. Each case is denoted by j where D_j contains the n_j most significant modes. The number n_j will be specified in subsection 4.3.2.

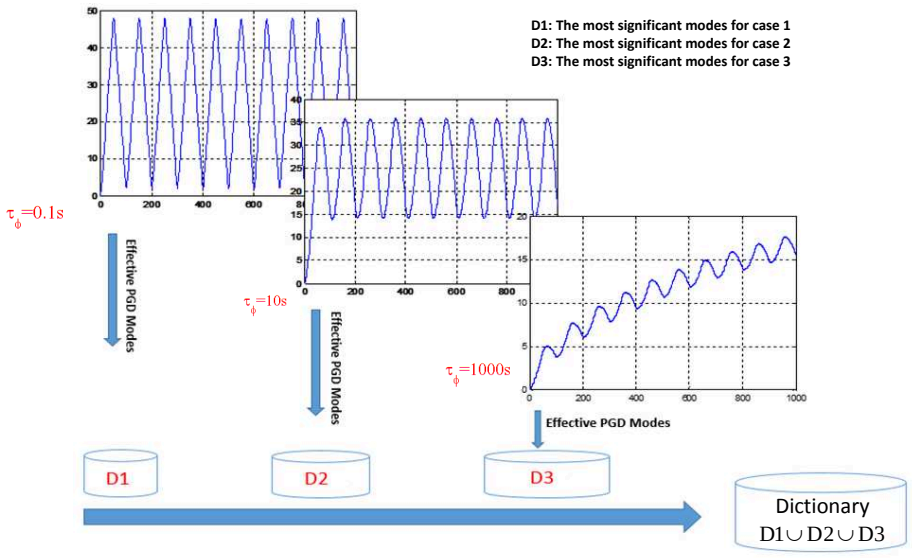


Figure 4.1: Creation of the dictionary issued from 3 different cases

4.3 Algorithm

4.3.1 Problem description

Consider a cube of side L subjected to a Robin boundary condition $\Phi = h(T - T_\infty)$ where Φ is the heat flux, h is the convection coefficient, T_∞ is cyclic (triangular form). In order to predict the temperature field $T(x, y, z, t)$ on the domain $\Omega = \Omega_x \times \Omega_y \times \Omega_z \times \Omega_t$, the thermal problem is written as follows:

$$\rho C_p \frac{\partial T}{\partial t} - k\Delta T = 0 \tag{4.1}$$

where k the conductivity coefficient is supposed constant in the domain. Let us note that the heat source is assumed null. The initial condition is supposed to vanish. Two different values for the convection coefficient will be considered in the simulations: a convection coefficient $h_{vertical}$ in the direction of x and y and a convection coefficient $h_{horizontal}$ in the z direction. Symmetry boundary conditions are considered.

4.3.2 Creation of the dictionary and algorithm of the proposed approach

The first step of our approach consists in creating the dictionary. The dictionary is composed by the significant modes of particular cases. Let us consider the illustrative example of Fig. 4.1 where the dictionary is composed by 3 cases. To determine the most significant modes, the procedure is as follows:

- The solution of each case j is computed by the PGD method where each solution $T^j(x, y, z, t)$ is sought under a separated representation given in Eq. (4.2). Let us recall that each space-time mode $F_i^j(x)G_i^j(y)H_i^j(z)U_i^j(t)$ is not known a priori but constructed through an iterative procedure. The interested reader can refer to [Ammar *et al.*, 2006]. Let us keep in mind that each function of the mode ($F_i^j(x)$, $G_i^j(y)$, $H_i^j(z)$ and $U_i^j(t)$) is normalized with respect to the L^2 norm in the usual PGD algorithm.

$$T^j(x, y, z, t) = \sum_{i=1}^{N^j} \alpha_i^j F_i^j(x)G_i^j(y)H_i^j(z)U_i^j(t) \tag{4.2}$$

- For each integer j among the N^j modes of the full PGD solution $T^j(x,y,z,t)$, the most significant modes are selected such as

$$\frac{\mid \alpha_i^j \mid}{\max\limits_i \mid \alpha_i^j \mid} \geq 10^{-4} \tag{4.3}$$

  n_j denotes the number of these modes for case j.

- Finally, the total number of the most significant modes is denoted by n and is equal to the sum of these modes for each case j. The dictionary is the collection of the most significant modes of each case.
  In our illustrative example where 3 cases are considered, the dictionary is given by the modes: $F_i^j(x)G_i^j(y)H_i^j(z)U_i^j(t)$ for i such as $1 \leq i \leq n_j$ and for $j = 1, 2, 3$.

To alleviate the solution, $F_k(x)G_k(y)H_k(z)U_k(t)$ denotes the space-time mode k in the dictionary.

The second step is using the modes of a given dictionary for a new simulation. The coefficients α_k are computed to build the solution. This step corresponds to the classical projection step of the PGD algorithm [Ammar *et al.*, 2006].
The field is written as follows:

$$T(x,y,z,t) = \sum_{k=1}^{n} \alpha_k F_k(x)G_k(y)H_k(z)U_k(t) \tag{4.4}$$

By taking into account the Robin condition, the Galerkin variational formulation can be written as follows:

$$\begin{aligned}
&\int_\Omega T^* \rho C_p \frac{\partial T}{\partial t} \mathrm{d}\Omega + k \int_\Omega [(\frac{\partial T^*}{\partial x}\frac{\partial T}{\partial x} + \frac{\partial T^*}{\partial y}\frac{\partial T}{\partial y} + \frac{\partial T^*}{\partial z}\frac{\partial T}{\partial z})]\mathrm{d}\Omega \\
&+ \int_{S_{yz}\times\Omega_t} T^*(\frac{L}{2},y,z,t)\ h_{vertical}(T(\frac{L}{2},y,z,t) - T_\infty)\mathrm{d}y\mathrm{d}z\mathrm{d}t \\
&+ \int_{S_{xz}\times\Omega_t} T^*(x,\frac{L}{2},z,t)\ h_{vertical}(T(x,\frac{L}{2},z,t) - T_\infty)\mathrm{d}x\mathrm{d}z\mathrm{d}t \\
+ \int_{S_{xy}\times\Omega_t} T^*(x,y,\frac{L}{2},t)\ h_{horizontal}(T(x,y,\frac{L}{2},t) - T_\infty)\mathrm{d}x\mathrm{d}y\mathrm{d}t &= 0
\end{aligned} \tag{4.5}$$

where Ω is the space-time domain, Ω_t is the time interval and S_{ij} refers to the surface $(i,j = x,y,z)$ on the boundary of the spatial domain.

The α_k coefficients can be computed by inserting Eq. (4.4) into the Galerkin variational formulation, where the virtual field T^* is written in this form:

$$T^*(x,y,z,t) = \sum_{k=1}^{n} \alpha_k^* F_k(x)G_k(y)H_k(z)U_k(t) \tag{4.6}$$

and where $F_k(x)G_k(y)H_k(z)U_k(t)$ is the most significant mode k, n is the finite number of the most significant modes. The α_k coefficients are then computed by projection as presented in [Ammar *et al.*, 2007]. Consequently, at step n, T is written in the following matrix form:

$$T(x,y,z,t) = \begin{bmatrix} N^T F_1 M^T G_1 P^T H_1 Q^T U_1 & \cdots & N^T F_n M^T G_n P^T H_n Q^T U_n \end{bmatrix} \begin{bmatrix} \alpha_1 \\ . \\ . \\ . \\ \alpha_n \end{bmatrix} \tag{4.7}$$

where N, M, P, and Q are the vector containing the value of the shape functions $N(x)$, $M(y)$, $P(z)$, and $Q(t)$ respectively. F_k, G_k, H_k, and U_k refer to the nodal values of the a priori most significant modes. The virtual field is written under a matrix form as follows:

$$T^*(x,y,z,t) = \left[\alpha_1^*...\alpha_n^*\right] \begin{bmatrix} N^T F_1 M^T G_1 P^T H_1 Q^T U_1 \\ . \\ . \\ . \\ N^T F_n M^T G_n P^T H_n Q^T U_n \end{bmatrix} \tag{4.8}$$

The gradient in the matrix form is shown below:

$$\begin{bmatrix} \frac{\partial T}{\partial x} \\ \\ \frac{\partial T}{\partial y} \\ \\ \frac{\partial T}{\partial z} \end{bmatrix} = \begin{bmatrix} dN^T F_1 M^T G_1 P^T H_1 Q^T U_1 ... dN^T F_n M^T G_n P^T H_n Q^T U_n \\ N^T F_1 dM^T G_1 P^T H_1 Q^T U_1 ... N^T F_n dM^T G_n P^T H_n Q^T U_n \\ N^T F_1 M^T G_1 dP^T H_1 Q^T U_1 ... N^T F_n M^T G_n dP^T H_n Q^T U_n \end{bmatrix} \begin{bmatrix} \alpha_1 \\ . \\ . \\ . \\ \alpha_n \end{bmatrix} \tag{4.9}$$

The vitual field of the gradient is written in this form:

$$\begin{bmatrix} \frac{\partial T^*}{\partial x} & \frac{\partial T^*}{\partial y} & \frac{\partial T^*}{\partial z} \end{bmatrix} = \left[\alpha_1^*...\alpha_n^*\right] \begin{bmatrix} F_1^T dN G_1^T M H_1^T P U_1^T Q & F_1^T N G_1^T dM H_1^T P U_1^T Q & F_1^T N G_1^T M H_1^T dP U_1^T Q \\ & . \ . \ . & \\ & . \ . \ . & \\ & . \ . \ . & \\ F_n^T dN G_n^T M H_n^T P U_n^T Q & F_n^T N G_n^T dM H_n^T P U_n^T Q & F_n^T N G_n^T M H_n^T dP U_n^T Q \end{bmatrix} \tag{4.10}$$

where dN, dM, and dP correspond to the vector containing the value of the shape functions derivatives with respect to the coordinate x, y, z, respectively. The virtual field can be written in the same manner. The notations of the field and its gradient are as follows:
$T = A\alpha$, $\nabla T = B\alpha$, $T^* = \alpha^* A^t$ and $\nabla T^* = \alpha^{*t} B^t$ with A^t and B^t the transpose of A and B, respectively, A and B being defined by Eq. (4.7) and Eq. (4.9) respectively.
Accordingly, the equation will be written as follows:

$$\begin{aligned} &\int_\Omega \alpha^* A^T \rho C_p \frac{\partial A}{\partial t} \alpha \mathrm{d}\Omega + \int_\Omega \alpha^{*T} B^T \ k \ B\alpha \mathrm{d}\Omega \\ &+ \int_{S_{yz}\times\Omega_t} \alpha^* A_{dx}^T \ h_{vertical}(A_{dx}\alpha)\mathrm{d}y\mathrm{d}z\mathrm{d}t \\ &+ \int_{S_{xz}\times\Omega_t} \alpha^* A_{dy}^T \ h_{vertical}(A_{dy}\alpha)\mathrm{d}x\mathrm{d}z\mathrm{d}t \\ &+ \int_{S_{xy}\times\Omega_t} \alpha^* A_{dz}^T \ h_{horizontal}(A_{dz}\alpha)\mathrm{d}x\mathrm{d}y\mathrm{d}t = \\ &\int_{S_{yz}\times\Omega_t} \alpha^* A_{dx}^T \ h_{vertical}(T_\infty)\mathrm{d}y\mathrm{d}z\mathrm{d}t \\ &+ \int_{S_{xz}\times\Omega_t} \alpha^* A_{dy}^T \ h_{vertical}(T_\infty)\mathrm{d}x\mathrm{d}z\mathrm{d}t \\ &+ \int_{S_{xy}\times\Omega_t} \alpha^* A_{dz}^T \ h_{horizontal}(T_\infty)\mathrm{d}x\mathrm{d}y\mathrm{d}t \end{aligned} \tag{4.11}$$

where Ω is the space-time domain and Ω_t is the time domain. S_{ij} refers to the surface $(i,j = x,y,z)$ on the boundary of the spatial domain, A_{di} represents the matrix A at the boundary. This equation is valid for all α^*.
Therefore, the equation Eq. (4.11) can be written in the form of a linear system

$$K\alpha = R \tag{4.12}$$

where K is the conductivity matrix of the discretized structure.

ρ	k	$h_{vertical}$	$h_{horizontal}$	T_∞
$950\ \mathrm{kg.m^{-3}}$	$0.45\ \mathrm{W.m^{-1}{}^\circ C^{-1}}$	$4.6\mathrm{W.m^{-2}.K^{-1}}$	$6.36\mathrm{W.m^{-2}.K^{-1}}$	$T_{min} = 0^\circ\mathrm{C}, \mathrm{T_{max}} = 50^\circ\mathrm{C}$

Table 4.1: Material properties and boundary conditions

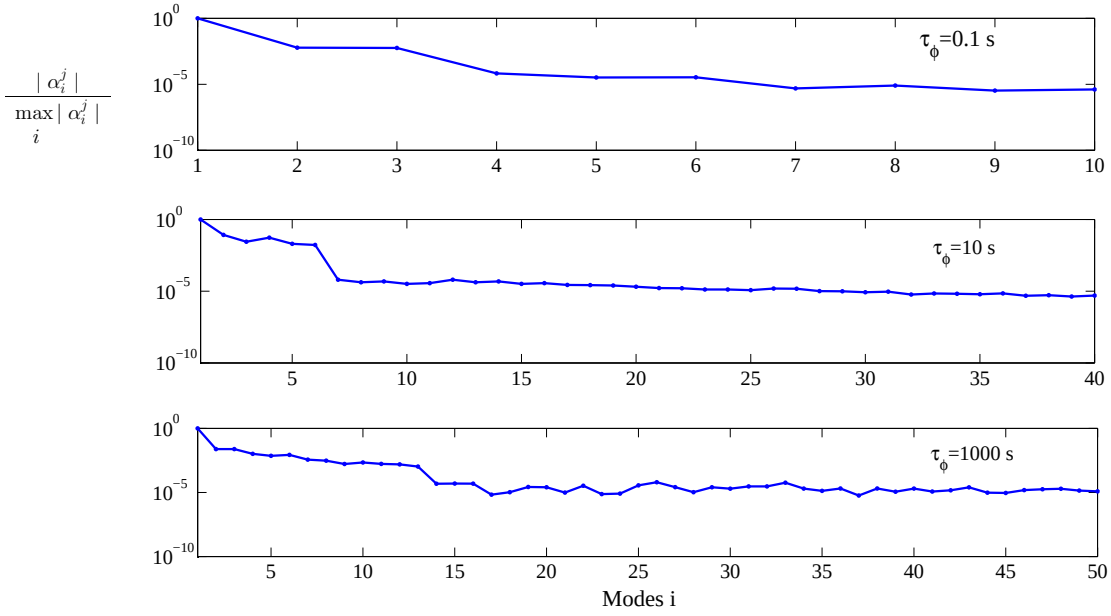


Figure 4.2: The evolution of $\frac{|\alpha_i^j|}{\max\limits_i |\alpha_i^j|}$ with respect to the number of modes for each case j

Let us mention that this approach based to the PGD method is not restricted to cubic domain and can be addressed in complex domains as presented in [Ghnatios *et al.*, 2016] for the PGD method.

4.4 Numerical results

Let us assume that the geometry is a cube with $L = 100\mathrm{mm}$ and the final time L_t equals $1000s$. The material properties and the boundary conditions are reported in Table 4.1. Note that two dictionaries will be created from the most significant modes of PGD modes. These modes are the space-time modes $F_k(x)G_k(y)H_k(z)U_k(t)$ as in section 4.3.2:

1. **Dictionary 1** for constant cycle time ($\tau_c = 20s$) and different physical times ($\tau_\phi = 0.1s$, $\tau_\phi = 10s$, $\tau_\phi = 1000s$).
2. **Dictionary 2** for constant physical time ($\tau_\phi = 10s$) and different cycle times ($\tau_c = 10s$, $\tau_c = 50s$, $\tau_c = 100s$).

Remark 1 The relative error is computed for each case as follows:

$$E(\%) = \frac{\|T_{ref} - T_{method}\|}{\|T_{ref}\|} \times 100 \tag{4.13}$$

where T_{ref} is the full PGD solution, T_{method} is the solution computed using a dictionary as presented in Section 4.3, and $\|\ \|$ is the L^2 norm.

C_p J.kg^{-1}.C^{-1}	0.075	7.5	757
τ_ϕ(s)	0.1	10	1000

Table 4.2: The physical time τ_ϕ with respect to the specific heat coefficient C_p

$\tau_\phi(s)$	0.1	10	1000
Number of modes full PGD	10	40	50
Number of most significant modes	3	6	13

Table 4.3: Number of modes for the full PGD and number of most significant modes with respect to the physical time τ_ϕ (dictionary 1 - $\tau_c = 20s$)

4.4.1 Dictionary 1 for a fixed cycle time and different physical times

4.4.1.1 Dictionary creation

In this part, a dictionary will be created from different physical times and a given cycle time ($\tau_c = 20s$). Three cases are considered:

- Case 1: τ_ϕ is smaller than the cycle time ($\tau_\phi = 0.1s$)
- Case 2: τ_ϕ is of the same order as the cycle time ($\tau_\phi = 10s$)
- Case 3: τ_ϕ is larger than the cycle time ($\tau_\phi = 1000s$).

To deal with different physical times, different specific heats are considered. Table 4.2 outlines the physical time τ_ϕ with respect to the specific heat C_p.

The three cases are solved using the Proper Generalized Decomposition (PGD) method. Fig. 4.2 depicts the evolution of $\frac{|\alpha_i^j|}{\max\limits_i |\alpha_i^j|}$ with respect to the number of modes for each case j ($j = 1, 2, 3$). Then the most significant modes are selected with the criterion (4.3). The number of most significant modes (space-time modes) needed in each case to generate an accurate solution are presented in Table 4.3. The results show that as the physical time increases, the number of most significant modes needed to capture the solution is more important. To illustrate for $\tau_\phi = 0.1s$, 3 modes are only needed. However, for $\tau_\phi = 10s$, 6 modes are required and for $\tau_\phi = 1000s$ the required modes are 13. The modes in the dictionary are ordered with respect to increasing τ_ϕ.
The question arises: how to use these most significant modes?

First, the efficiency of most significant modes is investigated compared to the full PGD solution. Fig. 4.3 depicts the evolution of the temperature under cyclic loading for $\tau_\phi = 0.1s$ for a fixed spatial point. The solution generated from 3 most significant modes is compared to the full PGD solution constructed with 10 modes. It is worth noting there is no significant difference between both solutions. The results reveal an accurate solution and relative error less than 0.9%.

Likewise, for $\tau_\phi = 10s$ the solution is depicted in Fig. 4.4 from the most significant modes versus the full PGD solution (40 modes). Both solutions match with a relative error less than 1%.
Let us note that in this case a greater number of modes is required since the solution is composed by two parts: a transient part and a stationary part.

Fig. 4.5 represents the solution for a large physical time $\tau_\phi = 1000s$. The most remarkable result is that we need 13 most significant modes only to generate accurate results compared to the full PGD solution (50 modes).
The marked observation and results are: the most significant modes can give an accurate result, the number of the most significant modes is related to the relationship between the cycle time τ_c and

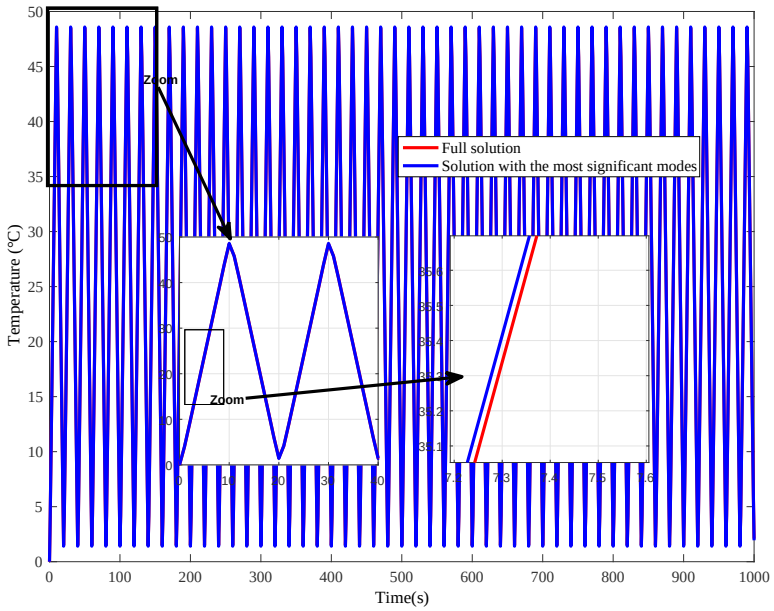


Figure 4.3: The evolution of the temperature under cyclic load $\tau_c = 20s$ (50 cycles) with $\tau_\phi = 0.1s$ at $(x, y, z) = (25, 25, 50)$

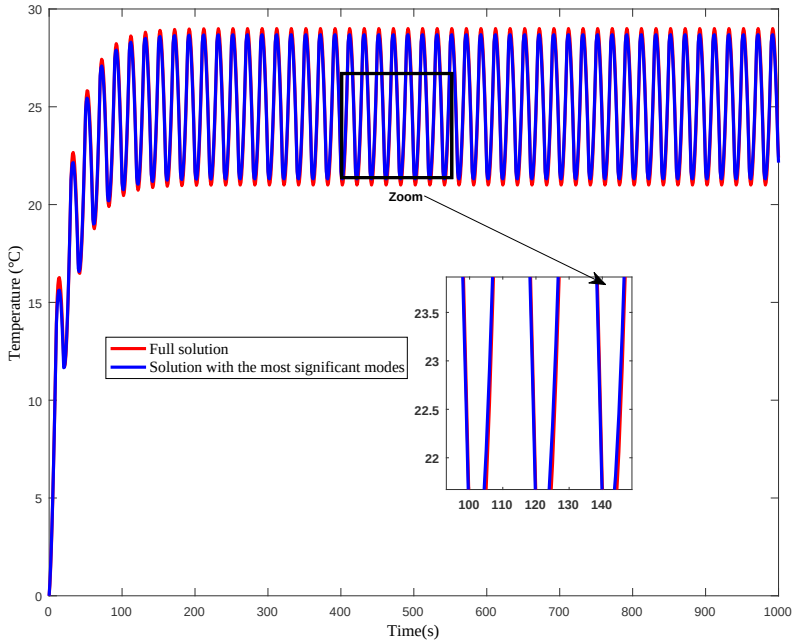


Figure 4.4: The evolution of the temperature under cyclic load $\tau_c = 20s$ (50 cycles) with $\tau_\phi = 10s$ at $(x, y, z) = (25, 25, 50)$

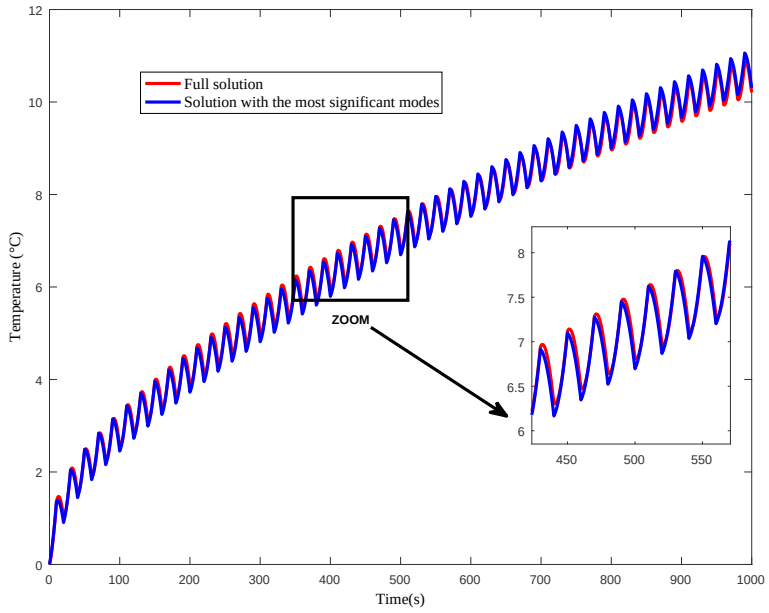


Figure 4.5: The evolution of temperature under cyclic load $\tau_c = 20s$ (50 cycles) with $\tau_\phi = 1000s$ at $(x, y, z) = (25, 25, 50)$

the physical time τ_ϕ (smaller, same order, larger).

Fig. 4.6 presents the first 12 spatial part of the most significant modes. It is noticed that:

- the modes are different.
- the modes components $F_i(x)$ and $G_i(y)$ given in Eq. (4.4) are the same. This can be explained by an identical convection coefficient in these two directions.

Fig. 4.7 represents the evolution with respect to time of some modes $F_i(x)G_i(y)H_i(z)U_i(t)$ for a fixed spatial point. The illustrated modes correspond to the first 4 most significant modes related to each case ($\tau_\phi = 0.1s, \tau_\phi = 10s, \tau_\phi = 1000s$). The modes are composed of a deviation and a periodic function. The period seems to be related to the cycle time. Large values of τ_ϕ imply important deviation of the modes. This dictionary denoted by dictionary 1 contains a large spectrum of responses.

4.4.1.2 Dictionary evaluation

To validate the present method, a collection of the most significant modes gathered in the dictionary 1 is used to solve different problems by changing, first, the physical time and, second, the boundary conditions.

Influence of the physical time. Let us consider a problem for which the physical time τ_ϕ is changed ($\tau_\phi = 3s$). A priori modes of the dictionary 1 associated with $\tau_\phi = 0.1s$, $\tau_\phi = 10s$, $\tau_\phi = 1000s$ are used to compute the solution for $\tau_\phi = 3s$. The variation of the α_i coefficient with respect to the modes of dictionary 1 is shown in Fig. 4.8. The mode number 4 is the most efficient associated with $\alpha_4 = 90$. It can be noticed that this mode is the first mode associated with $\tau_\phi = 10s$.
The solution is directly constructed from the modes of the dictionary 1 and the calculated α_i. Fig. 4.9 plots the solution for $\tau_\phi = 3s$ using this approach versus the full PGD solution. The results thus obtained are compatible with the reference solution, with a relative error less than 1.2% for different points in the domain as shown in Table 4.4.

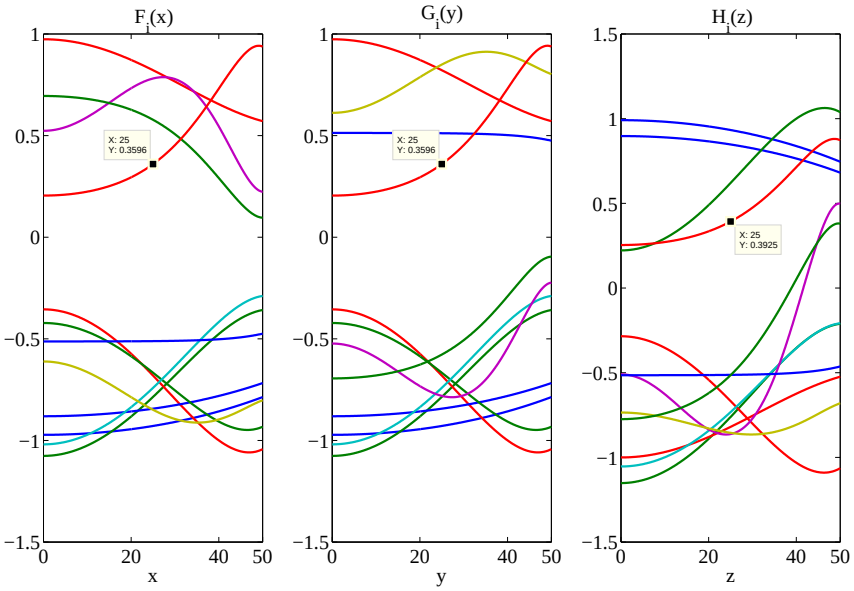


Figure 4.6: The partition of the first 12 most significant modes in x, y, z directions of the dictionary

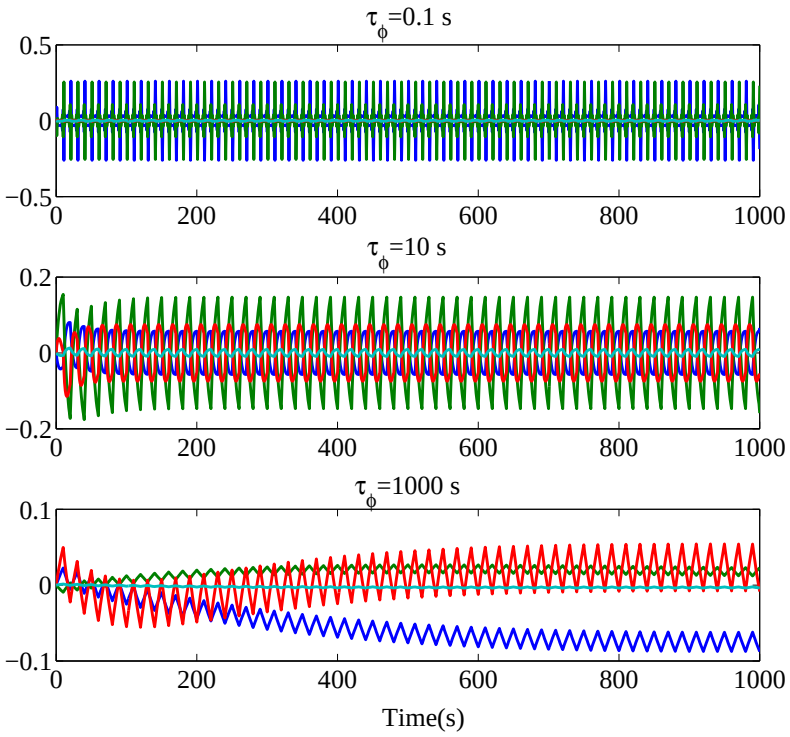


Figure 4.7: The time evolution of the modes $F_i(x)G_i(y)H_i(z)U_i(t)$ of the dictionary 1 at $(x, y, z) = (25, 25, 25)$

Spatial point (x,y,z)	$(25, 25, 25)$	$(37.5, 25, 25)$	$(37.5, 37.5, 37.5)$	$(37.5, 12.5, 37.5)$
Relative error $(\%)$	1.1	1.2	1	1.1

Table 4.4: The relative error calculated for different points for $\tau_\phi = 3s$ and dictionary 1

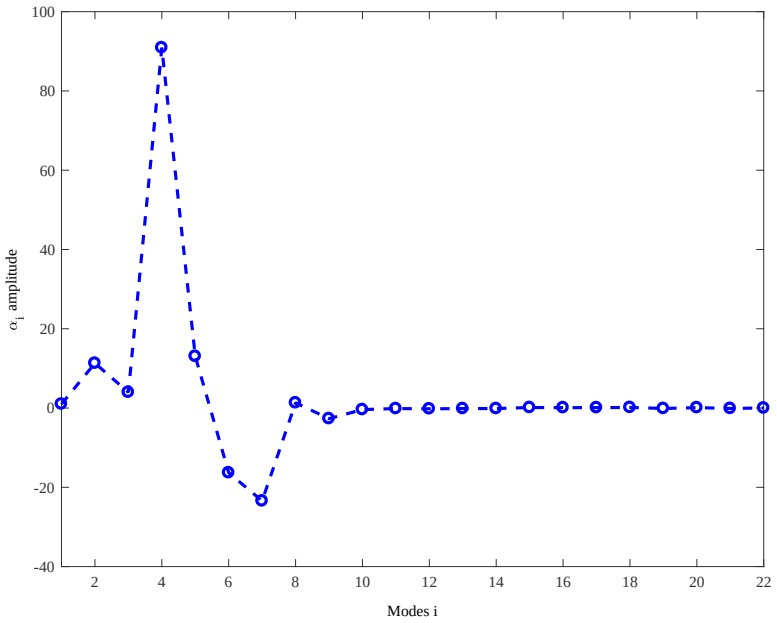


Figure 4.8: The evolution of the α_i coefficient for $\tau_\phi = 3s$ with respect to the modes of the dictionary 1

Different cases are studied and tested with this dictionary. Accurate results are obtained for different problems with small characteristic times or very large characteristic times. One of the big advantages of this approach is the computation time issue. This method leads to a saving time of ratio around 50 (calculation made by Finite Element Method (FEM)).

Influence of the boundary conditions. In this paragraph, the dictionary 1 is used to solve problems with different boundary conditions. Let us recall that the dictionary is created using Robin boundary conditions. The model now encounters cyclic temperature on the vertical faces of the cube (Dirichlet conditions instead of Robin conditions) equal to the value T_∞ defined as previously (triangular cyclic form, $T_{min} = 0$ and $T_{max} = 50°\mathrm{C}$). The boundary condition on the upper and lower faces is unchanged.
Two cases are investigated:

1. The specific heat $C_p = 10\mathrm{J.kg}^{-1}.\mathrm{C}^{-1}$ is taken, consequently $\tau_\phi \approx 10s$.
2. The specific heat $C_p = 75.75\mathrm{J.kg}^{-1}.\mathrm{C}^{-1}$, thus $\tau_\phi = 100s$

These cases are denoted by case 1-BC and case 2-BC, respectively.
Note that different values of C_p are used in order to check the ability of the dictionary for different boundary conditions and physical times. The chosen values of τ_ϕ are present in the dictionary 1 but not for the same boundary condition.

The results for case 1-BC are presented in Fig. 4.10. The use of the modes of the dictionary 1 generates an accurate result compared to the full PGD solution with a relative error less than 1.8% as shown in Table 4.5 for different points. This test highlights the efficiency of this dictionary. For the

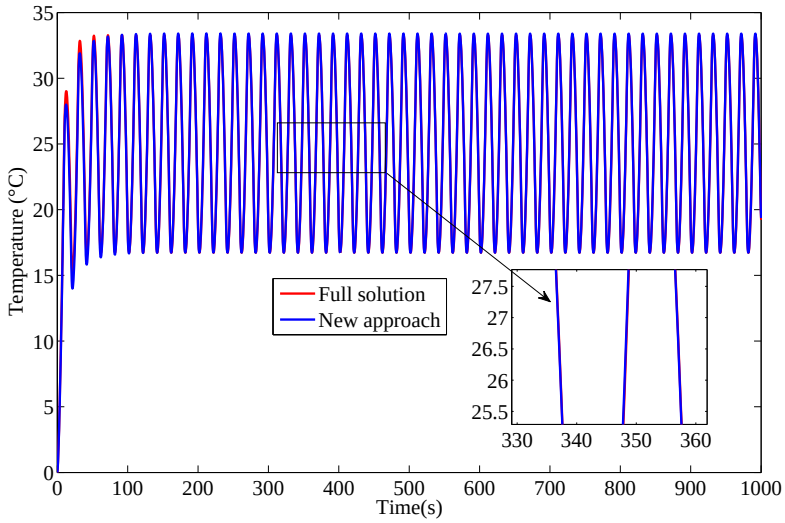


Figure 4.9: The evolution of temperature under cyclic load $\tau_c = 20s$ (50 cycles) with $\tau_\phi = 3s$ at $(x, y, z) = (25, 25, 50)$

Spatial point (x,y,z)	$(25, 25, 25)$	$(37.5, 25, 25)$	$(37.5, 37.5, 37.5)$	$(37.5, 12.5, 37.5)$
Relative error case 1-BC$(\%)$	1.8	1.7	1.8	1.6
Relative error case 2-BC$(\%)$	1.5	1.4	1.2	1.4

Table 4.5: The relative error for different spatial points in the domain for cases 1-BC and 2-BC

case 2-BC, accurate results with respect to the full PGD solution are depicted in Fig. 4.11. To check the percentage error at different points in the domain, the relative error Eq. (4.13) is calculated for different points as shown in Table 4.5. The results show that the modes of the dictionary 1 can give accurate results with a relative error less than 1.5%. The remarkable result that can be noticed is the ability of the dictionary to generate solutions for different physical times and different boundary conditions.

4.4.2 Dictionary 2 for fixed physical time and different cycle times

4.4.2.1 Dictionary creation

The idea here is to validate the possibility of creating a dictionary by varying the cycle time. The following question arises:

- Is it possible to use the collection of most significant modes associated with different cycle times for problems involving another cycle time?

To answer these questions, three different cases are investigated by keeping constant the physical time $\tau_\phi = 10s$:

- cycle time $\tau_c = 10s$,
- cycle time $\tau_c = 50s$,
- cycle time $\tau_c = 100s$.

As the time interval remains equal to $1000s$, the number of considered cycles is 100, 20 and 10 respectively. The number of modes for the full PGD solution is reported in Table 4.6 with respect to the cycle time. The number of modes increases while the cycle time decreases. In fact, the ratio $\frac{\tau_\phi}{\tau_c}$

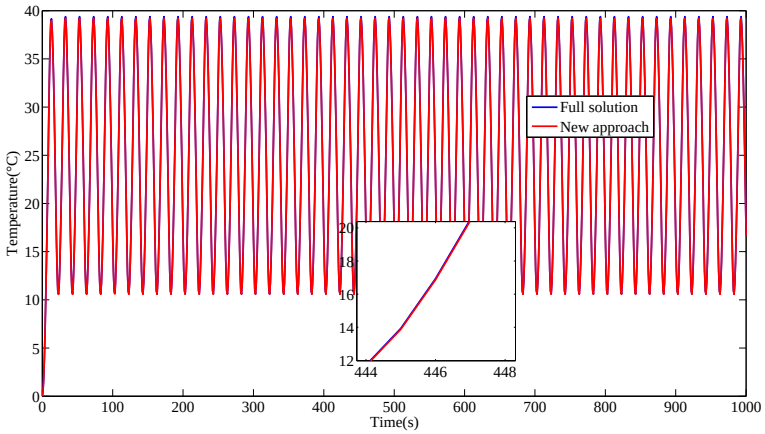


Figure 4.10: The evolution of temperature under $\tau_c = 20s$ with $\tau_\phi \approx 10s$ and different boundary conditions at $(x, y, z) = (25, 25, 50)$ - case 1-BC

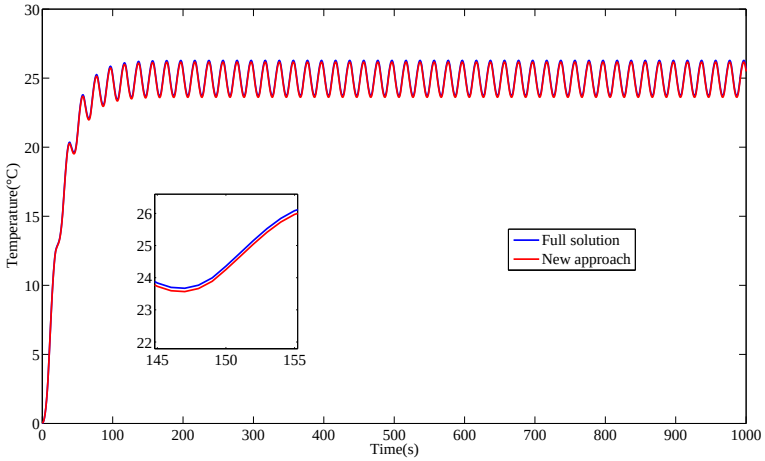


Figure 4.11: The evolution of temperature under $\tau_c = 20s$ with $\tau_\phi = 100s$ and different boundary conditions at $(x, y, z) = (25, 25, 50)$ - case 2-BC

Cycle time (s)	10	50	100
Number of modes full PGD	44	36	30
Number of most significant modes	9	6	6

Table 4.6: Number of modes for the full PGD and number of most significant modes for $\tau_\phi = 10s$ with respect to cycle time (dictionary 2).

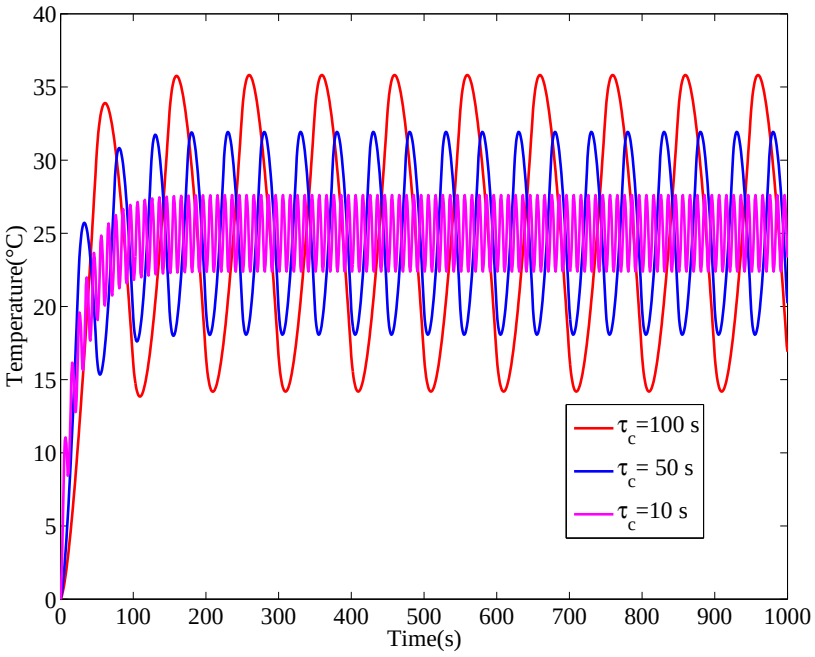


Figure 4.12: The evolution of temperature for different cycle times at $(x, y, z) = (25, 25, 50)$

increases, leading to compute a solution with larger transient part. The number of most significant modes is reported in Table 4.6 and is calculated by using (4.3). To illustrate the different responses, Fig. 4.12 depicts the evolution of the temperature with respect to time for a given spatial point for different cycle times. It is noticed that permanent response is reached for shorter times when decreasing the cycle time. By considering these three different cycle times, the dictionary 2 contains 21 most significant modes. The first 12 spatial part of the most significant modes are different from those in dictionary 1. The time component of the modes for the three cases are shown in Fig. 4.13. These modes are different than those in dictionary 1, the cycle time has a significant effect. Fig. 4.14 represents the evolution with respect to time of some modes $F_k(x)G_k(y)H_k(z)U_k(t)$ for the considered spatial point. The illustrated modes correspond to the first 4 most significant modes related to each case ($\tau_c = 10s, \tau_c = 50s, \tau_c = 100s$). Let us recall that τ_ϕ is fixed and equals $10s$. The fluctuation is different for each case, the cycle time being different. The form of the mode for $\tau_c = 50s$ and $\tau_c = 100s$ is similar. This is due to the closest value of the ratio $\frac{\tau_\phi}{\tau_c}$ equal to 0.2 and 0.1, respectively. For the case $\tau_c = 10s$, this ratio is equal to 1 leading to a more different form of the modes. It can be noticed that the time modes are periodic and the period equals τ_c.

4.4.2.2 Dictionary evaluation

Let us consider the case with a cycle time $\tau_c = 20s$. The total number of cycles is 50. This particular cycle time is in the range of modes collected in dictionary 2. By considering the modes from this dictionary, the α_i coefficients are then calculated. The variation of the α_i coefficient with respect to the modes of dictionary 2 is depicted in Fig. 4.15. The modes 2 and 17 are the most efficient.

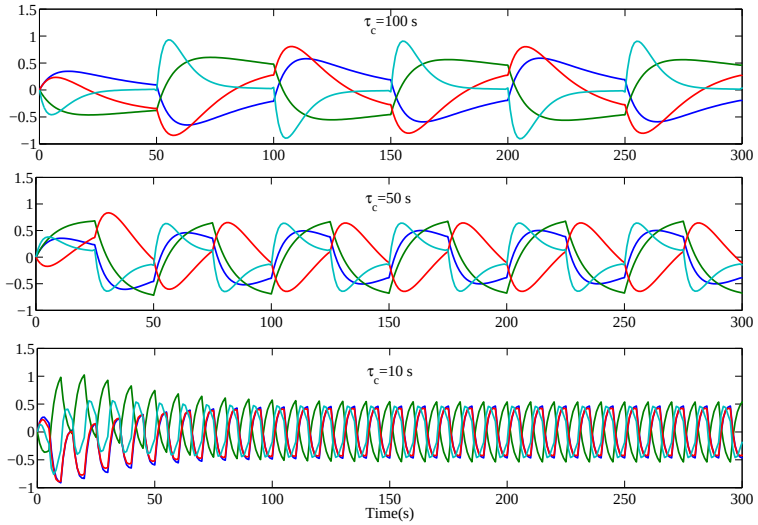


Figure 4.13: The time part of the first 12 most significant modes of the dictionary 2

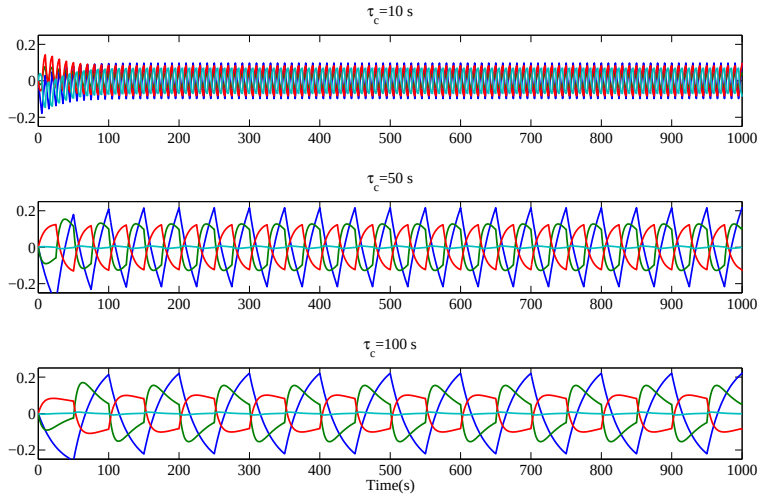


Figure 4.14: The time evolution of the modes $F_k(x)G_k(y)H_k(z)U_k(t)$ of the dictionary 2 at $(x, y, z) = (25, 25, 50)$

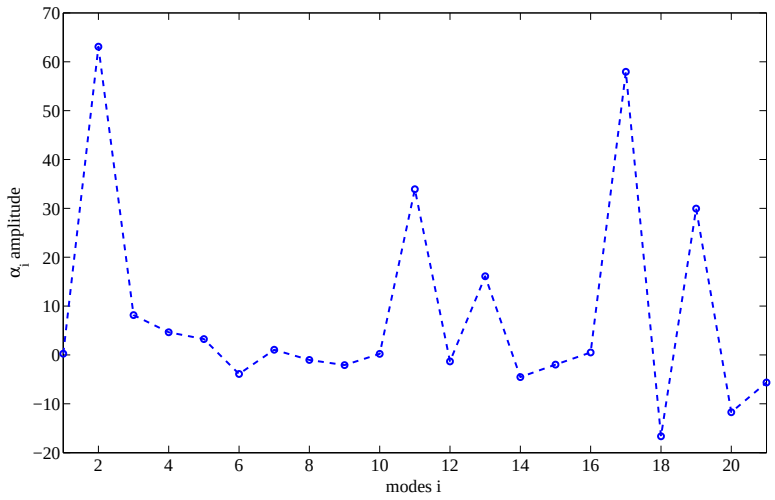


Figure 4.15: The evolution of the coefficient α for $\tau_c = 20s$ with respect to the modes of the dictionary 2

Cycle time (s)	10	20	50	100
Number modes	44	40	36	30
Number of the most significant modes	9	6	6	6

Table 4.7: Number of modes for the full PGD and number of the most significant modes for $\tau_\phi = 10s$ with respect to cycle time (dictionary 3).

They belong to the most significant modes related to $\tau_c = 10s$ and $\tau_c = 100s$. Fig. 4.16 compares the solution obtained from dictionary 2 to the full PGD solution. The solution obtained using this dictionary is not accurate, the period of the solution being $100s$ instead of $20s$. It corresponds to the largest period of the modes in the dictionary. Nevertheless, the global behavior is well predicted. Let us add in dictionary 2 the modes related to $\tau_c = 20s$. These 6 modes are added to the dictionary denoted by dictionary 3. The modes of dictionary 3 are reported in Table 4.7. The solution obtained with this dictionary matches the full PGD solution with a relative error less than 1%. The related α_i coefficients are given in Fig. 4.17. The most significant modes are the modes related to $\tau_c = 20s$. To predict correctly the solution, the modes corresponding to the cycle time must be present in the dictionary.

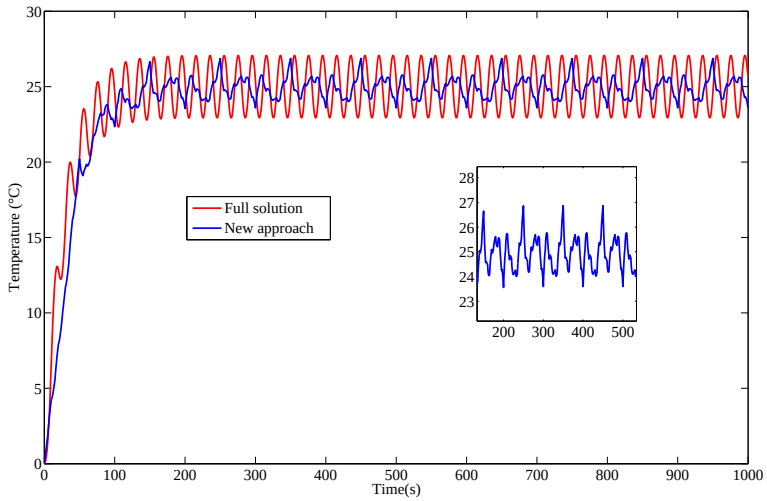


Figure 4.16: The evolution of temperature under $\tau_c = 20s$ with $\tau_\phi = 10s$ at $(x, y, z) = (25, 25, 25)$

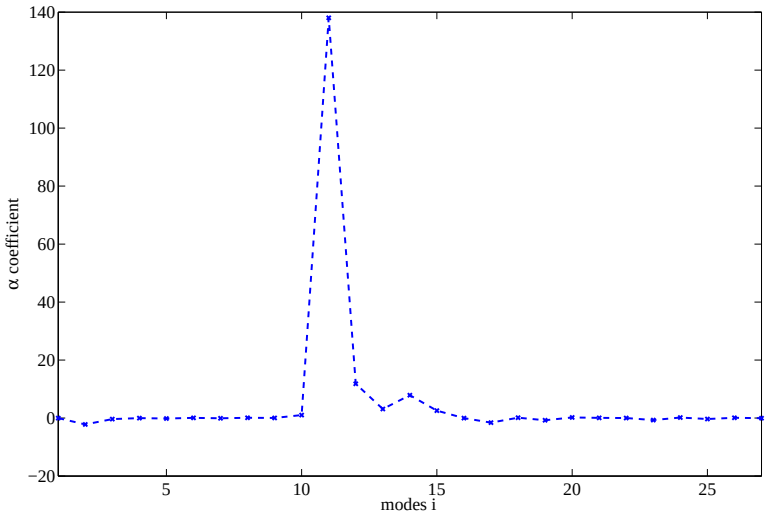


Figure 4.17: The evolution of the coefficient α for $\tau_c = 20s$ with respect to the modes of the dictionary 3

$\tau_\phi(s)$	0.1	10	100
Number of most significant modes $\tau_c = 10s$	3	6	14
Number of most significant modes $\tau_c = 50s$	3	6	12
Number of most significant modes $\tau_c = 100s$	3	6	9

Table 4.8: Number of most significant modes with respect to the physical time τ_ϕ and constant cycle time for dictionary 4

4.5 Extension to many harmonics

The objective here is to create a dictionary of significant modes with different cycle times (τ_c) and with variable physical times (τ_ϕ). This dictionary denoted by $D4$ for dictionary 4 will be composed of different harmonics as follows:

1. **Dictionary** $D4_{(\tau_c=10)}$ for constant cycle time ($\tau_c = 10s$) and different physical times ($\tau_\phi = 0.1$, $\tau_\phi = 10$, $\tau_\phi = 100s$)
2. **Dictionary** $D4_{(\tau_c=50)}$ for constant cycle time ($\tau_c = 50s$) and different physical times ($\tau_\phi = 0.1$, $\tau_\phi = 10$, $\tau_\phi = 100s$)
3. **Dictionary** $D4_{(\tau_c=100)}$ for constant cycle time ($\tau_c = 100s$) and different physical times ($\tau_\phi = 0.1$, $\tau_\phi = 10$, $\tau_\phi = 100s$)

Thus, the dictionary 4 (D4) is the combination of the three previous sub-dictionaries such as:

$$D4 = D4_{(\tau_c=10)} \sqcup D4_{(\tau_c=50)} \sqcup D4_{(\tau_c=100)} \tag{4.14}$$

Then, the most significant modes are chosen for each dictionary based on the criterion (4.3). The number of the significant modes (space-time modes) needed in each case are presented in Table 4.8.

Following this, each dictionary has been tested independently by changing the physical time. Let us consider a problem for which the physical time $\tau_\phi = 3s$ is changed and $\tau_c = 100s$. A priori modes of the dictionary $D4_{(\tau_c=100)}$ are used to compute the solution for $\tau_\phi = 3s$. The solution is directly constructed from the modes of the dictionary $D4_{(\tau_c=100)}$ and the calculated α_i using the approach. Fig. 4.18(a) plots the solution for $\tau_\phi = 3s$ using this approach versus the full PGD solution. The results obtained are compatible with the reference solution (full PGD solution), with a relative error less than 1.1% for different points in the domain.

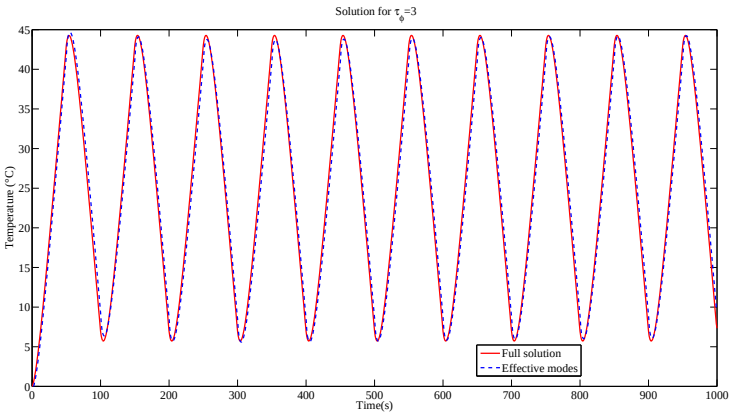
Similarly, dictionary $D4_{(\tau_c=50)}$ has been tested with a new physical time $\tau_\phi = 3s$. Fig. 4.18(b) depicts the evolution of the temperature obtained with our approach and the full PGD solution. The results show that the modes of the dictionary $D4_{(\tau_c=50)}$ can give accurate results with a relative error less than 1.2%. Further tests carried out with $D4_{(\tau_c=10)}$, leading to a good agreement as shown in Fig. 4.18(c). This confirms our earlier findings (Dictionary 1) where each dictionary has the ability to generate solutions for different physical times with a large time saving of order 50.

4.5.1 Dictionary evaluation

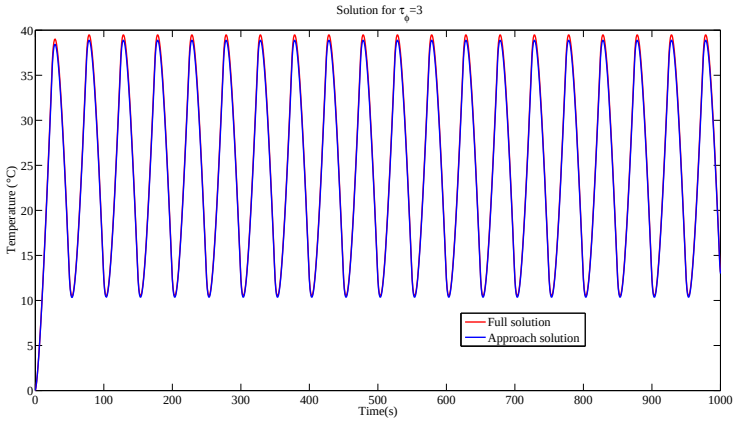
In this part, the dictionary 4, $D4$ equal to $(D4_{(\tau_c=10)} \sqcup D4_{(\tau_c=50)} \sqcup D4_{(\tau_c=100)})$, is being evaluated through an example with different harmonics.
Let us consider T_∞ with different harmonics:

$$T_\infty = T_\infty(\tau_c = 10) + T_\infty(\tau_c = 50) + T_\infty(\tau_c = 100)$$

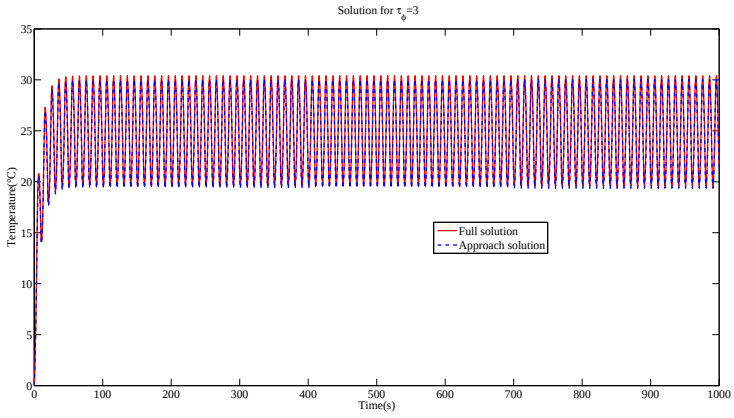
T_∞ is represented in Fig. 4.19 where it consists of different harmonics, the period of T_∞ is $\tau_c = 100s$. Consider the problem where the physical time is $\tau_\phi = 3s$. A priori modes of the dictionary $D4$ are used to compute the solution. The variation of the α_i coefficient with respect to



(a) The evolution of temperature under $\tau_c = 100s$ with $\tau_\phi = 3s$ using dictionary $D4(\tau_c = 10)$ at $(x, y, z) = (25, 25, 50)$



(b) The evolution of temperature under $\tau_c = 50s$ with $\tau_\phi = 3s$ using dictionary $D4(\tau_c = 50)$ at $(x, y, z) = (25, 25, 50)$



(c) The evolution of temperature under $\tau_c = 10s$ with $\tau_\phi = 3s$ using dictionary $D4(\tau_c = 100)$ at $(x, y, z) = (25, 25, 50)$

Figure 4.18: The evolution of temperature using different dictionaries

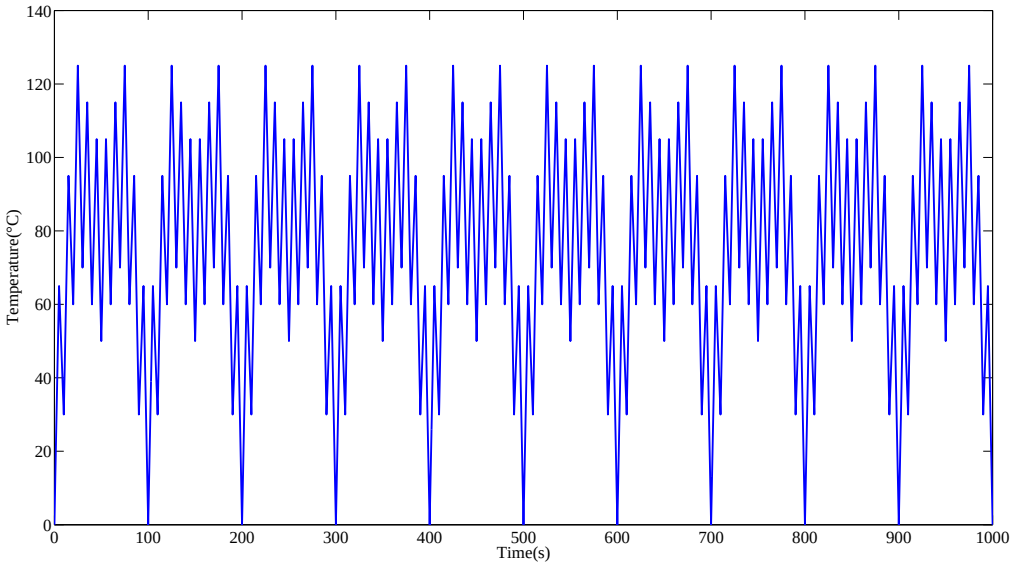


Figure 4.19: The evolution of T_∞ under $(T_\infty(\tau_c = 10) + T_\infty(\tau_c = 50) + T_\infty(\tau_c = 100))$

Relative error (%) at spatial point (x,y,z)	$(25, 25, 25)$	$(37.5, 25, 25)$	$(37.5, 37.5, 37.5)$	$(37.5, 12.5, 37.5)$
Approach solution with $D4$	1.1	1.4	1.32	1.51
Summation solution	1.9	1.8	1.85	1.96

Table 4.9: The relative error for different spatial points in the domain

the modes of dictionary 4 is shown in Fig. 4.20 (the order of modes is given by: $\tau_c = 10$, $\tau_c = 50$, and $\tau_c = 100s$ respectively). Interestingly, accurate results are obtained using this approach compared to the full solution. Fig. 4.21 depicts the evolution of the temperature using our approach and the full solution using PGD method with a relative error less than 2% as shown in Table 4.9. This result has further empowered the approach.
To summarize the ability of different dictionaries, Table 4.10 shows the different combination of the usage of each dictionary. The notation ✓ refers to valid and x refers to invalid. For example a dictionary generated from load F1($\tau_c = 10s$) associated with $\tau_c = 10s$ can be used for different boundary conditions, and different physical times. However it is restricted for load with a cycle time $\tau_c = 10s$.

Dictionary generated from \ Load	F1	F2	F3	F1+F2	F1+F3	F2+F3	F1+F2+F3
F1	✓	x	x	x	x	x	x
F2	x	✓	x	x	x	x	x
F3	x	x	✓	x	x	x	x
F1 ⊔ F2	✓	✓	x	✓	x	x	x
F1 ⊔ F3	✓	x	✓	x	✓	x	x
F2 ⊔ F3	x	✓	✓	x	x	✓	x
F1 ⊔ F2 ⊔ F3	✓	✓	✓	✓	✓	✓	✓

Table 4.10: Different combination of the dictionaries (✓ refers to valid and x refers to invalid)

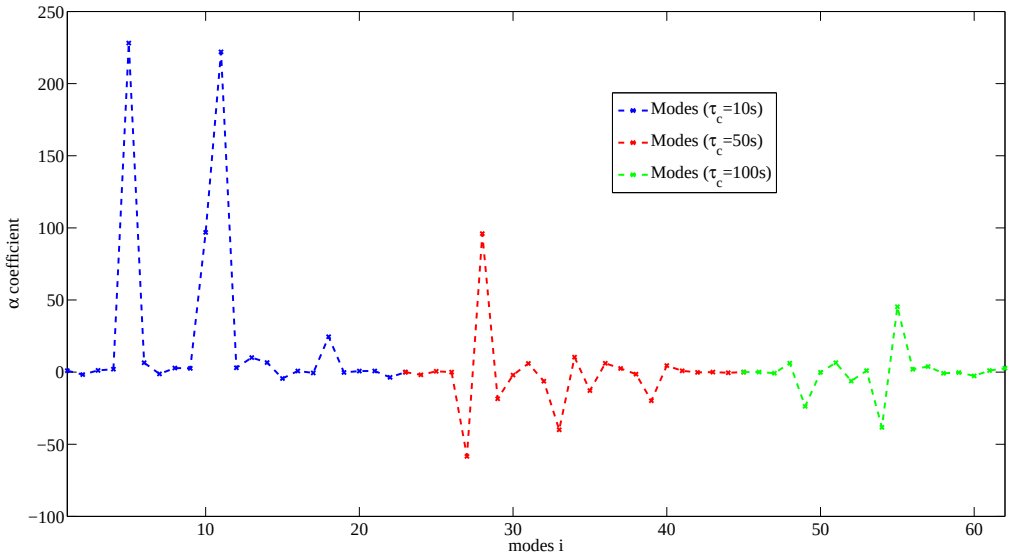


Figure 4.20: The evolution of the coefficient α for $\tau_\phi = 3s$ with respect to the modes of the dictionary 4

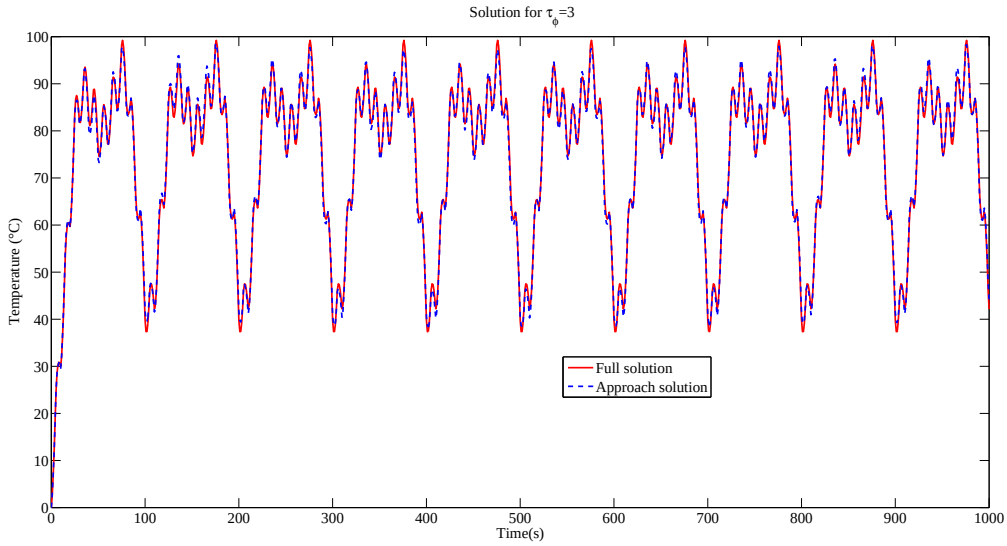


Figure 4.21: The evolution of temperature under $(\tau_\phi = 3s)$ and cycle time $(\tau_c = 10, \tau_c = 50, \tau_c = 100s)$ at $(x, y, z) = (25, 25, 50)$

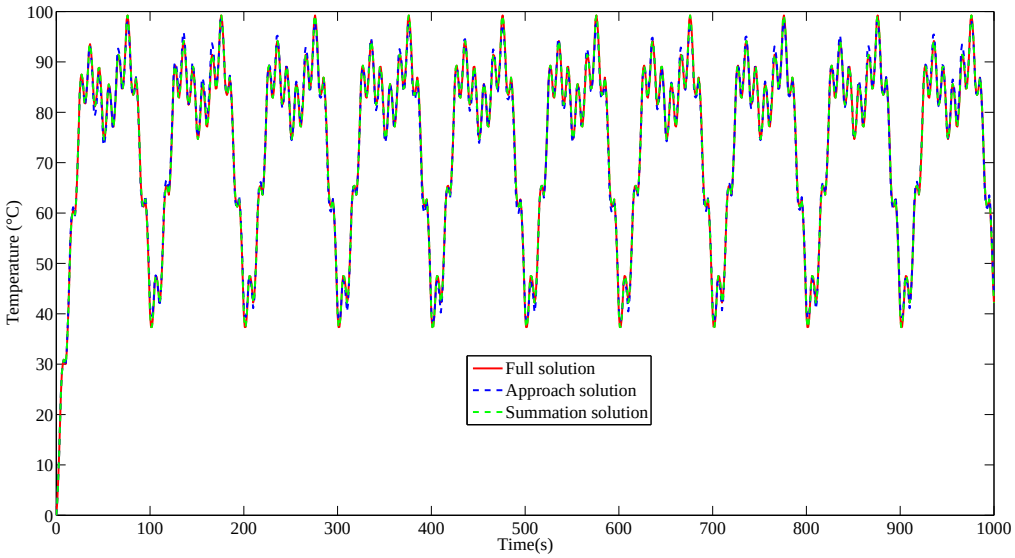


Figure 4.22: The evolution of temperature under ($\tau_\phi = 3s$) and cycle time ($\tau_c = 10$,$\tau_c = 50$, $\tau_c = 100s$) at $(x, y, z) = (25, 25, 50)$ using the summation of different solutions obtained from each dictionary independently.

Another meaning of construction of the solution obtained from the harmonic case: In this paragraph, an illustration of another way to construct the solution of the problem where the physical time is $\tau_\phi = 3s$ with harmonic load T_∞ ($T_\infty(\tau_c = 10) + T_\infty(\tau_c = 50) + T_\infty(\tau_c = 100)$) is presented. The response can be obtained by adding the solution generated from each dictionary independently since the PDE is linear (superposition principle). To illustrate, the solution can be generated from the summation of the following solutions: the evolution of temperature using the dictionary $D4(\tau_c = 10)$ with $\tau_\phi = 3s$, the evolution of temperature using the dictionary $D4(\tau_c = 50)$ with $\tau_\phi = 3s$, and the evolution of temperature using the dictionary $D4(\tau_c = 100)$ with $\tau_\phi = 3s$. Fig. 4.22 depicts the solution obtained from summation showing a good agreement compared to the reference solution and the approach solution (first way presented previously with the union of the dictionaries). Let us note that the relative error obtained from the different solutions showed that the approach solution (the full dictionary) generates more accurate solution as summarized in Table 4.9.

4.6 Extension to coupled problems

Our method is being now extended to a coupled thermo-diffusion problem with weak coupling. The effect of the concentration on the temperature is considered only. The coupling term appears only in the right-hand side of the thermal equation Eq. (4.16), the diffusion equation Eq. (4.15) being the uncoupled one.

4.6.1 Problem description

In this section, the cube is subjected to an heat source with null initial and boundary conditions. Let us consider the thermo-diffusion coupled problem, where Eq. (4.15) represents the diffusion problem and Eq. (4.16) represents the thermo-diffusion coupled equation.

$$\frac{\partial c}{\partial t} - D\Delta c = F_D(t) \tag{4.15}$$

$$\rho C_p \frac{\partial T}{\partial t} - K\Delta T = F_T(t) - \beta c \tag{4.16}$$

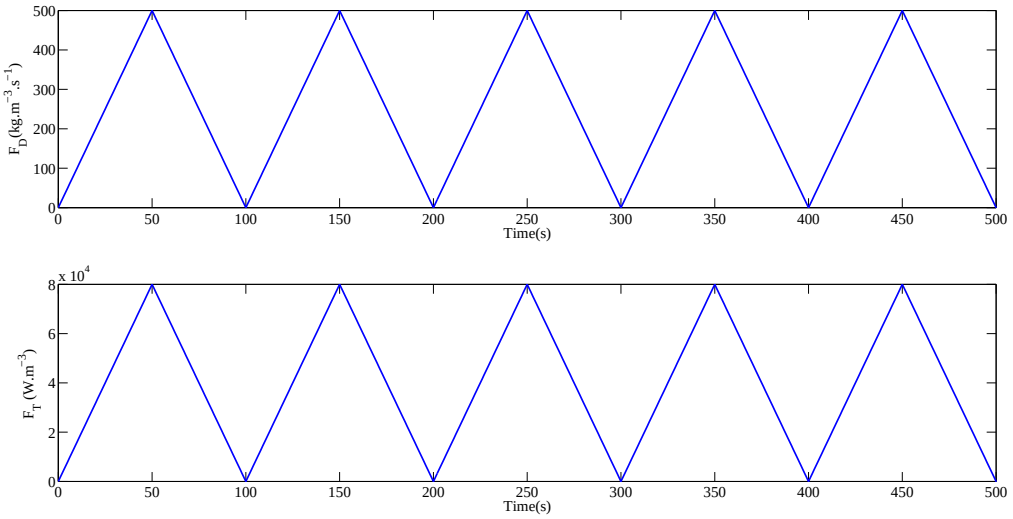


Figure 4.23: The first five cycles of the cyclic loading with a cycle time $\tau_c = 100s$

In the diffusion equation Eq. (4.15), c is the concentration, D is the diffusivity coefficient, and $F_D(t)$ referred to the mass source in the diffusion equation. This mass source can be due to chemical reactions for example. In the thermal-diffusion equation Eq. (4.16), T is the temperature, C_p is the specific heat, ρ is the density, k is the thermal conductivity, β is the coupling coefficient between the concentration and the temperature, and $F_T(t)$ is the heat source in the thermal-diffusion equation. The coupling term is here considered as proportional to the concentration, the coupling coefficient will be chosen such that the coupling doesn't not increase the temperature of more than 10%.

Provided that, the diffusion phenomenon has two characteristic times:

1. The cycle time of the load applied within the volumetric mass source F_D (denoted by τ_c^D).
2. The time associated with the physical properties ($\frac{L_c^2}{D}$) where L_c is the characteristic length. This physical time is denoted by τ_ϕ^D.

The thermo-diffusion problem has two characteristic times:

1. The cycle time of the load applied within the volumetric heat source F_T (denoted by τ_c^T).
2. The time associated with the physical properties ($\frac{\rho C_p L_c^2}{k}$) where L_c is the characteristic length. This physical time is denoted by τ_ϕ^T.

and the characteristic times associated with the diffusion phenomenon transferred by the coupling term.
Fig. 4.23 pinpoints the evolution of the load applied for the diffusion problem ($F_D(t)$) and the coupled thermo-diffusion problem ($F_T(t)$) in the particular case of $\tau_c = 100s$.

Table 4.11 outlines the physical time of the diffusion equation τ_ϕ^D for variable diffusivity coefficient, and the physical time of the thermo-diffusion equation τ_ϕ^T for variable specific heat. Small C_p leads to small τ_ϕ^T, the thermal-diffusion physical time and the specific heat being proportional. Comparatively, small D leads to high τ_ϕ^D, the diffusion physical time and the diffusivity coefficient being inversely proportional. The material properties and the coupling coefficient are reported in Table 4.12.

The concentration field of the diffusion equation is written as:

$$c(x,y,z,t) = \sum_{i=1}^{n} \alpha_i^D F_i^D(x) G_i^D(y) H_i^D(z) U_i^D(t) \tag{4.17}$$

D s.m^{-2}	6.25×10^{-3}	6.25×10^{-5}	6.25×10^{-6}
C_p J.kg^{-1}.C^{-1}	0.075	7.5	75.7
τ_ϕ(s)	0.1	10	100

Table 4.11: The physical times τ_ϕ^D and τ_ϕ^T with respect to the specific heat coefficient C_p and the diffusion coefficient D respectively

ρ	k	β
950 kg.m^{-3}	0.45 W.m^{-1}°C^{-1}	50 J.kg^{-1}.s^{-1}

Table 4.12: Material properties and the coupling coefficient

Keep in mind that each function of the mode $(F_i^D(x)G_i^D(y)H_i^D(z)U_i^D(t))$ is normalized with respect to the L^2 norm in the usual PGD algorithm.

4.6.2 Algorithm of the coupled thermo-diffusion problem

To solve the thermo-diffusion problem, we proceed as follows:

1. Construct a dictionary 5 such that:

   - **Dictionary** $D5^D_{(\tau_c=10)}$ for constant cycle time $(\tau_c = 10s)$ and different physical times $(\tau_\phi = 0.1,\ \tau_\phi = 10,\ \tau_\phi = 100s)$, this dictionary is related to the diffusion equation only.
   - **Dictionary** $D5^T_{(\tau_c=100)}$ for constant cycle time $(\tau_c = 100s)$ and different physical times $(\tau_\phi = 0.1,\ \tau_\phi = 10,\ \tau_\phi = 100s)$, this dictionary is related to thermal problem only (without the coupling term).

   Remark. The most significant modes of each dictionary are chosen based on the criterion (4.3). The number of the significant modes (space-time modes) needed for each case is presented in Table 4.13. Each of these dictionaries is evaluated with different physical times. Accurate results were obtained with a maximum relative error equal to 1.8%. It is worth noting, that the method is able to generate an accurate prediction of the solution even in case of null boundary condition and a cyclic heat source.

2. Solve the diffusion equation by computing the α_i^D coefficient.

3. The coupled term appears to be in the right-hand side which leads to a spatial-time effect. Thus, the load is now spatially variable. Consequently, the concentration term will be written as Eq. (4.17).

$\tau_\phi(s)$	0.1	10	100
$D5^D_{(\tau_c=10)}$	3	6	13
$D5^D_{(\tau_c=100)}$	3	6	10
$D5^T_{(\tau_c=10)}$	3	6	14
$D5^T_{(\tau_c=100)}$	3	6	9

Table 4.13: Number of most significant modes with respect to the physical time and cycle time τ_c of each dictionary for diffusion and thermal problem only (uncoupled problems)

4. A new dictionary $D5^{T-D}$ that includes both dictionaries (thermal and diffusion dictionaries) is created such that:

$$D5^{T-D} = D5^{T}_{(\tau_c=100)} \sqcup D5^{D}_{(\tau_c=10)} \tag{4.18}$$

5. The new dictionary $D5^{T-D}$ is used to compute the solution of the coupled thermal equation.

4.6.3 Dictionary evaluation of the thermo-diffusion problem

To validate the ability of the method to solve a thermo-diffusion problem, a collection of the most significant modes gathered in dictionary $D5^{T-D}$ are used to solve thermo-diffusion problem with different physical times:

- same physical times for diffusion and thermal phenomena,
- different physical time for each phenomenon.

Firstly, we consider the following coupled problem:

- Diffusion problem: the physical time is $\tau^D_\phi = 3s$ and the cycle time of the mass source is $\tau^D_c = 10s$
- Thermal problem: the physical time is $\tau^T_\phi = 3s$ and the cycle time of the heat source is $\tau^T_c = 100s$.

This problem represents the case with the same physical time for the two phenomena. The considered dictionary denoted by dictionary 5 is a combination of $D5^{T}_{(\tau_c=100)}$ and $D5^{D}_{(\tau_c=10)}$, thus the modes corresponding to the cycle time are present in the dictionary. The variation of the α_i coefficient with respect to the modes of dictionary 5 is shown in Fig. 4.24 for the temperature. The temperature solution is built from the modes of dictionary 5 and the calculated α_i. Fig. 4.25 depicts the temperature solution for $\tau_\phi = 3s$ using this approach versus the full PGD solution. An relative error of less than 2.6% is obtained. As the two physical times are equal, only the cycle time effect is visible: the solution is composed by a periodic function of $100s$ where a cycle time of $10s$ is added. To more illustrate the effect of the coupling, the evolution of the temperature for the uncoupled problem is shown in Fig. 4.28.
Secondly, we consider the following coupled problem:

- Diffusion problem: the physical time is $\tau^D_\phi = 20s$ and the cycle time of the mass source is $\tau^D_c = 10s$
- Thermal problem: the physical time is $\tau_\phi = 3s$ and the cycle time of the heat source is $\tau^T_c = 100s$.

This problem represents the case with two different physical times. The physical time for the diffusion phenomena is larger than the physical time of the temperature phenomena and is larger than the cycle time of the diffusion phenomena. The evolution of the concentration is different as illustrated in Fig. 4.28.
Dictionary 5 is used to solve this new thermo-diffusion problem. The variation of the α_i coefficient with respect to the modes of the dictionary 5 is shown in Fig. 4.26. The effect of the coupling term is more marked with larger values of the α_i coefficients assoiated with the modes related to the diffusion compared to the previous studied coupled case. The temperature solution is then built and compared to the full PGD solution for a given spatial point as shown in Fig. 4.27. The response is similar to the previous one for the effect of the cycle time. The minima and maxima of the temperature values are different and more precisely the first cycles (small deviation) due to the change in the physical time of the diffusion phenomenon.
The remarkable result is the ability of the method to generate accurate solutions for different physical times in case of a thermo-diffusion problem.

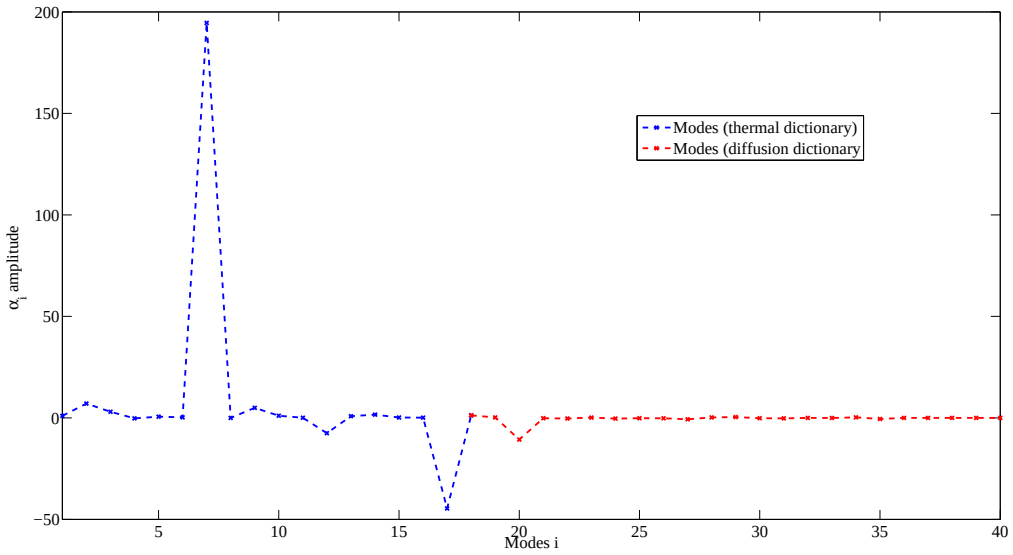


Figure 4.24: The evolution of the α_i coefficient for $\tau_\phi = 3s$ (same physical time) with respect to the modes of the coupled dictionary denoted by dictionary 5 in case of the coupled problem for the temperature

Remark. Since the uncoupled thermal and diffusion problems have the same nature, it is not necessary to distinguish a particular dictionnary related to the diffusion and another one related to the thermal, only dictionnaries related to the different cycle times have to be considered. For example dictionary $D5^{T-D} = D5^{T}_{(\tau_c=100)} \sqcup D5^{D}_{(\tau_c=10)}$ could be replaced by $D5^{D-D} = D5^{D}_{(\tau_c=100)} \sqcup D5^{D}_{(\tau_c=10)}$. The dictionary is finally similar to the dictionary for many harmonics.

4.7 Conclusion

To save computation time, many methods are already discussed in the bibliography. For this purpose, this chapter proposes to use an efficient (space-time) basis to greatly decrease the computation time for problems with different characteristic times such as physical time and cycle time.
The efficient basis is first created by building a dictionary with the significant modes calculated using the PGD. Unlike the POD, these modes are space-time modes. In this chapter, the solution of a cyclic heat problem is computed by projection on the significant modes of the dictionary. Different dictionaries have been evaluated: dictionary 1 with a given cycle time and different physical times; dictionary 2 with a given physical time and different cycle times. The solution built using dictionary 1 matches the full PGD solution with a saving computational time around 50 and a relative error less than 2%. However, the solution computed using dictionary 2 leads to less accurate results compared to the full PGD solution. This is due to the fact that the fluctuation is different for each particular cycle time. To obtain an accurate result, the modes related to the particular cycle time have to be added to the dictionary. It is noteworthy that accurate results were obtained in the case of a fixed cycle time and variable physical time for different boundary conditions. Further studies showed that an enriched dictionary denoted by D_4, union of the dictionaries of the different harmonics, can be used for a case with many harmonics. Let us notice that a large number of modes is required depending on the number of harmonics. Moreover, dictionary D_5 built from thermal and diffusion problems only can be used to solve a coupled thermo-diffusion problem generating accurate results. So far, the results are very promising and encouraging. Equally important, the approach has the potential to solve a thermo-diffusion problem with accurate results.
However, the method presents some limitations in the case of different cycle times as the modes related to the cycle times of the problem have to be added in the dictionary. This issue can be related

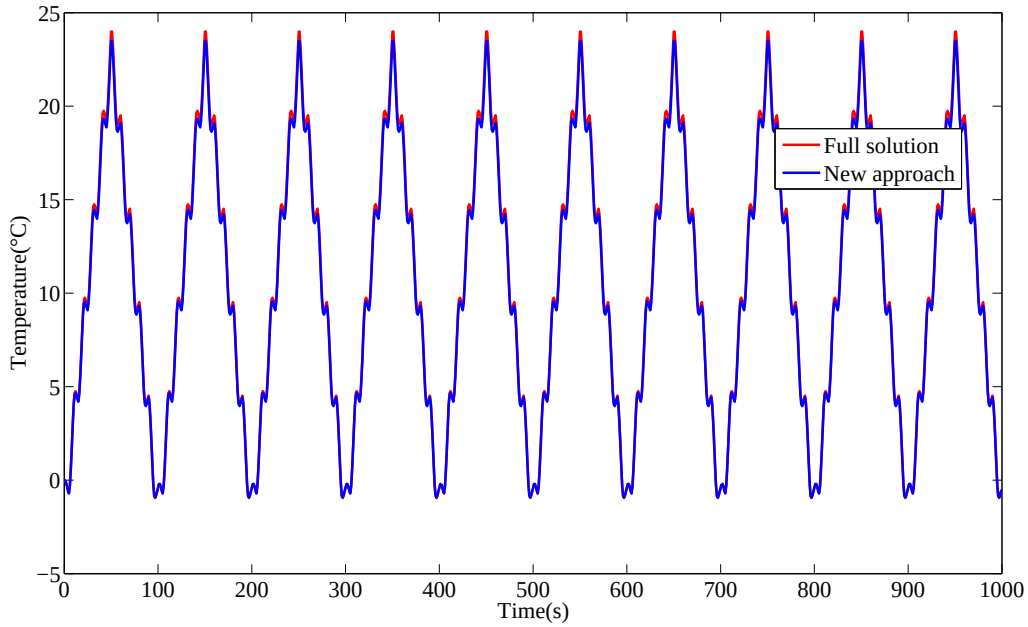


Figure 4.25: The evolution of temperature under same physical time ($\tau_\phi = 3s$) and $\tau_c^T = 100s$ and $\tau_c^D = 10s$ at $(x, y, z) = (25, 25, 25)$

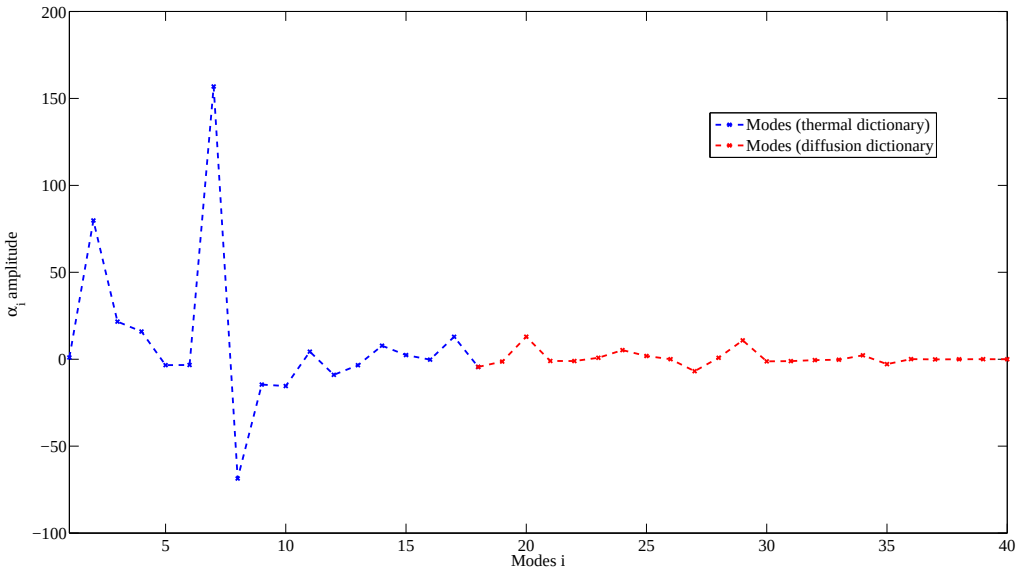


Figure 4.26: The evolution of the α_i coefficient for $\tau_\phi = 20s$ (different physical times) with respect to the modes of the dictionary 5 in case of the coupled problem for the temperature

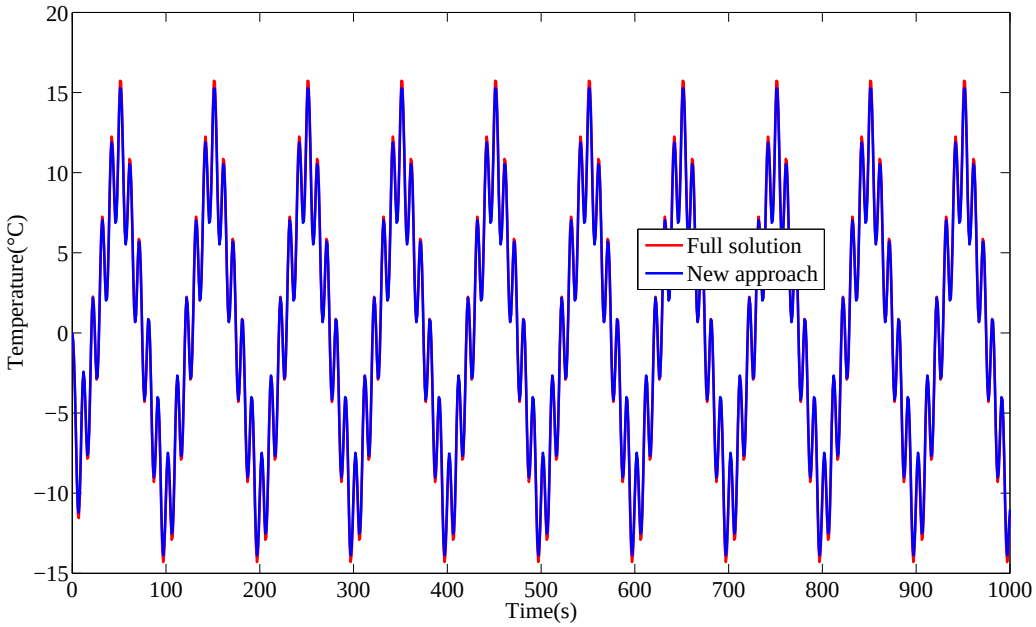


Figure 4.27: The evolution of temperature under $\tau_\phi^T = 3s$ and $\tau_c^T = 100s$ with $\tau_\phi^D = 20s$ and $\tau_c^D = 10s$ at (x, y, z) = (25, 25, 25)

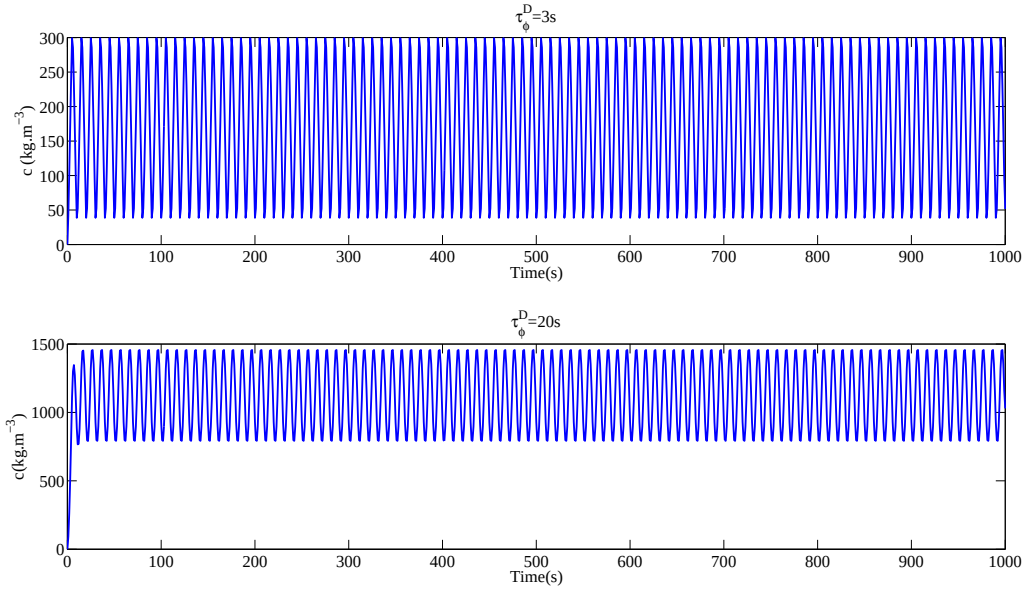


Figure 4.28: Uncoupled case : the evolution of concentration under $\tau_\phi^D = 3s$ and $\tau_\phi^D = 20s$ with $\tau_c^D = 10s$ at $(x, y, z) = (25, 25, 25)$

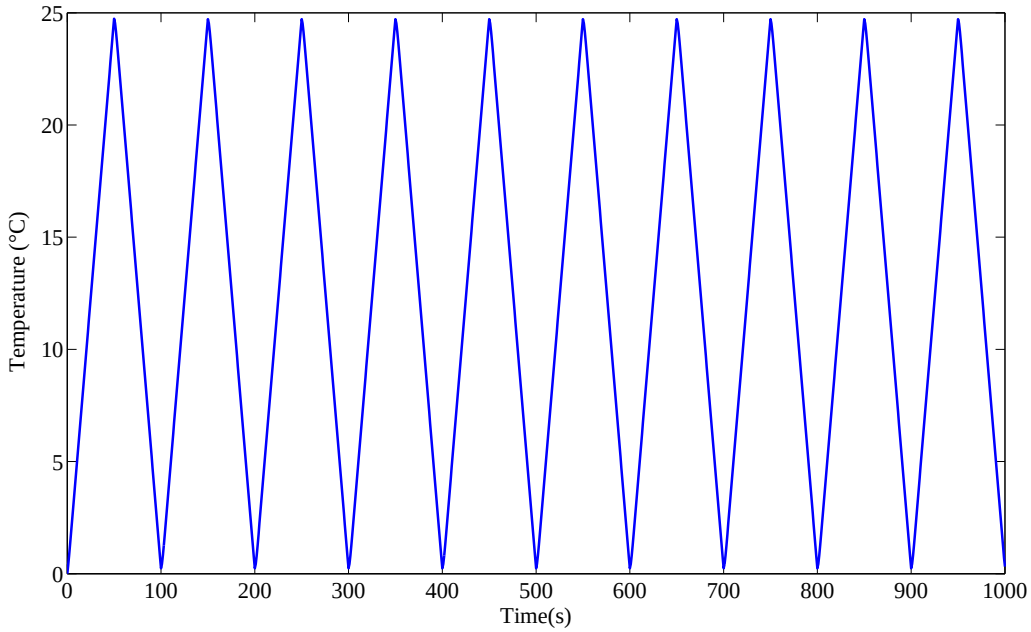


Figure 4.29: The evolution of temperature under $\tau_\phi = 3s$ and cycle time $\tau_c^T = 100$ without coupling effect

to the use of the temporal basis deduced from the PGD method. In the next chapter, a temporal basis parametrized by the cycle time and the physical time is investigated.

Chapter 5

Towards a priori timebasis - proposal of a mixed strategy

—

Research is to see what everybody else has seen, and to think what nobody else has thought.
Albert Gyorgyi

Contents

5.1 Introduction . . . 92
5.2 Presentation of the method . . . 92
5.3 Mixed strategy for 3D linear problem . . . 94
5.3.1 Algorithm . . . 94
5.3.1.1 Problem description . . . 94
5.3.1.2 Strategy to generate the time bases . . . 95
5.3.1.3 Algorithm to compute the spatial bases . . . 100
5.3.2 Numerical results . . . 101
5.3.2.1 Homogeneous Dirichlet boundary conditions . . . 101
5.3.2.2 Non-homogeneous Dirichlet boundary conditions . . . 104
5.3.2.3 Opposite non-homogeneous Dirichlet boundary conditions . . . 107
5.3.2.4 Robin boundary conditions . . . 109
5.3.2.5 Non-constant source and non-homogeneous Dirichlet with different cycle times . . . 109
5.3.3 Effect of the time basis order . . . 111
5.3.4 Usage of the time basis to generate solution with larger number of cycles . . . 113
5.3.5 Usage of the time basis to generate solution with larger time domain . . . 114
5.3.6 Influence of the load . . . 116
5.3.6.1 Sinusoidal . . . 117
5.3.6.2 Heaviside . . . 122
5.3.6.3 Influence of the ratio $(\frac{T_{min}}{T_{max}} = -1)$ . . . 126
5.3.6.4 Influence of the load amplitude . . . 127
5.3.7 Extension to coupled problem . . . 131
5.3.8 Discussion on the use of the mixed strategy for linear problem . . . 135
5.4 Mixed strategy for 3D non linear problem . . . 135
5.4.1 Algorithm . . . 135
5.4.1.1 Choice of the time bases . . . 135
5.4.1.2 Algorithm to compute spatial basis and to solve the non-linearity . . . 136
5.4.2 Numerical results . . . 136
5.4.2.1 Nonlinear heat equation with one cycle time . . . 136
5.4.2.2 Nonlinear heat equation with two cycle times . . . 143
5.4.3 Discussion on the use of the mixed strategy for nonlinear problem . . . 145
5.5 Conclusion . . . 145

5.1 Introduction

In this chapter, a new numerical strategy to reduce computation time by avoiding the use of an incremental scheme is presented. This strategy is based on the knowledge of an a priori known basis like the well-known Proper Orthogonal Decomposition method (POD) [Chatterjee, 2000]: the time basis, and the construction of the basis within an iterative procedure like the Proper Generalized Decomposition method (PGD) [Ladeveze et Nouy, 2003]: the spatial basis. The method can be seen similar to the LATIN method as the solution is sought under a space-time representation [Ladeveze *et al.*, 2010].
The originality of the approach is the construction of the a priori time basis. To propose an efficient time basis, the study of the solution within the frequency domain via the Fast Fourier Transform (FFT) is considered and an analytical expression of the time basis is provided.
In summary, the major issues treated in this chapter are:

1. Propose a new approach that can be applied for different cycle times. Note that the method proposed in Chapter 4 can not be generalized for different cycle times.
2. Create of a priori time basis with analytical expressions.
3. Check the feasibility of this approach called the mixed strategy for different problems: different physical times (τ_ϕ), cycle times (τ_c) and boundary conditions.
4. Enrich the dictionary by taking different types of loads.
5. Extend the approach to a coupled problem.
6. Propose an algorithm to solve the non-linear problem with this approach.

5.2 Presentation of the method

The basic idea of the method arises from the observation that, in the context of alternating time problems, the solution consists of the combination of a transient part (deviation) and a fluctuation (cyclic) as illustrated in Fig. 5.1 for the response of a 3D conduction problem under cyclic loading. With this in mind, for thermal problem, the solution illustrates the combination of the time scales present in the phenomenon. Provided that, two different time scales control this phenomenon: the physical time τ_ϕ related to the material properties and the cycle time τ_c associated with the loading. The approach is presented as follows: Fast Fourier Transform of a generic problem is done in order to construct a time basis in the frequency domain, followed by the decomposition of the FFT by peaks. Each peak generates a basis in the frequency domain.Then, the peaks are grouped into two types: one related to the physical time and the other related to the cycle time. After that, the bases are projected using the Inverse Fast Fourier Transform (IFFT) in real space (time domain) [AL Takash *et al.*, 2017], where an analytical expression is developed with respect to the type of the basis. The question arises to the representativeness of a priori basis, as well as the convergence of such a technique.

Thus, the main ingredients of this method are:

1. Fast Fourier Transform (FFT).
2. Proper Generalized Decomposition (PGD).

The FFT will be used to analyze different problems and as a tool to construct the time bases. However, the algorithm of the approach is similar to the classical PGD algorithm but the time bases are a priori known. Thus, the second ingredient (PGD) will be used to compute the spatial bases. Fig. 5.2 illustrates the algorithm of the proposed approach. In the following, the construction of a time basis a priori is investigated.

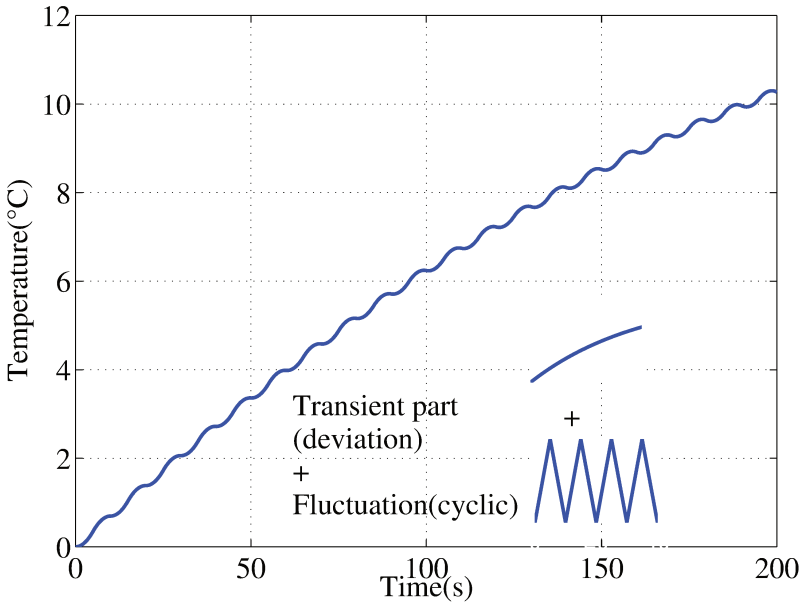


Figure 5.1: Combination between transient part and a fluctuation part

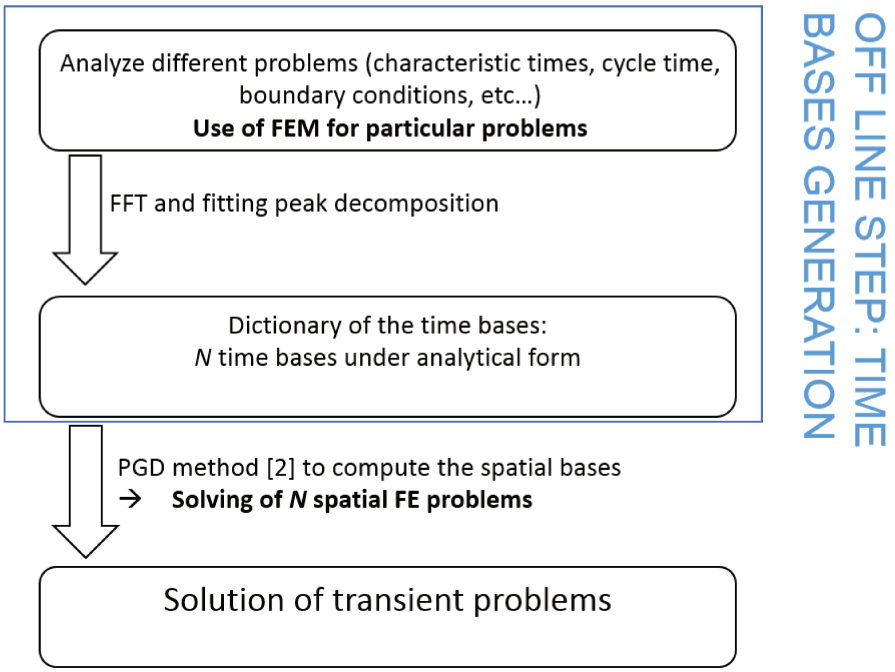
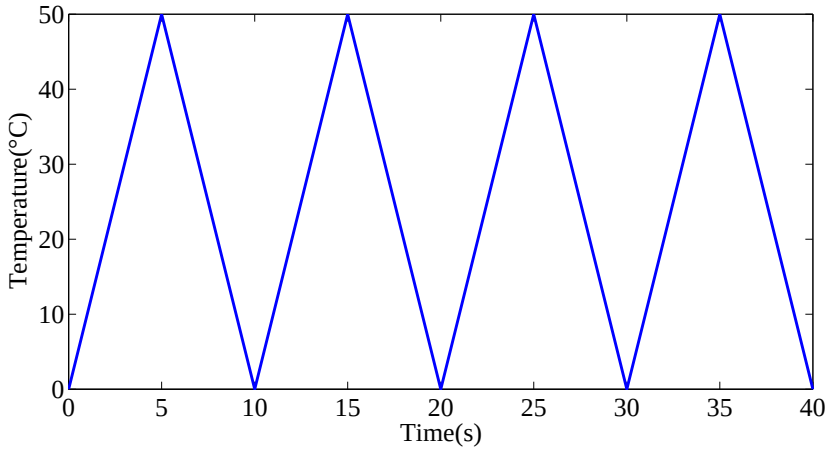
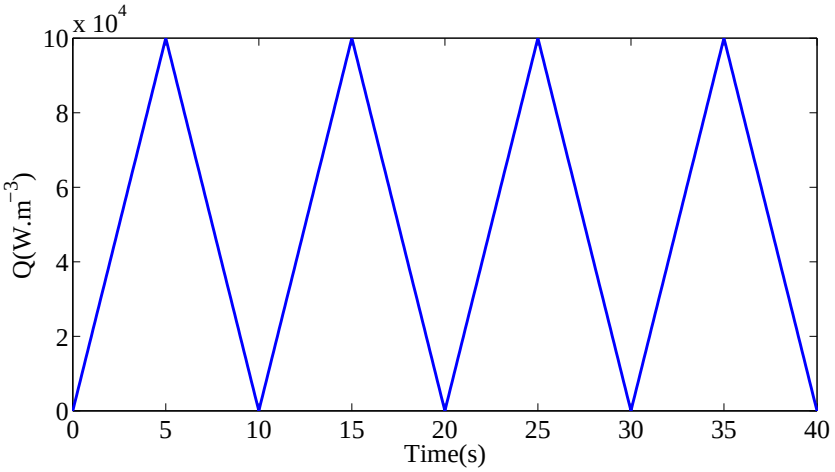


Figure 5.2: Presentation of the algorithm and the ingredient of the approach



(a) The evolution of temperature



(b) The evolution of heat source

Figure 5.3: The first four cycles of the cyclic loading with a cycle time $\tau_c = 10s$

5.3 Mixed strategy for 3D linear problem

5.3.1 Algorithm

5.3.1.1 Problem description

Consider a cube of side L subjected to a cyclic temperature in triangular form with a $\boldsymbol{R} = \frac{T_{\min}}{T_{\max}} = 0$ and a maximal temperature $T_{\max} = 50°\mathrm{C}$ as shown in Fig. 5.3. This load is imposed in different forms: volumetric heat source, heat flux boundary conditions which refers to Robin boundary conditions, and surface cyclic temperature which refers to Dirichlet boundary conditions.
The thermal problem studied is under Fourier law's assumption:

$$\begin{aligned} \rho C_p \frac{\partial T}{\partial t} &= k\Delta T + Q \\ T(x, y, z, t = 0) &= 0 \end{aligned} \tag{5.1}$$

where $T(\underline{x}, t)$ is the temperature field and $\underline{x} = (x, y, z)$, $t \in [0, L_t]$; ρ represents the density of the polymer, C_p its specific heat, k its thermal conductivity, Q the volumetric heat source and Δ represents the three-dimensional Laplacian.

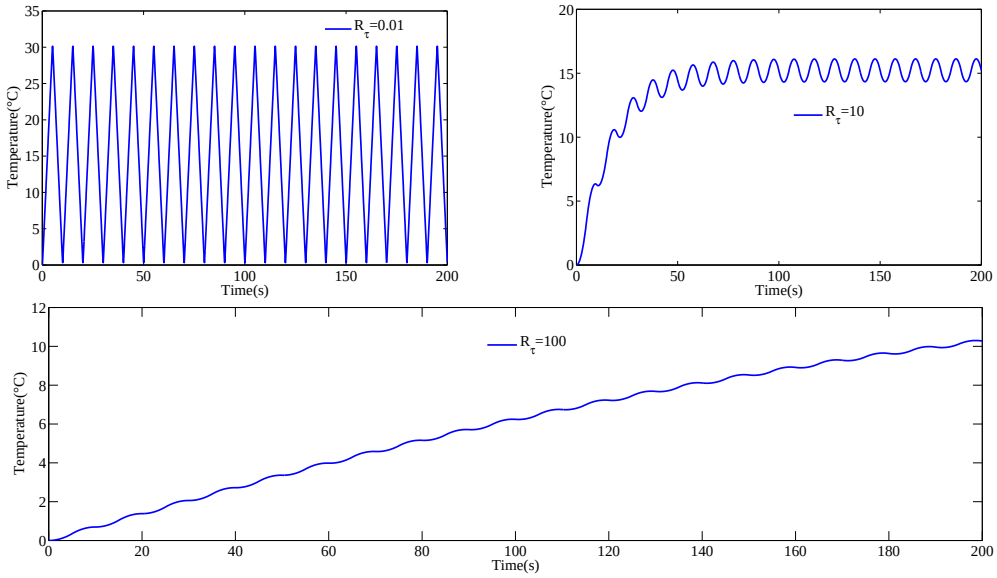


Figure 5.4: The evolution of the temperature for different values of $R_\tau = \frac{\tau_\phi}{\tau_c}$ with a constant cycle time $\tau_c = 10s$.

5.3.1.2 Strategy to generate the time bases

To generate the time bases, first assume that the model encounters a cyclic heat source in triangular form with a ratio $\boldsymbol{R} = 0$ and a cycle time $\tau_c = 10s$ as illustrated in Fig. 5.3(b); null initial and boundary conditions. Provided that, thermal problem has two characteristic times: the cycle time of the load applied within the volumetric heat source Q (denoted by τ_c) and the time associated with the physical properties $\left(\frac{\rho C_p}{k} L_c^2\right)$ (denoted by τ_ϕ) where L_c represents a characteristic length. The evolution of the temperature is controlled by the relationship between the cycle time and the physical time.
As an illustration, let us consider a heat problem under cyclic heat source with a cycle time τ_c equals $10s$ and with null boundary conditions. The solution depends on the relationship between the physical and the cycle times where the ratio $\frac{\tau_c}{\tau_\phi}$ is denoted by R_τ. Fig. 5.4 compares the different behaviors that are generated for different values of R_τ:

- When the physical time is smaller than the cycle time ($R_\tau < 1$), the evolution of the temperature is very fast, and the stabilized cycle is quickly reached.
- By way of contrast, when the physical time and cycle time are of the same order, the temperature reaches the stabilization after 4 cycles.
- For larger physical times ($R_\tau > 1$), the stabilization is not reached at the end of the simulation.

Different physical times are used, which illustrate the different responses. It is important to identify and analyze the effect of physical time on the frequency domain.
Preliminary, the problem is solved with the Finite Element Method (FEM) using ABAQUS software. In the first place, a fixed spatial point has been chosen (the center point). Nevertheless, the effect of spatial point is discussed. Notably, an efficient basis can be generated by considering different points.
A Fast Fourier Transform (FFT) is held on the time spectrum for different problems with different physical and cycle times. Let us note that to evaluate the effect of the physical time, the specific heat was changed where the conductivity and the density were kept constant. Table 5.1 summarizes the value of the physical time for variable specific heat with $\rho = 950\ \mathrm{kg.m^{-3}}$, $k = 0.45\ \mathrm{W.m^{-1}.C^{-1}}$ and $L_c = 25\mathrm{mm}$ (L_c being equal to one half of the cube). Small specific heat leads to small physical time, the physical time and the specific heat being proportional.

C_p [Joule.kg^{-1}.°C^{-1}]	0.075	0.75	7.5	75	757	7570
$\tau_\phi[s]$	0.1	1	10	100	1000	10000

Table 5.1: The physical time τ_ϕ with respect to the specific heat C_p

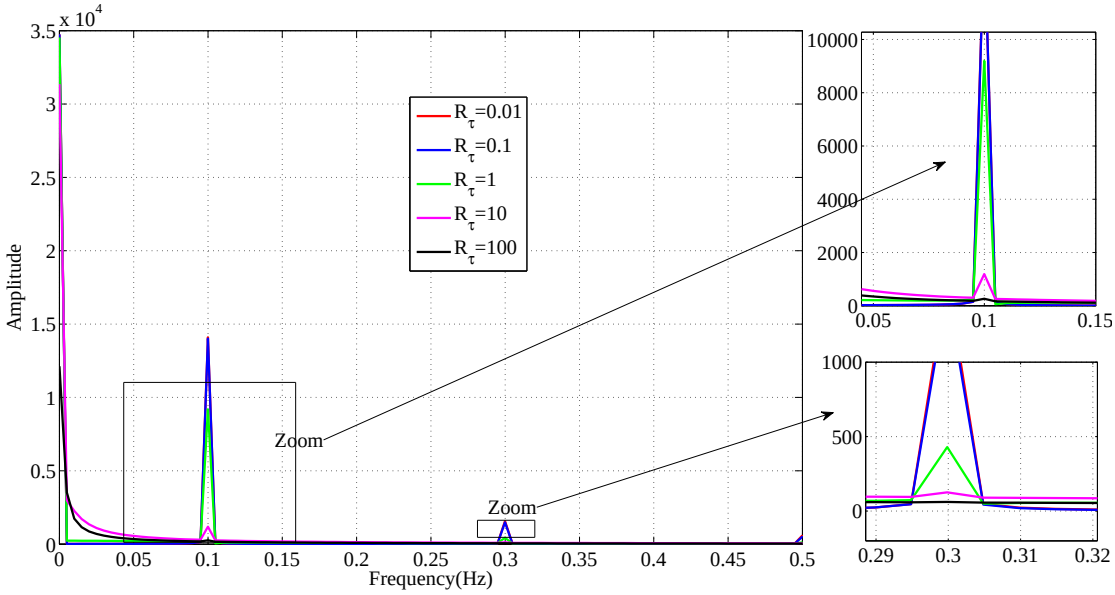


Figure 5.5: The FFT of a fixed spatial point at the center of the cube for different values of $R_\tau = \frac{\tau_\phi}{\tau_c}$ and a constant cycle time $\tau_c = 10s$

Let us recall that R_τ denotes the ratio between physical time and cycle time. For a visual representation of the effect of physical time with a fixed cycle time $\tau_c = 10s$ on the evolution of the spectrum in the frequency domain, the related time bases in frequency domain are presented in Fig. 5.5.

Obviously, the relationship between the physical time and the cycle time is comprehensive. It is important to realize, that three different behaviors were shown:

1. For small physical time compared to the cycle time ($R_\tau > 1$), the evolution of the spectrum in frequency matches together. In this case, the first peak seems to be linear. So far, the second peak which looks like Gaussian curve shows the effect of the importance of the applied load. To sum up, the most important information of the solution are present in the first and second peaks.

2. When $R_\tau = 1$, the cycle time and the physical time are equal, the amplitude of the peaks starts to decrease.

3. When $R_\tau < 1$ in which the physical time is larger than cycle time, the amplitude takes an exponential form and the second peak is less effective. In like manner, the amplitude of the third peak decreases with the increase of the physical time.

To highlight the effect of spatial points, a study with a large physical time $\tau_\phi = 1000s$ is done. The evolution of frequency spectrum is checked for 4 different points chosen from the cube.
Fig. 5.6 depicts the amplitude of the FFT of four different points. First, the observation shows that the spectrum is a combination of transient and Gaussian peaks, most compelling evidence is that transient part is related to the characteristic time and the Gaussian peaks refer to the effect of cyclic load. To emphasize, since in this case the applied load is the heat source, thus the maximum energy will be concentrated at the center of the cube which explains the highest amplitude at the

center $((x, y, z) = (25, 25, 25))$. Let us note that this variation shows that a fixed point is capable to capture the information for different points since they are varied by the magnitude.

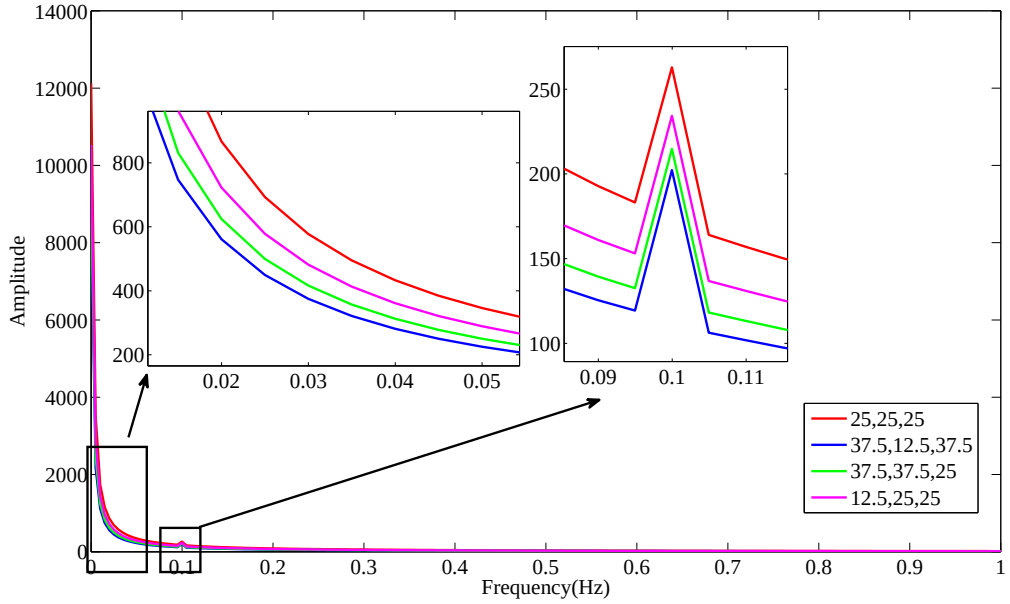


Figure 5.6: The variation of the amplitude of the peaks in the frequency domain for 4 different points

Accordingly, to build the basis from the first peak which is associated to the effect of the physical time, the first peak is projected for all different characteristic times, considered in these simulations, on the time domain using the Inverse Fast Fourier Transform (IFFT). An analytical expression of the related time basis is generated within a fitting step.

To clarify the time bases creation, an example, where $R_\tau = 10$, $\tau_c = 10s$ and $\tau_\phi = 100s$ is detailed. First, the solution of this particular problem is solved with FEM (or another method like PGD). The evolution of temperature at the center point and the FFT of this solution are shown in Fig. 5.7. Different peaks are seen where each peak is related to time basis. For peak 1 related to the average of the evolution and the effect of the transient, a time basis is generated from the IFFT of the peak and fitted within the function as shown in Fig. 5.8.
Same procedure has been developed for different R_τ so that we would be able to construct a priori time basis. Different time bases associated with the physical time are plotted in Fig. 5.9. The results obtained are compatible with the fact that as the physical time increases the evolution of the temperature decreases and becomes more exponential. Thus, the transformation from frequency to time domain shows the effect of the physical time.

The following empirical equation is used for the first time basis:

$$S_1^\phi(t) = a(1 - A \times \exp(-\frac{5}{\tau_\phi}t)) \qquad A = 1 - \exp(-0.7R_\tau) \tag{5.2}$$

where the coefficient *a* refers to the amplitude of the the time-basis which can be captured within the spatial modes, set to be 1, and $S_1^\phi(t)$ corresponds to the time basis related to the physical time τ_ϕ and the cycle time τ_c through the ratio R_τ.

The other peaks refer to the effect of the cycle time and physical time. To illustrate this, the cycle time is taken $10s$. Consequently, the frequency is $0.1Hz$ which explains the location of the second peak and the other peaks. With this intention, the location of these peaks can be noticed

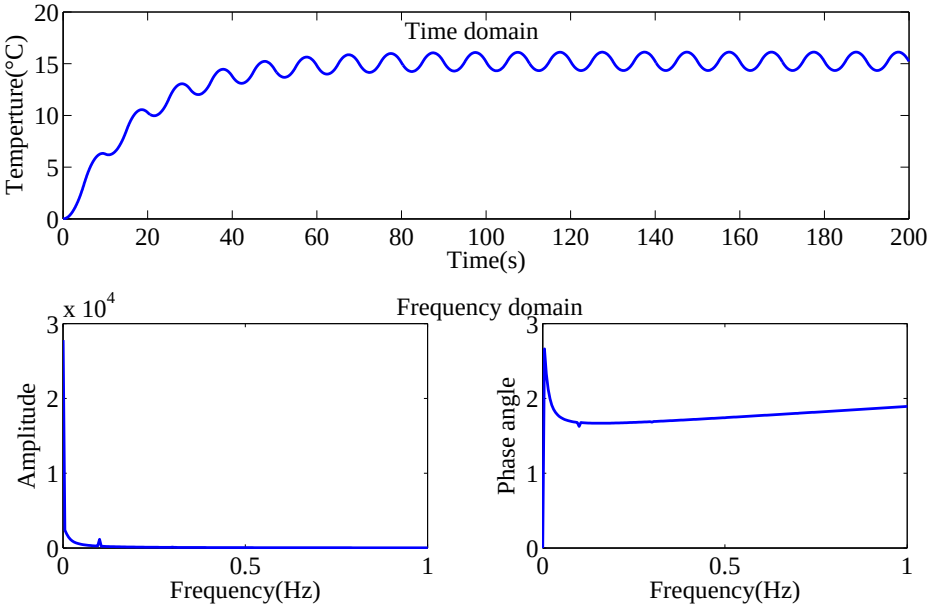


Figure 5.7: The evolution of the temperature in the time domain and frequency domain at the center point $(x, y, z) = (25, 25, 25)$

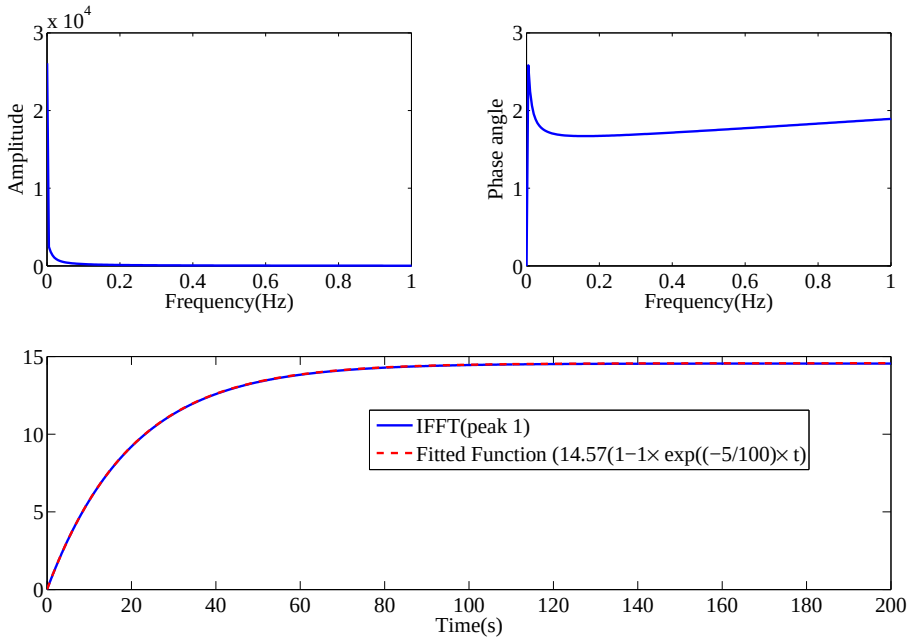


Figure 5.8: Generation of the time basis for the first peak

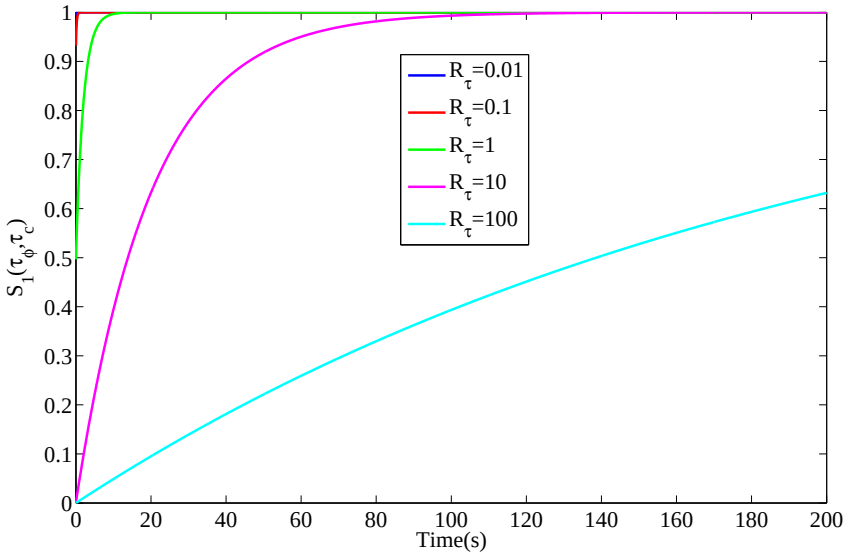


Figure 5.9: The time basis generated from the first peak with $S_1 = 1 - A \times exp(\frac{-5t}{\tau_\phi})$

from the FFT of the load applied as shown in Fig. 5.10. To generate a time basis for these peaks, FFT has been held for different characteristic times, then projected using IFFT in time domain where an empirical equation has been generated as shown in Eq. 5.3:

$$S_{i+2}(t) = A \times cos((2i+1)w \times t + \theta(R_\tau)) \tag{5.3}$$

where $i = 0...n$, n is the number of modes, $w = 2 \times \pi \times f$, and $f = \frac{1}{\tau_c}$. To calculate $\theta(R_\tau)$, an empirical equation has been developed:

$$\theta(R_\tau) = \begin{cases} \pi - tan^{-1}(1.04 \times R_\tau), & 0 \leq R_\tau \leq 10 \\ 1.007\pi - tan^{-1}(1.329 \times R_\tau), & 10 \leq R_\tau \leq 100 \end{cases}$$

.

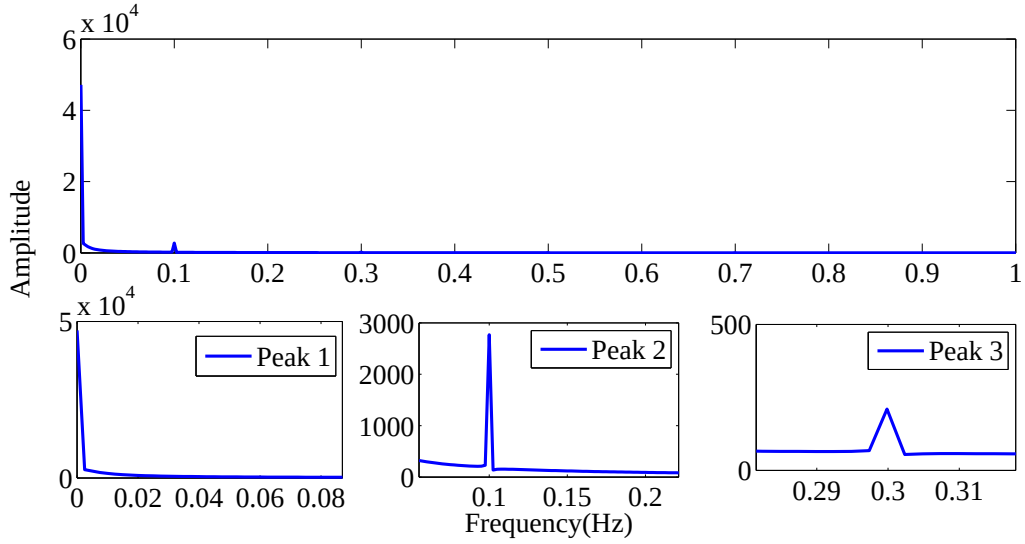


Figure 5.10: The FFT of the load applied

The evolution of the phase angle θ with respect to R_τ is depicted in Fig. 5.11. The evolution showed that as R_τ, the ratio of the physical time to the cycle time increases, $\theta(R_\tau)$ decreases to

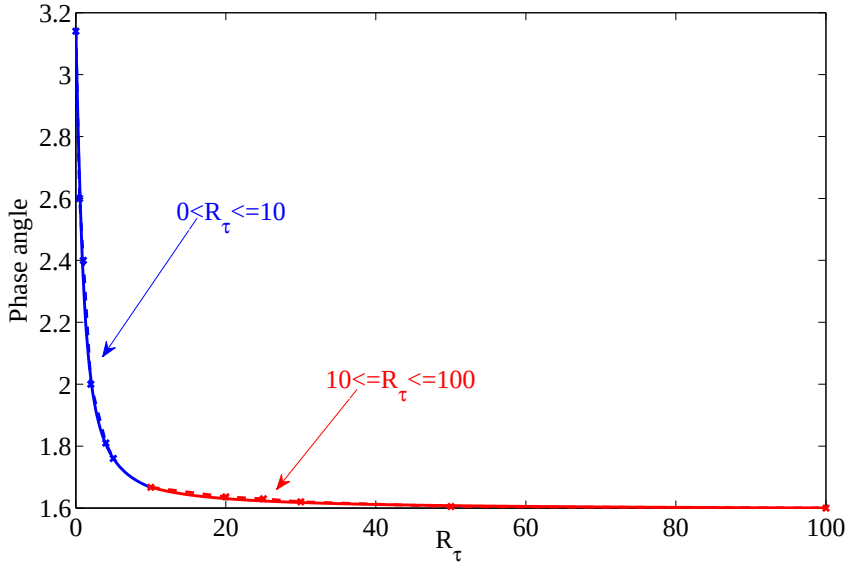


Figure 5.11: The evolution of the phase angle with respect to R_τ

reach a stabilized value ≈ 1.6.

To sum up, to create the dictionary of time bases, the first time basis is related to the effect of the physical time and the other time bases are related to the frequency of the load applied knowing that the physical time affects the evolution of the magnitude of the other peaks.

5.3.1.3 Algorithm to compute the spatial bases

The time bases are denoted by $S_i(t), i = 1..n$. There are a priori predicted as presented in the previous section and we look forward to the associated spatial bases $R_i(\underline{x}), i = 1..n$, $\underline{x} = (x, y, z)$ such that the space-time solution is written in the following separated form:

$$T(\underline{x}, t) = \sum_{i=1}^{n} R_i(\underline{x}) S_i(t) \tag{5.4}$$

The spatial modes are obtained via the following procedure.
Assume that the first k spatial modes are known and compute the next spatial mode $k+1$ that is $R_{k+1}(\underline{x})$, which is the solution of the Galerkin variational form of Eq.(5.1) with the real and virtual fields written as follows:

$$T(\underline{x}, t) = \sum_{i=1}^{k} R_i(\underline{x}) S_i(t) + R_{k+1}(\underline{x}) S_{k+1}(t) \tag{5.5}$$

$$T^*(\underline{x}, t) = R^*_{k+1}(\underline{x}) S_{k+1}(t) \tag{5.6}$$

The field R^*_{k+1} is assumed kinematically admissible.
After integrating by parts and taking into account the boundary conditions, this leads to the following equation:

$$\rho C_p \int_{\Omega \times \Omega_t} T^* \frac{\partial T}{\partial t} d\Omega dt + k \int_{\Omega \times \Omega_t} \vec{\nabla} T \, \vec{\nabla} T^* d\Omega dt = \int_{\Omega \times \Omega_t} Q T^* d\Omega dt \tag{5.7}$$

To find $R_{k+1}(\underline{x})$, it is enough to solve a spatial problem. Using the Finite Element Method, it leads to the following discrete form:

$$\begin{aligned}\left(\rho C_p \chi_t^{k+1\ k+1}[M] + k\gamma_t^{k+1\ k+1}[K]\right)\{R_{k+1}\} = \\ -\sum_{i=1}^{k}\left(\rho C_p \chi_t^{ik}[M]\{R_i\} + k\gamma_t^{ik}[K]\{R_i\}\right) + q_t^k[M]q_x\end{aligned} \tag{5.8}$$

with $\gamma_t^{ik} = \int_{\Omega_t} S_i(t)S_k(t)$, $\chi_t^{ik} = \int_{\Omega_t}(S_k(t)\frac{\partial S_i(t)}{\partial t})dt$, $q_t^k = \int_{\Omega_t} S_k(t)q_t(t)dt$,
$[K]$ is referred to the stiffness matrix, $[M]$ the conductance matrix, R_{k+1} are the nodal values of the spatial function and q_x are the nodal values of the spatial function associated with Q the volume heat source.
For the purpose of simplicity, Q is written under a space-time separated representation as follows: $Q = q_x(\underline{x})q_t(t)$ where q_t is cyclic.

5.3.2 Numerical results

In what follows, a priori time bases generated in section 5.3.1.2 through analytical forms given in Eq. (5.2) and Eq. (5.3) are used and the efficiency of the method is discussed through 5 different cases:

1. Homogeneous Dirichlet boundary condition, with different physical times and cyclic heat source.
2. Non-homogeneous Dirichlet boundary conditions with a cyclic load on all surfaces.
3. Opposite non-homogeneous Dirichlet boundary conditions.
4. Robin boundary conditions with cyclic T_∞ .
5. Non-constant source and non-homogeneous Dirichlet with different cycle times.

For all simulations, the values of the parameters ρ and k are fixed: $\rho = 950\ \mathrm{kg.m^{-3}}$, $k = 0.45\ \mathrm{W.m^{-1}.C^{-1}}$.
Let us note that to improve the accuracy of this approach the relative error is computed using the following equation for all cases:

$$E(\%) = \frac{\|T_{ref} - T_{method}\|}{\|T_{ref}\|} \times 100 \tag{5.9}$$

where T_{ref} is the Finite Element solution and T_{method} is the solution obtained with the proposed strategy. To choose the number of modes to be used, the following criteria is used with a stopping value of 10^{-4}

$$E(\%) = \frac{\|T_n\|}{\|T_{n-1}\|} \times 100 \tag{5.10}$$

5.3.2.1 Homogeneous Dirichlet boundary conditions

Throughout this section, the thermal model with a null initial and boundary conditions with a cyclic heat source is considered. The cyclic heat source, Q, consists of triangular form with $\boldsymbol{R} = \frac{Q_{\min}}{Q_{\max}} = 0$, $\tau_c = 10s$ and a maximum amplitude equal to $100000\ W.m^{-3}$. First, a priori basis issued from the analytical expressions are constructed. Then, the bases are used a priori to solve a spatial problem henceforth, build the solution from a priori time basis and spatial modes. A large physical time τ_ϕ equal to $1000s$ is used by considering the specific heat C_p equal to $757\ \mathrm{Joule.kg^{-1}.C^{-1}}$ (cf. Table 5.1). These time basis are then normalized using the L^2 norm and are shown in Fig. 5.12. They are called time modes. The number of the bases are chosen based on the stopping criteria. Fig. 5.13 depicts the convergence of Eq. (5.10) in function of the number of modes. Thus, 2 time

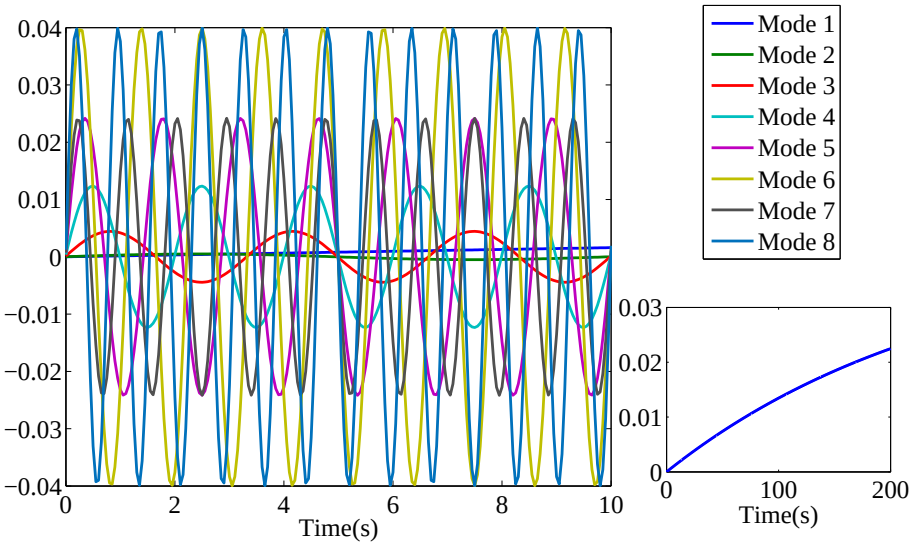


Figure 5.12: Normalized time modes for $\tau_\phi = 1000s$ issued from the analytical expressions

Spatial point (x,y,z)	$(25, 25, 25)$	$(37.5, 25, 25)$	$(37.5, 37.5, 37.5)$	$(37.5, 12.5, 37.5)$
Relative error for $\tau_\phi = 1000s$ (%)	1.6	2.3	2.8	2
Relative error for $\tau_\phi = 100s$(%)	1.8	2.1	2.6	1.9
Relative error for $\tau_\phi = 0.1s$(%)	1.1	1.6	1.5	1.6

Table 5.2: The relative error calculated for different points for $\tau_\phi = 1000s$, $\tau_\phi = 100s$ and $\tau_\phi = 0.1s$

bases will be used. The most significant mode corresponds to the second peak, notably, the modes are less effective as the frequency increases.

Fig. 5.14 illustrates the evolution of the temperature obtained with the FEM and the proposed approach. As expected, our approach captures and generates an accurate result compared to the FEM. The evolution of the temperature does not reach the stabilized cycle and it has a small amplitude due to the low thermal diffusivity.
To check the percentage error at different points in the model as represented in Fig. 5.15, the relative error is computed using (5.9) and presented in Table 5.2. The results show that the maximum relative error is 2.8%.

Similarly, for new physical time $\tau_\phi = 100s$, new time bases related to the new physical time and the load applied are generated using the analytical expression. The normalized basis using L^2 norm are shown in Fig. 5.16. It is clear that the first time basis is different from the previous case and the other time basis are similar but have different phase angle. The number of the basis are chosen based on the stopping criteria. Fig. 5.17 shows the evolution of equation Eq. (5.10) as function of the modes. 4 time bases will be then used. The evolution of the temperature is shown in Fig. 5.18 with a relative error equal to 1.6%. A maximum of the relative error equal to 2.6% using the L^2 norm in the whole domain is obtained as shown in Table 5.2.

To sum up, accurate results were obtained with high time-saving of order 54 (CPU time for the approach $= 1.932$s and CPU time for FEM$= 104.6$s). It can be explained by the fact that just 2 linear equations for $\tau_\phi = 1000s$ are solved with our approach (number of the priori time basis used) instead of 2000 linear equations with FEM (fixed time discretization with $\Delta t = 0.1$ and the total time $200s$). The approach is able to capture a large physical time problem.

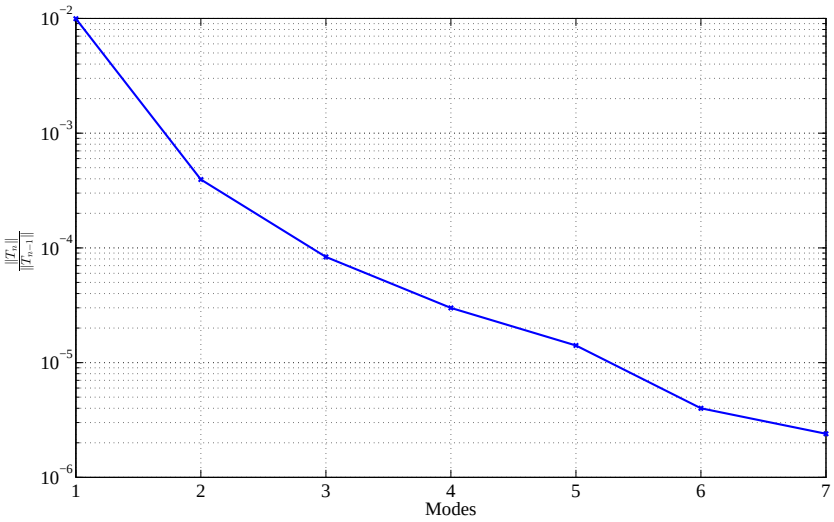


Figure 5.13: Convergence with respect to the number of modes for $\tau_\phi = 1000s$

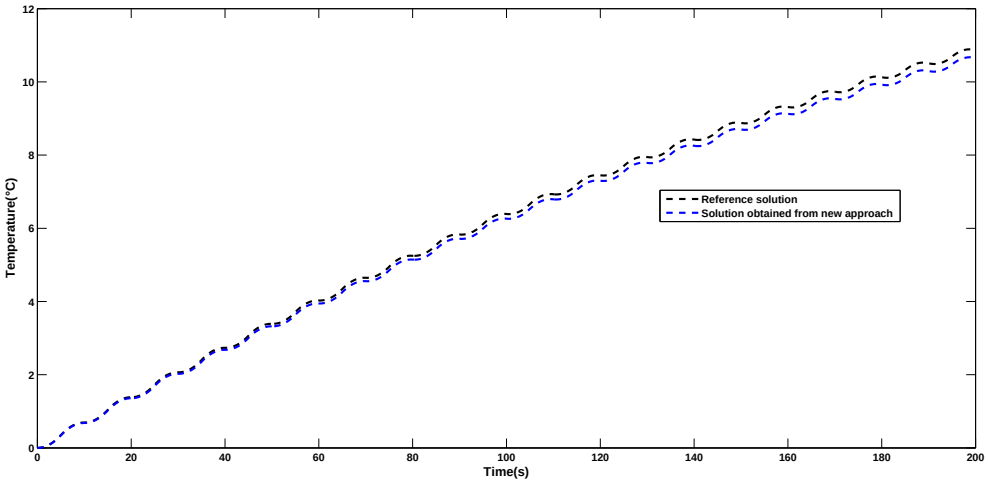


Figure 5.14: Comparison between the temperature for $\tau_\phi = 1000s$ resulting from the mixed strategy and FEM at $(x, y, z) = (25, 25, 25)$

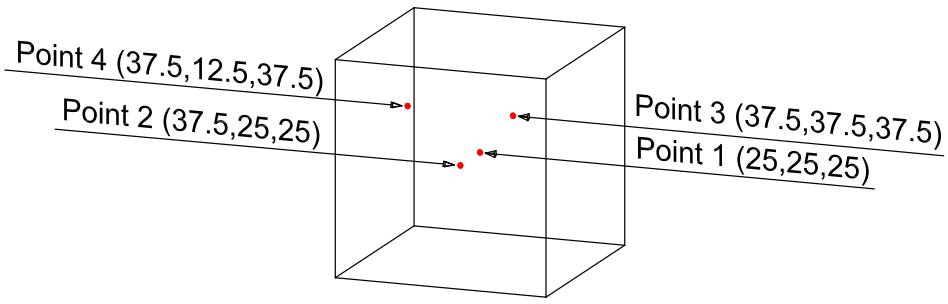


Figure 5.15: Different points in the model

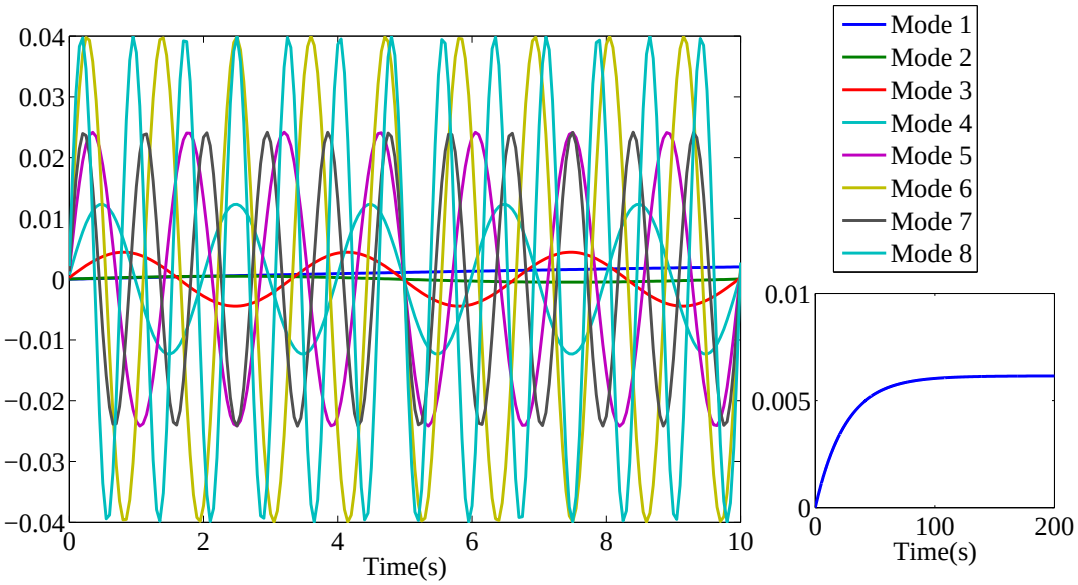


Figure 5.16: Normalized time modes for $\tau_\phi = 100s$ issued from the analytical expressions

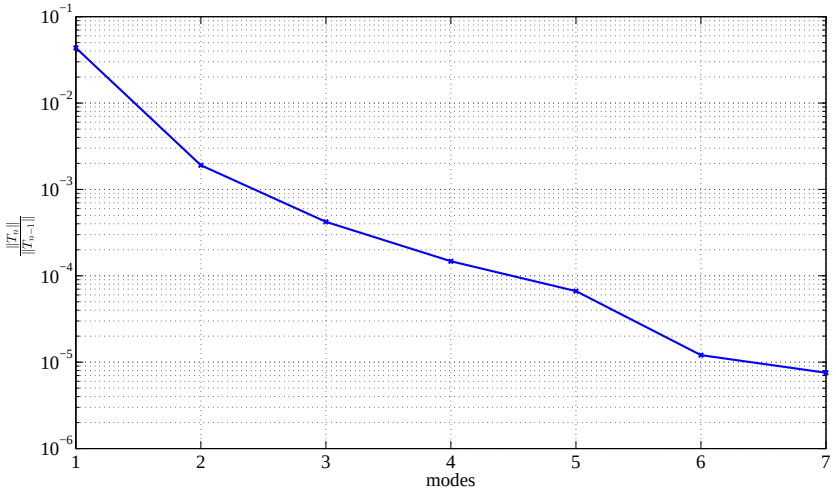


Figure 5.17: Convergence with respect to the number of modes for $\tau_\phi = 100s$

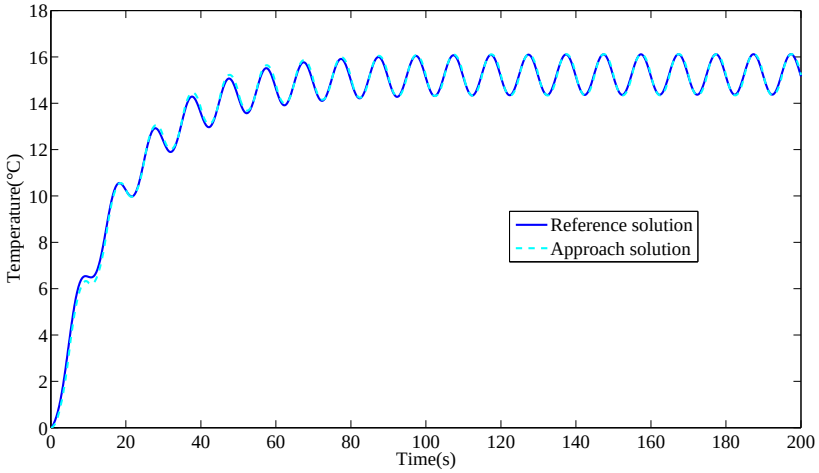


Figure 5.18: Comparison of the case where physical time $\tau_\phi = 100s$ resulting from the mixed strategy and FEM at $(x, y, z) = (25, 25, 25)$

5.3.2.2 Non-homogeneous Dirichlet boundary conditions

New boundary conditions are investigated in this section. The question arises here: Could the dictionary developed with null boundary condition be used for different boundary conditions? What are the limitations of the developed dictionary? So far, a cyclic temperature is applied on the whole surfaces of the domain. Non-homogeneous Dirichlet conditions along the boundaries are applied: $T(\underline{x}, t) = T_b(t)$ on $\partial\Omega$.

Algorithm to compute spatial modes.
In order to apply the separated form, a function $T^D(\underline{x}, t)$ that satisfies the Dirichlet conditions is considered. Consequently, the separated representation of the boundary condition is constructed as follows:

$$T^D(\underline{x}, t) = G(\underline{x})T_b(t) \tag{5.11}$$

where

- $G(\underline{x}, t) = 1$ at $\underline{x} \in \partial\Omega$ and $G(\underline{x}, t) = 0$ at $\underline{x} \in \Omega\backslash\partial\Omega$,
- $T_b(t)$ is the applied temperature.

The parameters of the simulations are:

- $T_b(t)$ has a cyclic triangular form (cycle amplitude $= 50$, $\tau_c = 20s$, number of cycles $= 10$),
- null heat source $Q = 0$,
- $\tau_\phi = 0.1s$.

Eq. (5.1) can be written under the following form:

$$\begin{aligned}\left(\rho C_p \chi_t^{k+1\ k+1}[M] + k\gamma_t^{k+1\ k+1}[K]\right)\{R_{k+1}\} = \\ -\sum_{i=1}^{k}\left(\rho C_p \chi_t^{ik}[M]\{R_i\} + k\gamma_t^{ik}[K]\{R_i\}\right) \\ -\left(\rho C_p \chi_t^{k+1\ k+1}[M] - k\gamma_t^{k+1\ k+1}[K]\right)\{G\}\end{aligned} \tag{5.12}$$

Remark. The equation shows that new terms are added compared to Eq. (5.8) to take into account the non-homogenous boundary conditions. Note that the term which refers to heat source is eliminated, $Q = 0$ in this particular case.

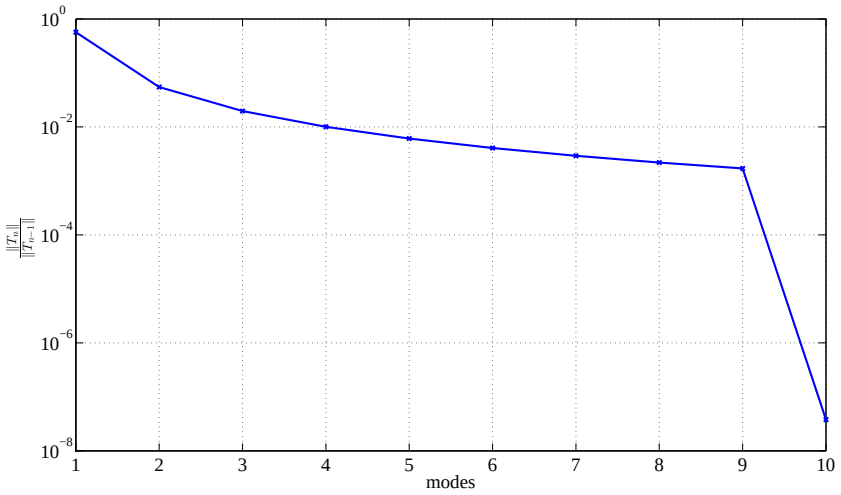


Figure 5.19: Convergence of the solution with respect to the number of modes

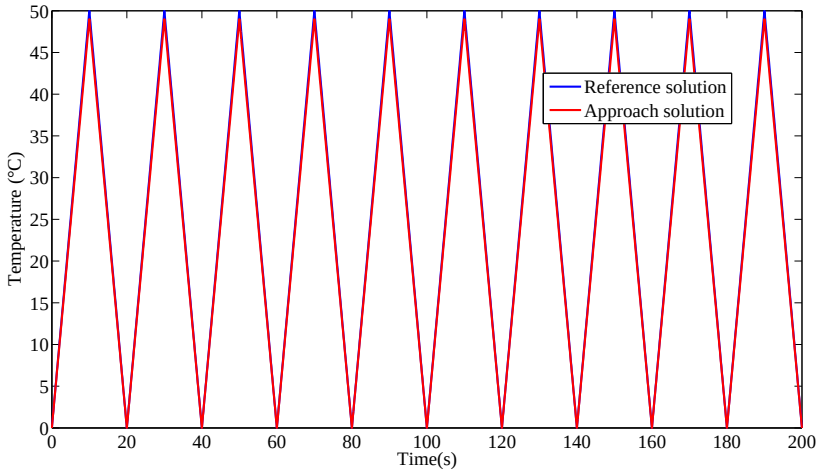


Figure 5.20: Comparison of the solution, for the case of non-homogeneous boundary condition, resulting from the mixed strategy and the FEM at $(x, y, z) = (25, 25, 25)$

Numerical result. The time bases are created using the analytical expression derived in section 5.3.1.2 by updating the values of the physical time and the cycle time.
Based on the stopping criteria, the number of a priori time bases is 9 as illustrated in Fig. 5.19.

Fig. 5.20 illustrates the accuracy compared to the FE solution with a maximum of relative error equals to 2% in the whole domain as shown in Table 5.3. It can be noticed that this error is slightly larger than in the homogeneous case for $\tau_\phi = 0.1s$ as referred to Table 5.2

Henceforth, this method can predict and solve problems with a non-homogeneous boundary conditions by considering the analytical expression for the time bases issued from a different case (cyclic temperature applied and homogeneous Dirichlet conditions). It means that the spatial modes can describe the new spatial gradients issue from new boundary conditions.

Spatial point (x,y,z)	$(25, 25, 25)$	$(37.5, 25, 25)$	$(37.5, 37.5, 37.5)$	$(37.5, 12.5, 37.5)$
Relative error $(\%)$	1.3	1.8	1.6	2

Table 5.3: The relative error calculated for different points for non-homogeneous Dirichlet boundary conditions

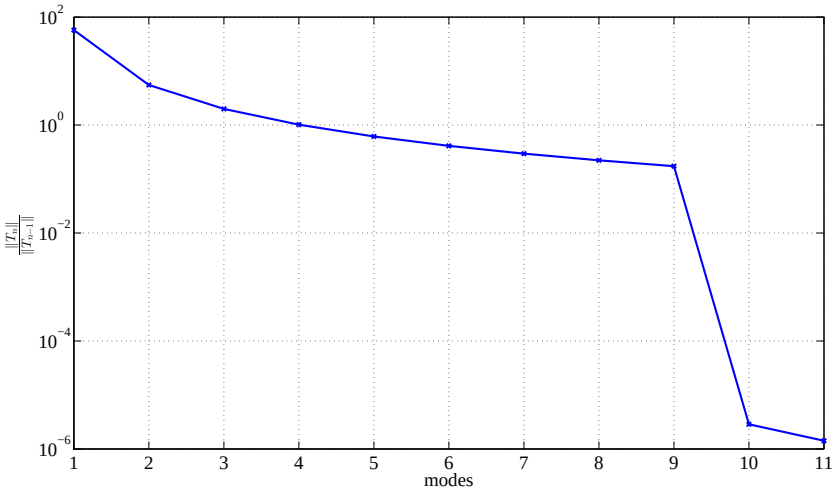


Figure 5.21: Convergence with respect to the number of modes for opposite loads

5.3.2.3 Opposite non-homogeneous Dirichlet boundary conditions

In this case, the model encountered two opposite loads in z direction while the other surfaces have null boundary conditions. The loads have the same cycle time but opposite magnitude. For this case the time basis are similar to the previous case with non-homogeneous boundary conditions since we have the same cycle time and physical time. However, the number of bases needed is 11 based on the stopping criteria as shown in Fig. 5.21, where the ratio decreases as the number of modes increases.

Remark. The equation will be the same as in the previous section 5.3.2.2, only the boundary conditions in z direction are changed.

In Fig. 5.22, the solution is for a fixed spatial point. This method is able to generate an accurate prediction of the solution even in the case of two opposite loads. Moreover, to clearly check the effect of applying two opposite loads, the results obtained at the center of the cube are shown in Fig. 5.23, the temperature is null as expected. Indeed, the method leads to an accurate prediction for different points in the model with a relative error less than 4.1% as show in Table 5.4. This method has the capability to predict the solution in the case of opposite loads, it illustrates the robustness of the analytical expression of the time bases.

5.3.2.4 Robin boundary conditions

In this section, Robin boundary conditions $q_r = h(T - T_\infty)$ are applied where h is the convection coefficient. Two different values of convection coefficient, $h_{vertical} = 4.6\ \mathrm{W.m^2.K^{-1}}$ and

Spatial point (x,y,z)	$(25, 25, 25)$	$(37.5, 25, 25)$	$(37.5, 37.5, 37.5)$	$(37.5, 12.5, 37.5)$
Relative error $(\%)$	2.6	3.4	4.1	3.9

Table 5.4: The relative error calculated for different points for opposite non-homogeneous Dirichlet boundary conditions

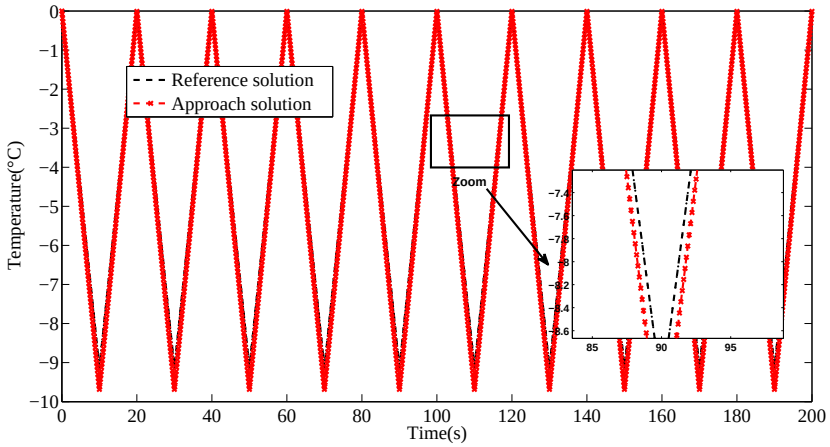


Figure 5.22: Comparison between the solution obtained within the mixed strategy and FEM for opposite loads at $(x, y, z) = (37.5, 25, 25)$

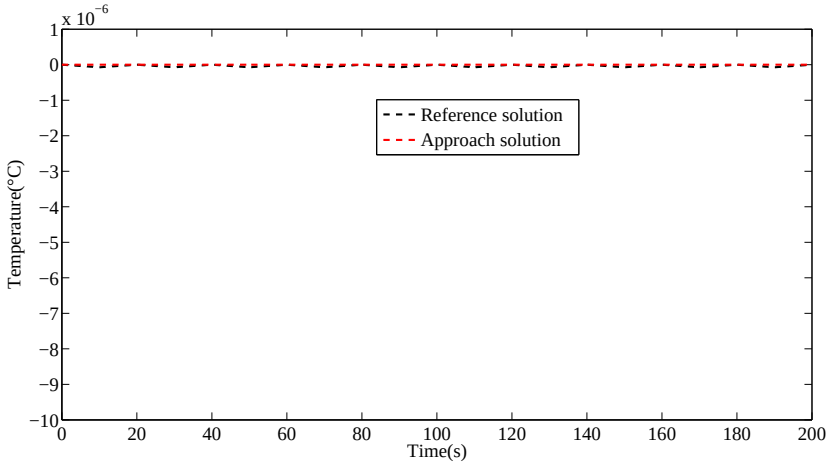


Figure 5.23: Comparison between the solution obtained using the mixed strategy and the FEM at the center point for opposite loads

Function	LHS	RHS
$h(T-T_\infty(t))T^*\overrightarrow{n}\mathrm{dSdt}$	$hTT^*\overrightarrow{n}\mathrm{dSdt}$	$hT_\infty(t)T^*\overrightarrow{n}\mathrm{dSdt}$

Table 5.5: Separated form of the LHS and RHS for Robin boundary conditions

Spatial point (x,y,z)	$(25,25,25)$	$(37.5,25,25)$	$(37.5,37.5,37.5)$	$(37.5,12.5,37.5)$
Relative error $(\%)$	1.41	1.61	1.52	1.65

Table 5.6: The relative error calculated for different points for Robin boundary conditions

$h_{horizontal} = 6.36\ \mathrm{W.m^2.K^{-1}}$, are used to illustrate the effect of density variation and geometry. Not to mention these values correspond to a study in [Nguyen *et al.*, 2013]. T_∞ is a cyclic temperature with amplitude equal to $50°C$ and cycle time equal to $20s$. Let us note that at the top of cube (z direction) vertical coefficient $h_{horizontal}$ is considered and at the surfaces of the cube (x, y directions) horizontal coefficient $h_{vertical}$ is considered. In this part, null heat source is assigned. The physical properties are as follows: $\rho = 950\mathrm{kg.m^{-3}}$, $C_p = 0.075\ \mathrm{Joule.kg^{-1}.C^{-1}}$ and $k = 0.45\ \mathrm{Wm^{-1}.C^{-1}}$, accordingly, the physical time $\tau_\phi = 0.01s$. The time bases are updated with the values of the physical time and the cycle time through the analytical expressions.

Algorithm to compute spatial modes.
Alongside the formulation will be written as follows:

$$\int_{\Omega_t}\int_{\Omega_{\underline{x}}} T^*\rho C_p\frac{\partial T}{\partial t}\mathrm{d\underline{x}dt} + \int_{\Omega_t}\int_{\Omega_{\underline{x}}} div(-k\overrightarrow{\nabla})T^*\mathrm{d\underline{x}dt} = 0 \tag{5.13}$$

Taking into account Robin conditions, Eq. (5.13) is written as follows

$$\int_{\Omega_t}\int_{\Omega_{\underline{x}}} T^*\rho C_p\frac{\partial T}{\partial t}\mathrm{d\underline{x}dt} + \int_{\Omega_t}\int_{\Omega_{\underline{x}}} k\nabla T\nabla T^*\mathrm{d\underline{x}dt} + \int_{\Omega_t}\int_{\partial\Omega_b} h(T-T_\infty(t))T^*\overrightarrow{n}\mathrm{dSdt} = 0 \tag{5.14}$$

Robin conditions, are now separated into Right Hand Side (RHS) and Left Hand Side (LHS) as shown in Table. 5.5

For example, at the first iteration, the real and test fields are $T_1 = R_1S_1(t)$ and $T^* = R^*S_1(t)$, respectively. Eq. (5.14) can be written as follows:

$$\int_{\Omega_t}\int_{\Omega_{\underline{x}}} KR^*S_1RS_1\mathrm{d}\overrightarrow{n}\mathrm{dt} = h\int_{\Omega_t} S_1S_1\mathrm{dt}\int_{\Omega_{\underline{x}}}\mathrm{d}\overrightarrow{n} \tag{5.15}$$

where $\overrightarrow{n}$ is the normal of the surface.

Numerical result. The method converges with 10 modes as shown in Fig. 5.24. Fig. 5.25 plots the evolution of the temperature for a fixed point, the center of the cube, using the new approach and compared to the FEM solution. These results show a good agreement and a large time saving of order 50 is obtained with a maximum of relative error less than 2% in the whole domain as shown in Table 5.6.

5.3.2.5 Non-constant source and non-homogeneous Dirichlet with different cycle times

In this case, the possibility of introducing two different cycle times is discussed. As in the previous cases, the thermal problem is considered. Two different cycle times are considered through:

- a cyclic heat generation source Q with $\tau_c = 20s$;
- Dirichlet boundary conditions on the whole surfaces with a cyclic temperature with $\tau_c = 50s$.

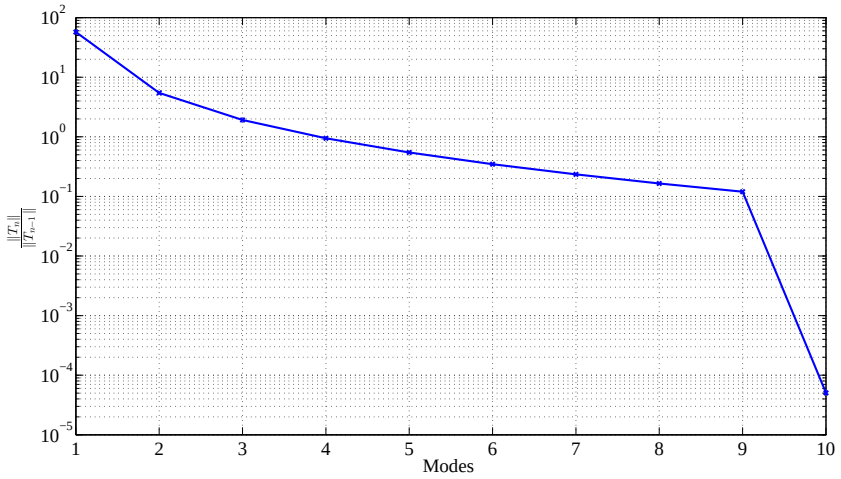


Figure 5.24: Convergence with respect to the number of modes for Robin boundary conditions

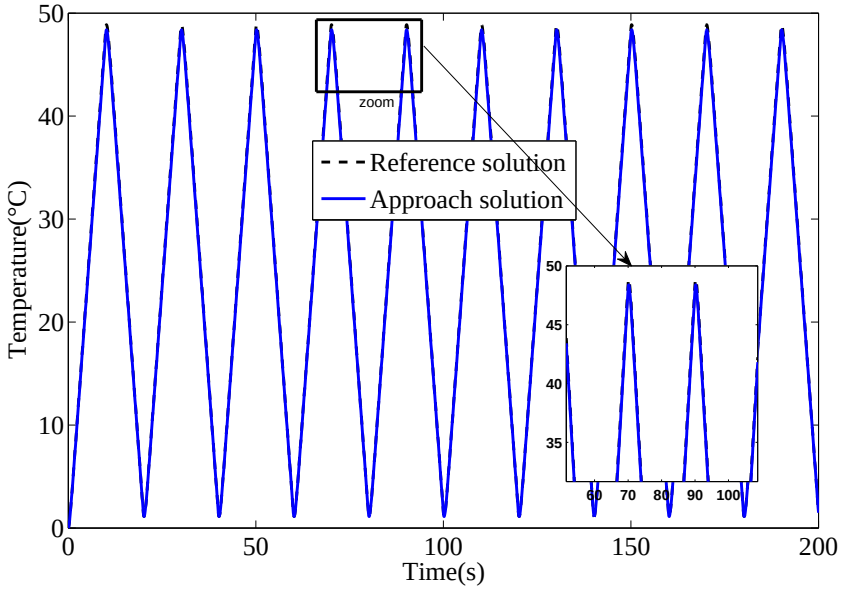


Figure 5.25: Solution from the mixed strategy compared to the Finite Element solution for Robin boundary conditions at $(x, y, z) = (25, 25, 25)$

Spatial point (x,y,z)	$(25, 25, 25)$	$(37.5, 25, 25)$	$(37.5, 37.5, 37.5)$	$(37.5, 12.5, 37.5)$
Relative error (%)	1.4%	1.6%	1.65%	1.8%

Table 5.7: The relative error calculated for different points for different cycle time

Let us denote the heat source by $Q(t)$ and $T_b(t)$ the cyclic temperature on the boundary. Straightaway, a priori basis is constructed using the analytical expressions derived in section 5.3.1.2 by updating the physical time and cycle time. In this case, the bases will be related to two different cycle times: 20 s and 50 s. The position of these peaks can be generated using FFT of the load applied, and later the IFFT by modifying the phase angle to fit with the physical time. As an illustration, Fig. 5.26 pinpoints the location of the peaks. S_1^b, S_2^b... S_n^b and S_1^q, S_2^q...S_n^q denote the time bases issued from the Dirichlet boundary conditions and the heat source respectively, where n refers to the number of basis. To alleviate the notations, n is used for the two different kinds of time bases but n can be different for S_i^b and S_i^q.
The first investigation of these bases show that the major information are contained in the first and second peaks. The results show that for loads with different cycle time and amplitude, different time bases are generated by changing the cycle time of the analytical expressions. However, these bases are essential to construct the solution.

Algorithm to compute spatial modes.
Let us specify, the non-homogeneous Dirichlet conditions are applied along the boundary $\partial\Omega$: $T(\underline{x}, t) = T_b(t)$. In order to apply the separated form we consider a function $T^D(\underline{x}, t)$ that satisfies the Dirichlet conditions as presented previously in section 5.3.2.2. Let us recall. The separated representation of the boundary condition is under the form:

$$T^D(\underline{x}, t) = G(\underline{x}, t)T_b(t) \tag{5.16}$$

where $G(\underline{x}, t) = 1$ at $\underline{x} \in \partial\Omega$ and $G(\underline{x}, t) = 0$ at $\underline{x} \in \Omega\backslash\partial\Omega$.
Besides, the heat source is written under a separated form $Q = q_x(\underline{x})q_t(t)$ where q_t is cyclic.
Eq. (5.1) is re-written as follows:

$$\begin{aligned} &\left(\rho C_p \chi_t^{k+1\ k+1}[M] + k\gamma_t^{k+1\ k+1}[k]\right)\{r_{k+1}\} = \\ -\sum_{i=1}^{k} &\left(\rho C_p \chi_t^{ik}[M]\{r_i\} + k\gamma_t^{ik}[k]\{r_i\}\right) + q_{tk}[M]q_x \\ &- \left(\rho C_p \chi_t^{k+1\ k+1}[M] - k\gamma_t^{k+1\ k+1}[k]\right)\{G\} \end{aligned} \tag{5.17}$$

Remark 2: Eq. (5.17) differs from Eq. (5.8) with a new term related to the non null Dirichlet condition.

Numerical result. The number of modes needed is 22. The time bases are alternative based on the location of the peaks that can be determined from the decomposition of the load. The results are shown in Fig. 5.27. There is accurate results compared to the FEM that leads us to conclude that the mixed strategy method is able to solve problems under different cycle times. Table 5.7 depicts the relative error for different spatial points, where the maximum relative error is equal to 1.8%.
Remark 3: Since in this case we have different cycle times due to the loads applied (through heat source and boundary conditions), the bases are related to both loads applied leading to two different values of R_τ.

5.3.3 Effect of the time basis order

Considering the model encountering two different loads with different cycle times ($\tau_c = 50s$, $\tau_c = 20s$) and $\tau_\phi = 10s$, the bases are established a priori using the analytical expression. To check the effect of the order of the time-basis, 3 different cases are discussed:

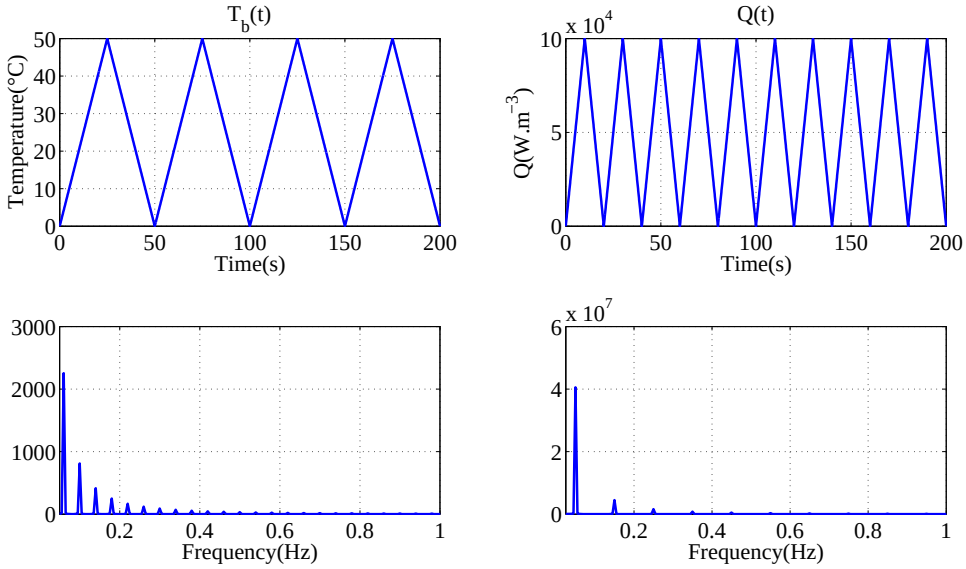


Figure 5.26: Bases issued from different cycle times imposed by a volumetric heat source (right) and a Dirichlet boundary condition (left)

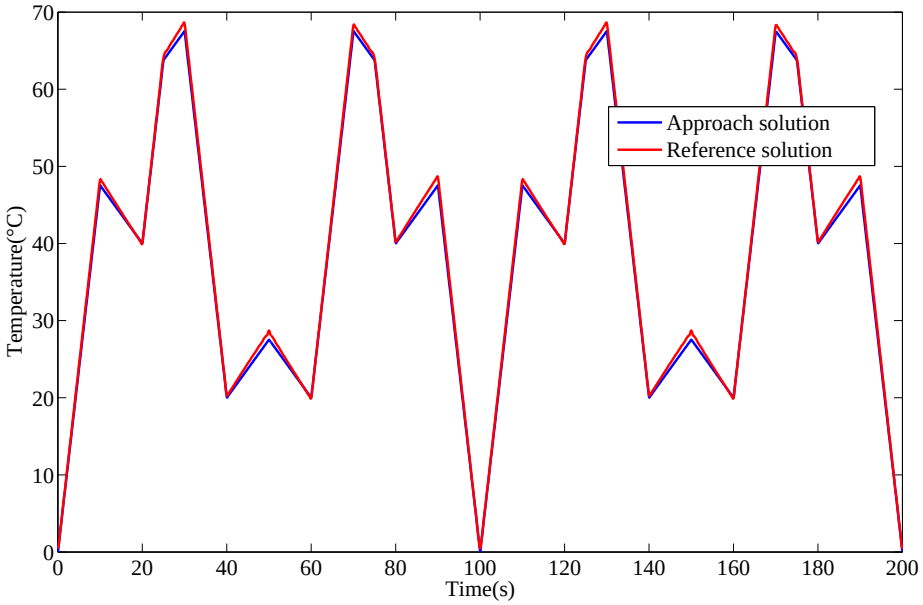


Figure 5.27: The evolution of temperature using the approach (using the order of bases from case 1) compared to FEM solution at $(x, y, z) = (25, 25, 25)$

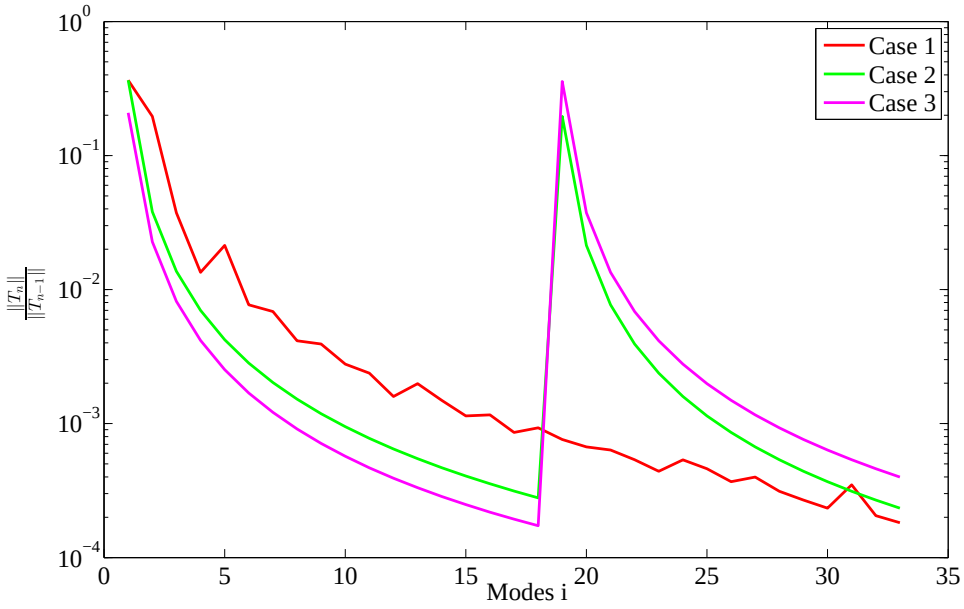


Figure 5.28: The evolution of $\frac{T_n}{T_{n-1}}$

1. case 1: the bases are chosen alternatively according to their related frequency.
2. case 2: the bases issued from $\tau_c = 50s$ are the first followed by the basis issued from $\tau_c = 20s$,
3. case 3: the bases issued from $\tau_c = 20s$ are the first followed by the basis issued from $\tau_c = 50s$.

The results are shown in Fig. 5.28. The evolution of the ratio shows that within case 2 and case 3, the number of modes are 9, and 10, respectively. However, for case 1, 20 modes are needed. But regarding the relative error compared to the FEM, it is noticed that for case 2 and case 3 the relative error is higher than 18%. However, for case 1 the relative error is 1.41%, thus the order of the basis is important: the time bases have to be ordered with increasing frequency. For this case, the time saving is 40 (where CPU using FEM is 80s, and using the approach is 2s) and an accurate prediction is obtained as illustrated in Fig. 5.27.
Remark. In the case of wrong cycle time, the method is able to distinguish the wrong bases which proved the robustness of the method.

5.3.4 Usage of the time basis to generate solution with larger number of cycles

In this section, the ability of the bases to capture larger number of cycles is discussed. The physical time $\tau_\phi = 1000s$ and the cycle time $\tau_c = 40s$ are considered.
Different number of cycles are studied:

1. case 1: 5 cycles with total time $L_t = 200s$
2. case 2: 10 cycles with total time $L_t = 400s$
3. case 3: 25 cycles with total time $L_t = 1000s$

The bases are build using the analytical expression with the following details: $\tau_\phi = 1000s$ and $\tau_c = 40s$. Let us note that the analytical expressions are fitted for a time domain equal to $L_t = 200s$. Table 5.8 summarizes the relative error and the number of modes for each number of cycles.

Fig. 5.29 depicts the evolution of temperature for 5 cycles, it is noticed that the solution is matching with the FEM solution with an error less than 2%. However, Fig. 5.30 and Fig. 5.31 depict the evolution of temperature for 10 and 25 cycles, respectively. Accurate results have been obtained

Number of cycles	5	10	25
Number of modes	2	3	6
Relative error (%)	1.74	3.4	5.6

Table 5.8: The relative error and the number of modes for different number of cycles

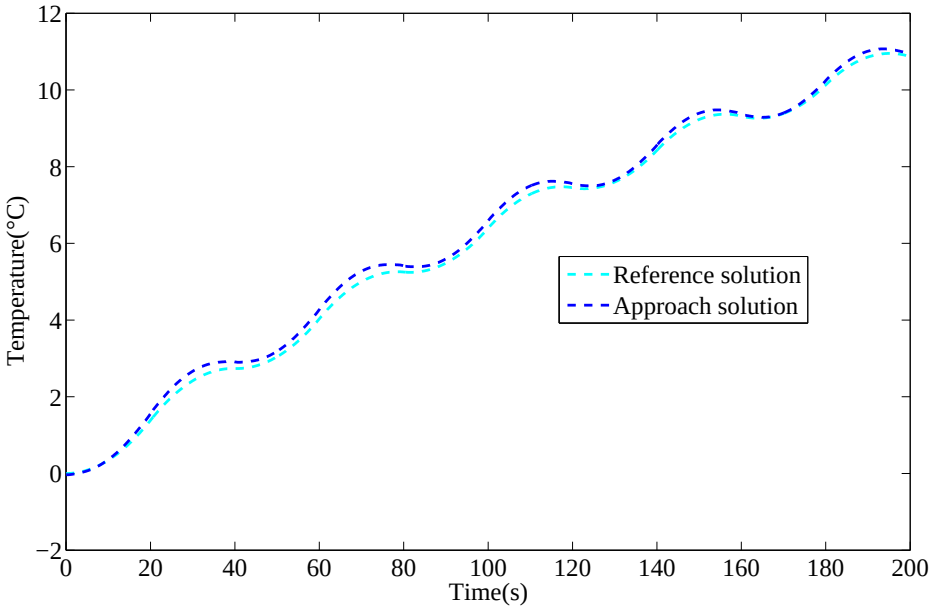


Figure 5.29: Evolution of temperature at $(x, y, z) = (25, 25, 25)$ for larger number of cycles: 5 cycles (case 1)

even when the number of cycles increases, indicating the efficiency of the approach to generate a solution with a different number of cycles and more particularly a number of cycles leading to a time domain larger than the fitted one.

5.3.5 Usage of the time basis to generate solution with larger time domain

Throughout this section, the model encounters a load with a larger time domain with the following properties: $\tau_\phi = 100s$, $\tau_c = 20s$ leading to $R_\tau = 5$ and the total time of the time domain is $L_t = 2000s$ (10 times larger than the fitting domain). The bases are used directly from the analytical expressions generated in the time bases generation section by taking into account the effect of cycle time and physical time. Let us note that we here assume that the analytical expressions are valid for large time domain, larger than that of the time domain used for fitting.
For example the analytical expression of the first time basis leads to:

$$S_1^{100} = 1 - \exp(-\frac{5}{100}t)$$

and the second time basis:

$$S_2 = cos(\frac{2\pi}{20} \times t + 1.76)$$

The results obtained with our approach are represented in Fig. 5.32 and compared to FE solution. The first set of analysis highlighted the impact of the physical time, where the stabilized cycle is obtained after 5 cycles. Interestingly, only 4 modes are needed to obtain an accurate solution with an error less than 3.45%. The error is calculated in different spatial points (near boundaries and at the center) using L^2 norm and are reported for some spatial points in Table 5.9.
This is an important issue that a priori bases generated from short time $L_t = 200s$ are used for larger

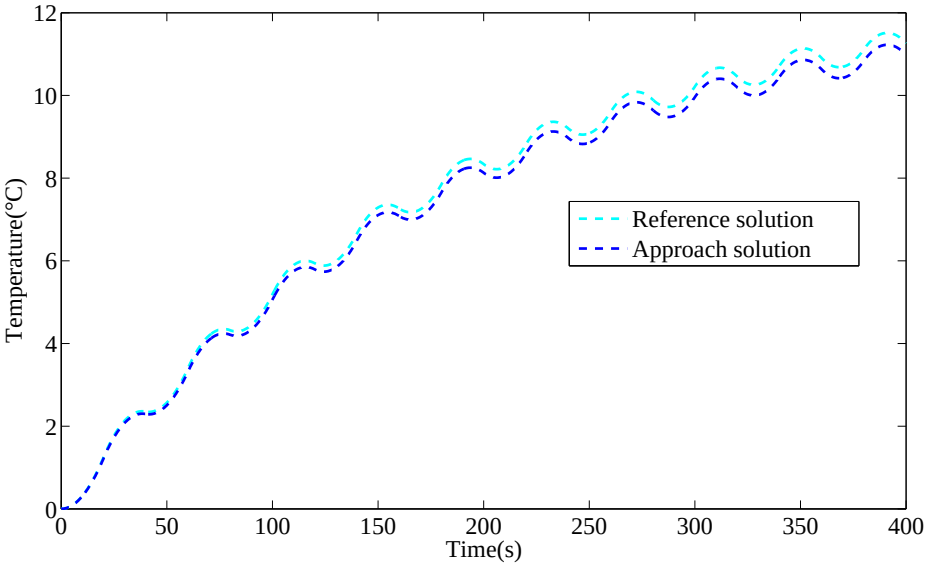


Figure 5.30: Evolution of temperature at $(x, y, z) = (25, 25, 25)$ for larger number of cycles: 10 cycles (case 2)

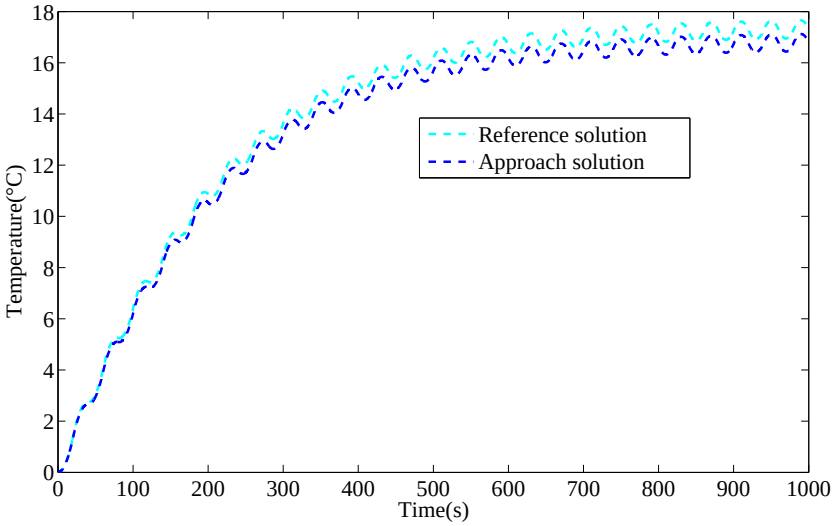


Figure 5.31: Evolution of temperature at $(x, y, z) = (25, 25, 25)$ for larger number of cycles: 20 cycles (case 3)

Spatial point (x,y,z)	$(25, 25, 25)$	$(37.5, 25, 25)$	$(37.5, 37.5, 37.5)$	$(37.5, 12.5, 37.5)$
Relative error (%)	2.3%	3.6%	3.45%	2.8%

Table 5.9: The relative error calculated for different points with larger time domain $L_t = 2000s$

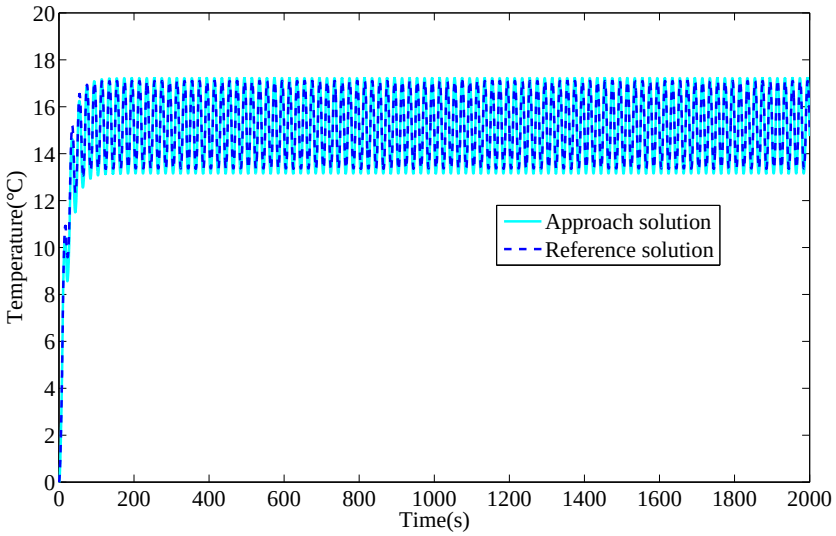


Figure 5.32: The evolution of the temperature with larger time domain $L_t = 2000s$ at $(x, y, z) = (25, 25, 25)$

time domain $L_t = 2000s$. Let us note that this is valid only if the model used is valid for larger domain. Thus, this method represents a viable technique to solve a physical problem with large time domain. A large time saving of order 80 has been obtained in this case.

5.3.6 Influence of the load

As stated in the introduction, one of the objectives is to discuss the efficiency of the dictionary or to enrich the dictionary by analyzing the influence of the load applied. Thus, 2 other types of loads are investigated:

- Sinusoidal load.
- Heaviside load.

Previously, we only consider a triangular load.
The influence of the ratio is discussed by considering a cyclic triangular load with $\boldsymbol{R} = -1$, and the influence of the amplitude by considering a cyclic triangular load with $\boldsymbol{R} = 0$ and changing the value of the amplitude.

The results point to answer the following questions:

1. Can the previous bases be used for different types of the loads such as sinusoidal, triangular and Heaviside?
2. Can the bases issued from the case where a triangular load with $\boldsymbol{R} = 0$ be used for $\boldsymbol{R} = -1$?
3. What is the effect of the amplitude?

To answer these questions, the study is extended here either to enrich the dictionary or to discuss the efficiency of analytical expressions to generated the a priori time basis.

5.3.6.1 Sinusoidal

The FFT of a sinusoidal signal generates only one peak related directly to the cycle time of the load applied, and another peak at zero frequency which is related to the effect of the physical time and the response of temperature. Based on the proposed approach, two time bases are generated.
Thus, the question arose here:

1. What is the effect of the sinusoidal load?
2. Can the convergence of our approach occurs with two bases only?
3. Can the bases directly be derived from the triangular load with ($\boldsymbol{R} = 0$) to generate the solution for a sinusoidal load?
4. What are the modifications needed in the analytical expression (if a modification is required)?

Two cases will be studied, where two sinusoidal loadings are investigated:

1. Load 1: $200000 \times (1 + 1 \times sin(\frac{2\pi}{20} \times t - \frac{\pi}{2}))$
2. Load 2: $100000 \times (1 + 1 \times sin(\frac{2\pi}{20} \times t))$

The first load (load 1) is shown in Fig.5.33(a). It satisfies the null initial condition and it is in phase with the triangular load applied to derive a priori time basis. However, Fig. 5.33(b) depicts the evolution of the second load (load 2) where the null initial conditions are not satisfied.

Load 1. A heat source in the form of the sinusoidal load 1 as shown in Fig. 5.33(b) has been applied with $\tau_c = 20s$ and $\tau_\phi = 1000s$. Two peaks are obtained, first peak is mainly related to the effect of physical time, while, the second peak is related to the effect of the cycle time and physical time. The two time bases are derived directly from the analytical expressions which are build on time bases generation section without any modification to the phase angle. The first time basis is:

$$S_1^{1000} = 1 - \exp(-\frac{5}{1000}t)$$

and the second time basis is:

$$S_2 = cos(\frac{2\pi}{20}t + 1.6)$$

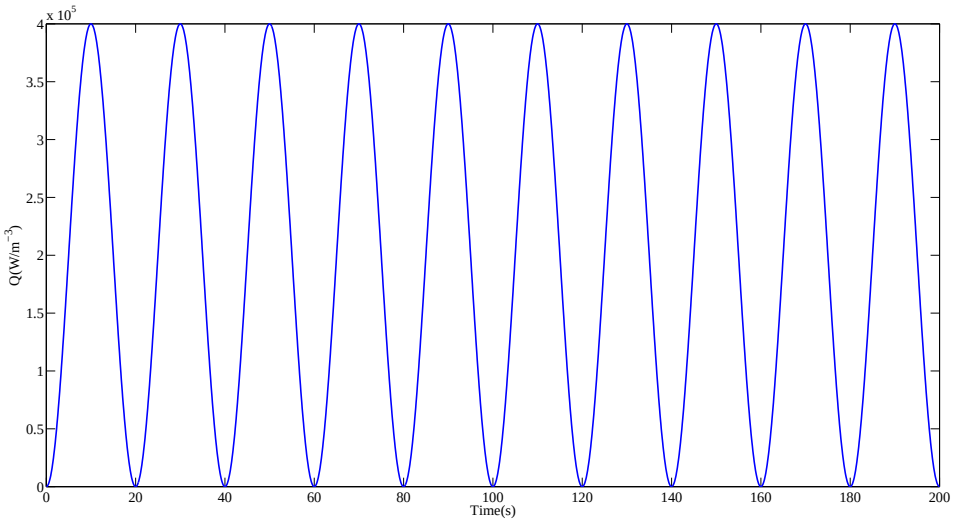
The spatial modes are computed within the approach and the solution is built. Fig. 5.34 depicts the evolution of temperature using the approach and is compared to the FEM. An accurate result has been obtained with a relative error less than 5% in the whole domain, and with a time-saving of order 60 compared to the FEM solution. It is well noticed that the temperature, regardless the type of the load, doesn't reach the stabilized cycle at the end of the simulation due to the effect of the physical time.

Load 2. The model now encounters a new sinusoidal load where modification has been applied to the previous load, in which the load has a non-null intial conditions. Thus it is out of the phase compared to the triangular signal. The heat source is in the form of sinusoidal load as shown in Fig. 5.33(b) with a ratio $\boldsymbol{R} = 0$.

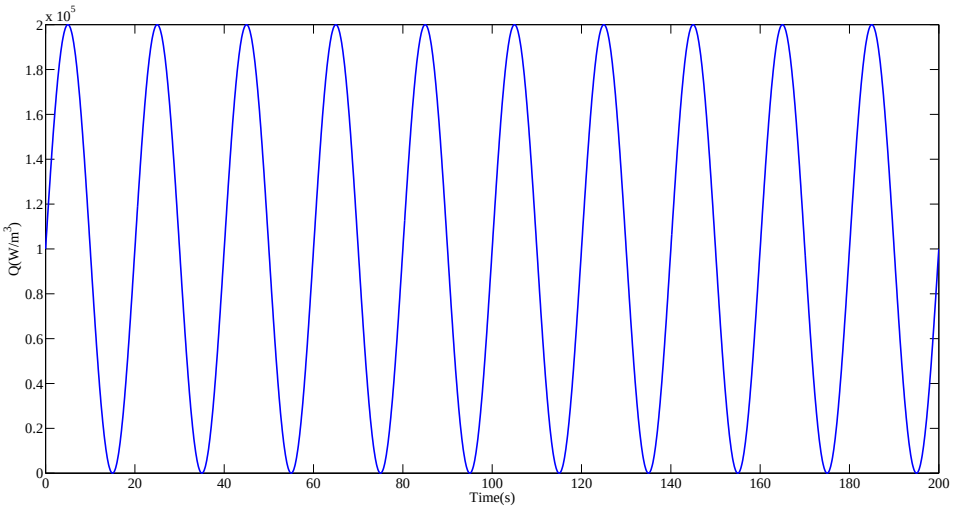
- Can the old time bases be used?
- What are the needed modifications to enrich the dictionary?

Three cases are to be investigated:

- case 1: $R_\tau = 50$, $\tau_c = 20s$, $\tau_\phi = 1000s$
- case 2: $R_\tau = 20$, $\tau_c = 20s$, $\tau_\phi = 400s$



(a) The evolution of the load 1: $200000 \times (1 + 1 \times sin(\frac{2\pi}{20} \times t - \frac{\pi}{2}))$



(b) The evolution of the load 2: $100000 \times (1 + 1 \times sin(\frac{2\pi}{20} \times t))$

Figure 5.33: The evolution of two types of sinusoidal load

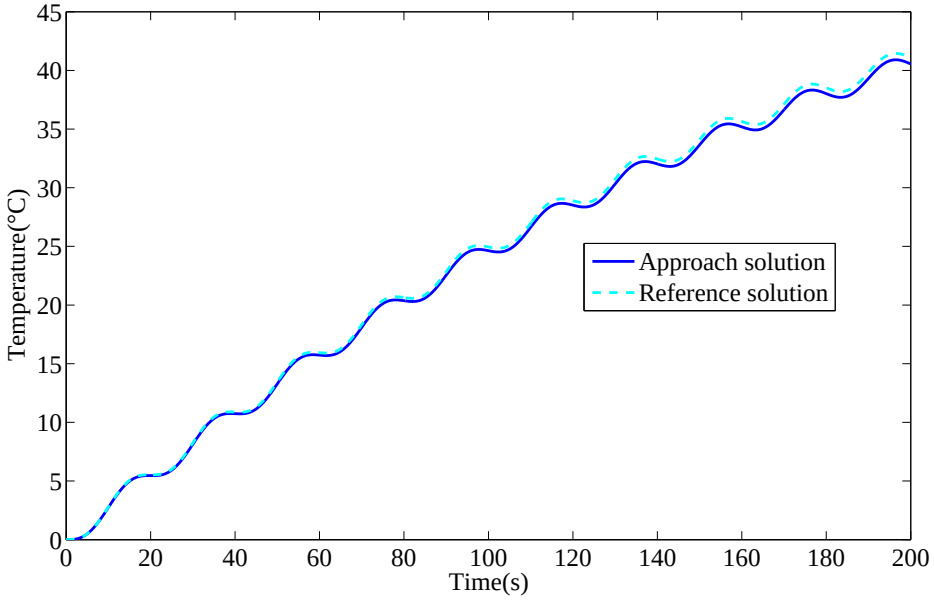


Figure 5.34: The evolution of the temperature for fixed spatial point (25,25,25) under sinusoidal load 1

- case 3: $R_\tau = 1000$, $\tau_c = 1s$, $\tau_\phi = 1000s$

Case 1 will be used to improve the dictionary and the two remaining cases (case 2 an case 3) to check the potential of the approach.

Case 1 ($R_\tau = 50$, $\tau_c = 20s$)
The model encounters a sinusoidal load with $\tau_c = 20s$, $\tau_\phi = 1000s$. Thus, the ratio of physical time to cycle time is 50, which is considered high. Therefore, the evolution of temperature will be in transient form.

First the old bases are used by updating only the values of τ_c and τ_ϕ.
The first time basis is:

$$S_1^{\text{old}} = 1 - \exp(-\frac{5}{1000}t)$$

and the second time basis is:

$$S_2^{\text{old}} = cos(\frac{2\pi}{20}t + 1.6)$$

The results showed the non-convergence of the method where the solution only matches the mean of the reference solution which indicates that both cases have the same physical time leading to a same deviation. This leads to improve the time bases by generating the new time bases. A FFT has been done on a fixed spatial point, and the two corresponding bases are compared to the old bases as shown in Fig. 5.35. Indeed, the first time basis is clearly the same as the old one. However, the second basis is shifted from the old one, thus a modification to the old basis is required. Adding a phase angle $\frac{\pi}{2}$ gives a similar evolution but in opposite sign which can be captured with the spatial modes.

In fact, using old bases leads to the non-convergence of the solution. A modification of the analytical expression is required, the modified bases are as follows:
The first time basis remains the same where:

$$S_1 = 1 - \exp(-\frac{5}{1000}t)$$

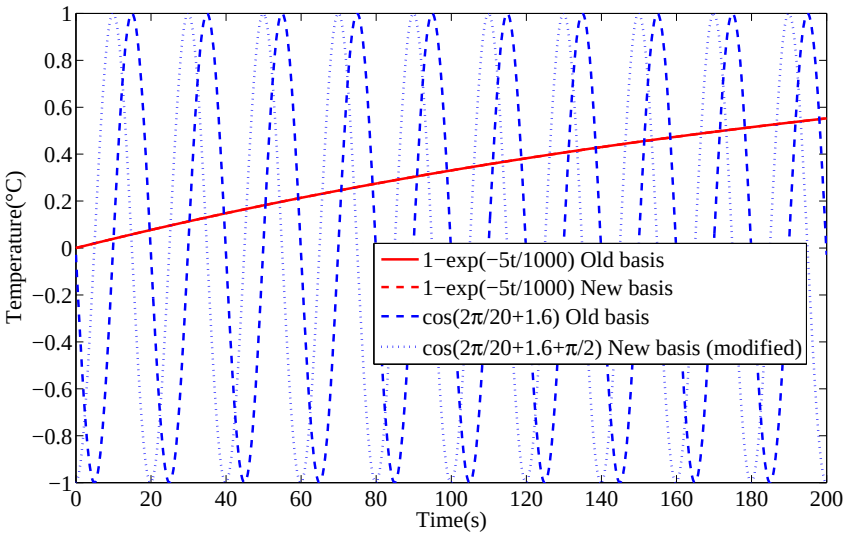


Figure 5.35: Comparison of the bases: old and new bases

Spatial point (x,y,z)	$(25, 25, 25)$	$(37.5, 25, 25)$	$(37.5, 37.5, 37.5)$	$(37.5, 12.5, 37.5)$
Relative error $(\%)$	3.3%	4.3%	4.5%	3.7%

Table 5.10: The relative error calculated for different points for the sinusoidal case

and the second time basis is modified by adding $\frac{\pi}{2}$

$$S_2 = cos(\frac{2\pi}{20}t + 1.6 + \frac{\pi}{2})$$

These modified bases are now used to generate the solution. An accurate solution is obtained as shown in Fig. 5.36 with a relative error less than 4.5% as reported in Table 5.10. The addition of a phase angle of $\frac{\pi}{2}$ corresponds to the phase angle of the load applied compared to load 1 (the load 1 being in phase with the triangular load used to fit the analytical expressions of the time bases). In fact, only two time bases are needed that leads to a large time saving of order 60. The evolution of temperature depicts that the temperature doesn't reach the stabilized cycle at the end of the simulation.

Case 2 ($R_\tau = 20$, $\tau_c = 20s$, $\tau_\phi = 400s$):
The model now encounters the same load, but the physical time has been changed to be equal to $\tau_\phi = 400s$ where $R_\tau = 20$. The modified bases obtained from the previous case (case 1) are now used. The results obtained are shown in Fig. 5.37, accurate results has been obtained with error less than 5%.

Case 3 ($R_\tau = 1000$, $\tau_c = 1s$, $\tau_\phi = 1000s$)
The efficiency of the bases are then tested with more complicated cases by taking 1000 cycles that is $\tau_c = 1s$ and $\tau_\phi = 1000s$, where $R_\tau = 1000$. The bases used are those of case 1 (the new one). Fig. 5.38 depicts the evolution of the temperature. Accurate results have been obtained with a relative error less than 5% for all the spatial points on the model. The solution using the approach leads to a very large time saving of order 80 compared to FEM (CPU time for FEM $= 184.77s$, CPU time for the approach $= 2.3097s$). As a summary by applying a sinusoidal load, two time bases are needed. The old bases can be used directly as the ones used to generate the analytical expression. However, $\frac{\pi}{2}$ can be added to some cases where the load applied is out of phase. The convergence of the approach by using only two-time bases has been validated and it proves the potential of the

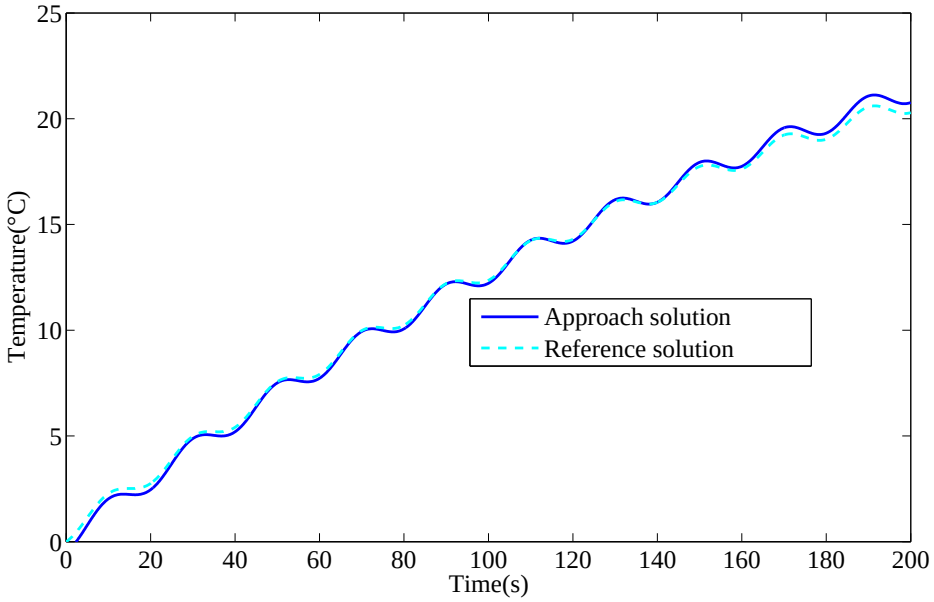


Figure 5.36: Case 1: Evolution of the temperature using the approach and the reference solution at $(x, y, z) = (25, 25, 25)$

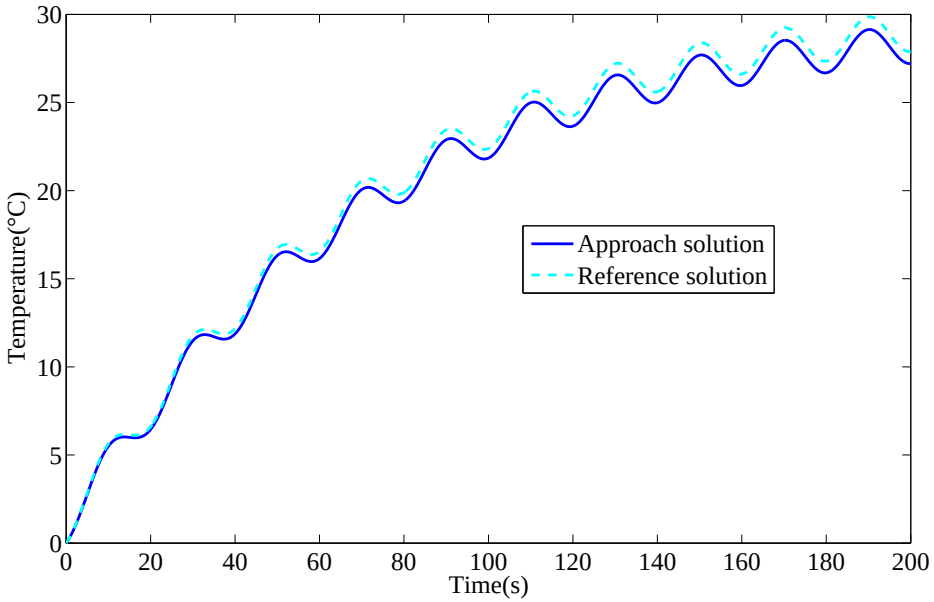


Figure 5.37: Case 2: Evolution of the temperature using the approach and the reference solution at $(x, y, z) = (25, 25, 25)$

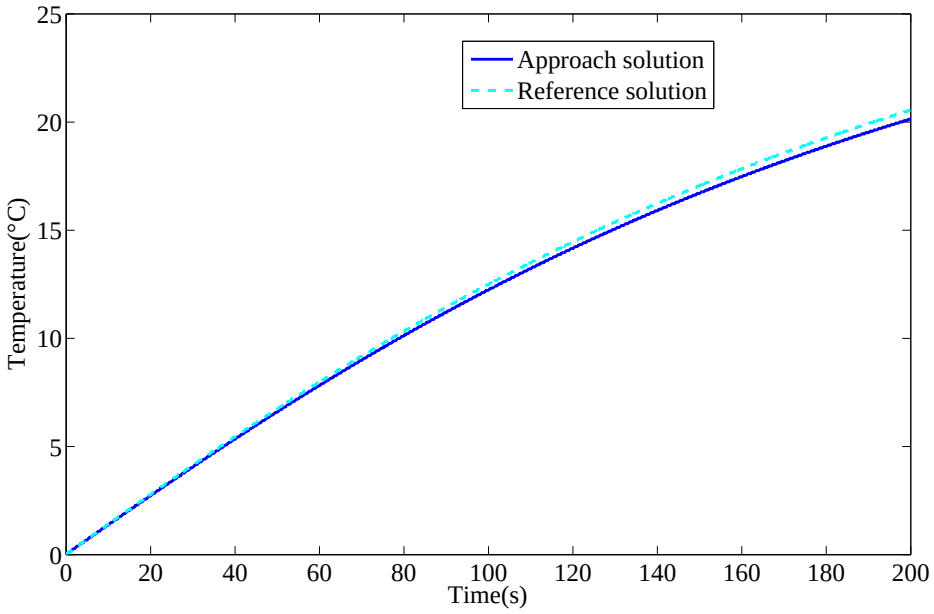


Figure 5.38: Case 3: Evolution of the temperature using the approach and the reference solution at $(x, y, z) = (25, 25, 25)$

approach. To clearly increase the robustness of the approach, more complicated cases are analyzed by applying a Heaviside load.

Remark. Let us consider a triangular form instead of a sinusoidal one. The conclusion of adding $\frac{\pi}{2}$ is true as it is related to the phase shift of the load. The conclusion of the number of modes is related to the form of the load. 4 modes are required for the triangular load instead of 2 for the sinusoidal load with a same order of accuracy.

5.3.6.2 Heaviside

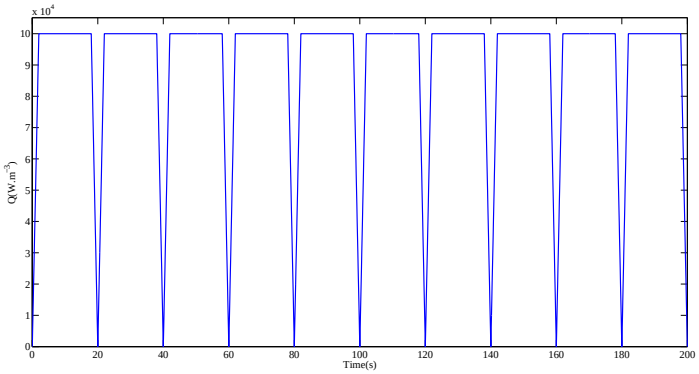
The aim of this section is to check the effect of introducing a load with many frequencies. To do this, a Heaviside load is studied. This case calls into the following questions:

1. Can this approach take into account the effect of this type of load (many frequencies)?
2. What are the time bases to be used?

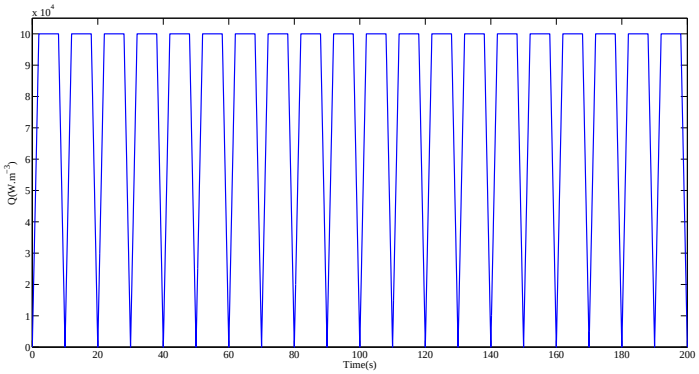
Four different types of Heaviside loads illustrated in Fig. 5.39 are investigated. Type 1 and type 2 differ from the cycle time, $\tau_c = 20s$ and $\tau_c = 10s$ respectively. Type 3 and type 4 have different plateaus at $T = 0°C$.

The present section seeks to address how to solve the problem under Heaviside load and the effect of the Heaviside load on the evolution of temperature.

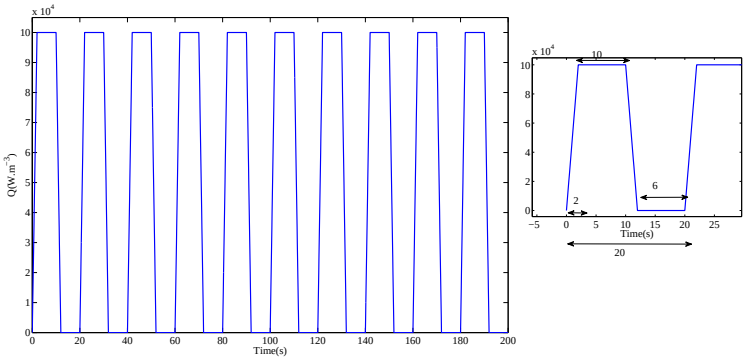
Heaviside type 1 and type 2. In this section, two cases are investigated. First the model encounters a Heaviside load such that the number of cycles is 10 which refers to the Heaviside of type 1. Then, another case where the load applied has 20 cycles. In order to understand the effect of the number of cycles, the FFT of the two loads is applied. It is found that the first peak of the load of 10 cycles (type 1) is related directly to the cycle time of the load which is 20 s where the fundamental frequency is $f = \frac{1}{20}$, the other fundamentals frequencies of this load are ($\frac{1}{10}$, $\frac{1}{5}$, $\frac{1}{2.5}$, $\frac{1}{1.25}$...). On the other hand, the load with 20 cycles, the first fundamental frequency is $\frac{1}{10}$ which is related directly to the cycle time 10 s, and the other fundamentals frequencies are ($\frac{1}{5}$, $\frac{1}{2.5}$, $\frac{1}{1.25}$). Let



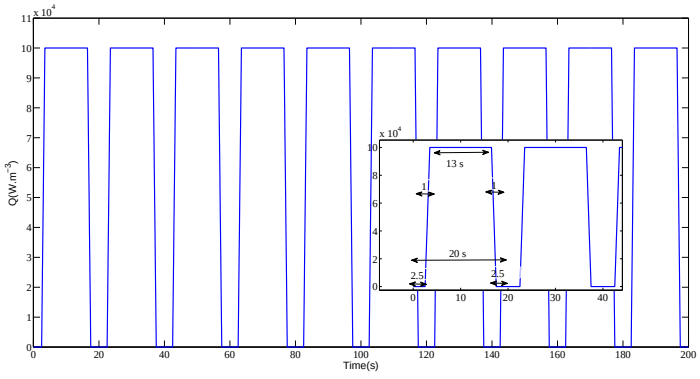
(a) Heaviside load type 1 with 10 cycles



(b) Heaviside load type 2 with 20 cycles



(c) Heaviside load type 3



(d) Heaviside load type 4

Figure 5.39: Different types of Heaviside load

Frequency (Hz)	Time (s)	f	$3 \times f$	$5 \times f$	$7 \times f$
0.05	20	0.05	0.15	0.25	0.35
0.1	10	0.1	0.3	0.5	0.7
0.2	5	0.2	0.6	1	1.4
0.4	2.5	0.4	1.2	2	2.8
0.8	1.25	0.8	2.4	4	5.6

Table 5.11: The location of the peaks for the case of load type 1 with $\tau_c = 20s$

Frequency	Cycle time	f	$3 \times f$	$5 \times f$	$7 \times f$
0.1	10	0.1	0.3	0.5	0.7
0.2	5	0.2	0.6	1	1.4
0.4	2.5	0.4	1.2	2	2.8
0.8	1.25	0.8	2.4	4	5.6

Table 5.12: The location of the peaks for the load of type 2 ($\tau_c = 10s$)

us note that the location of the peaks is determined by the frequency. Table 5.11 and Table 5.12 summarize respectively the first 5 locations of the peaks of the fundamental for the case $\tau_c = 10s$ and $\tau_c = 20s$ respectively.

With this in mind, the approach is used to solve the model under the Heaviside load. The first case is $\tau_c = 20s$ and $\tau_\phi = 100s$. Regarding the use of a priori time bases, the bases are developed according to their frequencies using the analytical expression developed in the time bases generation section 5.3.1.3. The first five bases used are:

$$S_1 = 1 - exp(-\frac{5}{100}t)$$

$$S_2 = 1 \times cos(w_1 \times t + (1.76))$$

$$S_3 = 1 \times cos(w_2 \times t + (1.66))$$

$$S_4 = 1 \times cos(w_3 \times t + (1.63))$$

$$S_5 = 1 \times cos(w_4 \times t + (1.62))$$

where $w_1 = 2 \times \pi \times \frac{1}{20}$; $w_2 = 2 \times \pi \times \frac{1}{10}$; $w_3 = 2 \times \pi \times \frac{1}{5}$; $w_4 = 2 \times \pi \times \frac{1}{2.5}$.
Note that more frequencies are added than in the triangular load.
Let us note that the variation of the phase angle is the same as the one used in the case of triangular load. For example, if we take cycle time $\tau_c = 5s$ then $R_\tau = 100/5 = 20$. This will generate a phase angle equal to 1.6305 (cf. S_4). The same procedure is applied for all cycle times $(20s, 10s, 5s, 2.5s)$. The time bases are similar to the triangular case but we have different frequencies due to the effect of the load.

It is interesting to note that these bases lead to the convergence of the approach where Fig. 5.40 depicts the evolution of the temperature for fixed spatial point with a relative error less than 5% for different spatial points on the model. The approach converge with 7 modes leading to a large time saving of order 50.
In the same manner, for the case of $\tau_c = 10s$ (case 2) the bases are used according to their frequencies leading to accurate results as shown in Fig. 5.41 with a relative error less than 5%. These results exhibit the robustness of the approach, and in particular the efficiency of the expression of the time bases.

Heaviside type 3 ($N_{cycles} = 10$). The model now encounters a new Heaviside load of type 3 with a physical time equal to 100 s, where the FFT of this load leads to generate only one fundamental frequency related to the cycle time $\tau_c = 20s$ and all the location of the other peaks is related to

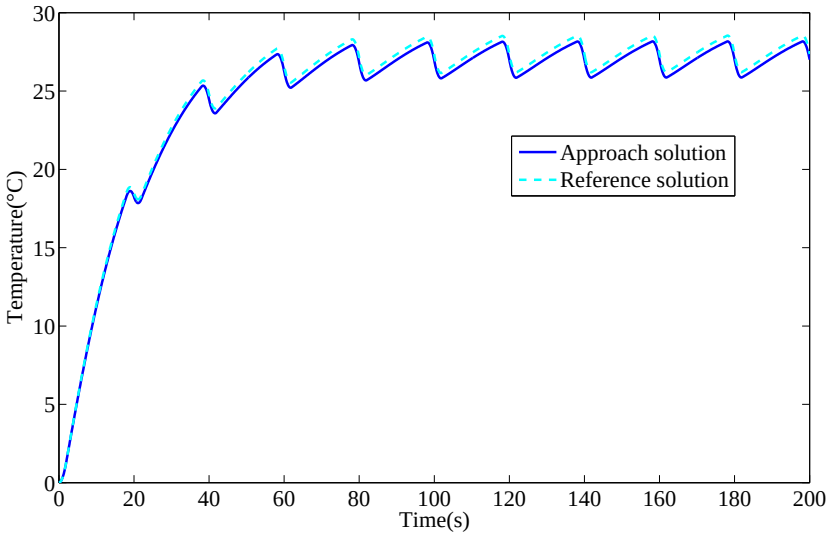


Figure 5.40: Load type 1: Solution using the approach at $(x, y, z) = (25, 25, 25)$ with $\tau_c = 20s$

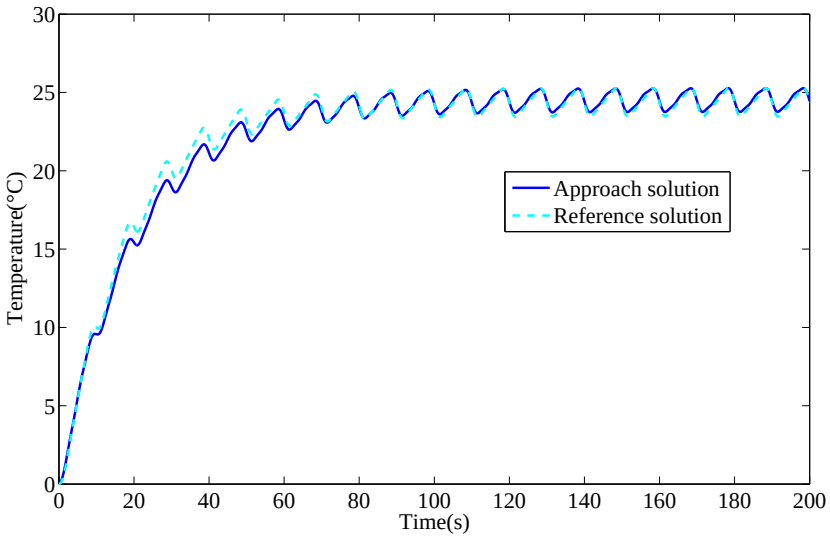


Figure 5.41: Load type 2: Solution using the approach at $(x, y, z) = (25, 25, 25)$ with $\tau_c = 10s$

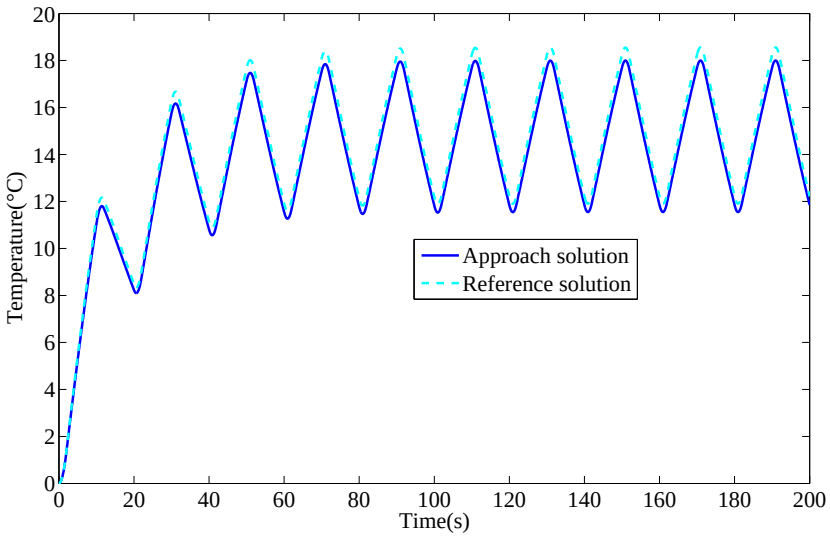


Figure 5.42: Solution using the approach at $(x, y, z) = (25, 25, 25)$ with $\tau_\phi = 100s$

this frequency. The bases need to be updated by adding $\frac{\pi}{2}$ to the analytical expression used and to modify the phase angle by doing the direct fitting with FFT. Thus, we can use directly the bases. The first two bases used are:

$$S_1 = 1 - 1 \times exp(-\frac{5}{100}t)$$

$$S_2 = 1 \times cos(\frac{2\pi}{20}t + (1.4 + \frac{\pi}{2}))$$

The evolution of temperature using the approach is compared to a reference solution as shown in Fig. 5.42 leading to a relative error less than 5%. This case leads us to generate an accurate result once we have updated the bases.

Heaviside type 4 ($N_{cycles} = 10$). By taking a more complicated load such as in Fig. 5.39(d), the bases are derived directly from the analytical expression. First the location of the peaks is determined from the FFT of the load. In fact the FFT of this load leads to the same location of the peaks as case 1.

$$S_1 = 1 - 1 \times exp(-\frac{5}{100}t)$$

$$S_2 = 1 \times cos(w_1 \times t + (1.76))$$

$$S_3 = 1 \times cos(w_2 \times t + (1.76))$$

$$S_4 = 1 \times cos(w_3 \times t + (1.66))$$

$$S_5 = 1 \times cos(w_4 \times t + (1.63))$$

where $w_1 = 2 \times \pi \times \frac{1}{20}$; $w_2 = 2 \times \pi \times \frac{1}{10}$; $w_3 = 2 \times \pi \times \frac{1}{5}$; $w_4 = 2 \times \pi \times \frac{1}{2.5}$.
The evolution of temperature using the approach is compared to a reference solution as shown in Fig. 5.43 leading to a relative error less than 4.6% and a large time saving of order 50.

The results point to validate the use of such approach with different kinds of load. The knowledge of the load applied is helpful to create an efficient dictionary.

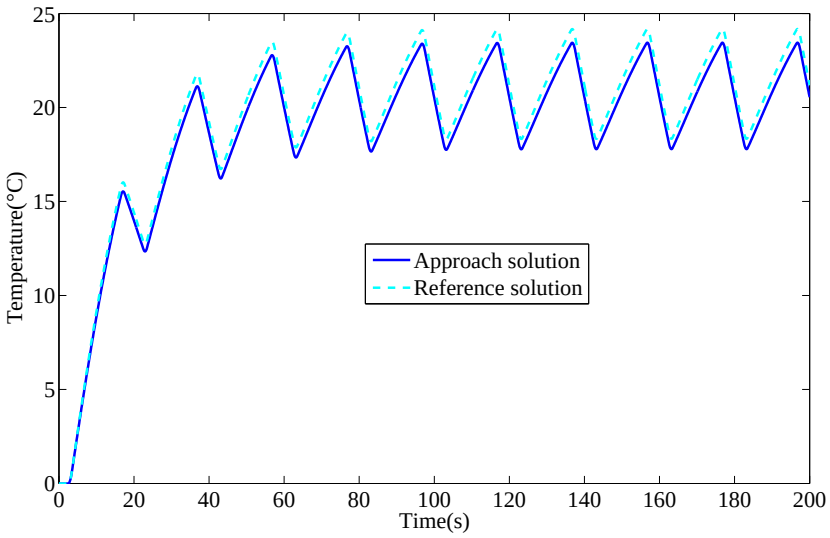


Figure 5.43: Load type 4: Solution using the approach at $(x, y, z) = (25, 25, 25)$ with $\tau_\phi = 100s$

5.3.6.3 Influence of the ratio ($\frac{T_{min}}{T_{max}} = -1$)

In this section, the effect of $\boldsymbol{R}$ is dealt with. In the first place, $\boldsymbol{R} = -1$ is used instead of $\boldsymbol{R} = 0$. Preliminary, the ratio will influence the evolution of temperature. To clearly understand the effect of the ratio, the model now encounters a heat source with triangular form $\frac{T_{min}}{T_{max}} = -1$ as shown in Fig. 5.44. The physical time considered is 10 s. In the first place, the old bases generated from $\boldsymbol{R} = 0$ are used. The mixed strategy is used to compute the spatial modes and the reconstructed solution is represented in Fig. 5.45. As expected, the method cannot capture the solution with the old bases, it leads to an error higher than 50%. The evidence from this case points towards the idea of enriching this dictionary by taking different cases of loads. However, to determine the new bases it is proposed to compare the FFT in both cases $\boldsymbol{R} = 0$ and $\boldsymbol{R} = -1$ with $\tau_\phi = 10s$. The evolution of the amplitude and the phase in the frequency domain are depicted in Fig. 5.46. There is a strong difference with the phase angle between the two cases. However, the evolution of the amplitude is similar. This leads to generate a new time bases, following the same procedure used in the construction of the old time bases:
The first two time bases are:

$$S_1 = 1 - A \times \exp(\frac{-5}{10}t)$$

with $A = 10$

$$S_2 = 1 \times cos(w \times t + (2.66 + \frac{\pi}{2}))$$

The first time basis is different compared to that of the triangular case. The amplitude in this case, $A = 10$ while in the triangular case ($\boldsymbol{R} = 0$), $A = 0.0676$.

The phase angle in the second time basis is also not the same. An adding of a phase angle $\frac{\pi}{2}$ is required compared to the case of the triangular load. It seems that there is an effect on the evolution of the first time basis. Thus, it is required to analyze different cases to generate a more general expression for the case of $\boldsymbol{R} = -1$. However, the solution is here obtained with these time bases.
Fig. 5.47 shows the evolution of the temperature with a relative error less than 5%. The findings from this case support the idea of constructing a priori time bases and the convergence of the approach. Nevertheless, in this case, a new analytical expression has to be developped.

5.3.6.4 Influence of the load amplitude

A priori time bases can be used for different cases with different load forms as proved in the past sections. In this section, an additional support for the approach is provided by studying the influence

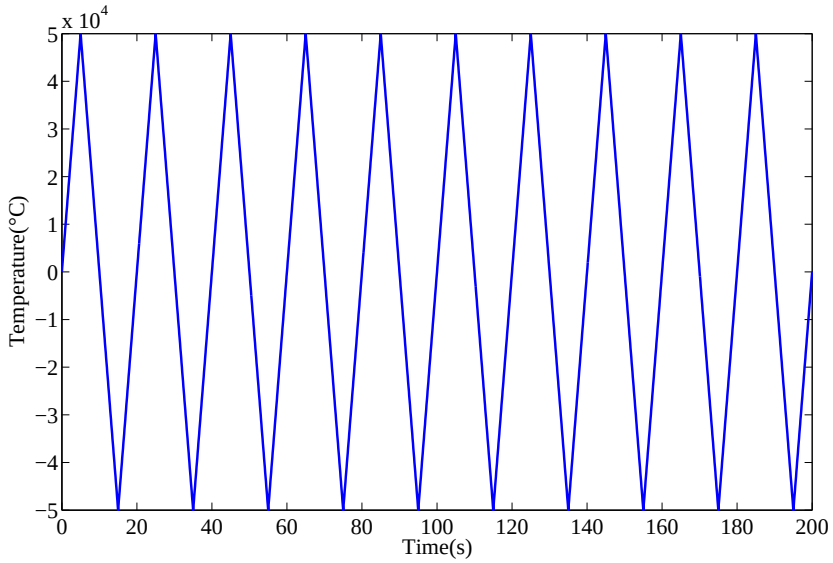


Figure 5.44: Heat source $\boldsymbol{R} = -1$, $\tau_c = 20s$, $n_{cycles} = 10$

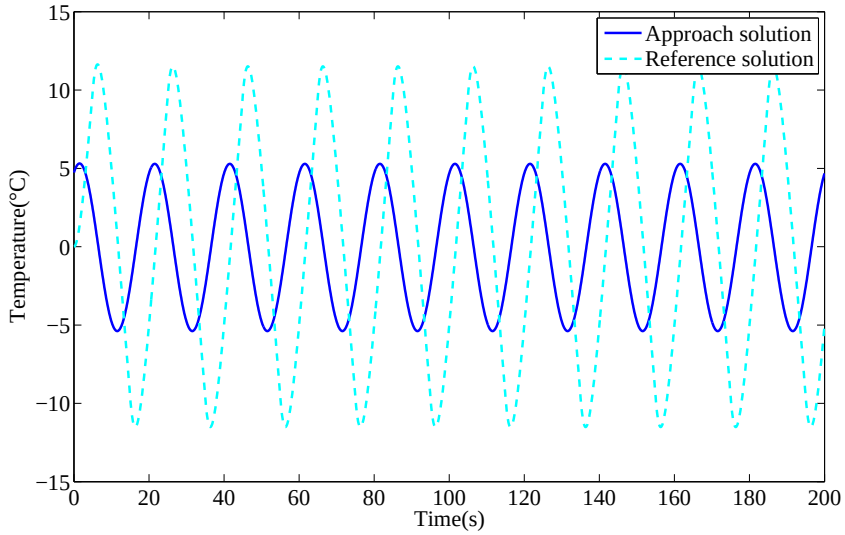


Figure 5.45: The evolution of temperature using the old bases at $(x, y, z) = (25, 25, 25)$

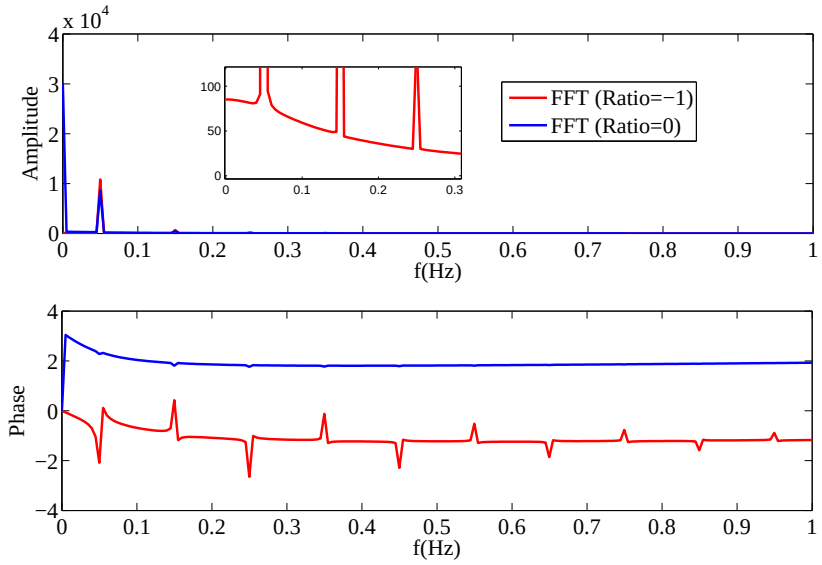


Figure 5.46: The variation of the amplitude and the phase angle in frequency domain for fixed spatial point $(x, y, z) = (25, 25, 25)$, $(\boldsymbol{R} = -1)$ and $(\boldsymbol{R} = 0)$

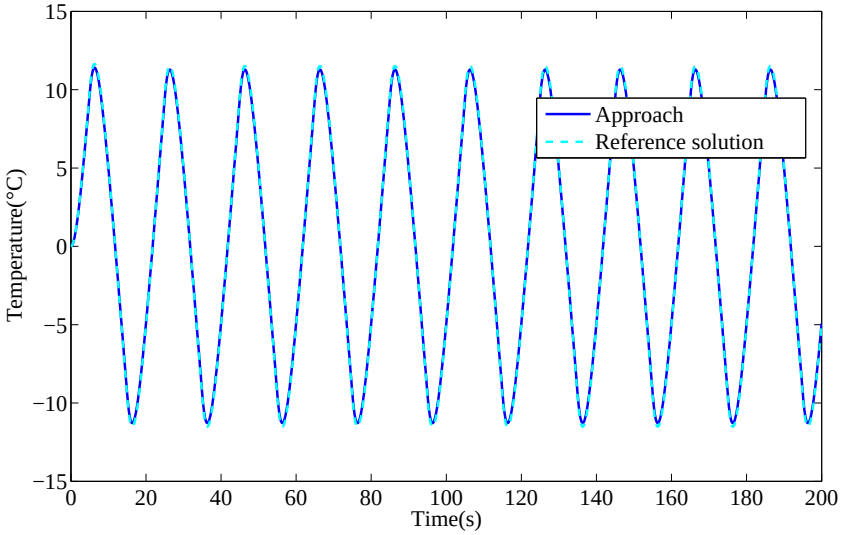


Figure 5.47: Solution using the approach compared to reference solution at $(x, y, z) = (25, 25, 25)$

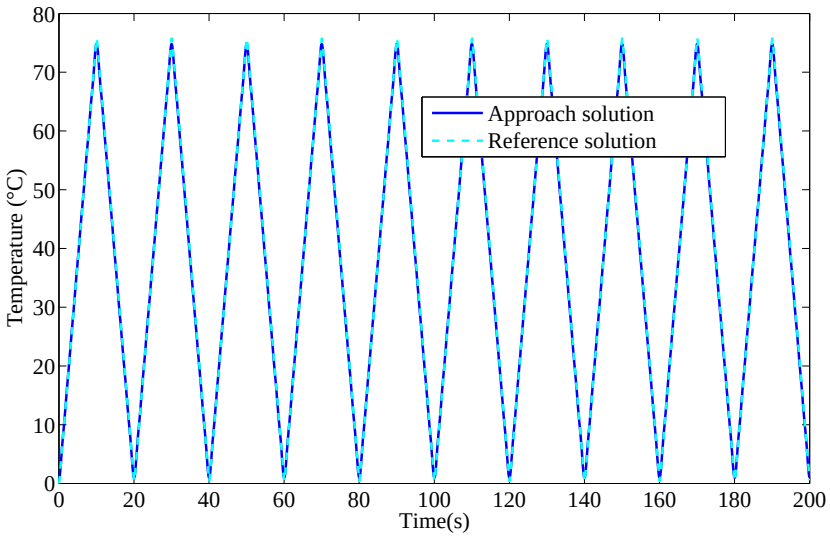


Figure 5.48: Evolution of temperature for new amplitude with old bases at $(x, y, z) = (25, 25, 25)$

of the amplitude of the load applied. For example, take a load with (amplitude 250000 instead of 100000) with ($\tau_\phi = 0.1s$ and $\tau_c = 20s$). A priori time bases are used from the old dictionary developed. The spatial modes are calculated, then the solution is reconstructed. The results at a fixed spatial point is shown in Fig. 5.48 with a relative error using L^2 norm less than 5%. The evolution of the temperature highlights the effect of the load amplitude where the difference is just related to the amplitude of the temperature. These observations strengthen the spatial modes which take into account the amplitude effect.

Remark: The summary of the simulations using the approach compared to FEM with respect to the computation time and the relative error are shown in the Appendix C and prove the potential of the approach.

5.3.7 Extension to coupled problem

The mixed strategy is being now extended to a coupled thermo-diffusion problem with a weak coupling. Let us recall the coupled problem previously presented in section 4.6: Eq. (5.18) represents the diffusion problem and Eq. (5.19) represents the thermo-diffusion coupled problem.

$$\frac{\partial c}{\partial t} - D\Delta c = F_D(t) \tag{5.18}$$

$$\rho C_p \frac{\partial T}{\partial t} - K\Delta T = F_T(t) - \beta c \tag{5.19}$$

In the diffusion equation Eq. (5.18), c is the concentration, D is the diffusivity coefficient, and $F_D(t)$ refers to the mass source in the diffusion equation. In the thermal-diffusion equation Eq. (5.19), T is the temperature, C_p is the specific heat, ρ is the density, k is the thermal conductivity, β is the coupling coefficient between the concentration and the temperature, and $F_T(t)$ is the heat source in the thermal-diffusion equation. The diffusion phenomenon has two characteristic times (cycle time of the load applied (denoted by τ_c^D), and the physical time ($\tau_\phi^D = \frac{L_c^2}{D}$)). While, the thermo-diffusion problem has two characteristic times (cycle time of the load applied (denoted by τ_c^T), and the physical time ($\tau_\phi^T = \frac{\rho C_p L_c^2}{k}$)), and the characteristic time associated with the diffusion phenomenon transferred by the coupling term.

The cube is subjected to an heat source and a mass source with null initial and boundary conditions. The material properties are summarized in Table 5.13. Fig. 5.49 pinpoints the evolution of the load applied for the diffusion problem ($F_D(t)$) with $\tau_c^D = 2.5s$ (the total number of cycles is 80) and for the coupled thermo-diffusion problem ($F_T(t)$) with $\tau_c = 50s$ (the total number of cycles is 4).
We here consider that the diffusion and the thermal phenomena have the same physical time $\tau_\phi = 3s$. To solve the coupled thermo-diffusion problem with the mixed strategy, the concentration field of the diffusion equation is written as:

$$c(\underline{x}, t) = \sum_{i=1}^{n} R_i^D(\underline{x}) S_i^D(t) \tag{5.20}$$

where S_i^D are a priori time bases computed using the analytical expression (see Eqs. (5.2) and (5.3)) and R_i^D referred to the spatial modes computed from the diffusion equation. For the diffusion equation $R_\tau = \frac{3}{2.5} = 1.2$, $\theta(R_\tau = 1.2) = 2.2606$ according to Eq. (5.3). The first 2 time bases for the diffusion equation are:

$$S_1^D = 1 - 0.5683 \times exp(-\frac{5}{3}t)$$

$$S_2^D = 1 \times cos(\frac{2\pi}{2.5}t + 2.2606)$$

Remark. The spatial modes for the diffusion equation ($\tau_\phi^D = 3s$, and $\tau_c^D = 2.5s$) are computed with the mixed strategy where 7 time bases are needed to achieve an error of less than 2.2% while, for the thermal problem ($\tau_\phi^T = 3s$, and $\tau_c^T = 50s$), 10 time bases are needed.

The first 2 time bases for thermal problem ($R_\tau = \frac{3}{50} = 0.06$, $\theta(R_\tau = 0.06) = 3.0811$) are:

$$S_1^T = 1 - 0.0411 \times exp(-\frac{5}{3}t)$$

$$S_2^T = 1 \times cos(\frac{2\pi}{50}t + 3.0811)$$

To solve the thermal-diffusion equation with $\tau_\phi = 3s$, the time bases have to be ordered with increasing frequency, in this problem, two frequencies ($f_1 = \frac{1}{\tau_c^T} = 0.02$, and $f_2 = \frac{1}{\tau_c^D} = 0.4$) are considered, where $\tau_c^T = 50$ and $\tau_c^D = 2.5$, with $\tau_\phi^D = \tau_\phi^T = 3s$ The time bases used are collected

ρ	C_p	k	β	D
$950\ \mathrm{kg.m^{-3}}$	$2.273\ \mathrm{J.kg^{-1}.C^{-1}}$	$0.45\ \mathrm{W.m^{-1}{\circ}C^{-1}}$	$50\ \mathrm{J.kg^{-1}.s^{-1}}$	$2.08 \times 10^{-4}\ \mathrm{s.m^{-2}}$

Table 5.13: Material properties and the coupling coefficient

from the diffusion and thermal problems (17 time bases).
For the purpose of simplicity, F_T is written under a space-time separated representation as follows: $F_T = F_x(\underline{x})F_t(t)$. Eq. (5.19) will be written as:

$$\rho C_p \int_{\Omega\times\Omega_t} T^* \frac{\partial T}{\partial t} d\Omega dt + k \int_{\Omega\times\Omega_t} \vec{\nabla}\, T\, \vec{\nabla}\, T^* d\Omega dt = \int_{\Omega\times\Omega_t} F_T T^* d\Omega dt - \beta \int_{\Omega\times\Omega_t} cT^* d\Omega dt \quad (5.21)$$

where c is written as in Eq. (5.20). The evolution of temperature is depicted in Fig. 5.50 for a given spatial point. An relative error of less than 3.2% is obtained. As the two physical times are equal, only the cycle time is visible (the solution is composed of a periodic function of $50s$ where a cycle time of $2.5s$ is added (it is clear from the zoom see Fig. 5.50)). To more clearly understand the effect of the coupling effect, Fig. 5.51 depicts the evolution of temperature for the uncoupled problem. This approach leads to a time saving of order 7.86 compared to the PGD method (CPU time for the approach $= 3.603s$ and CPU time for the PGD $= 28.326s$)

To support the efficiency of this approach, we here consider a more general case with different physical times and cycle times. Compared to the previous case, the time bases have to be changed with respect to the new physical time: $\tau_\phi^D = 10s$ instead of $\tau_\phi = 3s$. For the diffusion, the ratio between the cycle time and the physical time becomes $R_\tau = \frac{10}{2.5} = 4$ and the phase angle becomes $\theta(R_\tau = 4) = 1.8067$. Thus, the first time bases for the diffusion are:

$$S_1^D = 1 - 0.9392 \times exp(-\frac{5}{10}t)$$

$$S_2^D = 1 \times cos(\frac{2\pi}{2.5}t + 1.8067)$$

The results obtained using the approach by considering 6 time basis for diffusion and 10 for thermal are illustrated in Fig. 5.52. The effect of a different physical time is more marked at the beginning (cf. Fig. 5.50 and Fig. 5.52). A relative error less than 4% compared to the PGD solution is obtained with a time saving of order 7.67 (CPU time for the approach = 3.48s and CPU time for the PGD = 26.6916s).

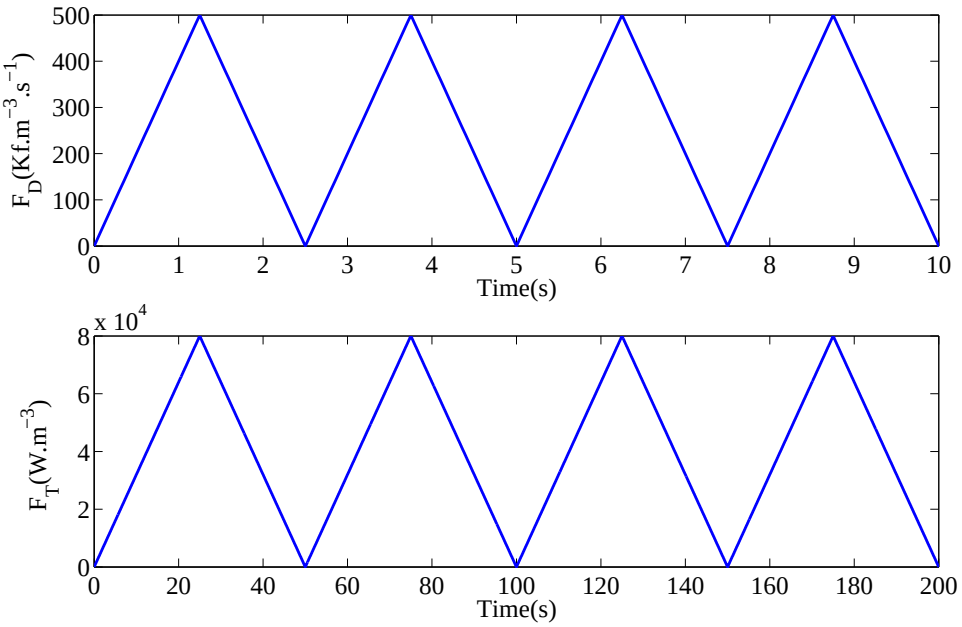


Figure 5.49: The first 4 cycles of the cyclic loading with a cycle time $\tau_c^D = 2.5s$ for $F_D(t)$ and $\tau_c^T = 50s$ for $F_T(t)$

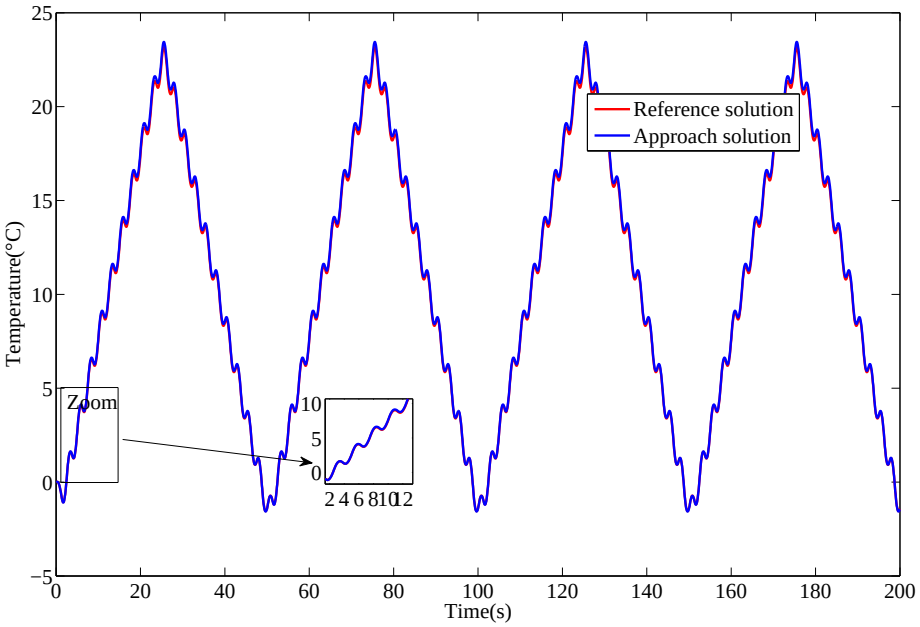


Figure 5.50: The evolution of temperature under the same physical time ($\tau_\phi = 3s$) and $\tau_c^T = 50s$ and $\tau_c^D = 2.5s$ at $(x, y, z) = (25, 25, 25)$

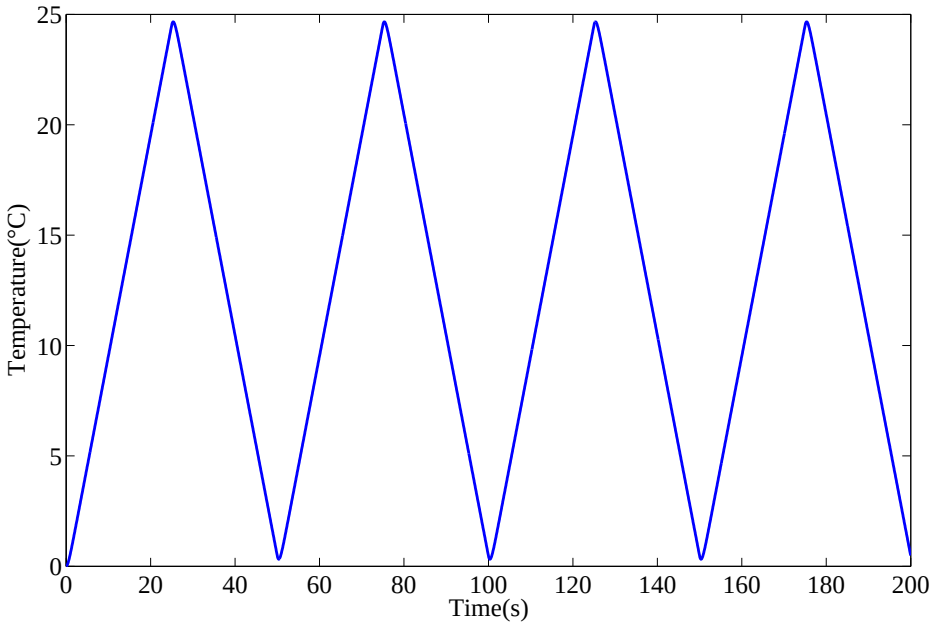


Figure 5.51: The evolution of temperature under ($\tau_\phi = 3s$) and $\tau_c^T = 50s$ without coupling effect

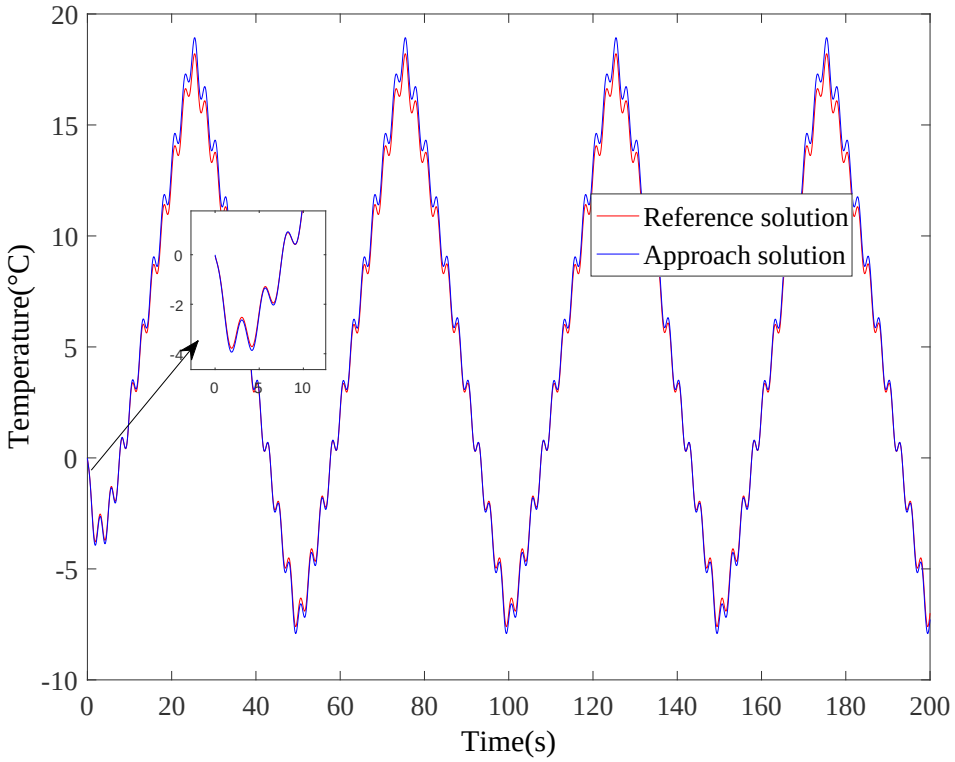


Figure 5.52: The evolution of temperature under different physical times ($\tau_\phi^T = 3s$ and $\tau_\phi^D = 10s$) and $\tau_c^T = 50s$ and $\tau_c^D = 2.5s$ at $(x, y, z) = (25, 25, 25)$

5.3.8 Discussion on the use of the mixed strategy for linear problem

Solving physical problems under cyclic loadings may lead to a large computation time when one uses an incremental method. The present study focuses on finding an innovative way to enhance the computation time. The evidence from this study intimates that due to the presence of different time scales in the problem, the solution will be affected by the relationship between these characteristic times (physical time and cycle time) which lead to think about the correlation and the effect of each time scale. Therefore, this study is the first step towards enhancing and developing a priori time basis. In fact, a new approach based on building a priori time basis was presented. It leads to the generation of a dictionary to be used on certain family of problems. To sum up, our study provides that a priori time basis can be generated by using only Fast Fourier Transform (FFT) analysis and the knowledge of time scales. This approach has been investigated with different cases such as an homogeneous boundary conditions, non-homogeneous boundary conditions, Robin boundary conditions, and different types of the applied load. To illustrate, a priori bases were found when two different loads with different cycle time and amplitude were considered. Equally important, when opposite surfaces encountered opposite loads in each surface a priori time basis has been used to solve the problem. Further studies showed that the dictionary can be used with different types of loads (Heaviside and sinusoidal). Moreover, this dictionary has been enriched by taking many cases.

5.4 Mixed strategy for 3D non linear problem

5.4.1 Algorithm

In the previous sections, the mixed strategy has been introduced and applied to the solution of linear transient heat conduction problems. Generally speaking, the physical properties have been assumed to be non-temperature dependent. An important issue is to introduce the non-linearity with the material properties such as the specific heat. The aim of this chapter is to answer the following questions and to evaluate the approach through different non-linear cases.

1. How to extend the mixed strategy to the nonlinear case?
2. What are the effects of the non-linearity on the evolution of the temperature?
3. How to choose the time bases?

The model considered is the same as the linear case with null initial and boundary conditions and a heat source is applied. However, in what follows we will consider the dependency of the specific heat on the temperature.
In summary, the major issues treated in this section are:

1. Propose the algorithm to solve the non-linear problem.
2. Check the feasibility of this approach.

Choosing a priori of time bases for a nonlinear case is complicated since the effect of the specific heat depends on the variation of temperature. With this in mind, the time bases are depending on physical time which in turn depends on the specific heat. Thus, the choice of the time bases is the main concern.

5.4.1.1 Choice of the time bases

The basic idea in choosing the bases in the nonlinear case arises from the observation that, the specific heat varies between two values: maximum specific heat generated from the maximum temperature (T_{max}) and the minimum specific heat generated from the minimum temperature (T_{min}). Thus, linear time bases are used based on the range of the physical time.
But, can the bases chosen capture the non-linearity effect? In the following, the algorithm to solve a non-linear problem is illustrated.

5.4.1.2 Algorithm to compute spatial basis and to solve the non-linearity

As discussed in the previous section, to solve the nonlinear problem, Picard's algorithm has been chosen, as illustrated in Chapter 1. In the mixed strategy, the procedure consists in three steps. Step 1 and step 2 deal with the a priori time bases and step 3 computes the spatial within the Picard's iterative procedure. The procedure can be summarized as follows:

1. Find the range of the specific heat.
   This range is related to the range of the cyclic imposed temperature.
   - Minimum range at T_{min} leading to a given value of the physical time: $\tau_\phi = \frac{\rho C(T_{min})}{K} L^2$
   - Maximum range at T_{max} leading to a given value of the physical time: $\tau_\phi = \frac{\rho C(T_{max})}{K} L^2$
2. Choose the time bases according to the two different physical times and with respect to the cycle time of the load applied. The time bases related to the different values of R_τ are defined through the analytical expressions given in section 5.3.1.2. Let us note that these time bases are used for each Picard's iteration.
3. Solve Picard iterations to deal with the non linearity.
   - Choose a starting guess T_1 where the index refers to the numbering of the Picard's iteration. Here we will choose $T_1 = 0$ leading to C_p equals a constant value (solution of a linear case) and an user defined value of ϵ (stopping criteria of the Picard's procedure).
   - **for** k=1,2,3... **do**
   - Compute the next solution $T_{k+1} = f(T_k)$ with the algorithm to compute the spatial modes proposed in section 5.3.1.3 in the previous Chapter.
   - **if** $\delta^k < \epsilon$, where $\delta^k = \frac{\|T_{k+1} - T_k\|}{\|T_k\|}$ with $\epsilon = 10^{-3}$ then
   - **stop**
   - **end if**
   - **else** update C_p with the new value T_{k+1}
   - **end for**

The nonlinear cases studied can be classified as follows:

- cases with only one cycle time
  - Linear dependence of specific heat with respect to temperature ($Cp(T) = aT + b$).
  - Quadratic dependence of specific heat with respect to temperature ($Cp(T) = aT^2 + bT + c$).
  - Rectangular dependence of specific heat with respect to temperature.
- cases with two cycle times
  - Sinusoidal dependence of specific heat ($Cp(T)$) with respect to temperature.

5.4.2 Numerical results

5.4.2.1 Nonlinear heat equation with one cycle time

Throughout this section, the thermal model with a null initial and boundary condition with a cyclic heat source is considered (same as in the linear case). The cyclic heat source is in a triangular form with $\boldsymbol{R} = 0$, $\tau_c = 10\ s$ and amplitude equal to $100000\ W.m^{-3}$. To detail, the following material and thermal properties are used: $\rho = 950\ \mathrm{kg.m^{-3}}$, $k = 0.45\ \mathrm{W.m^{-1}.C^{-1}}$. However, the specific heat is temperature dependent. Different dependencies are here investigated but these dependencies do not add another cycle time.

Linear dependence of specific heat with respect to temperature $(C_p(T) = aT + b)$**.** Let us consider a linear dependence of specific heat with respect to temperature as follows:

$$C_p = aT + b \tag{5.22}$$

where a and b are constants to be chosen.
With attention to the value of a and b that will determine the range of the physical time, three cases will be considered:

1. Case 1: $Cp = 9.2 \times T + 1366.6$. These values of a and b have been used in [Nguyen, 2013]. For these particular values, the range of the ratio of physical time to cycle time is $180 < R_\tau < 241$
2. Case 2: $C_p = T + 25$ leading to $3.2 < R_\tau < 10$
3. Case 3: $C_p = 27 \times T + 25$ leading to $3.2 < R_\tau < 181.4$

Case 1 In the first place, a priori bases issued from the analytical expression derived in section 5.3.1.2 are constructed based on the values of R_τ. Notably, the ratio varies between 180 and 241 considered as high ratio. For this reason, the bases can be constructed with one of the ratios since both will lead to the construction of the same time bases (see Eqs. (5.2) and (5.3)).
The two time bases that are used are as the followings:

$$\begin{aligned} S_1^{\tau_\phi=1800} &= 1 - \exp(-\frac{5}{1800}t) \\ S_2 &= cos(\frac{2\pi}{10}t + 1.6) \end{aligned} \tag{5.23}$$

Fig. 5.53 represents the evolution of the temperature obtained with FEM and the present approach. As expected, the approach captures and generates a satisfactory results compared to FEM. Not to mention, the highly transient evolution of temperature support the behavior with a large range of ratio. The non-linearity is solved with the algorithm discussed in section 5.4.1.2. So far, 3 iterations were required to obtain an accurate solution with an error less than 2% using L^2 norm as shown in Table 5.14. A time saving of order 45 compared to FEM is obtained. Fig. 5.54 depicts the evolution of the error with respect to the number of iterations.

Case 2 Similarly, for the case of $C_p = T + 25$ with $3.2 < R_\tau < 10$. New time bases issued from the analytical expressions has been built. Then, the bases used are related to both $R_\tau = 3.2$ and $R_\tau = 10$ (4 time bases). The time bases are ordered with respect to the physical time.

$$\begin{aligned} S_1^{\tau_\phi=32} &= 1 - 1.1065 \times \exp(-\frac{5}{32}t) \\ S_2 &= cos(\frac{2\pi}{10}t + 1.8627) \\ S_3^{\tau_\phi=100} &= 1 - 1.0009 \times \exp(-\frac{5}{100}t) \\ S_4 &= cos(\frac{2\pi}{100}t + 1.6667) \end{aligned} \tag{5.24}$$

As expected, the approach converged with 4 iterations as shown in Fig. 5.55 leading to accurate results compared to FEM with an error less than 3.9%. A time saving of order 40 compared to FEM is obtained. The evolution of the temperature compared to the reference solution for a fixed point is shown in Fig. 5.56. Indeed, the solution is a combination of the smallest R_τ and the largest R_τ. It shows that the approach can predict the solution within a small range of the ratio of physical time to the cycle time.

Case 3 In this case, two different behaviors from the range of R_τ can be noticed. For a small range $(R_\tau = 3.2)$, the evolution of the temperature can reach the stabilized cycle after a while. However, for the larger value $(R_\tau = 181.4)$ the evolution of temperature will not reach the stabilized

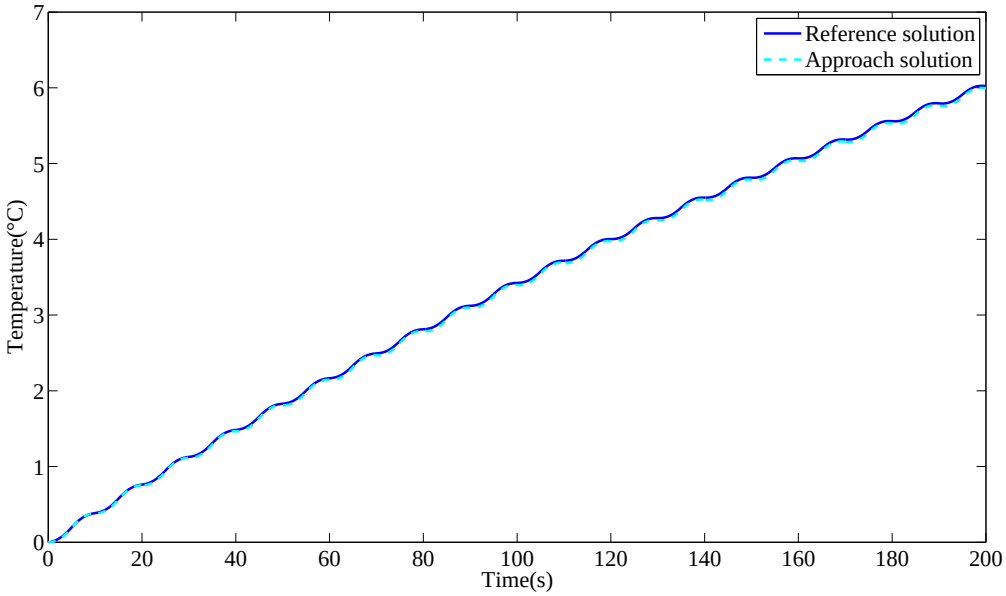


Figure 5.53: The evolution of the temperature with $\tau_c = 10s$ and $Cp = 9.2 \times T + 1366.6$ at $(x, y, z) = (25, 25, 25)$ - case 1

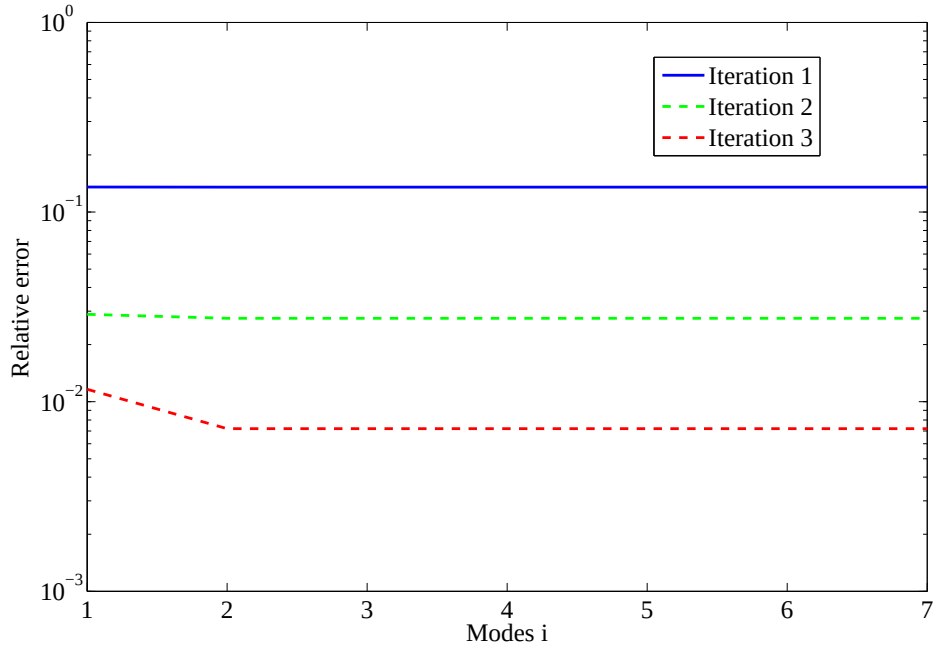


Figure 5.54: The evolution of the relative error with respect to the Picard iterations and the number of modes - case 1

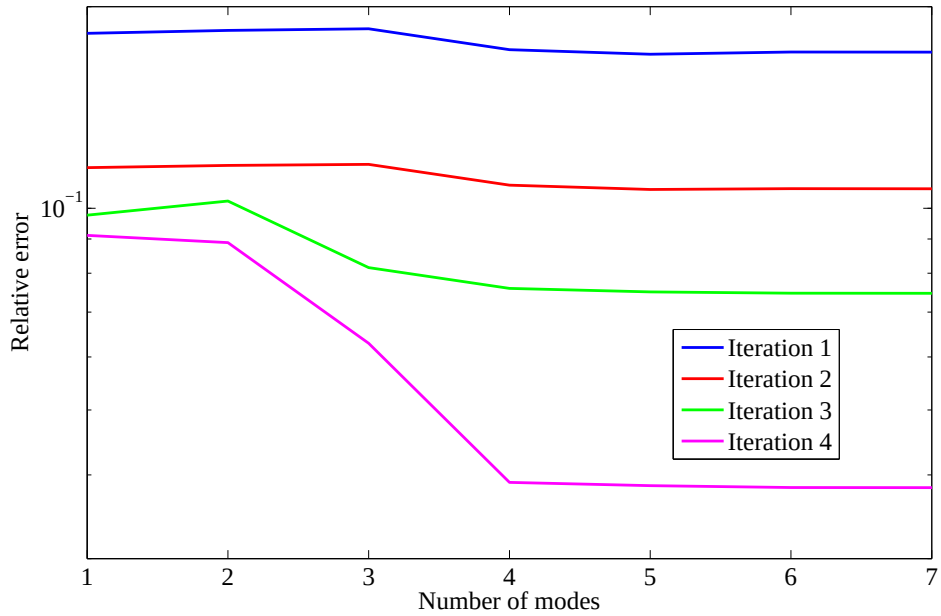


Figure 5.55: The evolution of the relative error with respect to the number of Picard iterations - case 2

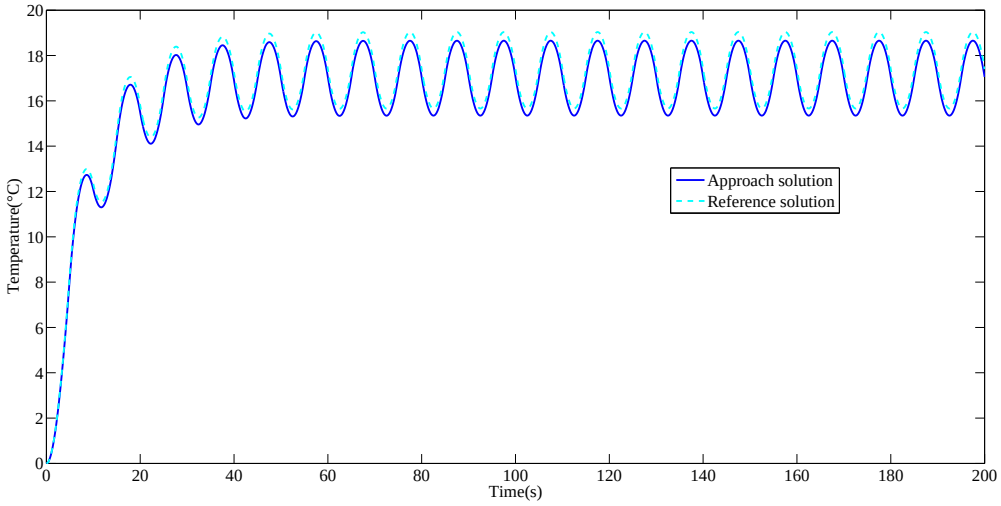


Figure 5.56: The evolution of temperature with $\tau_c = 10s$, $C_p = T + 25$ and $3.2 < R_\tau < 10$ at $(x, y, z) = (25, 25, 25)$ - case 2

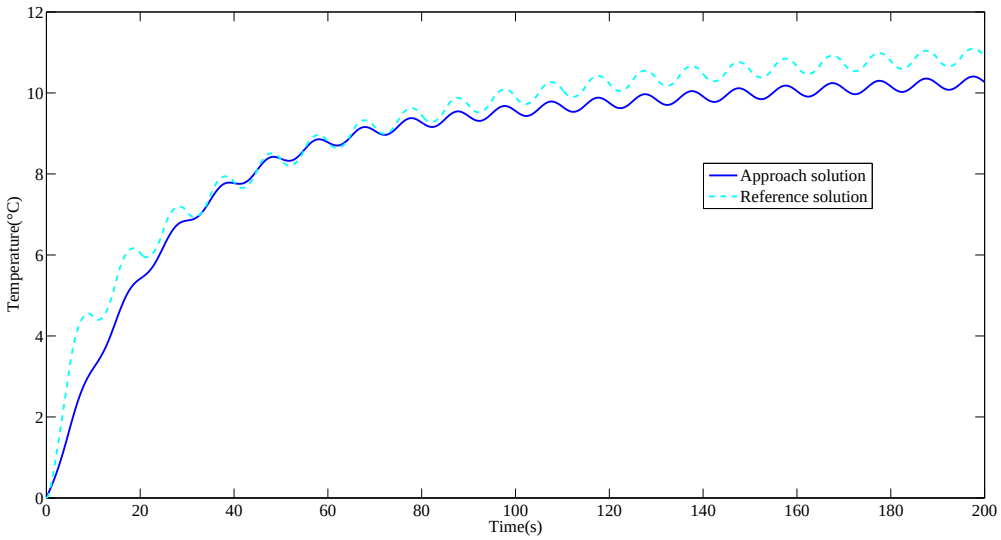


Figure 5.57: The evolution of temperature with $\tau_c = 10s$, $C_p = 27 \times T + 25$ with $3.2 < R_\tau < 181.4$ at $(x, y, z) = (25, 25, 25)$ - case 3

Spatial point (x,y,z)	$(25, 25, 25)$	$(37.5, 25, 25)$	$(37.5, 37.5, 37.5)$	$(37.5, 12.5, 37.5)$
Case 1 (%)	0.8%	1.2%	2%	1.6%
Case 2 (%)	3.44%	3.8%	3.9%	3.6%
Case 3 (%)	9.3%	10.7%	10.5%	8.7%

Table 5.14: The relative error calculated for different points for linear dependence of specific heat

cycle. Thus, what is the behavior of the temperature? Can we capture the solution within the time bases issued from the linear cases? First, let us note that, six time bases related to ($R_\tau = 3.2$, and $R_\tau = 181.1$) are chosen according to the physical time and a solution with an relative error equal to 20% is obtained.
How to enrich the bases? We here propose to add more time bases for example by taking the time bases related to $R_\tau = \frac{(R_\tau=3.2)+(R_\tau=181.1)}{2} = 92.3$ (a mean value of R_τ) to describe more continously the transition between the two different behaviors. The error has been reduced to 11% with the new 9 time bases (4 related to $R_\tau = 3.2$, 3 related to $R_\tau = 92.3$ and 2 related to $R_\tau = 181.1$). This strategy seems to be efficient. To enrich these bases, another 6 time bases are added by taking other values of R_τ ($R_\tau = 10$, and $R_\tau = 100$), the number of bases is here 15. Fig. 5.57 represents the evolution of temperature compared to FEM solution with an error of 10.7%. Let us note that this error has been decreased from 20% when different R_τ were taken into account. A time saving of order 16.5 compared to FEM is obtained.
As a conclusion, bases can not capture exactly the behavior of the solution when the range of R_τ is very large, and a large number of time bases has to be added for an accurate prediction. To sum up, the finding from the three previous cases show that the method can solve the non-linearity issued from the material properties. However, the most important limitation is related to the large range of the ratio where a priori time bases don't capture clearly the solution. Table 5.14 summarizes the relative error for different spatial points for the three cases.

Quadratic dependence of specific heat with respect to temperature $(C_p(T) = aT^2 + bT + c)$**.** In this subsection, the form of the specific heat has been changed to:

$$Cp = a \times T^2 + b \times T + c \tag{5.25}$$

Spatial point (x,y,z)	$(25, 25, 25)$	$(37.5, 25, 25)$	$(37.5, 37.5, 37.5)$	$(37.5, 12.5, 37.5)$
Case rectangular (%)	5%	4.8%	4.7%	4.3%

Table 5.15: The relative error calculated for different points for the quadratic case

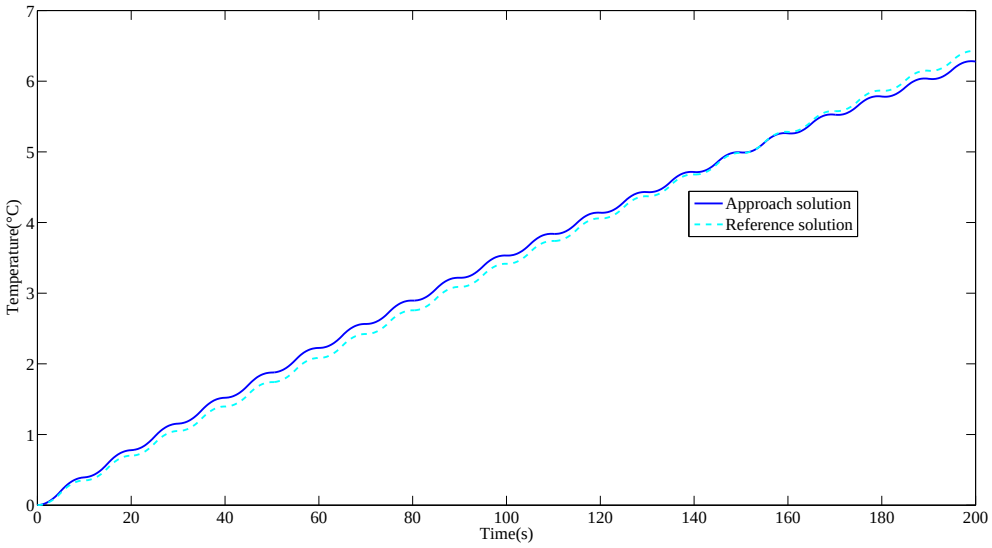


Figure 5.58: The evolution of temperature using the approach compared to the FEM at $(x, y, z) = (25, 25, 25)$ - quadratic dependence of $C_p(T)$

with $a = b = 0.25$, and $c = 1500$ leading to the following range of $197 < R_\tau < 282$. The bases used are issued from the analytical expression with $R_\tau = 197$. Two time bases are used:

$$\begin{aligned} S_1^{\tau_\phi=1970} &= 1 - \exp(-\frac{5}{1970}t) \\ S_2 &= cos(\frac{2\pi}{10}t + 1.6) \end{aligned} \tag{5.26}$$

Fig. 5.58 pinpoints the evolution of the temperature using the approach and compared to the FEM solution. Table 5.15 depicts the relative for different spatial points. The results obtained with 5 Picard iterations and only 2 a priori time bases are compatible with the reference solution with an average error less than 5%.

Rectangular dependence of specific heat with respect to temperature. In this case, the possibility of introducing new form of the dependence of the specific heat is being discussed. As in the previous cases, the thermal problem is considered Eq. (5.1) with an heat generation source with $\tau_c = 10s$. The form of the specific heat is represented in Fig. 5.59. Shortly, the form of the load is rectangular leading to a sharp reduction of the specific heat. Straightaway, a priori bases are constructed using the analytical expression. The bases used are:

$$\begin{aligned} S_1 &= 1 - \exp(-\frac{5}{1800}t) \\ S_2 &= cos(\frac{2\pi}{10}t + 1.6) \end{aligned} \tag{5.27}$$

Obviously, the effect is only related to the evolution of the temperature amplitude. Accurate results with the approach are obtained as shown in Fig. 5.60. Table 5.16 depicts the relative error for different spatial points. Notably, 13 Picard iterations and 2 a priori time bases are required to have accurate results with a relative error less than 4.2%.

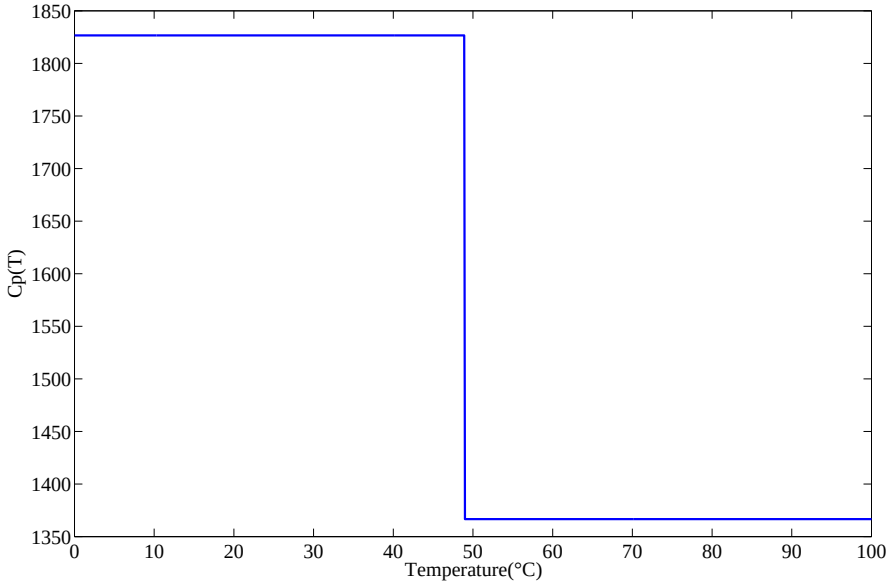


Figure 5.59: The evolution of the specific heat with respect to the temperature - rectangular dependence of $C_p(T)$

Spatial point (x,y,z)	$(25, 25, 25)$	$(37.5, 25, 25)$	$(37.5, 37.5, 37.5)$	$(37.5, 12.5, 37.5)$
Case rectangular (%)	4.1%	4.2%	3.9%	4.1%

Table 5.16: The relative error calculated for different spatial points - rectangular dependence of $C_p(T)$

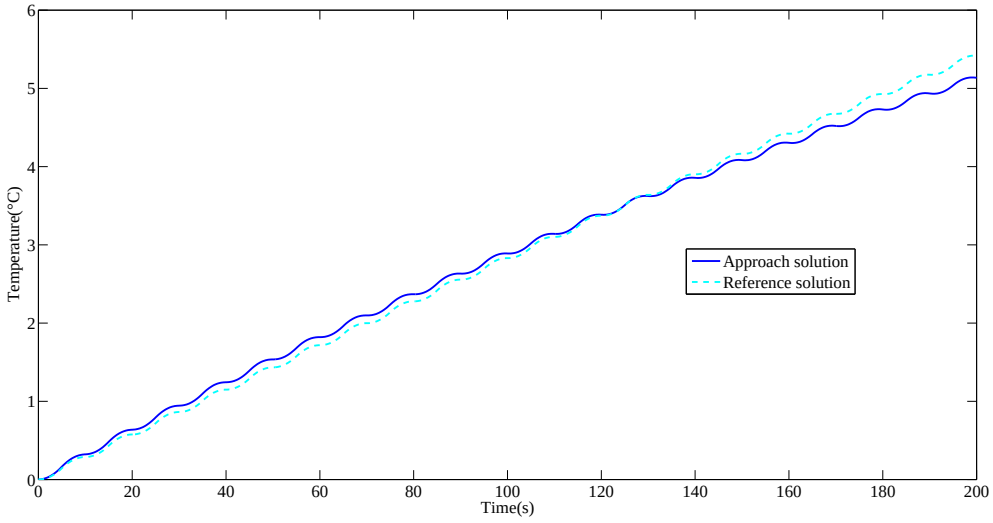


Figure 5.60: The evolution of temperature using the approach compared to the FEM at $(x, y, z) = (25, 25, 25)$- rectangular dependence of $C_p(T)$

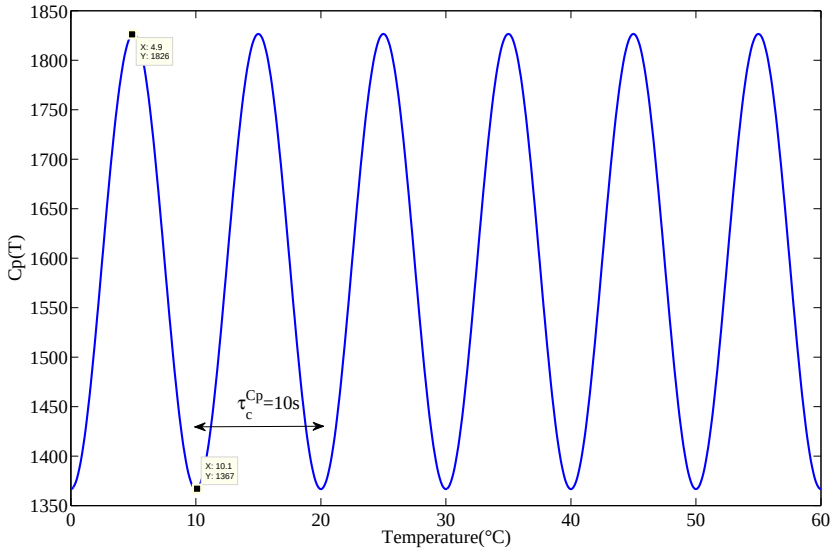


Figure 5.61: The evolution of specific heat C_p with respect to the temperature - case 1 sinusoidal dependence

5.4.2.2 Nonlinear heat equation with two cycle times

The objective of this section is to study the effect of introducing a new characteristic time. The nonlinear problem which deals with two cycle times is achived trough a sinusoidal dependence of specific heat with respect to temperature.
Two different cases are investigated:

1. Case 1: The variation of the specific heat with respect to the temperature is represented in Fig. 5.61 with a cycle time equal to 10s, same value as the cycle time of the load applied: two cycle times with a same value.

2. Case 2: The variation of specific heat with respect to temperature is represented in Fig. 5.62 with a cycle time equal to 20s, larger than the cycle time of the load applied: two cycle times with two different values.

This raises different questions:

- How does the new characteristic time affects the evolution of temperature?
- What are the time bases used?

To begin with, the evolution of the temperature for the two cases for fixed spatial point $(25, 25, 25)$ is represented in Fig. 5.63. The new characteristic time related to the specific heat evolution with respect to the temperature affects only the amplitude (the behavior is the same). Can the same time basis be used to solve both behaviors since the difference is only related to a change of the amplitude? In that case, spatial modes can capture the effect proved in the linear case. Let us take the time bases issued from a priori time bases with $R_\tau = 180$ which corresponds to the minimum value of Cp. This value has been chosen instead of the maximum since both are located in the same regimes (transient).
The first two time bases used are:

$$\begin{aligned} S_1 &= 1 - \exp(-\frac{5}{1800}t) \\ S_2 &= cos(\frac{2\pi}{10}t + 1.6) \end{aligned} \tag{5.28}$$

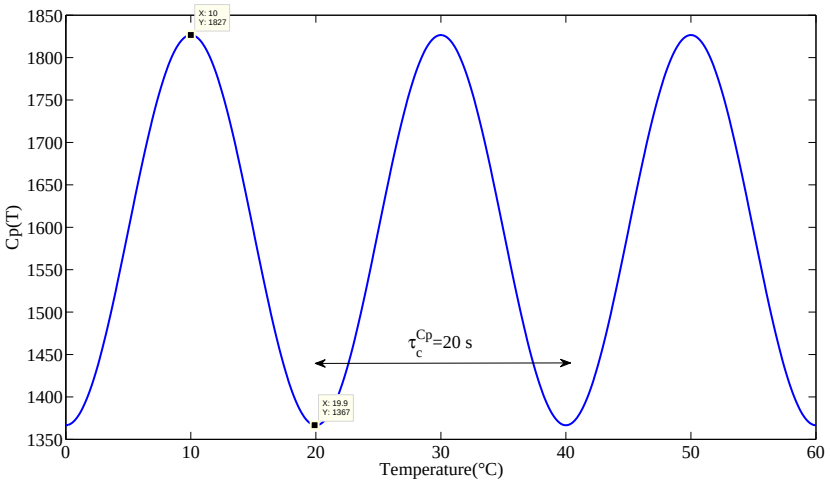


Figure 5.62: The evolution of specific heat C_p with respect to the temperature - case 2 sinusoidal dependence

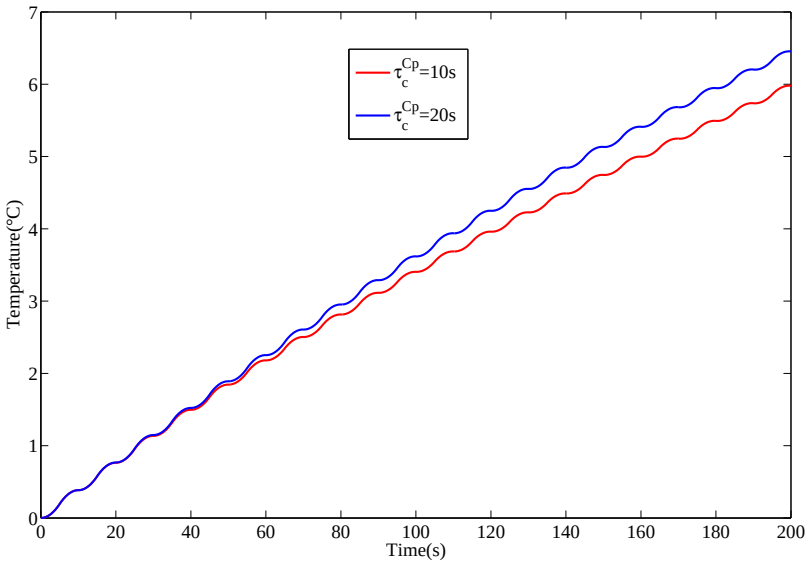


Figure 5.63: The evolution of temperature case 1 and case 2 using FEM at $(x, y, z) = (25, 25, 25)$

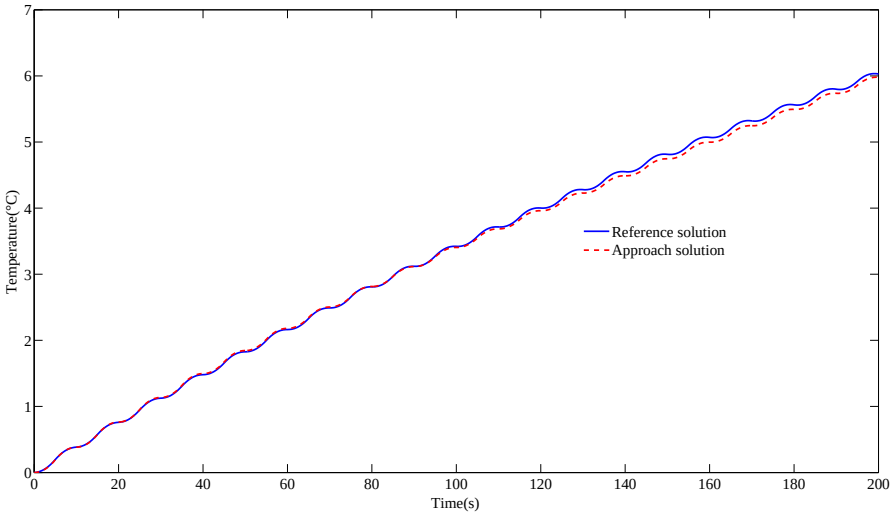


Figure 5.64: The evolution of temperature using the approach and compared to the FEM - case 1 ($\tau_c^{C_p} = 10s$) at $(x, y, z) = (25, 25, 25)$

Spatial point (x,y,z)	$(25, 25, 25)$	$(37.5, 25, 25)$	$(37.5, 37.5, 37.5)$	$(37.5, 12.5, 37.5)$
Case 1 (%)	3.3%	3.2%	3.7%	3.6%
Case 2 (%)	3.2%	3.1%	3.8%	3.5%

Table 5.17: The relative error calculated for different points for the sinusoidal case

Fig. 5.64 and Fig. 5.65 depict the evolution of the temperature for both cases respectively compared to FEM. The results showed that mixed strategy method is able to solve problems with different characteristic times (τ_c, $\tau_\phi(T)$, $\tau_c^{C_p}$). Table 5.17 depicts the relative error for different spatial points showing that an accurate result is obtained.

5.4.3 Discussion on the use of the mixed strategy for nonlinear problem

This work illustrates that the approach can be extended to a non-linear problem. The finding of this study indicates that a combination with a linearization scheme can be used to compute the spatial basis for a nonlinear problem, the time basis being the time basis issued for linear problems for different values of the ratio $R_\tau = \frac{\tau_\phi}{\tau_c}$. These values are issued from the minimal and maximal values of the range of temperature, leading to particular values of the specific heat and then particular values of τ_ϕ. Accurate results are obtained with a limited number of Picard iterations. Nevertheless, the method is limited for case 3 where the ratio range is very large. Of course, this is a complex case as the behavior changes significantly with respect to the temperature in this range (small characteristic times and large characteristic times). To overcome this problem, more time bases are added (corresponding to different values of τ_ϕ), it leads to a decreasing value of the error (less than 10.7% instead of 20%). The results are very encouraging for all other cases regardless the form of the specific heat. In general, using a linear priori time bases to solve non linear leads to an accurate answer with an average error less than 4% and a large time saving of order 50 compared to FEM.

5.5 Conclusion

To sum up, a mixed strategy has been proposed and tested in the case of linear transient problems, coupled problems and nonlinear transient problems under cyclic loadings. This strategy is based on the use of an a priori time basis. This time basis are known under an analytical expression with

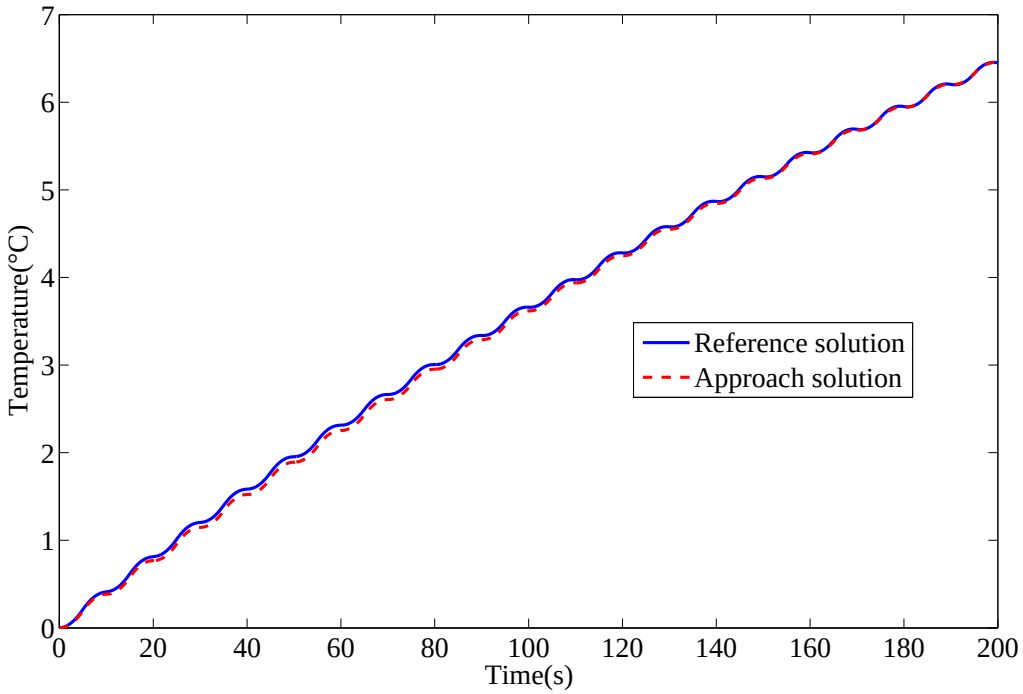


Figure 5.65: The evolution of temperature using the approach and compared to the FEM - case 2 ($\tau_c^{C_p} = 20s$) at $(x, y, z) = (25, 25, 25)$

respect to the different times: physical times and cycle times. This expression is obtained after the peak decomposition of the time evolution of the temperature for different characteristic times in the frequency domain by using the FFT, the fitting is then done in the time domain for each peak function. Once these time basis known, a PGD algorithm is used to compute the spatial modes. Let us note that the interest of this strategy is the non use of an incremental scheme such as in the FEM. If the number of time basis is smaller that the number of iterations of the incremental procedure in the FEM, the computation will be largely reduced. Let us recall the different results discussed:

- The mixed strategy has proved its capacity to solve 3D linear transient problem with different cycle times, physical times, boundary conditions, and load types. Accurate results compared to FEM have been obtained with a large time saving around 50 times.
- The approach has been successfully extended to a coupled problem by considering the time basis related to each physical time and cycle time for each separated phenomenon.
- The mixed strategy has been extended for nonlinear heat equation where the analytical expression generated in linear cases has been used. The non-linearity has been studied by considering different dependencies of the specific heat with respect to temperature. More precisely, the used time basis are the time basis related to the linear problem but for different values of the ratio $R_\tau = \frac{\tau_\phi}{\tau_c}$. These values are issued from the minimal and maximal values of the range of temperature, leading to particular values of the specific heat and then particular values of τ_ϕ. Once the time basis are known, the spatial basis are computed with a PGD algorithm combined to a linearization procedure such as a Picard scheme. Accurate results have been obtained with a limited number of iterations in the case where the non-linearity doesn't change significantly the behavior. If not, more basis have to be added corresponding to other values of the temperature (and not only max and min) which can lead to a large number of time basis.

The mixed strategy allows to alleviate the limitation to the previous proposed approach for more than one cycle time by making use of only a priori time basis based on an analytical expression.

Nevertheless, this strategy has to be evaluated in more complex problem presenting more cycle times such as thermoviscoelasticity.

Conclusions and perspectives

***

Conclusions

This thesis sets out and discusses alternative approaches to predict the solution of thermal transient problems under fatigue.

The findings of this study are summarized by:

- From the outcomes of the literature review, many possibilities exist to solve multitime problems. The methods can be classified into two main categories:
  - the incremental methods (which making use of an incremental scheme for the time integration)
  - the non-incremental methods

  The literature on the use of incremental method such as FEM in the polymers fatigue problems may lead to very large computation times (due to the time scales, the number of cycle to reach the stabilized cycle), non-convergence of the computations (due to the difficulty to achieve stability) and a large memory storage (time dependent history and large number of variables to be stored). To solve this issue, researchers have proposed various methods such as Model Order Reduction methods which allows to significantly reduce computation time and storage memory. Some of these methods belong to non-incremental methods as the LATIN method or its extension to multidimensional case the PGD method (under a space-time separation). Straightaway, the review of the nonlinear models showed that the non-linearities in a thermal conduction problem are often related to temperature dependent parameters. Different linearization schemes can be used to solve the non-linearity within the PGD method. Some of these linearization schemes such as the Newton Raphason method encounters the following difficulties: the computation time (due to the updating of the operators) and the storage memory. However, another technique related to the coupling between PGD-DEIM is recently used, and showed an efficient way to reduce the computational cost by evaluating the non-linearities on a reduced domain.

- In this study, the PGD method is used to solve a 3D cyclic linear transient problem. This method can capture the different behaviors generated from different time scales (different ratios between the cycle time related to the loading and the physical time related to the material properties). The results obtained with the PGD lead to a large computation time-saving compared to the FEM of order 30 with an accuracy and average error less than 1%. Moreover, a way to decrease the computation time was presented. It consists in decreasing the time step depending on the physical time: for larger physical time a coarse time step can be used which is not the case for smaller physical time. Also, the effect of the spatial position with respect to the physical time showed that for high physical time, the cyclic effect vanishes far from the boundaries where the load is applied.
  The PGD-based DEIM method is then used to solve a nonlinear thermal problem issued from the dependence of the parameters on temperature such as the specific heat and the convection coefficient. The upshot of the DEIM-based PGD generates accurate results (error less than 5%) with a significant time-saving of order 12 compared to FEM. This PGD-based DEIM technique can be useful for applications that encounter a fluctuation in temperature such as a nuclear reactor, aircraft turbines.

- The second major finding is the development of a new numerical approach based on the use of a collection of the most significant modes (space-time modes) to solve cyclic transient thermal problems involving different time scales. The basic idea comes from the context of the different responses obtained in the first finding. The significant modes (space-time modes) generated from PGD modes are collected in a dictionary instead of only spatial modes in the famous reduction method, the POD method. Once the significant modes are known (offline calculation), the solution of cyclic heat problem is computed by projection on the dictionary modes (online calculation). Different dictionaries have been evaluated:

- Dictionary 1 with a given cycle time and different physical times. The solution built using this dictionary matches the full PGD solution with a saving computational time around 50 compared to FEM and a relative error less than 2%. This dictionary is also used for problems involving different boundary conditions and variable physical times.
- Dictionary 2 with a given physical time and different cycle times. This dictionary leads to less accurate results compared to the full PGD solution for a problem with a different cycle time. This is explained by the fact the fluctuation differs for each particular cycle time. To obtain accurate results, the modes related to the tested cycle time have to be added to the dictionary.
- Another dictionary given by different cycle times and different physical times can be used to solve a problem that involves harmonic loads. Nevertheless, each particular cycle times have to be added to the dictionary. It can lead to a dictionary which a large number of modes.
- A dictionary built from thermal and diffusion problems separately can be used to solve a weak coupled thermo-diffusion problem and leads to accurate results.

This approach has considerably decreased the computation time for problems with several characteristic times like the physical time and the cycle time. Nevertheless, the main limitation of this approach is for problems which a large number of cycles times. As all the space-modes corresponding to each cycle has to be added to the dictionary, the dictionary can be very large. It can lead to large computation either to a too large memory storage.

- Finally, a mixed strategy which makes use of the PGD and a priori time basis is developed to reduce the computation time by overcoming the limitation of the previous strategy. Let us note that this strategy is an non incremental strategy like the two previous strategies. The mixed strategy is based on the knowledge of a priori time bases, where an analytical expression has been developed using the FFT method.
  This approach has been investigated in different linear transient heat cases like homogeneous, non-homogeneous, and Robin boundary conditions in the particular case of a triangular form of the load. Moreover, various types of the applied load (like the Heaviside, and sinusoidal load) have been studied and an extension of the analytical expression has been proposed. Equally important, when opposite loads are considered (leading to different gradients), the time basis can always be used. Let us note that the an ordered bases with respect to the frequency leads to a more accurate results with a smaller number of basis. Importantly, the approach has been extended to coupled problem. To sum up, the approach proved its capacity to solve 3D linear transient problem with different time scales (cycle time and physical time), boundary conditions, and load types. Furthermore, the mixed strategy has been used to solve a non-linear problem. It consists in using the time basis generated for linear cases associated with the threshold values of the temperature and by combining the PGD algorithm to a non-linear solver (Picard's method) to compute the spatial basis. This strategy leads to accurate results for small nonlinearites (leading to a same behaviors type). Less accurate results are obtained for large non-linearities. A solution consists in adding more time basis allowing to describe all the different behaviors.

As a summary, all the approaches tested in this thesis seem an appealing solution to deal with thermal transient problems under cycle loadings. The mixed strategy seems to be the more efficient as it allows to deal with a large number of cycle times without increasing the number of time basis. Finally, this strategy is based on the use of a separated space-time representation of the solution like the LATIN method (avoiding the use of an incremental scheme) but a known time basis is assumed. One of the potency of the approach is the use of an analytical expression of the time basis (the offline time is also decreased compared to the second approach).

Perspectives

In this thesis, alternative approaches have been used to solve the linear transient, non-linear transient and coupled heat problems. The results were very promising and convincing. However, the following perspectives for the developments of the approaches can be drawn:

- The model used in this thesis accounts for only a cube geometry. The model should be extended to more complex geometry. This point is not a sticking point as the PGD can be applied to non parallelepipedic domain.
- In this thesis, the two last approaches (a priori space-time modes and a priori time basis) have been used to solve a weak coupled problem (thermo-diffusion). It can be a limitation for the prediction of thermoviscoelasticity of polymers where all the phenomena (viscosity and thermal) influence each other. The approaches have to be extended to solve a strongly coupled problem.
- There is a lack of error indicator for the second approach (dictionary with the most significant modes) and the third approach (towards a priori time basis). It is recommended to develop intrinsic or extrinsic error indicators allowing quantifying the solution accuracy. For the second approach, the error indicator can be based on the use of different number of significant modes. That is to say by considering different threshold values to choose the number of significant modes. For the third approach which is iterative, an error indicator based on a stagnation criterion such as for the PGD method can be used.
- The second approach has to be extended to non-linear case. At this moment, a Picard scheme has been studied and seems a non robust scheme. Other linearization schemes have to be evaluated.
- Additional work on the third approach, the mixed strategy, needs to be carried out to establish with a general way a priori basis in the frequency domain. The generation of a priori time basis can be enriched by analyzing different problems.

Significantly, the idea is to take the advantages of each approach to solve thermoviscoelastic problems efficiently.

Résumé substantiel

***

Introduction

Dans le domaine de la mécanique des matériaux, il est important de disposer d'outils permettant de prédire correctement des durées de vie de pièces soumises à des sollicitations cycliques. Les matériaux concernés sont notamment les polymères et les métaux. Ces matériaux sont soumis lors de leur utilisation à des contraintes thermomécaniques qui peuvent être plus dommageables si le matériau est soumis à des chargements cycliques dépendant de la température. Dans le cadre de cette thèse, on se focalisera sur la mise en place de méthodes numériques destinées à long terme aux matériaux polymères. La mise en place de critères de fatigue requiert généralement la description du cycle stabilisé. Ce dernier nécessite généralement un plus grand nombre de cycles pour être atteint dans le cas des matériaux polymères en comparaison des métalliques. En conséquence, le temps de calcul des simulations est donc plus élevé pour ces matériaux.
D'un point de vue numérique, l'utilisation de la Méthode des Eléments Finis (MEF) combiné à un schéma incrémental dans le contexte de la fatigue des polymères mène aux verrous suivants : temps de calcul important, stockage de mémoire important voire non-convergence de la solution notamment dans le cas où un grand nombre d'échelles (échelles spatiales et temporelles) est présent.

Pour palier ces limitations, des approches alternatives (non incrémentales) et de type réduction de modèles telle que par exemple la décomposition propre généralisée (PGD) peuvent être utilisées.

Dans cette thèse trois approches sont proposées et discutées:

- La première approche est la méthode PGD avec une décomposition $x \times y \times z \times t$ de la solution.
- La deuxième approche est basée sur l'utilisation d'une collection de modes spatio-temporels les plus significatifs. Ces modes sont des modes PGD issus de différents problèmes représentatifs et sont regroupés dans un dictionnaire. La solution est ensuite recherchée par projection sur les modes du dictionnaire. Cette approche est similaire à la décomposition propre orthogonale (POD), à la différence que les modes connus sont ici des modes spatio-temporels et non pas uniquement des modes spatiaux.
- La troisième approche appelée stratégie mixte est basée sur la connaissance de modes temporels pour réduire le temps de calcul des simulations. Elle évite l'utilisation du schéma incrémental. L'originalité dans cette approche est la construction de la base temporelle a priori qui utilise l'analyse de Fourier et permet d'avoir une expression analytique de la base temporelle qui dépend de la forme du chargement (triangulaire, carré, sinusoidal), de son amplitude, de son ratio (max-min), des temps physiques (dépendant des paramètres matériaux) et des temps de cycle considérés. Les modes spatiaux sont ensuite calculés à travers un algorithme type PGD en supposant connus les modes temporels.

Ces trois approches permettent de réduire considérablement les temps de calculs des simulations en comparaison à des simulations EF classiques (avec schéma incrémental). Néanmoins, elles nécessitent pour les deux dernières de connaitre des bases a priori.

Dans cette thèse, pour évaluer ces différents approches numériques, un problème 3D thermique transitoire linéaire, non linéaire ainsi qu'un problème faiblement couplé (thermo-diffusion) sous chargements cycliques seront étudiés.

Le manuscript de thèse est organisé en 5 chapitres en plus de l'introduction et la conclusion:

- Le premier chapitre dresse l'état de l'art des méthodes numériques pour le traitement de problèmes transitoires sous chargements cycliques qui permettent de palier les limitations de l'approche éléments finis couplée à un schéma incrémental.
  Plus particulièrement, les méthodes de réduction de modèles sont brièvement décrites. Le focus est mis sur l'une de ces méthodes: la méthode PGD ainsi que son utilisation dans le contexte de la fatigue et les algorithmes combinés à la PGD pour résoudre les nonlinéarités.
  Enfin, l'analyse de Fourier qui sera utilisée dans la troisième approche de la thèse est succintement décrite.

- Le deuxième chapitre se focalise sur la modélisation des problèmes transitoires linéaires (conduction uniquement) et nonlinéaires. Les différents temps de ces modèles ainsi que leurs expressions en fonction des paramètres matériaux sont précisées. Leur résolution via la méthode des éléments finis est rappelée.

- Le troisième chapitre présente la première approche, la méthode PGD, pour le traitement d'un problème de conduction transitoire linéaire et non linéaire sous chargements cycliques.
  L'algorithme dans le cas linéaire est rappelé brièvement ainsi que dans le cas non linéaire où la méthode d'interplation empirique (DEIM) est couplée à la méthode PGD.
  Ces algorithmes ont largement été utilisés dans la littérature. Ils sont éprouvés ici pour des sollicitations cyclées. Les résultats obtenus sont validés et comparés à la MEF en terme de précision et de temps de calcul.

- Le quatrième chapitre présente la deuxième approche basée sur la connaissance a priori de modes spatiaux-temporels issus de la PGD les plus significatifs. Ces modes sont regroupés dans un dictionnaire. Ces modes correspondent aux modes PGD de différents problèmes linéaires transitoires relatifs à différentes échelles temporelles (temps physiques et ou temps du cycle). L'efficacité de ces modes est évaluée et le dictionnaire est ensuite testé pour résoudre différents problèmes. Cette approche est aussi évaluée pour des problèmes à plusieurs harmoniques et un problème faiblement couplé (problème de thermo-diffusion - équations de même nature). La limitation de cette méthode par rapport aux temps de cycle est discutée.

- Le cinquième chapitre présente la troisième approche basée sur la connaissance a priori de modes temporels uniquement. Ces modes sont issus de l'analyse de Fourier de différents problèmes (différents temps). Cette analyse permet de déduire une expression analytique de ces modes en fonction du temps du cycle et du temps physique. Une fois les modes temporels connus, l'algorithme PGD est ensuite utilisé pour calculer les modes spatiaux. La nouveauté de cette approche réside dans la construction de la base temporelle a priori.
  Dans un premier temps la méthode est étudiée et validée pour des problèmes présentant différents temps. Elle est ensuite étendue à un problème faiblement couplé de thermodiffusion ainsi qu'à un problème non linéaire.

La partie conclusion présente un résumé du travail ainsi que les différentes perspectives.

Chapitre 1

Ce chapitre présente l'état de l'art. Il est composé de quatre parties:

- La première partie se focalise sur l'utilisation d'un schéma incrémental comme c'est le cas avec la MEF lors du traitement de problèmes transitoires. Les difficultés rencontrées lors de l'utilisation du schéma incrémental sont illustrées comme par exemple un temps de calcul élevé et mènent à la question : existe-t'il des méthodes pour palier ces difficultés?

- La deuxième partie traite de l'utilisation des méthodes de réduction de modèles pour palier ces difficultés. Les méthodes de réduction de modèles sont exposées brièvement en distinguant les méthodes a priori et les méthodes a posteriori. Les méthodes a posteriori utilisent la simulation directe pour créer une base où la solution sera projetée, la plus connue est la décomposition propre orthogonale (POD). Les méthodes a priori ne nécessitent aucune information préalable sur le problème à traiter, la décomposition propre généralisée (PGD) est l'une de ces méthodes. La littérature a montré que la PGD est capable de résoudre un grand nombre de problèmes dans différents domaines et de générer des résultats impressionnants notamment d'un point de vue réduction du temps de calcul. Ceci est lié au fait qu'une représentation séparée de la solution est postulée. La méthode PGD a notamment été utilisée dans la résolution de problèmes de fatigue.

- La troisième partie est liée aux algorithmes utilisés pour résoudre des problèmes non linéaires. Dans le cadre de la réduction de modèles, différents schémas de linéarisation sont utilisés tels que la méthode de Newton, la méthode de Picard, menant néanmoins à des temps de calcul et de mémoire élevés (évaluation de la non linéarité dans le cadre d'une représentation séparée). Une technique alternative permet de réduire le temps de calcul : la méthode d'interpolation empirique dicrète (DEIM).

- La quatrième partie est une présentation succinte de la transformée de Fourier Rapide (TFR) qui permet de transformer une fonction du domaine temporel dans le domaine fréquentiel et qui sera utilisée dans la troisième approche étudiée dans la thèse.

Partie 1. MEF et le schéma incrémental

Dans le cas des problèmes transitoires, un schéma incrémental doit être utilisé. Dans le cadre des éléments finis classiques, à chaque pas de temps, la résolution spatiale est faite par la MEF. Ceci augmente le temps de calcul dans le cas où un grand nombre de pas de temps est nécessaire. De plus, le pas de temps est choisi afin de satisfaire des critères de stabilité ainsi que pour une bonne description des phénomènes physiques et du chargement cyclique. Pour des simulations 3D, le temps de calcul peut être très important, d'autant plus que le pas de temps est petit et la discrétisation spatiale est fine.
Pour l'intégration temporelle, plusieurs schémas existent dans la littérature comme par exemple le schéma explicite et le schéma implicite . L'analyse de stabilité des schémas implicites et explicites [Ascher *et al.*, 1997] montre qu'une stabilité inconditionnelle est obtenue avec le schéma implicite et qu'un pas de temps critique est nécessaire pour le schéma explicite [Hughes et Liu, 1978].
De nombreuses recherches consistent à trouver des approches numériques alternatives pour réduire le temps de calcul des simulations ainsi que le stockage des données (problèmes dépendant de l'histoire). Les approches les plus utilisées sont les approches de type réduction de modèles qui consistent notamment à réduire le temps de calcul en utilisant des bases de dimension réduite. Les méthodes de réduction de modèles diffèrent notamment en fonction du choix de la base.

Partie 2. Modèles d'Ordre Réduits (MOR)

Les MOR ont été développés pour résoudre des problèmes multiphysiques, complexes [Chinesta *et al.*, 2011b, Benner *et al.*, 2015, Stein *et al.*, 2004, Guérin *et al.*, 2018] et ont mené à des résultats précis

avec des temps de calculs réduits.
Les MOR sont en général classés en deux catégories:

- Les MOR a posteriori. Une méthode a posteriori utilise des simulations directes pour créer la base. La méthode a posteriori la plus connue est la décomposition propre orthogonale (POD) [Chatterjee, 2000]. La méthode POD a été utilisée dans un grand nombre d'applications telles que par exemple le traitement d'images [Benaarbia et Chrysochoos, 2017] ou encore le traitement de problème thermique transitoire linéaire [Białecki *et al.*, 2005]

- Les MOR a priori. Les méthodes de cette catégorie ne nécessitent aucune connaissance préalable de la base. Les fonctions de base ne sont pas connues a priori mais sont calculées à l'aide d'une procédure itérative. L'une de ces méthodes est la méthode PGD.

La méthode PGD est issue du travail de Pierre Ladevèze dans le cadre de la méthode à grands incréments de temps (LATIN) où une représentation séparée de la solution (séparation espace-temps) est utilisée pour réduire le temps de calcul des simulations de problèmes de mécanique [Ladeveze *et al.*, 2010]. A noter que cette limitation du temps de calcul est notamment liée à l'utilisation d'un schéma non incrémental [Ladeveze et Nouy, 2003]. Dans les travaux de 2006 de Ammar et al. [Ammar *et al.*, 2006], la représentation séparée a été généralisée aux problèmes multidimensionnels (séparation selon chaque direction de l'espace) et les auteurs l'ont appelée plus tard la méthode PGD pour Proper Generalized Decomposition. Cette méthode a été largement utilisée par de nombreux chercheurs dans de nombreux domaines [Chinesta *et al.*, 2013a, Chinesta *et al.*, 2011a] comme par exemple le multiphysique, la viscoélasticité, la dynamique, etc ...
La méthode PGD a aussi été utilisée dans le contexte de la fatigue où on peut citer les travaux de Bergheau et al. [Bergheau *et al.*, 2016] pour traiter des problèmes élastoplastiques. D'autres études dans le domaine de la viscosité ont été menées par Hammoud et al. [Hammoud *et al.*, 2014] pour du fluage et des chargements cycliques ainsi que par Ammar et al. [Ammar *et al.*, 2015]. Plus récemment, Nasri el al. [Nasri *et al.*, 2018] ont résolu un problème de polycristaux sous chargement cyclique. En 2018, Bhattacharyya et al., [Bhattacharyya, 2018] utilisent les techniques LATIN-PGD pour résoudre des problèmes d'endommagement afin de prédire la durée de vie des composants soumis à de la fatigue cyclique.

Partie 3. Problèmes numériques pour traiter les non-linéarités dans le cadre de la PGD

Dans le cadre de la méthode PGD, une méthode de linéarisation doit être combinée à la méthode PGD pour traiter les problèmes non linéaires. Ces méthodes consistent généralement à linéariser le problème continu à l'aide d'une procédure itérative. A chaque itération le problème linéaire est ensuite résolu par la méthode PGD. Les différentes méthodes de linéarisation étudiées dans le cadre de la méthode PGD sont:

1. la méthode de Newton-Raphson [Larson et Bengzon, 2013]
2. la méthode de Picard [Larson et Bengzon, 2013]
3. la méthode asymptotique numérique (MAN) [Chinesta *et al.*, 2013b]
4. la méthode d'interpolation empirique discrète (DEIM) [Aguado *et al.*, 2013]

La dernière méthode est plus efficace dans la mesure où la non linéarité est évaluée sur une base plus réduite. L'évaluation de non linéarité lorsqu'une représentation séparée est utilisée reste à ce jour un thème exploré, ce n'est néanmoins pas l'objet de cette thèse où la méthode DEIM sera utilisée.

Partie 4. Analyse de Fourier

L'analyse de Fourier sera appliquée dans la troisième approche étudiée dans cette thèse pour l'étude d'une fonction temporelle. Elle consiste à transformer la fonction en une représentation dans le

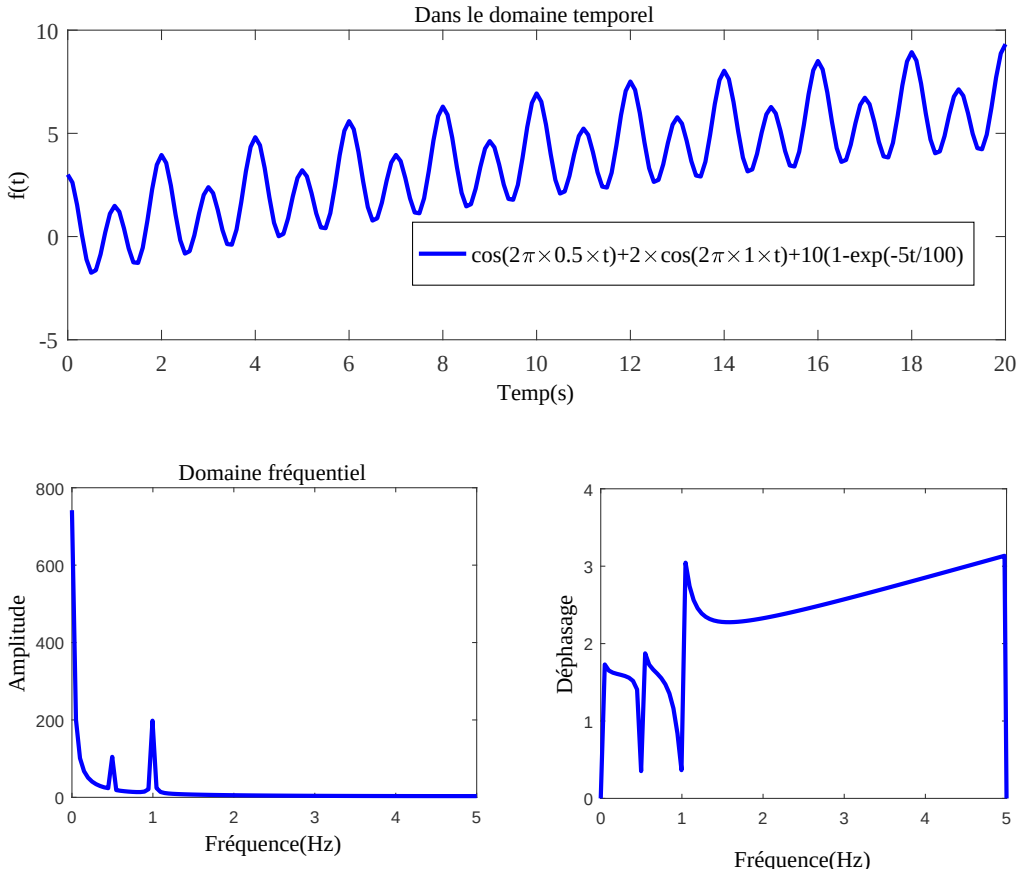


Figure 5.66: Représentation de la Transformée de Fourier Rapide (TFR) de $f(t)$

domaine fréquentiel en terme d'amplitude et de phase. Elle sera utilisée dans cette thèse comme une boite noire.
Le type de réprésentation obtenue est illustré à travers l'exemple de la fonction suivante (combinaison de fonctions périodiques et exponentielle):

$$f(t) = cos(2\ \pi\ f_1\ t) + 2cos(2\ \pi\ f_2\ t) + 10(1 - exp(\frac{5}{100}t) \tag{5.29}$$

où $f_1 = 0.5Hz$, $f_2 = 1Hz$ et t(s) est le domaine temporel. La Figure 5.66 représente l'évolution de la fonction dans le domaine temporel ainsi que sa réprésentation dans le domaine fréquentiel via la Transformée de Fourier Rapide. On peut noter que:

- Dans le domaine temporel, la fonction étudiée consiste en une combinaison d'une partie transitoire (due à la présence d'une fonction exponentielle) et d'une fluctuation (cyclique liée à la présence des fonctions périodiques en cosinus).

L'analyse de Fourier est largement utilisée dans le traitement du signal ainsi que dans l'analyse des données en mécanique comme par exemple dans les travaux de Harcarik et al. [Harčarik *et al.*, 2012] où la TFR est utilisée pour analyser les propriétés du matériau. À notre connaissance, la FFT n'a pas été utilisée comme outil direct pour établir des bases temporelles dans le cadre de la réduction de modèles comme c'est le cas dans l'approche que nous proposons.

Conlusion

En résumé, dans ce chapitre, un aperçu des différentes approches numériques pour résoudre des problèmes transitoires multitemps est présenté. Dans le cadre de la méthode des éléments finis,

un grand nombre d'articles souligne les limitations de cette approche notamment pour l'étude de la fatigue des polymères : temps de calcul important, non-convergence et besoin d'une grande capacité mémoire. Pour surmonter ces limitations, les méthodes de réduction du modèles semblent être un moyen efficace et plus particulièrement la méthode PGD.

Chapitre 2.

Introduction

Ce chapitre présente la modélisation et le traitement par la MEF d'un problème linéaire transitoire thermique et non linéaire. Il est composé de deux parties :

- La première partie présente la modélisation du problème linéaire thermique 3D ainsi que sa résolution avec la MEF.
  De plus, les temps caractéristiques associés au problème thermique sont définis : la première échelle de temps appelée le temps physique dépend des propriétés du matériau telles que la masse volumique, la chaleur spécifique et la conductivité; la deuxième échelle de temps appelée le temps de cycle est liée au temps de cycle du chargement.

- La deuxième partie présente la modélisation du problème non linéaire. Un autre temps physique peut apparaître dans ce cas comme par exemple lorsqu'une dépendance sinusoïdale de la chaleur spécifique par rapport à la température est considérée.

Dans ce chapitre, l'algorithme utilisé dans le cadre de la Méthode des Eléménts Finis (MEF) pour résoudre les problèmes linéaires et non linéaires transitoires est présenté et plus particulièrement dans le cadre du logiciel éléments finis commercial Abaqus.

Partie 1. Problème thermique linéaire 3D

A l'équilibre, la chaleur produite sur une partie du solide est égale au flux de chaleur sortant. L'équilibre thermique s'écrit comme suit:

$$\forall\ \Omega_A,\quad \int_{\Omega_A} Q dv = \int_{\partial\Omega_A} \overrightarrow{\Phi}.\overrightarrow{n} ds \tag{5.30}$$

où $\overrightarrow{\phi}$ est le vecteur associé au flux de chaleur ($W.m^{-2}$), $\overrightarrow{n}$ est la normale unitaire extérieure à la surface et Q est une source volumique interne de chaleur ($W.m^{-3}$).

La loi de Fourier stipule que la variation de température selon une direction de l'espace ($\overrightarrow{grad}(T)$) génère un flux de chaleur selon cette même direction :

$$\overrightarrow{\Phi} = -\underline{k}.\overrightarrow{grad}(T) \tag{5.31}$$

où $\underline{k}$ est un tenseur symétrique du second ordre dans lequel chaque composante donne l'influence d'un gradient thermique dans une direction donnée sur la densité du flux de chaleur dans une autre direction. En introduisant l'Eq. (5.31) dans Eq. (5.30), il vient :

$$div(\underline{k}.\overrightarrow{grad}(T)) + Q = 0 \tag{5.32}$$

En effet, selon la première loi de la thermodynamique, l'état d'équilibre produit un changement d'énergie interne qui peut s'exprimer comme $\rho\dot{H}$ où $\dot{H}$ représente la variation par rapport au temps de l'enthalpie spécifique H et ρ est la masse volumique. En cas d'état stable, $\dot{H}$ est nul.
L'équation transitoire Eq. (5.32) s'écrit :

$$div(\underline{k}.\overrightarrow{grad}(T)) + Q = \rho\dot{H} \tag{5.33}$$

Différentes conditions aux limites thermiques peuvent être appliquées au solide et en particulier :

1. une densité de flux connue q sur la frontière $\partial\Omega$ de Ω (condition de Neuman) :

$$\overrightarrow{\Phi}.\overrightarrow{n} = -q(T) \tag{5.34}$$

2. une température connue T_d sur la frontière (condition de limite de Dirichlet).

3. des échanges par convection de la forme $q = h(T - T_\infty)$, où h est un coefficient d'échange thermique local ($W.m^{-2}.K^{-1}$) et T_∞ est la température du milieu extérieur (K) (condition de Robin).

On souhaite trouver $T(x, y, z, t)$ en tous points $\mathbf{x} = (x, y, z) \in \Omega$ et à tout moment $t \ \in 0 < t < t_f$ vérifiant les conditions aux limites et initiales :

$$\begin{cases} \bullet \ \text{Condition initiale} \\ T(\overrightarrow{\mathbf{x}}, 0) = T_0(\mathbf{x}) \\ \mathbf{x} = (x, y, z) \\ \bullet \ \forall t, \ t \in \ 0 < t < t_f : \\ R(T, t) = div(\underline{k}.\overrightarrow{grad}(T)) + Q - \rho\dot{H} = 0 \\ \bullet \ \text{Conditions aux bords} \\ (\underline{k}.\overrightarrow{grad}(T)).\overrightarrow{n} = q \text{ on } \partial\Omega_q \\ T = T_d \text{ on } \partial\Omega_T \end{cases} \tag{5.35}$$

où $\partial\Omega_T \cup \partial\Omega_q = \partial\Omega$ et $R(T, t)$ représente le résidu du problème.

Les différentes échelles de temps impliquées dans un phénomène de transfert de chaleur transitoire [Marin, 2010] sont abordées ici. Il est bien connu que la chaleur se propage de la région où la température est la plus élevée vers la température où la température est la plus basse. Ce transfert dépend des éléments suivants:

1. L'échelle de temps physique qui est principalement liée aux propriétés du matériau (conductivité, masse volumique et chaleur spécifique) et à la taille de l'échantillon. Le temps physique τ_ϕ (s) est donnée par la relation :

$$\tau_\phi = \frac{\rho C_p L_c^2}{k} \tag{5.36}$$

2. L'échelle de temps liée à la charge appliquée (temps de cycle (τ_c) si le chargement imposé est cyclique).

En utilisant l'approximation par éléments finis, après assemblage, le vecteur résidu du problème thermique linéaire se réduit à :

$$\{R(T)\} = \{F\} - [M] \cdot \left\{\dot{T}\right\} - [K] \cdot \{T\} \tag{5.37}$$

où $\{F\}$ représente le vecteur de chargement, $[M]$ fait référence à la matrice de capacité thermique et $[K]$ est la matrice de conductivité thermique.

Partie 2. Problème thermique 3D non linéaire

La non-linéarité dans un problème de conduction thermique peut apparaître sous différentes formes :

- La dépendance des propriétés physiques à la température telle que par exemple la chaleur spécifique ($C_p(T)$).

- La dépendance de la source volumique de chaleur à la température ($Q(T)$).
- La dépendance du flux thermique à la température ($q(T)$).

Lorsque les propriétés du matériau telles que la conductivité k, la chaleur spécifique C_p et la masse volumique ρ dépendent de la température, les matrices $[K]$ et $[M]$ dépendent elles aussi de la température. Ainsi, le vecteur résidu est une fonction non linéaire de la température :

$$\{R(T)\} = \{F\} - [M(T)] \,.\, \left\{\dot{T}\right\} - [K(T)] \,.\, \{T\} \tag{5.38}$$

Pour résoudre la non-linéarité, une méthode de linéarisation est utilisée. La plus utilisée dans les codes de calcul éléments finis est la méthode de Newton-Raphson.

Conlusion

En résumé, ce chapitre présente la modélisation et la résolution d'un problème thermique 3D linéaire et non linéaire transitoire. Les expressions des temps caractéristiques du problème thermique sont données. Il s'agit du temps physique τ_ϕ lié aux propriétés du matériau et du temps de cycle τ_c associé au chargement.

Chapitre 3.

Introduction

Ce chapitre concerne l'utilisation de la méthode PGD pour résoudre un problème thermique transitoire et est divisé en deux parties :

- Une fois l'algorithme de la PGD présenté, la première partie illustre l'efficacité de la PGD par rapport à la MEF en terme de temps de calcul pour la résolution de problèmes thermiques transitoires linéaires. La solution PGD est précise et une erreur inférieure à 1% par rapport à la MEF avec un gain de temps de l'ordre de 50 pour différentes échelles de temps est obtenu. Dans le cas de chargements cycliques, l'influence du pas de temps en fonction des temps physiques est étudiée : pour un temps physique élevé, un pas de temps grossier est suffisant ; une discrétisation fine est nécessaire pour un temps physique réduit. L'influence de la position spatiale sur l'évolution temporelle de la température est ensuite étudiée : pour un temps physique élevé, l'effet cyclique disparaît plus le point spatial est loin des bords où la charge est appliquée. On notera que ce même type de réponse a déjà été obtenue pour un problème viscoélastique 1D sous chargement cyclique par Hammoud et al [Hammoud *et al.*, 2014].

- Dans la deuxième partie, la méthode PGD est combinée à la méthode d'interpolation empirique discrète (DEIM) [Aguado *et al.*, 2013] pour résoudre un problème transitoire non linéaire 3D. Le terme non linéaire est interpolé en utilisant la base réduite. Notons que la non-linéarité étudiée consiste en une dépendance linéaire de la chaleur spécifique par rapport à la température. Les résultats obtenus grâce à la combinaison de PGD-DEIM permettent d'obtenir des résultats précis avec des temps de calcul réduits de l'ordre de 30.

La question posée maintenant est : est-il possible de réduire encore plus le temps de calcul ? Deux autres approches sont étudiées dans les autres chapitres de la thèse pour répondre à cette question.

Partie 1. PGD pour un problème 3D transitoire linéaire

La simulation étudiée est un cube de côté L soumis à une condition aux limites de type Robin $\phi = h(T - T_\infty)$ où ϕ est le flux de chaleur, h est le coefficient de convection, T_∞ est la température extérieure. La température extérieure est considérée cyclique avec une forme triangulaire, un rapport $\boldsymbol{R} = \frac{T_{min}}{T_{max}} = 0$ et un temps de cycle fixé noté τ_c et égal à $20s$.
Pour prédire le champ de température $T(x, y, z, t)$ sur le domaine $\Omega = \Omega_x \times \Omega_y \times \Omega_z \times \Omega_t$, le problème thermique s'écrit :

$$\rho C_p \frac{\partial T}{\partial t} - k\Delta T - Q = 0 \tag{5.39}$$

où k est la conductivité thermique du matériau, ρ sa masse volumique et C_p sa chaleur spécifique.
Remarque. La source volumique de chaleur Q est supposée nulle pour toutes les simulations étudiées dans ce chapitre.
Deux valeurs différentes de coefficient de convection sont considérées : un coefficient de convection $h_{vertical}$ dans la direction de x et y, et un coefficient de convection $h_{horizontal}$ dans la direction z. La symétrie du problème est considérée ce qui permet de simuler uniquement un huitième du cube.

Le problème linéaire transitoire 3D s'écrit :

$$\rho C_p \frac{dT}{dt} - k(\frac{\partial^2 T}{\partial^2 x} + \frac{\partial^2 T}{\partial^2 y} + \frac{\partial^2 T}{\partial^2 z}) - Q = 0 \tag{5.40}$$

avec une condition initiale nulle et des conditions aux bords de type Robin. En prenant en compte

les conditions aux limites, la formulation variationnelle de Galerkin s'écrit :

$$\begin{aligned}\int_\Omega T^*\rho C_p\frac{\partial T}{\partial t}\mathrm{d}\Omega + k\int_\Omega[(\frac{\partial T^*}{\partial x}\frac{\partial T}{\partial x}+\frac{\partial T^*}{\partial y}\frac{\partial T}{\partial y}+\frac{\partial T^*}{\partial z}\frac{\partial T}{\partial z})]\mathrm{d}\Omega\\ +\int_{S_{yz}\times\Omega_t} T^*(\frac{L}{2},y,z,t)\ h_{vertical}(T(\frac{L}{2},y,z,t)-T_\infty)\mathrm{d}y\mathrm{d}z\mathrm{d}t\\ +\int_{S_{xz}\times\Omega_t} T^*(x,\frac{L}{2},z,t)\ h_{vertical}(T(x,\frac{L}{2},z,t)-T_\infty)\mathrm{d}x\mathrm{d}z\mathrm{d}t\\ +\int_{S_{xy}\times\Omega_t} T^*(x,y,\frac{L}{2},t)\ h_{horizontal}(T(x,y,\frac{L}{2},t)-T_\infty)\mathrm{d}x\mathrm{d}y\mathrm{d}t=0\end{aligned} \tag{5.41}$$

Le problème est résolu avec la PGD en supposant une représentation séparée de la solution sous la forme :

$$T(x,y,z,t)=\sum_{i=1}^{N}F_i(x)G_i(y)H_i(z)U_i(t) \tag{5.42}$$

Dans la PGD, nous choisissons de séparer par rapport à chaque coordonnée x, y, z et t.
En supposant connue la solution à l'enrichissement $n-1$ soit

$$T(x,y,z,t)=\sum_{i=1}^{n-1}F_i(x)G_i(y)H_i(z)U_i(t) \tag{5.43}$$

on cherche la solution à l'enrichissement n telle que :

$$T(x,y,z,t)=\sum_{i=1}^{n-1}F_i(x)G_i(y)H_i(z)U_i(t)+F_n(x)G_n(y)H_n(z)U_n(t). \tag{5.44}$$

Pour cela, on suppose que le champ virtuel s'écrit sous la forme :

$$\begin{aligned}T^*(x,y,z,t)=F_n^*(x)G_n(y)H_n(z)U_n(t)+F_n(x)G_n^*(y)H_n(z)U_n(t)\\ +F_n(x)G_n(y)H_n^*(z)U_n(t)+F_n^*(x)G_n(y)H_n(z)U_n^*(t).\end{aligned} \tag{5.45}$$

En remplaçant dans la formulation variationnelle les expressions des champs réels et virtuels, cela mène à la résolution d'un système non linéaire pour déterminer le n ième mode $F_n(x)G_n(y)H_n(z)U_n(t)$.
Ce système non linéaire est classiquement résolu par une méthode de point fixe à directions alternées. Elle consiste à résoudre à chaque itération de point fixe alternativement 4 systèmes linéaires :

1. Le premier système linéaire permet de déterminer $F_n(x)$ en supposant $G_n(y)$, $H_n(z)$ et $U_n(t)$ connus.
2. Le deuxième système linéaire permet de déterminer $G_n(x)$ en supposant $F_n(x)$, $H_n(z)$ et $U_n(t)$ connus.
3. Le troisième système linéaire permet de déterminer $H_n(z)$ en supposant $F_n(x)$, $G_n(y)$, $U_n(t)$ connus.
4. Le quatrième système linéaire permet de déterminer $U_n(t)$ en supposant $F_n(x)$, $G_n(y)$, $H_n(z)$ connus.

La taille de chaque système linéaire est égale au produit de la taille de chaque dimension séparément ce qui permet de réduire considérablement le temps de calcul des simulations (produit de chaque dimension pour la méthode des éléments finis).
Cette procédure itérative est arrêtée lorsque une valeur seuil du résidu est atteint. Il en est de même pour les étapes d'enrichissement.

Dans cette partie, une simulation EF avec un chargement cyclique est considérée et comparée à un chargement constant. Deux cas sont étudiés :

τ_ϕ	CPU(MEF)	CPU(PGD)	Rapport gain en temps
0.1	1342.2	8.48	158.51
10	780	9.89	78.86
1000	373.31	16.75	22.28

Table 5.18: Gain en temps PGD VS FEM en fonction des différents temps physiques

1. Cas 1 : conditions aux limites de type Robin avec $T_\infty = 25°C$ (charge constante par rapport au temps).
2. Cas 2 : conditions aux limites de type Robin avec T_∞ triangulaire cyclique avec $T_{max} = 50°C$, $R = 0$, $\tau_c = 20s$.

Le temps de calcul pour le chargement cyclique (cas 2) est beaucoup plus important que dans le cas avec une charge constante (cas 1) pour un maillage spatial identique. Un rapport de l'ordre de 27 est obtenu. En fait, cela s'explique par la présence des différentes échelles de temps - liées au temps caractéristique thermique et au temps de cycle, le pas de temps devant être adapté à ces phénomènes.
Le même problème est maintenant résolu avec la PGD pour trois temps physiques différents : $\tau_\phi = 0.1s$ inférieur au temps de cycle $\tau_c = 20s$; $\tau_\phi = 10s$ du même ordre de grandeur que le temps de cycle; $\tau_\phi = 1000s$ supérieur au temps de cycle. Trois comportements différents sont observés :

1. Cas 1: Le cycle stabilisé est rapidement atteint.
2. Cas 2: Le cycle stabilisé est atteint après 4 cycles.
3. Cas 3: Le cycle stabilisé n'est pas atteint à la fin de la simulation (1000 cycles sont nécessaires pour l'atteindre).

Pour les trois cas, la PGD mène à une solution précise en comparaison de la MEF. Le gain de temps obtenu avec la PGD par rapport à la MEF est résumé dans le Tableau 5.18. On remarque que la méthode PGD réduit le temps de calcul d'un facteur au moins égal à 22 pour les différents cas, ce facteur diminuant lorsque le temps physique augmente. En effet, pour τ_ϕ supérieur au temps du cycle, plus de modes PGD sont nécessaires pour prédire la solution pour une précision donnée (la solution restant transitoire dans ce cas) ce qui limite le gain en temps.

Partie 2. PGD pour un problème thermique 3D non-linéaire sous chargement cyclique

On considère maintenant un problème non linéaire. Pour cela, une non linéarité due aux propriétés du matériau est considérée. Une technique de linéarisation est combinée à la PGD pour résoudre ce problème. La méthode d'interpolation empirique discrète est considérée dans ce travail (DEIM) [Aguado *et al.*, 2013]. Pour cela la chaleur spécifique est considérée comme variant linéairement en fonction de la température :

$$Cp = a \times T + b \tag{5.46}$$

Différentes valeurs de a et b sont testées permettant de décrire les 3 différents comportements. Pour tous les cas, la solution PGD est précise (erreur inférieure à 0.6% par rapport à la MEF). Le nombre d'itérations du procédé de linéarisation varie entre 2 et 6 selon les cas menant à un facteur de réduction du temps de calcul par rapport à la MEF entre 12.55 et 50.94. La Figure 5.67 illustre l'évolution de la température obtenue pour $a = 27$ et $b = 25$.

Conlusion

Dans ce chapitre, la méthode PGD est utilisée pour résoudre un problème 3D thermique transitoire linéaire avec un chargement cyclique. Elle permet de réduire d'un facteur 30 le temps de calcul par

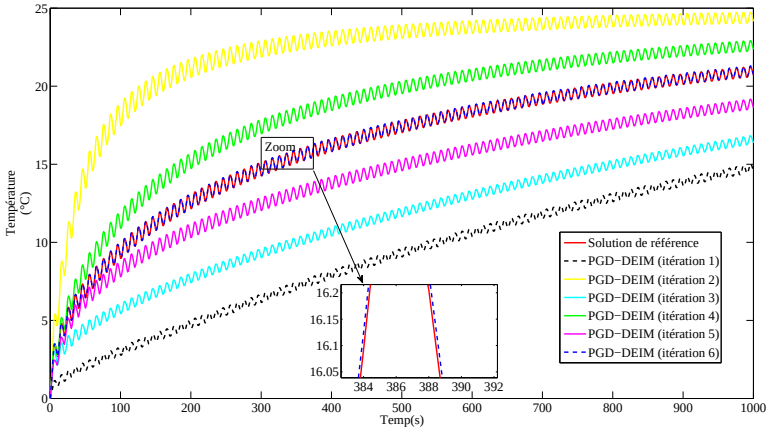


Figure 5.67: Evolution de la température pour le cas 3 $Cp = 27 \times T + 25$

rapport à la MEF. La PGD est ensuite combinée à la DEIM [Aguado *et al.*, 2013] pour résoudre un problème thermique non linéaire, la non linéarité étant due à la dépendance de la chaleur spécifique par rapport à la température. Même dans ce cas, la méthode PGD permet une réduction du temps de calcul d'un facteur d'au moins 12.55 pour une très bonne précision (inférieure à 0.6%) pour différentes valeurs du temps physique. La question qui se pose maintenant est : existe-t'il des méthodes plus performantes en terme de réduction du temps de calcul ?

Chapitre 4.

Introduction

Dans ce chapitre, une nouvelle approche est développée afin de réduire encore plus le temps de calcul des simulations. Cette approche consiste à collectionner les modes les plus significatifs issus de la résolution de différents problèmes thermiques transitoires cycliques pour résoudre d'autres problèmes thermiques transitoires cycliques (différentes conditions aux limites et temps physiques). Le chapitre est divisé en 4 parties :

- Dans la première partie, la méthode ainsi que l'algorithme sont présentés. Rappelons que pour les problèmes transitoires thermiques cycliques, les réponses diffèrent selon les différents temps caractéristiques: le temps physique et le temps de cycle. L'idée de cette approche est de construire un dictionnaire de modes significatifs générés à partir des modes PGD de problèmes représentatifs. Le dictionnaire est ensuite utilisé pour calculer la solution d'autres problèmes par projection. L'originalité réside dans le fait que des modes spatio-temporels sont considérés comme connus alors que dans la POD seuls les modes spatiaux sont considérés connus.

- Dans la deuxième partie, différents dictionnaires sont créés et évalués afin de discuter l'efficacité du dictionnaire et la convergence de l'algorithme.

- Dans la troisième partie, un dictionnaire pour traiter différentes harmoniques est proposé et discuté.

- La quatrième partie traite d'un problème faiblement couplé de thermo-diffusion (équations de même nature).

Partie 1. Présentation de la méthode

L'approche proposée consiste à construire un dictionnaire de modes significatifs générés à partir des modes PGD de problèmes particuliers. Les modes sont ensuite regroupés dans un dictionnaire. Le dictionnaire est ensuite utilisé pour calculer la solution d'autres problèmes par projection sur les modes spatio-temporels du dictionnaire. Détaillons la procédure pour créer le dictionnaire contenant les modes les plus significatifs ainsi que leur utilisation.

- Comme étape préliminaire, des solutions pour différentes échelles de temps données (temps physique et temps de cycle) sont recherchées. Le temps physique est défini comme $\tau_\phi = \frac{\rho C_p}{k} L^2$ où ρ est la masse volumique, k est la conductivité et C_p est la chaleur spécifique, et L est une longueur caractéristique de la géométrie de l'échantillon. Chaque temps physique (ou temps de cycle) conduit à une réponse différente. Dans cet esprit, l'idée est de trouver la solution pour un intervalle de temps physiques (ou plage de temps de cycle) avec des modes significatifs définis.

- Les modes significatifs sont alors regroupés dans un dictionnaire. Tout d'abord, ces modes significatifs sont testés en construisant la solution directe (modes spatio-temporels), les modes significatifs consistent à prendre les modes PGD les plus prépondérants pour chaque cas d'étude.

- Ensuite, une solution dans la même famille (nouvelle échelle de temps ou autre condition aux limites) est recherchée. Dans cette étape, les modes sont connus a priori (ceux sont les modes du dictionnaire) et une projection de la solution sur la base du dictionnaire est effectuée pour calculer les coefficients de projection notés $(\alpha) = (\alpha_i)$ dans cette thèse pour chaque mode i.

- Enfin, la solution est reconstruite en utilisant les coefficients calculés (α_i) et les modes a priori.

$\tau_\phi(s)$	0.1	10	1000
Nombre de modes PGD	10	40	50
Nombre de modes les plus significatifs	3	6	13

Table 5.19: Nombre de modes PGD et nombre de modes les plus significatifs pour différents temps physiques (dictionnaire 1 - $\tau_c = 20s$)

Partie 2. Création et évaluation du dictionnaire

Dans cette partie, deux dictionnaires sont évalués :

- Dictionnaire 1 : un temps de cycle fixé et différents temps physiques - $\tau_c = 20s$ et $\tau_\phi = 0.1, 10, 1000s$.
- Dictionnaire 2 : un temps physique fixé et différents temps de cycle - $\tau_\phi = 10s$ et $\tau_c = 10, 50, 100s$.

Dans le cas du dictionnaire 1, les modes les plus significatifs sont sélectionnés pour chaque valeur de τ_ϕ et sont résumés dans le Tableau. 5.19. Ils consistent à tronquer les modes PGD pour une certaine précision de la solution. Ce dictionnaire est ensuite évalué en modifiant d'abord le temps physique et ensuite les conditions aux limites. Les résultats montrent que les modes du dictionnaire 1 mènent à des résultats précis avec une erreur relative inférieure à 3% pour des temps physiques différents et des conditions aux limites différentes.

Le dictionnaire 2 est ensuite évalué pour différents temps de cycle. La solution obtenue n'est pas bonne car le temps de cycle choisi n'est pas présent dans le dictionnaire. Néanmoins, le comportement moyen (la déviation) est prédit correctement mais pas le cycle stabilisé. En ajoutant dans le dictionnaire 2, les modes liés au temps de cycle considéré, les résultats obtenus sont précis. Néanmoins, ceci constitue une limitation de l'approche dans la mesure où cela augmente le nombre de modes dans le dictionnaire.

Partie 3. Extension à plusieurs harmoniques

L'approche proposée est maintenant testée pour un cas de chargement constitué de plusieurs harmoniques (plus précisement trois harmoniques liés à 3 temps de cycle donnés) :

$$T_\infty = T_\infty(\tau_c = 10) + T_\infty(\tau_c = 50) + T_\infty(\tau_c = 100).$$

Le dictionnaire utilisé noté dictionnaire 4 est composé des modes associés à toutes les harmoniques

$$D4 = D4_{(\tau_c=10)} \sqcup D4_{(\tau_c=50)} \sqcup D4_{(\tau_c=100)} \tag{5.47}$$

Considérons le problème où le temps physique est $\tau_\phi = 3s$. Les modes a priori du dictionnaire $D4$ sont utilisés pour calculer la solution. Des résultats précis sont obtenus, plus précis que ceux obtenus par la solution du problème associé à chaque harmonique. La Figure 5.68 illustre la solution pour la température en un point de l'espace obtenue avec notre approche et avec la PGD. Une erreur relative inférieure à 2% est obtenue.

Partie 4. Extension aux problèmes couplés

L'approche est maintenant appliquée à un problème faiblement couplé thermo-diffusion écrit comme suit :

$$\frac{\partial c}{\partial t} - D\Delta c = F_D(t) \tag{5.48}$$

$$\rho C_p \frac{\partial T}{\partial t} - K\Delta T = F_T(t) - \beta c \tag{5.49}$$

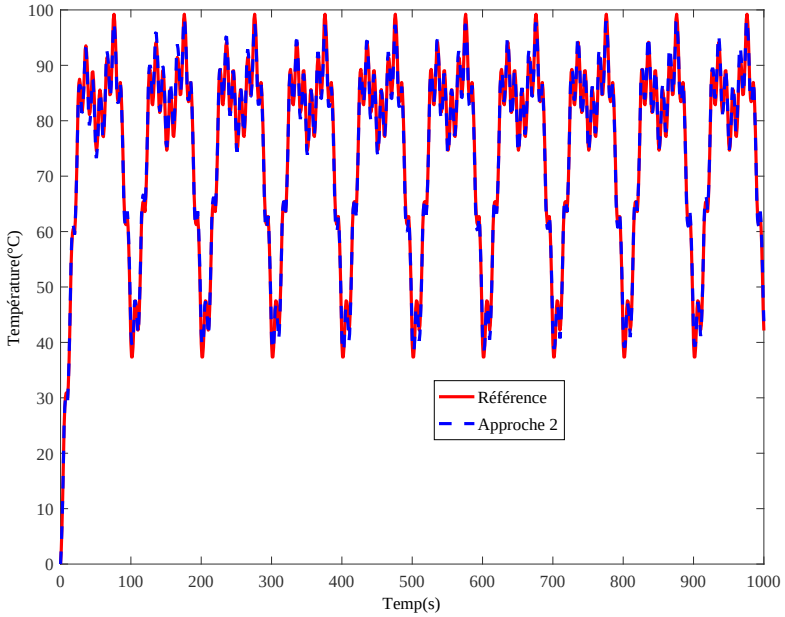


Figure 5.68: Evolution de la température pour $(\tau_\phi = 3s)$ et le dictionnaire 4 ($\tau_c = 10$,$\tau_c = 50$,$\tau_c = 100$) en (x, y, z) = (25, 25, 50)

L' équation (5.48) représente le problème de diffusion où une source massique est considérée et l'équation (5.49) représente l'équation de thermique couplée où une source volumique de chaleur est considérée. Des conditions initiales et aux bords nulles sont imposées.
Le phénomène de diffusion présente deux temps caractéristiques: le temps de cycle lié à la charge appliquée et le temps physique associé aux propriétés matériau. Le problème de la thermo-diffusion présente deux temps caractéristiques - le temps de cycle lié à la charge appliquée via la source volumique de chaleur et le temps physique associé aux propriétés matériau et en plus les temps caractéristiques associés au phénomène de diffusion transférés via le terme de couplage.
Le dictionnaire utilisé noté dictionnaire 5 contient les modes significatifs des deux problèmes découplés (thermique uniquement et diffusion uniquement). Pour illustrer, le dictionnaire considéré désigné par dictionnaire 5 est une combinaison de $D5^T_{\tau_c=100}$ (thermique sans le terme de couplage) et $D5^D_{\tau_c=10}$ (diffusion seulement). Une fois la solution du problème découplé de diffusion calculée, ce dictionnaire est ensuite utilisé pour prédire la solution du problème couplé par projection sur les modes du dictionnaire. Cette méthode mène à un résultat précis. Plus précisément, le dictionnaire 5 est évalué dans le cas suivant :

- Problème de diffusion: le temps physique est $\tau^D_\phi = 20s$ et le temps de cycle de la source de masse est $\tau^D_c = 10s$
- Problème thermique: le temps physique est $\tau_\phi = 3s$ et le temps de cycle de la source de chaleur est $\tau^T_c = 100s$.

Les coefficients de pondération devant les modes sont calculés via une projection sur les modes du dictionnaire 5. La solution obtenue est illustrée Figure 5.69. Elle est composée d'une fonction périodique d'une période de $100s$ (correspondant au temps du cycle le plus grand) où une fluctuation cyclique de $10s$ est ajoutée.

Conlusion

L'approche proposée dans ce chapitre qui consiste à regrouper les modes PGD les plus significatifs (associés à différents problèmes avec des temps particuliers) dans un dictionnaire et à déterminer

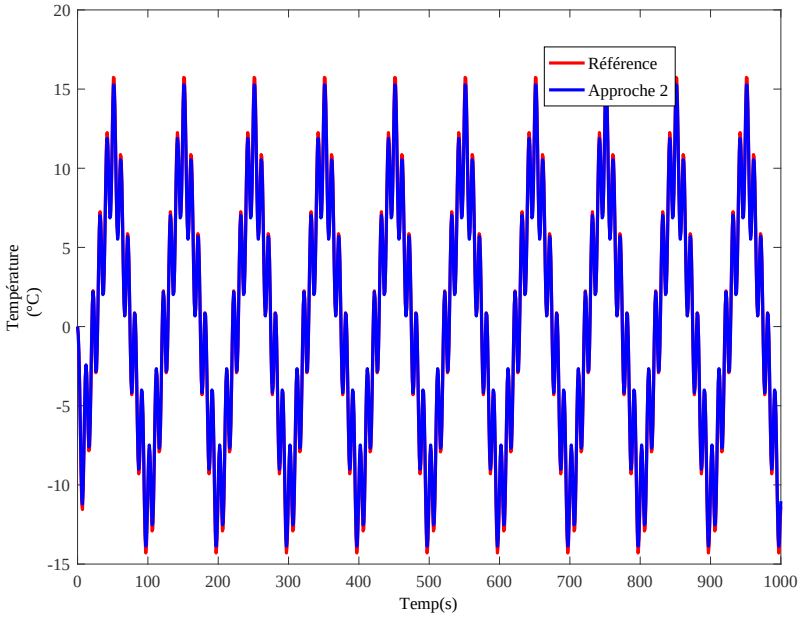


Figure 5.69: Evolution de la température pour $\tau_\phi^T = 3s$ et $\tau_c^T = 100s$ avec $\tau_\phi^D = 20s$ et $\tau_c^D = 10s$ à (x, y, z) = (25, 25, 25)

la solution d'un autre problème par projection sur les modes du dictionnaire est particulièrement efficace lorsque la solution recherchée diffère seulement par le temps physique. Si le temps de cycle est différent, les modes associés à ce temps de cycle doivent être contenus dans le dictionnaire ce qui risque de limiter l'utilisation de cette approche notamment lorsqu'un grand nombre de cycles est considéré. En effet, un grand nombre de modes doit être contenu dans le dictionnaire, ceci pouvant limiter la réduction en terme de temps de calcul de cette approche. Pour palier cette limitation, une nouvelle proposition est étudiée dans le chapitre 5.

Chapitre 5.

Introduction

Dans ce chapitre, une stratégie numérique alternative est proposée. Ce chapitre se compose de 4 parties :

- Dans la première partie, l'idée de base de la méthode est présentée.
- Dans la deuxième partie, la stratégie de génération des bases temporelles est présentée.
- Dans la troisième partie, l'extension de la méthode à un problème faiblement couplé est investiguée et mène à des résultats satisfaisants.
- Dans la quatrième partie, l'algorithme de la méthode est étendu pour la prise en compte des non linéarités. Des premiers résultats encourageants ont été obtenus même si plus de bases temporelles doivent être considérées lorsque la nonlinéarité est plus marquée.

Partie 1. Idée de base de la méthode

L'idée de base de l'approche proposée découle de l'observation que, pour les problèmes transitoires cycliques, la réponse consiste en la combinaison d'une partie transitoire (déviation) et d'une fluctuation (cyclique), mettant en évidence le lien de la réponse avec le temps physique et le temps du cycle. L'approche proposée est constituée de deux ingrédients principaux : la Transformée de Fourier Rapide (TFR) et la décomposition propre généralisée (PGD). La TFR est utilisée pour analyser les différentes réponses transitoires et comme outil pour construire les bases temporelles qui seront considérées comme a priori dans l'approche proposée. L'algorithme pour déterminer les bases spatiales est l'algorithme PGD classique, si ce n'est que les bases temporelles sont connues a priori. Cette nouvelle stratégie est appelée stratégie mixte.

Partie 2. Stratégie mixte pour un problème linéaire 3D

Le problème thermique étudié est le même que celui du chapitre précédent si ce n'est qu'une source volumique de chaleur est considérée, les conditions initiales et aux bords sont considérées comme nulles :

$$\begin{aligned} \rho C_p \frac{\partial T}{\partial t} &= k\Delta T + Q \\ T(x,y,z,t=0) &= 0 \end{aligned} \tag{5.50}$$

Stratégie pour générer les bases temporelles Une expression analytique des bases temporelles a priori est créée à partir d'une étude paramétrique de différentes réponses dans le domaine fréquentiel (ingrédient TFR). Par exemple, pour générer les bases temporelles, nous supposons d'abord que le modèle est soumis à une source de chaleur cyclique de forme triangulaire avec un rapport $R = 0$ et un temps de cycle $\tau_c = 10s$ et nous considérons des problèmes pour différents paramètres matériau soit différents temps physiques. Les TFR des solutions montrent la présence de différents pics. Notons que le premier pic est associé à l'effet du temps physique alors que les autres pics sont liés à l'effet du temps de cycle combiné à l'effet du temps physique. La réponse dans le domaine fréquentiel est analysée pic par pic. La Transformée de Fourier Inverse de chaque pic est ensuite considérée. Dans le domaine temporel, chaque évolution temporelle est fittée afin que l'expression analytique obtenue soit valable quelque soit le temps physique et le temps du cycle.
Pour le premier pic, soit la première fonction temporelle $S_1^{\phi}(t)$, l'expression suivante est obtenue :

$$\begin{aligned} S_1^{\phi}(t) &= a(1 - A \times \exp(-\frac{5}{\tau_{\phi}}t)) \\ A &= 1 - \exp(-0.7R_{\tau}) \end{aligned} \tag{5.51}$$

où le coefficient *a* fait référence à l'amplitude de la base temporelle qui peut être prise en compte par les modes spatiaux (elle est donc prise à 1). Comme $S_1^{\phi}(t)$ correspond à la première base temporelle, elle dépend principalement du temps physique τ_ϕ et du temps de cycle τ_c via le rapport $R_\tau = \frac{\tau_\phi}{\tau_c}$.
Pour les autres pics soient les autres fonctions temporelles, l'expression suivante est obtenue :

$$S_{i+2}(t) = \sum_{i}^{n} A \times cos((2i+1)w \times t + \theta(R_\tau)) \tag{5.52}$$

où $i = 0...n$, n est le nombre de modes, $w = 2 \times \pi \times f$ où $f = \frac{1}{\tau_c}$ et la fonction de déphasage $\theta(R_\tau)$ est donnée par l'expression :

$$\theta(R_\tau) = \begin{cases} \pi - tan^{-1}(1.04 \times R_\tau), & 0 \leq R_\tau \leq 10 \\ 1.007\pi - tan^{-1}(1.329 \times R_\tau), & 10 \leq R_\tau \leq 100 \end{cases}$$

Une fois, les bases temporelles connues, l'algorithme pour calculer les bases spatiales est un algorithme type PGD.

Résultats numériques Différents tests numériques ont été envisagés. Ils considèrent l'expression analytique des bases temporelles obtenue précédemment et consistent à tester la robustesse de ces bases dans différentes configurations : conditions aux limites de Dirichlet homogènes ; conditions aux limites de Dirichlet non homogènes ; conditions aux limites de Dirichlet non homogènes opposées ; conditions aux limites de Robin ; source non constante et Dirichlet non homogène avec différents temps de cycle. Pour ce dernier cas, il a été montré que les bases temporelles doivent être ordonnées en fonction de la fréquence pour une meilleure convergence de la méthode. Des résultats précis ont été obtenus avec la stratégie mixte pour tous ces cas avec une erreur relative inférieure à 3% et un gain en temps de l'ordre de 50.
L'influence de différents paramètres tels que la forme de la charge appliquée (Heaviside et sinusoïdale), le rapport entre la température maximale et la température minimale, l'amplitude de la charge a ensuite été étudiée afin de mieux cerner le domaine d'application de la méthode. Dans certains de ces cas, l'expression analytique des bases temporelles peut encore être déduite de l'expression donnée précédemment (et mise en place pour un signal triangulaire).

Partie 3. Extension au problème couplé La stratégie mixte est maintenant étendue à un problème de thermo-diffusion couplé avec un couplage faible comme discuté dans le chapitre précédent. Pour résoudre le problème de thermo-diffusion couplé avec la stratégie mixte, le champ de concentration de l'équation de diffusion s'écrit :

$$c(\underline{x}, t) = \sum_{i=1}^{n} R_i^D(\underline{x}) S_i^D(t) \tag{5.53}$$

où S_i^D sont des bases temporelles a priori calculées à l'aide de l'expression analytique (voir Eqs. (5.51) et (5.52)) et R_i^D représente le i ème mode spatial calculé à partir de l'équation de diffusion avec la strategie mixte.
Pour le problème de diffusion considéré $\tau_c = 2.5s$, $\tau_\phi = 3s$ ce qui mène à $R_\tau = \frac{3}{2.5} = 1.2$, $\theta(R_\tau = 1.2) = 2.2606$ selon Eq. (5.52). Les deux premières bases temporelles pour l'équation de diffusion sont : $S_1^D = 1 - 0.5683 \times exp(-\frac{5}{3}t)$ et $S_2^D = 1 \times cos(\frac{2\pi}{2.5}t + 2.2606)$. 7 bases temporelles sont nécessaires pour déterminer précisément la solution.
Pour le problème thermique considéré $\tau_\phi^T = 3s$ et $\tau_c^T = 50s$, 10 bases temporelles sont nécessaires. Les 2 premières bases temporelles pour le problème thermique ($R_\tau = \frac{3}{50} = 0.06$, $\theta(R_\tau = 0.06) = 3.0811$) sont : $S_1^T = 1 - 0.0411 \times exp(-\frac{5}{3}t)$ et $S_2^T = 1 \times cos(\frac{2\pi}{50}t + 3.0811)$.
Pour résoudre l'équation de thermo-diffusion couplé avec $\tau_\phi = 3s$, les bases temporelles sont d'abord ordonnées en fréquence croissante. 17 bases temporelles sont utilisées pour prédire la solution du problème (concaténation des bases temporelles associées à chaque problème découplé). L'évolution de la température est représentée sur la Figure 5.70 pour un point spatial donné, la solution est composée d'une fonction périodique de période $50s$ où un temps de cycle de $2.5s$ est ajouté.

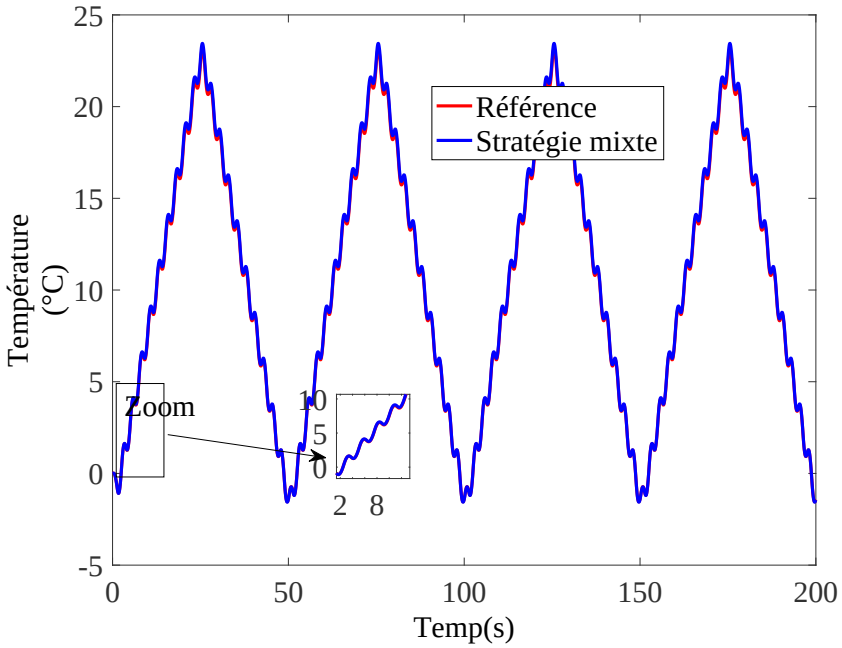


Figure 5.70: Evolution de la température pour un même temps physique ($\tau_\phi = 3s$) pour les deux phénomènes et deux temps de cycle différents $\tau_c^T = 50s$ et $\tau_c^D = 2.5s$ à $(x, y, z) = (25, 25, 25)$

Partie 4. Stratégie mixte pour un problème 3D non linéaire

Pour résoudre le problème non linéaire obtenue à travers une dépendence de la chaleur spécifique à la température, l'algorithme de Picard est combiné à la stratégie mixte. La procédure consiste en trois étapes : l'étape 1 et l'étape 2 consistent à déterminer les bases temporelles a priori ; l'étape 3 consiste à calculer les bases spatiales dans la procédure itérative de Picard. La procédure peut être résumée comme suit :

1. Trouver la plage de chaleur spécifique du problème considéré.
   Cette plage est liée à la plage de variation de température du problème (facile à déterminer dans le cas où une température cyclique est imposée).

   - La température minimale notée T_{min} mène à une valeur particulière de C_p et donc du temps physique $\tau_\phi = \frac{\rho C(T_{min})}{K} L^2$.
   - La température maximale notée T_{max} mène à une valeur particulière de Cp et donc du temps physique $\tau_\phi = \frac{\rho C(T_{max})}{K} L^2$.

2. Choisir les bases temporelles associées aux deux temps physiques et au temps de cycle de la charge appliquée. Les bases temporelles associées aux deux valeurs différentes de R_τ sont définies par les expressions analytiques données précédemment (c'est-à-dire via des expressions analytiques associées au cas linéaire).

3. Considérer les bases temporelles a priori définies aux étapes 1 et 2 et les utiliser pour déterminer les bases spatiales à chaque itération de Picard. L'initialisation de la procédure itérative peut être faite en considérant $T = 0$, ce qui mène à la résolution d'un système linéaire.

Différents cas non linéaires ont été résolus. Les résultats sont encourageants en ce qui concerne la précision de la solution et le gain en temps dans le cas où la non linéarité ne modifie pas trop la réponse du matériau (la réponse doit être du même type). Sinon, la base temporelle doit être enrichie en considérant des valeurs intermédiaires de la température.

Conlusion

En résumé, la stratégie mixte basée sur l'utilisation d'une base temporelle a priori issue d'une analyse de Fourier permet de résoudre des problèmes transitoires linéaires 3D avec différents temps de cycle, temps physique, conditions aux limites et types de charge (triangulaire, sinusoïdale, heaviside). Elle permet notamment de palier la limitation de la précédente approche au niveau des temps de cycle. La stratégie mixte permet d'obtenir un facteur de réduction de 50 par rapport à la MEF. De plus le temps pour déterminer les bases (dit temps de calcul offline) est lui aussi réduit dans la mesure où ces dernières sont connues via une expression analytique qui permet de considérer un grand nombre de problèmes différents. Cette approche a été mise en place et validée pour un problème faiblement couplé de thermo-diffusion. La stratégie mixte a ensuite été étendue pour les problèmes non-linéaires avec une méthode de linéarisation de type Picard et des bases temporelles a priori issues du cas linéaire. Des résultats encourageants ont été obtenus dans le cas d'une faible nonlinéarité. Pour des fortes non linéarités, l'approche doit encore être éprouvée.

Conclusion.

L'objectif principal de cette thèse est atteint dans la mesure où les trois différentes approches étudiées permettent de réduire notablement le temps de calcul des simulations (dit temps de calcul online) cycliques comparativement à l'utilisation de la MEF.
Les résultats de cette thèse pour les trois différentes approches sont les suivants:

- La première approche numérique testée est la méthode PGD. Elle est utilisée pour résoudre des problèmes transitoires cycliques linéaires. Cette méthode peut prédire les différents comportements liés aux différents échelles de temps du problème : le temps physique caractéristique du phénomène considéré et le temps du cycle lié au chargement imposé. Les résultats obtenus avec la PGD mènent à un gain en temps de calcul important - rapport de 50 par rapport à la MEF avec une bonne précision de la solution. Une manière de diminuer encore plus le temps de calcul a été présentée, elle consiste à adapter le pas de temps aux différents problèmes : pour des temps physique grand un maillage temporel grossier peut être utilisé ce qui n'est pas le cas pour des temps physiques petits. L'effet de la position spatiale sur la réponse montre que pour des temps physiques grands, l'effet du temps de cycle s'estompe loin des conditions aux bords où ce dernier est imposé.
  La méthode PGD combinée à la DEIM permet de réduire significativement le temps de calcul dans le cas de problèmes cycliques nonlinéaires avec un facteur de l'ordre de 30 pour les cas étudiés (ce rapport est inférieur au cas linéaire mais reste du même ordre de grandeur).

- Une deuxième approche basée sur l'utilisation d'un dictionnaire constitué des modes PGD les plus significatifs (spatio-temporels) correspondant à des problèmes thermiques cycliques transitoires à différents temps est ensuite évaluée. Les modes du dictionnaire sont générés par la PGD et sont donc spatiaux-temporels et non pas uniquement spatiaux comme dans le cas de la POD. Une fois que les modes sont connus (calcul offline), la solution d'un problème cyclique différent est calculée par projection sur les modes du dictionnaire (temps online). Différents dictionnaires ont été évalués : dictionnaire 1 avec un temps de cycle donné et des temps physiques différents, dictionnaire 2 avec un temps physique donné et des temps de cycle différents. Dans le cas du dictionnaire 1, l'approche est très efficace en terme de prédiction et de temps de calcul pour des problèmes avec différents temps physiques et différentes conditions aux limites. Dans le cas du dictionnaire 2, l'approche ne permet pas de prédire correctement la solution que si les modes associés au temps du cycle considérés font partie du dictionnaire. Cette approche a été testée pour un chargement avec différentes harmoniques et un problème couplé, elle permet de prédire correctement la solution si les temps de cycle considérés sont contenus dans le dictionnaire. Cette approche permet de générer un temps de calcul largement réduit pour une bonne précision des résultats. Le plus coûteux dans cette approche est de générer la base spatio-temporelle a priori (temps offline). Néanmoins cette approche est limité lorsque trop de temps de cycles sont considérés.

- Une autre approche basée sur la connaissance de la base temporelle a priori permet de palier la limitation de l'approche précédente. Cette approche est appelée stratégie mixte dans la mesure où elle utilise une analyse paramétrique utilisant la transformée de Fourier pour déterminer une expression analytique de la base temporelle en fonction du temps du cycle et du temps physique; un algorithme type PGD pour déterminer la base spatiale. Dans cette approche, la construction de la base temporelle est rapide dans la mesure où une fois l'étude paramétrique faite, celle-ci est connue sous une forme analytique (temps offline réduit). Les bases spatiales sont ensuite calculées à l'aide d'un algorithme type PGD. Cette approche a été validée pour des problèmes transitoires 3D cycliques, linéaires, non linéaires et faiblement couplés et permet d'obtenir des gains en temps important pour une bonne précision de la solution. Plus précisément, pour la résolution des problèmes non linéaires, l'expression analytique de la base temporelle obtenue dans le cas linéaire est utilisée. La base temporelle considérée est celle associée aux valeurs limites de la température pour le problème considéré menant à deux valeurs de la chaleur spécifique différentes et donc deux valeurs différentes du temps physique. Pour calculer les bases

spatiales, l'algorithme PGD est combiné à un algorithme de Picard. Cette stratégie mène à des résultats précis pour des faibles non linéarités (au sens où la réponse reste du même type). Pour des nonlinéarités plus importantes, une solution consiste à ajouter des bases temporelles associées à des valeurs intermédiaires de la température.

En résumé, toutes les approches testées dans cette thèse semblent être des bons candidats pour réduire le temps de calcul des simulations transitoires cycliques. La stratégie mixte semble être la plus efficace car elle permet de considérer un grand nombre de cycles sans forcément augmenter trop la base à considérer comme dans le cas de la seconde approche qui a cette faiblesse. Finalement, cette stratégie est basée sur la recherche d'une solution séparée espace-temps comme dans le cas de la LATIN, seulement la base temporelle est supposée connue. Un des potentiels de cette approche est l'utilisation d'une expression analytique pour la création de la base temporelle.

Suite aux différents résultats obtenus dans cette thèse, un certain nombre de perspectives peut être envisagé :

- Etude d'une géométrie plus complexe. Dans la thèse, seul un cube a été considéré. L'extension des approches à des géométries plus complexes ne semblent pas poser de problèmes dans la mesure où la PGD elle même peut être étendue à des géométries complexes.
- Dans cette thèse, les deux dernières approches ont été testées uniquement dans le cas faiblement couplé. Il est envisagé d'étendre la troisième approche à la prédiction de réponses thermo-viscoélastiques des polymères sous chargements cycliques et donc à des problèmes fortement couplés. La principale limitation devrait être le traitement des nonlinéarités générées par le couplage.
- Un indicateur d'erreur pour la deuxième approche doit être étudié ainsi que pour la troisième approche. Pour la deuxième approche qui n'est pas itérative, un indicateur basé sur le nombre de modes significatifs utilisé pourrait être étudié. Pour la troisième approche qui est itérative, un indicateur d'erreur basé sur un critère de stagnation comme celui de la PGD peut être envisagé.
- Pour la troisième approche, l'étude sur la possibilité de proposer une expression analytique plus générale doit être étayée même si les premiers résultats de la thèse sont prometteurs.

Bibliography

***

[Aghighi *et al.*, 2013] Aghighi, M., Ammar, A., Metivier, C., Normandin, M. et Chinesta, F. (2013). Non-incremental transient solution of the rayleigh–bénard convection model by using the pgd. *Journal of Non-Newtonian Fluid Mechanics*, 200:65 – 78. Special Issue: Advances in Numerical Methods for Non-Newtonian Flows.

[Aguado, 2015] Aguado, J. (2015). *Advanced strategies for the separated formulation of problems in the Proper Generalized Decomposition framework*. Thèse de doctorat, Ecole Centrale de Nantes.

[Aguado *et al.*, 2013] Aguado, J. V., Chinesta, F., Leygue, A., Cueto, E. et Huerta, A. (2013). Deim-based pgd for parametric nonlinear model order reduction. *In Centre Internacional de Mètodes Numèrics en Enginyeria (CIMNE)*, pages 29–34.

[AL Takash *et al.*, 2017] AL Takash, A., Beringhier, M., Hammoud, M. et Grandidier, J. C. (2017). Utilisation d'une base temporelle a priori issue d'une analyse tfr pour accélérer la prédiction du comportement d'un polymère sous chargement cyclique. *In Congrès Français de Mécanique*.

[AL Takash *et al.*, 2018] AL Takash, A., Beringhier, M., Hammoud, M. et Grandidier, J. C. (2018). Numerical approach based on the collection of the most significant modes to solve cyclic transient thermal problems involving different time scales. *Journal of Computational Physics*.

[AL Takash *et al.*, 2019] AL Takash, A., Beringhier, M., Hammoud, M. et Grandidier, J. C. (2019). On the validation of the proper generalized decomposition method with finite element method: 3d heat problem under cyclic loading. *In Mechanism, Machine, Robotics and Mechatronics Sciences*, pages 3–13, Cham. Springer International Publishing.

[Ammar *et al.*, 2006] Ammar, A., Mokdad, B., Chinesta, F. et Keunings, R. (2006). A new family of solvers for some classes of multidimensional partial differential equations encountered in kinetic theory modeling of complex fluids. *Journal of Non-Newtonian Fluid Mechanics*, 139(3):153–176.

[Ammar *et al.*, 2007] Ammar, A., Mokdad, B., Chinesta, F. et Keunings, R. (2007). A new family of solvers for some classes of multidimensional partial differential equations encountered in kinetic theory modelling of complex fluids: Part ii: Transient simulation using space-time separated representations. *Journal of Non-Newtonian Fluid Mechanics*, 144(2):98–121.

[Ammar *et al.*, 2010] Ammar, A., Normandin, M., Daim, F., Gonzalez, D., Cueto, E. et Chinesta, F. (2010). Non-Incremental Strategies Based on Separated Representations : Applications in Computational Rheology. *Communications in Mathematical Sciences*, 8(3):671–695.

[Ammar *et al.*, 2015] Ammar, A., Zghal, A., Morel, F. et Chinesta, F. (2015). On the space-time separated representation of integral linear viscoelastic models. *Comptes Rendus Mécanique*, 343(4):247–263.

[Anderson, 1991] Anderson, T. L. (1991). *Fracture mechanics-fundamentals and applications*. Taylor and Francis group.

[Anderson, 2017] Anderson, T. L. (2017). *Fracture mechanics-fundamentals and applications*. Taylor and Francis group.

[Annaratone, 2011] Annaratone, D. (2011). *Transient Heat Transfer*. SpringerBriefs in Applied Sciences and Technology. Springer Berlin Heidelberg.

[Ascher *et al.*, 1997] Ascher, U. M., Ruuth, S. J. et Spiteri, R. J. (1997). Implicit-explicit runge-kutta methods for time-dependent partial differential equations. *Applied Numerical Mathematics*, 25(2):151 – 167. Special Issue on Time Integration.

[Barrault *et al.*, 2004] Barrault, M., Maday, Y., Nguyen, N. C. et Patera, A. T. (2004). An 'empirical interpolation' method: application to efficient reduced-basis discretization of partial differential equations. *Comptes Rendus Mathematique*, 339(9):667 – 672.

[Benaarbia et Chrysochoos, 2017] Benaarbia, A. et Chrysochoos, A. (2017). Proper orthogonal decomposition preprocessing of infrared images to rapidly assess stress-induced heat source fields. *Quantitative InfraRed Thermography Journal*, 14(1):132–152.

[Benjamin *et al.*,] Benjamin, B., Julia, M. et Paul, S. Reduced-order modelling for linear heat conduction with parametrised moving heat sources. *GAMM-Mitteilungen*, 39(2):170–188.

[Benner *et al.*, 2015] Benner, P., Gugercin, S. et Willcox, K. (2015). A survey of projection-based model reduction methods for parametric dynamical systems. *SIAM review*, 57(4):483–531.

[Bergheau et Fortunier, 2010] Bergheau, J.-M. et Fortunier, R. (2010). *Finite Element Simulation of Heat Transfer*. Wiley Online Books.

[Bergheau *et al.*, 2016] Bergheau, J.-M., Zuchiatti, S., Roux, J.-C., Feulvarch, E., Tissot, S. et Perrin, G. (2016). The proper generalized decomposition as a space-time integrator for elastoplastic problems. *Comptes Rendus Mécanique*, 344(11):759 – 768.

[Beringhier *et al.*, 2010] Beringhier, M., Gueguen, M. et Grandidier, J. (2010). Solution of strongly coupled multiphysics problems using space-time separated representations—application to thermoviscoelasticity. *Archives of Computational Methods in Engineering*, 17(4):393–401.

[Berrehili, 2010] Berrehili, A. (2010). *Comportement cyclique et tenue en fatigue sous chargement multiaxial d'un polyéthylène : expériences et critère d'endurance*. Thèse de doctorat, ISAE-ENSMA Ecole Nationale Supérieure de Mécanique et d'Aérotechique - Poitiers.

[Bhattacharyya, 2018] Bhattacharyya, M. (2018). *A model reduction approach in space and time for fatigue damage simulation*. Thèse de doctorat, Université Paris-Saclay.

[Bhattacharyya *et al.*, 2016] Bhattacharyya, M., Néron, D., Ladeveze, P., Fau, A. et Nackenhorst, U. (2016). New latin-pgd technique for fatigue loading. *In European Congress on Computational Methods in Applied Sciences and Engineering*.

[Bhatti, 2005] Bhatti, M. A. (2005). Fundamental finite element analysis and applications. *Hoboken, New Jersey: John Wiley & Sons*.

[Białecki *et al.*, 2005] Białecki, R., Kassab, A. et Fic, A. (2005). Proper orthogonal decomposition and modal analysis for acceleration of transient fem thermal analysis. *International journal for numerical methods in engineering*, 62(6):774–797.

[Bognet *et al.*, 2012] Bognet, B., Bordeu, F., Chinesta, F., Leygue, A. et Poitou, A. (2012). Advanced simulation of models defined in plate geometries: 3d solutions with 2d computational complexity. *Computer Methods in Applied Mechanics and Engineering*, 201-204:1 – 12.

[Boisse *et al.*, 1990] Boisse, P., Bussy, P. et Ladeveze, P. (1990). A new approach in non-linear mechanics: The large time increment method. *International Journal for Numerical Methods in Engineering*, 29(3):647–663.

[Brandolini, 2004] Brandolini, L. (2004). *Fourier analysis and convexity*. Springer Science & Business Media.

[Capaldo *et al.*, 2014] Capaldo, M., Néron, D., Guidault, P.-A. et Ladevèze, P. (2014). An approximation framework dedicated to PGD-based nonlinear solver . *In 11th World Congress on Computational Mechanics (WCCM XI)*, Barcelone, Spain.

[Carslaw et Jaeger, 1986] Carslaw, H. et Jaeger, J. (1986). *Conduction of Heat in Solids*. Oxford science publications. Clarendon Press.

[Chama *et al.*, 2018] Chama, A., Gerber, S. et Wang, R. J. (2018). Newton raphson solver for finite element methods featuring nonlinear hysteresis models. *IEEE Transactions on Magnetics*, 54(1):1–8.

[Chatterjee, 2000] Chatterjee, A. (2000). An introduction to the proper orthogonal decomposition. *Current science*, 78:808–817.

[Chaturantabut et Sorensen, 2010] Chaturantabut, S. et Sorensen, D. (2010). Nonlinear model reduction via discrete empirical interpolation. *SIAM Journal on Scientific Computing*, 32(5):2737–2764.

[Chinesta *et al.*, 2010a] Chinesta, F., Ammar, A. et Cueto, E. (2010a). On the use of proper generalized decompositions for solving the multidimensional chemical master equation. *European Journal of Computational Mechanics/Revue Européenne de Mécanique Numérique*, 19(1-3):53–64.

[Chinesta *et al.*, 2010b] Chinesta, F., Ammar, A. et Cueto, E. (2010b). Recent advances and new challenges in the use of the proper generalized decomposition for solving multidimensional models. *Archives of Computational methods in Engineering*, 17(4):327–350.

[Chinesta *et al.*, 2016] Chinesta, F., Ammar, A. et Cueto, E. (2016). Proper generalized decomposition of multiscale models. *International Journal for Numerical Methods in Engineering*, 83:1114–1132.

[Chinesta *et al.*, 2007] Chinesta, F., Ammar, A., Falco, A. et Laso, M. (2007). On the reduction of stochastic kinetic theory models of complex fluids. *Modelling and Simulation in Materials Science and Engineering*, 15(6):639–652.

[Chinesta *et al.*, 2011a] Chinesta, F., Ammar, A., Leygue, A. et Keunings, R. (2011a). An overview of the proper generalized decomposition with applications in computational rheology. *Journal of Non-Newtonian Fluid Mechanics*, 166(11):578–592.

[Chinesta *et al.*, 2013a] Chinesta, F., Keunings, R. et Leygue, A. (2013a). *The proper generalized decomposition for advanced numerical simulations: a primer*. Springer Science & Business Media.

[Chinesta et Ladevèze, 2014] Chinesta, F. et Ladevèze, P. (2014). *Separated Representations and PGD-Based Model Reduction*. Springer.

[Chinesta *et al.*, 2011b] Chinesta, F., Ladeveze, P. et Cueto, E. (2011b). A short review on model order reduction based on proper generalized decomposition. *Archives of Computational Methods in Engineering*, 18(4):395–404.

[Chinesta *et al.*, 2013b] Chinesta, F., Leygue, A., Beringhier, M., Nguyen, L. T., Grandidier, J.-C., Schrefler, B. et Pasavento, F. (2013b). Towards a Framework for Non-Linear Thermal Models in Shell Domains. *International Journal of Numerical Methods for Heat and Fluid Flow*, 23(1):55–73.

[Chinesta *et al.*, 2013c] Chinesta, F., Leygue, A., Bordeu, F., Aguado, J. V., Cueto, E., Gonzalez, D., Alfaro, I., Ammar, A. et Huerta, A. (2013c). Pgd-based computational vademecum for efficient design, optimization and control. *Archives of Computational Methods in Engineering*, 20(1):31–59.

[Cochelin *et al.*, 1994a] Cochelin, B., Damil, N. et Potier-Ferry, M. (1994a). The asymptotic-numerical method: an efficient perturbation technique for nonlinear structural mechanics. *Revue Européenne des Éléments Finis*, 3(2):281–297.

[Cochelin *et al.*, 1994b] Cochelin, B., Damil, N. et Potier-Ferry, M. (1994b). Asymptotic–numerical methods and pade approximants for non-linear elastic structures. *International Journal for Numerical Methods in Engineering*, 37(7):1187–1213.

[Cognard et Ladevèze, 1993] Cognard, J.-Y. et Ladevèze, P. (1993). A large time increment approach for cyclic viscoplasticity. *International Journal of plasticity*, 9(2):141–157.

[Comte *et al.*, 2006] Comte, F., Maitournam, H., Burry, P. et Nguyen, T. M. L. (2006). A direct method for the solution of evolution problems. *Comptes Rendus Mécanique*, 334(5):317–322.

[Constantinescu *et al.*, 2004] Constantinescu, A., Charkaluk, E., Lederer, G. et Verger, L. (2004). A computational approach to thermomechanical fatigue. *International Journal of fatigue*, 26(8):805–818.

[Cooley, 1987] Cooley, J. W. (1987). The re-discovery of the fast fourier transform algorithm. *Microchimica Acta*, 93(1):33–45.

[Cueto et Chinesta, 2014] Cueto, E. et Chinesta, F. (2014). Real time simulation for computational surgery: a review. *Advanced Modeling and Simulation in Engineering Sciences*, 1:1–11.

[Cueto *et al.*, 2016] Cueto, E., González, D. et Alfaro, I. (2016). *Proper Generalized Decomposition: An Introduction to Computer Implementation with Matlab*. SpringerBriefs in Applied Sciences and Technology.

[Damil et Potier-Ferry, 1990] Damil, N. et Potier-Ferry, M. (1990). A new method to compute perturbed bifurcations: Application to the buckling of imperfect elastic structures. *International Journal of Engineering Science*, 28(9):943 – 957.

[Dokainish et Subbaraj, 1989] Dokainish, M. et Subbaraj, K. (1989). A survey of direct time-integration methods in computational structural dynamics. explicit methods. *Computers & Structures*, 32(6):1371 – 1386.

[dos Santos *et al.*, 2013] dos Santos, W., de Sousa, J. et Gregorio, R. (2013). Thermal conductivity behaviour of polymers around glass transition and crystalline melting temperatures. *Polymer Testing*, 32(5):987 – 994.

[Efe et Ozbay, 2003] Efe, M. O. et Ozbay, H. (2003). Proper orthogonal decomposition for reduced order modeling: 2d heat flow. *In Control Applications, 2003. CCA 2003. Proceedings of 2003 IEEE Conference on*, volume 2, pages 1273–1277. IEEE.

[Eyre et Milton, 1999] Eyre, D. et Milton, G. (1999). A fast numerical scheme for computing the response of composites using grid refinement. *The European Physical Journal Applied Physics*, 6(1):41–47.

[Feeny et Kappagantu, 1998] Feeny, B. et Kappagantu, R. (1998). On the physical interpretation of proper orthogonal modes in vibrations. *Journal of sound and vibration*, 211(4):607–616.

[Felder *et al.*, 2017] Felder, S., Kochamann, J., Wulfinghoff, S. et Reese, S. (2017). Multiscale fe-fft-based thermo-mechanically coupled modeling of viscoplastic polycrystalline materials. *In 7th GACM Colloquium on Computational Mechanics for Young Scientists from Academia and Industry*, Stuttgart, Germany.

[Fritzen *et al.*, 2016] Fritzen, F., Haasdonk, B., Ryckelynck, D. et Schöps, S. (2016). An algorithmic comparison of the hyper-reduction and the discrete empirical interpolation method for a nonlinear thermal problem. *Mathematical and Computational Applications*, 23:8–31.

[Fu *et al.*, 2018] Fu, H., Wang, H. et Wang, Z. (2018). Pod/deim reduced-order modeling of time-fractional partial differential equations with applications in parameter identification. *Journal of Scientific Computing*, 74(1):220–243.

[Ghavamian *et al.*, 2017] Ghavamian, F., Tiso, P. et Simone, A. (2017). Pod–deim model order reduction for strain-softening viscoplasticity. *Computer Methods in Applied Mechanics and Engineering*, 317:458 – 479.

[Ghnatios *et al.*, 2016] Ghnatios, C., Damil, G. X., Leygue, A., Visonneau, M., Chinesta, F. et Cimetiere, A. (2016). On the space separated representation when addressing the solution of pde in complex domains. *Discrete and Continuous Dynamical Systems - S*, 9:475 – 500.

[Giner *et al.*, 2013] Giner, E., Bognet, B., Ródenas, J. J., Leygue, A., Fuenmayor, F. J. et Chinesta, F. (2013). The proper generalized decomposition (pgd) as a numerical procedure to solve 3d cracked plates in linear elastic fracture mechanics. *International Journal of Solids and Structures*, 50(10):1710 – 1720.

[Grepl, Martin A. *et al.*, 2007] Grepl, Martin A., Maday, Yvon, Nguyen, Ngoc C. et Patera, Anthony T. (2007). Efficient reduced-basis treatment of nonaffine and nonlinear partial differential equations. *ESAIM: M2AN*, 41(3):575–605.

[Guérin *et al.*, 2018] Guérin, N., Thorin, A., Thouverez, F., Legrand, M. et Almeida, P. (2018). Thermomechanical model reduction for efficient simulations of rotor-stator contact interaction. *In ASME Turbo Expo 2018: Turbomachinery Technical Conference and Exposition*, Oslo, Norway. American Society of Mechanical Engineers.

[Hammoud *et al.*, 2014] Hammoud, M., Beringhier, M. et Grandidier, J.-C. (2014). A reduced simulation applied to the viscoelastic fatigue of polymers. *Comptes Rendus Mécanique*, 342(12):671–691.

[Harčarik *et al.*, 2012] Harčarik, T., Bocko, J. et Masláková, K. (2012). Frequency analysis of acoustic signal using the fast fourier transformation in matlab. *Procedia Engineering*, 48:199 – 204. Modelling of Mechanical and Mechatronics Systems.

[Holmes, 2012] Holmes, P. (2012). *Turbulence, coherent structures, dynamical systems and symmetry*. Cambridge university press.

[Hughes et Liu, 1978] Hughes, T. J. R. et Liu, W. K. (1978). Implicit-explicit finite elements in transient analysis stability theory. *Journal of Applied Mechanics*, 45:371 – 374.

[Ichihashi *et al.*, 2010] Ichihashi, F., Jeng, S.-M. et Cohen, K. (2010). Proper orthogonal decomposition and fourier analysis on the energy release rate dynamics of a gas turbine combustor. *In 48th AIAA Aerospace Science Meeting*.

[Khennane, 2013] Khennane, A. (2013). *Introduction to finite element analysis using MATLAB® and abaqus*. CRC Press.

[Ladevèze, 1985] Ladevèze, P. (1985). Sur une famille d'algortithmes en mécanique de structure. *Comptes-rendus de l'Académie des Sciences*, (2):41–44.

[Ladeveze et Nouy, 2003] Ladeveze, P. et Nouy, A. (2003). On a multiscale computational strategy with time and space homogenization for structural mechanics. *Computer Methods in Applied Mechanics and Engineering*, 192(28):3061–3087.

[Ladeveze *et al.*, 2010] Ladeveze, P., Passieux, J.-C. et Néron, D. (2010). The latin multiscale computational method and the proper generalized decomposition. *Computer Methods in Applied Mechanics and Engineering*, 199(21):1287–1296.

[Larson et Bengzon, 2013] Larson, M. et Bengzon, F. (2013). *The Finite Element Method: Theory, Implementation, and Applications*. Mathematics and statics. Springer, Berlin, Heidelberg.

[Le Bris, 2006] Le Bris, C. (2006). Mathematical and numerical analysis for molecular simulation: Accomplishments and challenges. *In Proceedings of the International Congress of Mathematicians*, volume 3, pages 1507–1522.

[Lebensohn *et al.*, 2011] Lebensohn, R., Rollett, A. et Suquet, P. (2011). Fast fourier transform-based modeling for the determination of micromechanical fields in polycrystals. 63:13–18.

[Lebensohn *et al.*, 2012] Lebensohn, R. A., Kanjarla, A. K. et Eisenlohr, P. (2012). An elasto-viscoplastic formulation based on fast fourier transforms for the prediction of micromechanical fields in polycrystalline materials. *International Journal of Plasticity*, 32-33:59 – 69.

[Liang *et al.*, 2002] Liang, Y., Lee, H., Lim, S., Lin, W., Lee, K. et Wu, C. (2002). Proper orthogonal decomposition and its applications-part i: Theory. *Journal of Sound and vibration*, 252(3):527–544.

[Lihong *et al.*, 2017] Lihong, F., Michael, M. et Peter, B. (2017). Adaptive pod–deim basis construction and its application to a nonlinear population balance system. *AIChE Journal*, 63(9): 3832–3844.

[Maday *et al.*, 2009] Maday, Y., Nguyen, N. C. et Patera, A. T. (2009). A general multipurpose interpolation procedure: the magic points. *Communications on Pure and Applied Analysis*, 8:383–404.

[Marin, 2010] Marin, E. (2010). Characteristic dimensions for heat transfer. *Latin-American Journal of Physics Educationl*, 4:56–60.

[Miled *et al.*, 2013] Miled, B., Ryckelynck, D. et Cantournet, S. (2013). A priori hyperreduction method for coupled viscoelastic–viscoplastic composites. *Computers & Structures*, 119: 95–103.

[Montebello, 2015] Montebello, C. (2015). *Analysis of the stress gradient effect in Fretting-Fatigue through a description based on nonlocal intensity factors*. Thèse de doctorat, Université Paris-Saclay.

[Nasri, 2017] Nasri, M. A. (2017). *Dimensional reduction for the simulation of metal fatigue*. Thèse de doctorat, Ecole nationale supérieure d'arts et métiers - ENSAM.

[Nasri *et al.*, 2018] Nasri, M. A., Robert, C., Ammar, A., Arem, S. E. et Morel, F. (2018). Proper generalized decomposition (pgd) for the numerical simulation of polycrystalline aggregates under cyclic loading. *Comptes Rendus Mécanique*, 346(2):132 – 151.

[Nayebi et Hamidpour, 2016] Nayebi, A. et Hamidpour, M. (2016). Thermo-mechanical cyclic loading analysis of pipes with different type of defects: Temperature dependent properties. *Proceedings of the Institution of Mechanical Engineers, Part L: Journal of Materials: Design and Applications*, 230(1):303–310.

[Néron et Ladevèze, 2010] Néron, D. et Ladevèze, P. (2010). Proper generalized decomposition for multiscale and multiphysics problems. *Archives of Computational Methods in Engineering*, 17(4):351–372.

[Néron *et al.*, 2004] Néron, D., Ladevèze, P., Dureisseix, D. et Schrefler, B. A. (2004). Accounting for nonlinear aspects in multiphysics problems: Application to poroelasticity. *Lecture notes in computer science*, 3039:612–620.

[Newman, 1996] Newman, A. J. (1996). Model reduction via the karhunen-loeve expansion part i: An exposition. Rapport technique.

[Nguyen, 2013] Nguyen, S. T. T. (2013). *Caractérisation expérimentale et modélisation thermo-mécanique de l'accommodation cyclique du polyéthylene.* Thèse de doctorat, ISAE-ENSMA Ecole Nationale Supérieure de Mécanique et d'Aérotechique-Poitiers.

[Nguyen *et al.*, 2013] Nguyen, S. T. T., Castagnet, S. et Grandidier, J.-C. (2013). Nonlinear viscoelastic contribution to the cyclic accommodation of high density polyethylene in tension: Experiments and modeling. *International journal of fatigue*, 55:166–177.

[Nguyen, 2012] Nguyen, T. L. (2012). *La Décomposition propre généralisée pour la résolution de problèmes multiphysiques transitoires couplés dédiés à la mécanique des matériaux*. Thèse de doctorat, Chasseneuil-du-Poitou, Ecole nationale supérieure de mécanique et d'aérotechnique.

[Niroomandi *et al.*, 2009] Niroomandi, S., Alfaro, I., Cueto, E. et Chinesta, F. (2009). Model order reduction for hyperelastic materials. *International Journal for Numerical Methods in Engineering*, 81(9):1180–1206.

[Noack, 2013] Noack, B. R. (2013). *Turbulence, Coherent Structures, Dynamical Systems and Symmetry*. American Institute of Aeronautics and Astronautics.

[Noor et Peters, 1980] Noor, A. K. et Peters, J. M. (1980). Reduced basis technique for nonlinear analysis of structures. *AIAA Journal*, 18(4):455–462.

[Nouy, 2010] Nouy, A. (2010). A priori model reduction through proper generalized decomposition for solving time-dependent partial differential equations. *Computer Methods in Applied Mechanics and Engineering*, 199(23):1603 – 1626.

[Othman et Abbas, 2012] Othman, M. et Abbas, I. (2012). Fundamental solution of generalized thermo-viscoelasticity using the finite element method. *Computational Mathematics and Modeling*, 23:158–167.

[Peigney et Stolz, 2003] Peigney, M. et Stolz, C. (2003). An optimal control approach to the analysis of inelastic structures under cyclic loading. *Journal of the Mechanics and Physics of Solids*, 51(4):575–605.

[Prulière *et al.*, 2010a] Prulière, E., Chinesta, F. et Ammar, A. (2010a). On the deterministic solution of multidimensional parametric models using the proper generalized decomposition. *Mathematics and Computers in Simulation*, 81(4):791–810.

[Prulière *et al.*, 2010b] Prulière, E., Férec, J., Chinesta, F. et Ammar, A. (2010b). An efficient reduced simulation of residual stresses in composite forming processes. *International Journal of Material Forming*, 3(2):1339–1350.

[Rao, 2010] Rao, S. S. (2010). *The finite element method in engineering*. Elsevier.

[Reddy, 1993] Reddy, J. N. (1993). *An introduction to the finite element method*, volume 2. McGraw-Hill New York.

[Rizk et Awad, 2018] Rizk, R. et Awad, M. (2018). *Mechanism, Machine, Robotics and Mechatronics Sciences*. Mechanisms and Machine Science. Springer International Publishing.

[Ryckelynck, 2002] Ryckelynck, D. (2002). Réduction a priori de modèles thermomécaniques. *Comptes Rendus Mécanique*, 330(7):499–505.

[Ryckelynck, 2005] Ryckelynck, D. (2005). A priori hyperreduction method: an adaptive approach. *Journal of computational physics*, 202(1):346–366.

[Ryckelynck et Benziane, 2010] Ryckelynck, D. et Benziane, D. M. (2010). Multi-level a priori hyper-reduction of mechanical models involving internal variables. *Computer Methods in Applied Mechanics and Engineering*, 199(17):1134–1142.

[Ryckelynck *et al.*, 2006] Ryckelynck, D., Chinesta, F., Cueto, E. et Ammar, A. (2006). On the a priori model reduction: overview and recent developments. *Archives of Computational methods in Engineering*, 13(1):91–128.

[Ryckelynck *et al.*, 2015] Ryckelynck, D., Gallimard, L. et Jules, S. (2015). Estimation of the validity domain of hyper-reduction approximations in generalized standard elastoviscoplasticity. *Advanced Modeling and Simulation in Engineering Sciences*, 2(1):6–25.

[Sauer et Richardson, 1980] Sauer, J. A. et Richardson, G. C. (1980). Fatigue of polymers. *International Journal of Fracture*, 16(6):499–532.

[Spiliopoulos, 2002] Spiliopoulos, K. (2002). A simplified method to predict the steady cyclic stress state of creeping structures. *Journal of applied mechanics*, 69(2):148–153.

[Stehly et Remond, 2002] Stehly, M. et Remond, Y. (2002). On numerical simulation of cyclic viscoplastic and viscoelastic constitutive laws with the large time increment method. *Mechanics of Time-Dependent Materials*, 6(2):147–170.

[Stein *et al.*, 2004] Stein, E., de Borst, R. et Hughes, T. J. (2004). *Encyclopedia of computational mechanics*, volume 1. Wiley Online Library.

[Subbaraj et Dokainish, 1989] Subbaraj, K. et Dokainish, M. (1989). A survey of direct time-integration methods in computational structural dynamics. implicit methods. *Computers & Structures*, 32(6):1387 – 1401.

[Sutherland, 1996] Sutherland, H. J. (1996). Frequency domain analysis of the fatigue loads on typical wind turbine blades. *Journal of Solar Engineering*, 118.

[Szabó, 2009] Szabó, T. (2009). On the discretization time-step in the finite element theta-method of the discrete heat equation. *In Numerical Analysis and Its Applications*, pages 564–571, Berlin, Heidelberg. Springer Berlin Heidelberg.

[Van Loan, 1992] Van Loan, C. (1992). *Computational Frameworks for the Fast Fourier Transform*. Society for Industrial and Applied Mathematics.

[Walnut, 2013] Walnut, D. F. (2013). *An introduction to wavelet analysis*. Springer Science & Business Media.

[Zienkiewicz et Taylor, 2000] Zienkiewicz, O. C. et Taylor, R. L. (2000). *The finite element method: solid mechanics*, volume 2. Butterworth-heinemann.

[Zienkiewicz et Taylor, 2005] Zienkiewicz, O. C. et Taylor, R. L. (2005). *The finite element method for solid and structural mechanics*, volume 6. Butterworth-heinemann.

Appendix A

***

A.1 Progressive construction of the PGD

The explicit form of the operation discussed in section 1.3.2.3 for the PGD steps with k as an extra coordinate:

1. Computing $R(x)$ from $S(t)$ and $W(k)$ The field and the test functions are written as:

$$u^n(x,t,k) = \sum_{i=1}^{n-1} X_i(x).T_i(t).k_i(k) + R(x).S(t)W(k) \tag{A.1}$$

$$u^*(x,t,k) = R(x)^*.S(t)W(k) \tag{A.2}$$

Substitute Eq. (A.1) and Eq. (A.2) in the weak formulation. The equation writes:

$$\begin{aligned}\int_{\Omega\times\Omega_t\times\Omega_k} R^*.S.W(D.\frac{\partial S}{\partial t}.W - k.\Delta R.S.W)dx.dt.dk = \\ \int_{\Omega\times\Omega_t\times\Omega_k} R^*.S.W(\sum_{i=1}^{n-1} X_i.\frac{\partial T_i}{\partial t}.k_i - \sum_{i=1}^{n-1} k.\Delta X_i.T_i.k_i - f)\end{aligned} \tag{A.3}$$

The functions of time and diffusivity are known, the Eq. A.3 is integrated over $\Delta_t \times \Delta_k$ using the notation that are summarized in Table A.1, Eq. A.3 becomes:

$$\int_\Omega R^*.(a_1.b_2.R - a_2.b_1.\Delta R)dx = -\int_\Omega R^*.(\sum_{i=1}^{n-1} a_4^i.b_4^i.X_i - \sum_{i=1}^{n-1} a_5^i.b_5^i.\Delta X_i - a3.b3.f)dx \tag{A.4}$$

For the unknown $R(x)$ can be solved by means of any suitable discretization.

Notation	Integral	Notation	Integral	Notation	Integral
a_1	$\int_{\Omega_k} W^2 dk$	b_1	$\int_{\Omega_t} S^2 dt$	c_1	$\int_\Omega R^2 dx$
a_2	$\int_{\Omega_k} kW^2 dk$	b_2	$\int_{\Omega_t} S\frac{dS}{dt} dt$	c_2	$\int_\Omega R.\Delta R dx$
a_3	$\int_{\Omega_k} W dk$	b_3	$\int_{\Omega_t} S dt$	c_3	$\int_\Omega R dx$
a_4^i	$\int_{\Omega_k} WK_i dk$	b_4^i	$\int_{\Omega_t} S\frac{dT_i}{dt} dt$	c_4^i	$\int_\Omega R.\Delta X_i dx$
a_5^i	$\int_{\Omega_k} kWK_i dk$	b_5^i	$\int_{\Omega_t} ST_i dt$	c_5^i	$\int_\Omega RX_i dx$

Table A.1: The notation for different integrals

2. Computing $S(t)$ from $R(x)$ and $W(k)$ The virtual field is written as:

$$u^*(x,t,k) = R(x).S^*(t)W(k) \tag{A.5}$$

using the notation that are summarized in Table A.1, Eq. A.3 becomes:

$$\int_\Omega S^*.(a_1.c_1.\frac{dS}{dt} - a_2.c_2.S)dt = -\int_\Omega S^*.(\sum_{i=1}^{n-1} a_4^i.c_5^i.\frac{dT_i}{dt} - \sum_{i=1}^{n-1} a_5^i.c_4^i.T_i - a3.c3.f)dt \tag{A.6}$$

3. Computing $W(k)$ from $R(x)$ and $S(t)$ The virtual field is written as:

$$u^*(x,t,k) = R(x).S(t)W^*(k) \tag{A.7}$$

using the notation that are summarized in Table A.1, Eq. A.3 becomes:

$$\int_\Omega W^*.(c_1.b_2.W - c_2.b_1.k.W)dk = -\int_\Omega W^*.(\sum_{i=1}^{n-1} c_5^i.b_4^i.K_i - \sum_{i=1}^{n-1} c_4^i.b_5^i.k.K_i - c3.b3.f)dk \tag{A.8}$$

A.2 Sampling in the frequency domain

This Appendix is related to the fourier analysis. The objective of this study is to show the effect of the sampling that is to say the effect of the number of samples taken from the time domain on the representation in the frequency domain.

Let us consider the following function:

$$f(t) = cos(2\ \pi\ f_1\ t) + 2cos(2\ \pi\ f_2\ t) \tag{A.9}$$

where $f_1 = 0.5Hz$, $f_2 = 1Hz$ The variation in the time domain of $(f(t))$ and the amplitude in the frequency domain (normalized by the maximum amplitude) are depicted in Fig. A.1 for two different samplings. It is noted that:

1. Two fundamental frequencies appeared regardless the sampling number $((f_1 = 0.5)$ and $(f_2 = 1))$ which are related to the frequency of the spectrum.
2. When the sampling number increases, a small unnecessary peaks appeared as shown in Fig. A.1.

To sum up, the minimum sampling number can show the fundamental frequencies in the spectrum. Large sampling can lead to non physical fluctuations.

A.3 Finite Element Method using ABAQUS software

A.3.1 Linear 3D transient thermal problem

Numerical analysis of thermal conduction phenomenon with dependence of material properties on temperature (latent heat effect (internal energy) and boundary convection) is performed using uncoupled heat transfer model in ABAQUS (commercial finite element software).

Transient analysis: The backward Euler method (known as Crank-Nicholson operator) is used as the time integration scheme for the transient problems. This method is unconditionally stable for the linear problems. The backward Euler's method is an implicit method, that finds the solution by solving the equation involving the current state of the system and the later one such that:

$$Y_{k+1} = Y_k + f(t_k, Y_{k+1})\Delta t$$

To recall, implicit method generates a solution by solving an equation involving both the current state and the later one of the system, however the explicit method uses the state of the current time

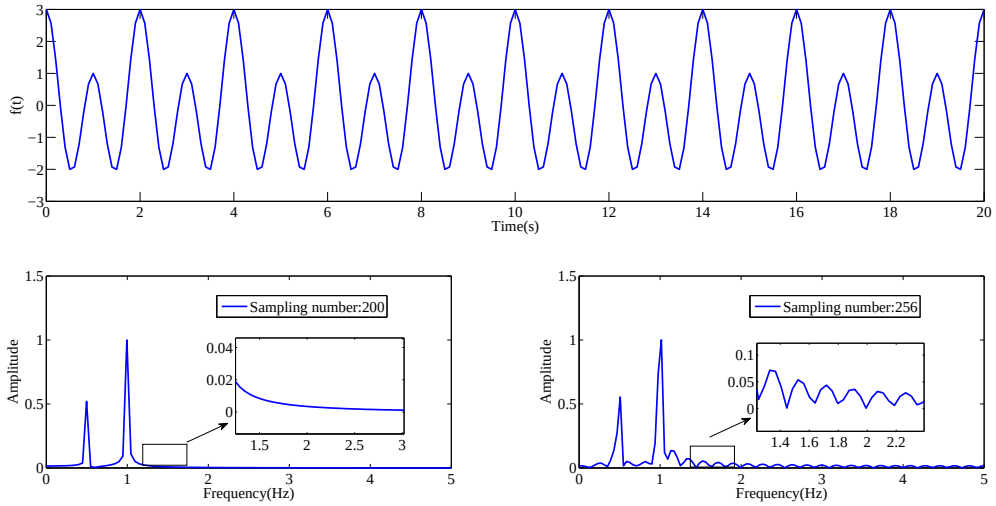


Figure A.1: The Fast Fourier Transform of $f(t)$ with different sampling numbers

Symbol	Element
DC3D4	4-node linear tetrahedron
DC3D6	6-node linear triangular prism
DC3D8	8-node linear brick
DC3D10	10-node quadratic tetrahedron
DC3D15	15-node quadratic triangular prism
DC3D20	20-node quadratic brick

Table A.2: Diffusive heat transfer or mass diffusion elements

to calculate the state of the system at a later time. Practically speaking, implicit method is time consuming. But, in case of the explicit schemes solving stiff equations (partial differential equation and ordinary differential equation) require very small time steps to satisfy the numerical stability. Thus, implicit scheme takes less computational time with larger time steps.

In case automatic step is used in ABAQUS, ABAQUS will adjust the time step to satisfy the stability limit. It provides tolerance parameters to indicate the level of accuracy required in the time integration of transient heat transfer analysis that involves physical times. The accuracy measure used in ABAQUS is denoted by (S^j), and the tolerance is denoted by (T^j). The accuracy measure is calculated for each time step In case $S^j > T^j$, that is in step j, the time step is too large to satisfy the time integration accuracy requirement, thus a new increment begun again such that:

$$\Delta t_{new} = 0.85 \frac{T^j}{S^j} \Delta t \tag{A.10}$$

Element type: In ABAQUS, the diffusive elements are provided for use in heat transfer. This kind of elements allows the heat storage and generates an output temperature. Therefore, the diffusive elements have only temperature degree of freedom. In fact, the diffusive elements can be either linear interpolation (first order), or quadratic interpolation (second order). For the heat transfer problem, an 8 node linear heat transfer brick (DC3D8) is used. Table A.2 depicts the other elements for diffusive heat transfer.

A.3.2 Nonlinear problem

Heat transfer problems can be nonlinear because of the dependence of the material properties on the temperature and the dependence of boundary conditions on the temperature. For instance, the convection coefficient can be a function of temperature. In fact, in the case of a nonlinear problem, ABAQUS implements an iterative scheme. This scheme is referred to Newton method, where in the presence of non-linear effects and in order to improve the stability, some modifications are needed.

Appendix B

***

B.1 Construction of the separated representation

This appendix is dedicted to illustrate the progressive construction of the PGD method.

First, let us note that Eq. 3.4 is divided into a Left Hand Side (LHS) and a Right Hand Side (RHS):

1. First term: $\int_\Omega T^* \rho C_p \frac{\partial T}{\partial t} \mathrm{d}\Omega + k \int_\Omega [(\frac{\partial T^*}{\partial x}\frac{\partial T}{\partial x} + \frac{\partial T^*}{\partial y}\frac{\partial T}{\partial y} + \frac{\partial T^*}{\partial z}\frac{\partial T}{\partial z})]\mathrm{d}\Omega$. The LHS and RHS are represented in Table B.1.

2. Second term: $\int_{S_{yz}\times\Omega_t} T^*(\frac{L}{2}, y, z, t)\ h_{horizontal}(T(\frac{L}{2}, y, z, t) - T_\infty)\mathrm{d}y\mathrm{d}z\mathrm{d}t$ The LHS is represented in Table B.2.

3. Third term:$\int_{S_{xz}\times\Omega_t} T^*(x, \frac{L}{2}, z, t)\ h_{vertical}(T(x, \frac{L}{2}, z, t) - T_\infty)\mathrm{d}x\mathrm{d}z\mathrm{d}t$ The LHS and RHS are represented in Table B.3.

4. Fourth term: $\int_{S_{xy}\times\Omega_t} T^*(x, y, \frac{L}{2}, t)\ h_{horizontal}(T(x, y, \frac{L}{2}, t) - T_\infty)\mathrm{d}x\mathrm{d}y\mathrm{d}t$ The LHS and RHS are represented in Table B.4.

The weighted residual form is written as in Eq. (B.1). Let us recall the dependencies of the functions: $F_n(x)$, $G_n(y)$, $H_n(z)$ and $(U_n(t))$.

Function	$\int_\Omega T^* \rho C_p \frac{\partial T}{\partial t} \mathrm{d}\Omega$	$k \int_\Omega (\frac{\partial T^*}{\partial x} \frac{\partial T}{\partial x} \Omega$	$k \int_\Omega \frac{\partial T^*}{\partial y} \frac{\partial T}{\partial y} \Omega$	$k \int_\Omega \frac{\partial T^*}{\partial z} \frac{\partial T}{\partial z}) \mathrm{d}\Omega$
x	$\rho C_p \cdot T(x) \cdot T^*(x)$	$k \cdot \frac{\partial}{\partial x} T(x) \cdot \frac{\partial}{\partial x} T^*(x)$	$k \cdot T(x) \cdot T^*(x)$	$k \cdot T(x) \cdot T^*(x)$
y	$T(y) \cdot T^*(y)$	$T(y) \cdot T^*(y)$	$\frac{\partial}{\partial y} T(y) \cdot \frac{\partial}{\partial y} T^*(y)$	$T(y) \cdot T^*(y)$
z	$T(z) \cdot T^*(z)$	$T(z) \cdot T^*(z)$	$T(z) \cdot T^*(z)$	$\frac{\partial}{\partial z} T(z) \cdot \frac{\partial}{\partial z} T^*(z)$
t	$\frac{\partial}{\partial t} T(t) \cdot T^*(t)$	$T(t) \cdot T^*(t)$	$T(t) \cdot T^*(t)$	$T(t) \cdot T^*(t)$

Table B.1: Separated forms of the LHS of the first term

$$
\begin{aligned}
&\int_\Omega F_n^*.G_{n-1}.H_{n-1}.U_{n-1}.(\rho C_p.F_n.G_{n-1}.H_{n-1}.\frac{\partial U_{n-1}}{\partial t}\mathrm{d}\Omega)\\
&+k[\int_\Omega[(G_{n-1}.H_{n-1}.U_{n-1}\frac{dF_n^*}{dx}.(G_{n-1}.H_{n-1}.U_{n-1}\frac{dF_n}{dx})]\\
&+\int_\Omega[(F_n^*.H_{n-1}.U_{n-1}\frac{dG_{n-1}}{dy}.(F_n.H_{n-1}.U_{n-1}\frac{dG_{n-1}}{dy})]\\
&+\int_\Omega[(F_n^*.G_{n-1}.U_{n-1}\frac{dH_{n-1}}{dz}.(F_n.G_{n-1}.U_{n-1}\frac{dH_{n-1}}{dz})]]\\
&+\int_{S_{yz}\times\Omega_t} h_{vertical}F_n^*(\frac{L}{2}).G_{n-1}.H_{n-1}.U_{n-1}.(F_n(\frac{L}{2}).G_{n-1}.H_{n-1}.U_{n-1})\mathrm{d}y\mathrm{d}z\mathrm{d}t\\
&+\int_{S_{xz}\times\Omega_t} h_{vertical}F_n^*.G_{n-1}(\frac{L}{2}).H_{n-1}.U_{n-1}.(F_n.G_{n-1}(\frac{L}{2}).H_{n-1}.U_{n-1})\mathrm{d}x\mathrm{d}z\mathrm{d}t\\
&+\int_{S_{xy}\times\Omega_t} h_{horizontal}F_n^*.G_{n-1}.H_{n-1}(\frac{L}{2}).U_{n-1}.(F_n.G_{n-1}.H_{n-1}(\frac{L}{2}).U_{n-1})\mathrm{d}x\mathrm{d}y\mathrm{d}t\\
&-\int_\Omega F_n^*.G_{n-1}.H_{n-1}.U_{n-1}.(\rho C_p.\sum_{i=1}^{n-1}.F_i.G_i.H_i.\frac{\partial U_i}{\partial t}\mathrm{d}\Omega)\\
&-k[\int_\Omega[(G_{n-1}.H_{n-1}.U_{n-1}\frac{dF_n^*}{dx}.(\sum_{i=1}^{n-1}G_i.H_i.U_i\frac{dF_i}{dx})]\\
&+\int_\Omega[(F_n^*.H_{n-1}.U_{n-1}\frac{dG_{n-1}}{dy}.(\sum_{i=1}^{n-1}F_i.H_i.U_i\frac{dG_i}{dy})]\\
&+\int_\Omega[(F_n^*.G_{n-1}.U_{n-1}\frac{dH_{n-1}}{dz}.(\sum_{i=1}^{n-1}F_i.G_i.U_i\frac{dH_i}{dz})]]\\
&+\int_{S_{yz}\times\Omega_t} F_n^*(\frac{L}{2}).G_{n-1}.H_{n-1}.U_{n-1}.(T_\infty)\mathrm{d}y\mathrm{d}z\mathrm{d}t\\
&+\int_{S_{xz}\times\Omega_t} F_n^*.G_{n-1}(\frac{L}{2}).H_{n-1}.U_{n-1}.(T_\infty)\mathrm{d}x\mathrm{d}z\mathrm{d}t\\
&+\int_{S_{xy}\times\Omega_t} F_n^*.G_{n-1}.H_{n-1}(\frac{L}{2}).U_{n-1}.(T_\infty)\mathrm{d}x\mathrm{d}y\mathrm{d}t\\
&-\int_{S_{yz}\times\Omega_t} h_{vertical}F_n^*(\frac{L}{2}).G_{n-1}.H_{n-1}.U_{n-1}.(\sum_{i=1}^{n-1}F_i(\frac{L}{2}).G_i.H_i.U_i)\mathrm{d}y\mathrm{d}z\mathrm{d}t\\
&-\int_{S_{xz}\times\Omega_t} h_{vertical}F_n^*.G_{n-1}(\frac{L}{2}).H_{n-1}.U_{n-1}.(\sum_{i=1}^{n-1}F_i.G_i(\frac{L}{2}).H_i.U_i)\mathrm{d}x\mathrm{d}z\mathrm{d}t\\
&-\int_{S_{xy}\times\Omega_t} h_{horizontal}F_n^*.G_{n-1}.H_{n-1}(\frac{L}{2}).U_{n-1}.(\sum_{i=1}^{n-1}F_i.G_i.H_i(\frac{L}{2}).U_i)\mathrm{d}x\mathrm{d}y\mathrm{d}t
\end{aligned}
\tag{B.1}
$$

Function	LHS	RHS
x	$h_{horizontal} \cdot T(x) \cdot T^*(x)$	$h_{horizontal} \cdot T^*(x) \cdot T_\infty$
y	$T(y) \cdot T^*(y)$	$T^*(y) \cdot T_\infty$
z	$T(z) \cdot T^*(z)$	$T^*(z) \cdot T_\infty$
t	$T(t) \cdot T^*(t)$	$T^*(t) \cdot T_\infty$

Table B.2: Separated forms of the LHS and RHS of the second term

Function	LHS	RHS
x	$h_{vertical} \cdot T(x) \cdot T^*(x)$	$h_{vertical} \cdot T^*(x) \cdot T_\infty$
y	$T(y) \cdot T^*(y)$	$T^*(y) \cdot T_\infty$
z	$T(z) \cdot T^*(z)$	$T^*(z) \cdot T_\infty$
t	$T(t) \cdot T^*(t)$	$T^*(t) \cdot T_\infty$

Table B.3: Separated forms of the LHS and RHS of the third term

Function	LHS	RHS
x	$h_{horizontal} \cdot T(x) \cdot T^*(x)'$	$h_{horizontal} \cdot T^*(x) \cdot T_\infty$
y	$T(y) \cdot T^*(y)$	$T^*(y) \cdot T_\infty$
z	$T(z) \cdot T^*(z)$	$T^*(z) \cdot T_\infty$
t	$T(t) \cdot T^*(t)$	$T^*(t) \cdot T_\infty$

Table B.4: Separated forms of the LHS and RHS of the fourth term

Appendix C

***

C.1 Chapter 5: simulations summary

This Appendix is related to a summary of the simulations presented in Chapter 5 where the mixed strategy is investigated. The thermal model with a null initial and boundary conditions and with a cyclic heat source is considered. The cyclic heat heat source consists of triangular form with $R = \frac{q_{min}}{q_{max}} = 0$, and a maximum amplitude equal to $100000 W.m^{-3}$. Three different cycle times are considered:

1. Table C.1 summarizes the different results for different physical times with $\tau_c = 10s$, with homogenous boundary conditions.
2. Table C.2 summarizes the different results for different physical times with $\tau_c = 20s$, with homogenous boundary conditions.
3. Table C.3 summarizes the different results for different physical times with $\tau_c = 40s$, with homogenous boundary conditions.

The different cases dealt with the mixed strategy are summarized in Table C.4, where it shows the number of time bases needed for each case and the boundary conditions applied (the results are detailed in Chapter 5).

τ_ϕ	CPU(FEM)	CPU(Approach)	Ratio time saving	Relative error compared to FEM
$\tau_\phi = 0.1$	103	3.2	32.18	1.3%
$\tau_\phi = 1$	104.6	3.105	33.68	2.3%
$\tau_\phi = 5$	101.5	3.002	33.81	2%
$\tau_\phi = 10$	100.3	2.95	34	2.5%
$\tau_\phi = 20$	101.2	2.81	36.01	4.1%
$\tau_\phi = 30$	96.7	2.75	35.16	5%
$\tau_\phi = 40$	96.36	2.633	36.59	5.3%
$\tau_\phi = 50$	95.7	2.52	38	5%
$\tau_\phi = 60$	104.5	2.5103	41.63	4.6%
$\tau_\phi = 70$	105.6	2.313	45.65	5.3%
$\tau_\phi = 100$	108	2.21	48.86	3.77%
$\tau_\phi = 200$	103.1	2.103	49.025	5.1%
$\tau_\phi = 300$	104	2.004	51.89	4%
$\tau_\phi = 500$	106.9	1.98	53.98	3.89%
$\tau_\phi = 750$	109.2	1.97	55.431	3.2%
$\tau_\phi = 1000$	104.6	1.932	54.14	2.8%
$\tau_\phi = 1800$	107.1	1.93201	55.43	2%

Table C.1: The relative error calculated for different spatial points for $\tau_c = 10s$ with heat source and null boundary conditions

τ_ϕ	CPU(FEM)	CPU(Approach)	Ratio time saving	Relative error compared to FEM
$\tau_\phi = 0.1$	86.4	2.5	36.56	1.2%
$\tau_\phi = 1$	87.7	2.43	36.1	2.6%
$\tau_\phi = 5$	88	2.31	38.1	3.1%
$\tau_\phi = 10$	87.65	2.2	40	2.1%
$\tau_\phi = 20$	88.3	2.05	43.07	4.3%
$\tau_\phi = 30$	87.5	2.01	43.53	5.4%
$\tau_\phi = 40$	89.2	2.01	44.37	3.25%
$\tau_\phi = 50$	88.7	2	44.35	2.07%
$\tau_\phi = 60$	88.3	2	42.84	3.3%
$\tau_\phi = 60$	88.4	1.98	44.6	4.14%
$\tau_\phi = 100$	89.6	1.96	45.71	3.65%
$\tau_\phi = 200$	88.3	1.93	45.75	2.41%
$\tau_\phi = 300$	88.3	1.94	45.51	4.3%
$\tau_\phi = 500$	88.5	1.93	45.85	3.45%
$\tau_\phi = 750$	88.7	1.86	47.68	2.82%
$\tau_\phi = 1000$	88.6	1.71	51.81	1.78%
$\tau_\phi = 1800$	88.6	1.65	53.69	1.81%

Table C.2: The relative error calculated for different spatial points for $\tau_c = 20s$ with heat source and null boundary conditions

τ_ϕ	CPU(FEM)	CPU(Approach)	Ratio time saving	Relative error compared to FEM
$\tau_\phi = 0.1$	102.1	2.8	36.46	1.3%
$\tau_\phi = 1$	100.7	2.75	36.6	2.1%
$\tau_\phi = 5$	99.5	2.66	37.4	2%
$\tau_\phi = 10$	99.3	2.61	38	2.5%
$\tau_\phi = 20$	94.2	2.505	37.6	5.1%
$\tau_\phi = 30$	96.7	2.5	38.68	5%
$\tau_\phi = 40$	96	2.3	41.74	5.3%
$\tau_\phi = 50$	94.2	2.235	42.14	5%
$\tau_\phi = 60$	94.7	2.2105	42.84	4.6%
$\tau_\phi = 60$	93.3	2.105	44.32	5.3%
$\tau_\phi = 100$	101	2.1	48.1	2.77%
$\tau_\phi = 200$	102	1.91	53.4	5.1%
$\tau_\phi = 300$	99	1.94	51.03	4%
$\tau_\phi = 500$	97	1.80003	50.55	3.89%
$\tau_\phi = 750$	97	1.8	53.88	3.2%
$\tau_\phi = 1000$	98.5	1.702	57.87	2.8%
$\tau_\phi = 1800$	98.5	1.606100	61.33	2%

Table C.3: The relative error calculated for different spatial points for $\tau_c = 40s$ with heat source and null boundary conditions

Simulation number	τ_c	τ_ϕ	Type of the load	$q(W/m^3)$ or $T°C$	Initial condition T(x,y,z,$t=0$)	length	Number of time basis	Time saving/FEM	Error/FEM	Stopping criteria
1	$10s$	0.1	Heat source	$100000(W/m^3)$	0	50	21	32.18	1.3%	10^{-4}
2	$10s$	1	Heat source	$100000(W/m^3)$	0	50	20	33.68	4.3%	10^{-4}
3	$10s$	10	Heat source	$100000(W/m^3)$	0	50	11	34	2.5%	10^{-4}
4	$10s$	100	Heat source	$100000(W/m^3)$	0	50	4	48.86	4%	10^{-4}
5	$10s$	1000	Heat source	$100000(W/m^3)$	0	50	2	54.14	2.8%	10^{-4}
6	$20s$	0.1	Dirichlet boundary conditions	$T = 50°C$	0	50	10	48	2.4%	10^{-4}
7	$20s$	0.1	Opposite Dirichlet boundary conditions	$T = 50°C$	0	50	11	47	4%	10^{-4}
8	$20s$	0.01	Robin boundary conditions	$T = 50°C$	0	50	10	50	3.7%	10^{-4}
9	$20\&50s$	0.1	Heat source and Dirichlet boundary conditions	$100000W/m^3\&T = 50°C$	0	50	22	50	1.4%	10^{-4}

Table C.4: Summary of the simulations